Stony Brook University

Biophysical Insights into the Initiation and Inhibition of Amyloid Formation by Islet Amyloid Polypeptide

A Dissertation Presented

by

Hui Wang

to

The Graduate School

in Partial Fulfillment of the

Requirements

for the Degree of

Doctor of Philosophy

in

Chemistry

Stony Brook University

May 2014

Stony Brook University

The Graduate School

Hui Wang

We, the dissertation committee for the above candidate for the

Doctor of Philosophy degree, hereby recommend

acceptance of this dissertation.

Daniel P. Raleigh –Dissertation Advisor
Professor and Vice Chair of Chemistry

Jin Wang – Chair Person of Defense
Associate Professor of Chemistry

Joseph W. Lauher – Third Member of Defense
Professor of Chemistry

Markus Seeliger - Outside Member of Defense
Assistant Professor of Pharmacological Sciences
School of Medicine, Stony Brook University

This dissertation is accepted by the Graduate School

Charles Taber
Interim Dean of the Graduate School

Abstract of the Dissertation

Biophysical Insights into the Initiation and Inhibition of Amyloid Formation by Islet Amyloid Polypeptide.

by

Hui Wang

Doctor of Philosophy

in

Chemistry

Stony Brook University

2014

Amyloid formation, the aggregation of normally soluble proteins or polypeptides into highly ordered β-sheet structures, is a characteristic feature of many human diseases including Alzheimer's disease, Parkinson's disease and type 2 diabetes. I centered my research on islet amyloid polypeptide (IAPP), a neuroendocrine hormone that forms fibrillar amyloid deposits in the extracellular space of the pancreatic islets of Langerhans in type 2 diabetes. Although whether IAPP amyloid formation is a cause or consequence of the disease is controversial, the aggregation process has been shown to induce β-cell apoptosis and reduce β-cell mass, which is a hallmark feature of type 2 diabetes. The mechanism of islet amyloid formation is not understood yet. Moreover, although there are some reported IAPP amyloid inhibitors, either peptide-based or small-molecule, lack of the clear modes of their actions impedes further

development and their clinical use. A better understanding of the amyloidsis and inhibition mechanism could help explain the pathogenesis of type 2 diabetes and could lead to improved treatment for the disease.

My work included a study of the effects of glycosaminoglycans, the main component of extracellular matrix which was believed to play a role in *in vivo* islet amyloid initiation and progression, on *in vitro* amyloid formation and inhibition; an investigation of the possible role of impaired proIAPP processing in islet amyloid formation; a rational design of several IAPP analogs with better solubility at neutral pH than a FDA approved drug, promising better adjunct drug candidates to insulin therapy for diabetes patients; a study to elucidate the factors which lead to optimum peptide based inhibitors of IAPP amyloid formation by examining the ability of a set of designed polypeptide analogs of IAPP; a critical examination of the inhibition of IAPP amyloid formation by inositol.

Table of Contents

List of Figures

List of Tables

List of Abbreviations

CD	Circular dichroism
CPE	Carboxypeptidase E
DM	H18R, I26P double mutant of hIAPP
DMSO	Dimethyl sulfoxide
DOPG	1,2-dioleoyl-sn-glycero-3-phospho-(1'-rac-glycerol)
EGCG	(−)-epigallocatechin 3-gallate
EM	Electron microscopy
F23L PM	Phe23Leu pramlintide
FBS	Fetal bovine serum
FLH	Fluorescein labeled heparin
Fmoc	9-fluornylmethoxycarbonyl
GAG	Glycosaminoglycan
GalNAc	N-acetyl--galactosamine
GlcA	Glucuronic acid
GlcNAc	N-acetylglucosamine
H18R PM	His18Arg pramlintide
HFIP	Hexafluoroisoproponal
hIAPP	Human islet amyloid polypeptide
HS	Heparan sulfate
HSPG	Heparan sulfate proteoglycan
I26P-IAPP	I26P point mutant of human IAPP

IAPP	Islet amyloid polypeptide
IdoA	Iduronic acid
INS-1	Rat insulinoma-1
LUV	Large unilamellar vesicles
MD	Molecular dynamics
NMe-G24, NMe-I26-IAPP	G24-N-Methyl, I26-N-Methyl-IAPP
PAL-PEG	5-(4'-fmoc-aminomethyl-3',5-dimethoxyphenol) valeric acid
PAM	Peptidyl amidating mono-oxygenase complex
PM	Pramlintide
QM	H18R, Ala-25, Ser-28, Ser-29 quadruple mutant of hIAPP
rIAPP	Rat IAPP
RP-HPLC	Reverse-phase high-performance liquid chromatography
T2D	Type 2 diabetes
TEM	Transmission electron microscopy
TFA	Trifluoroacetic acid
TM-a	G24P I26P triple mutant of hIAPP
TM-b	S20R G24P I26P triple mutant
v/v	Volume to volume

Acknowledgments

The whole work is supervised by my research advisor, Prof. Daniel P. Raleigh. Without his continuous guidance, support and encouragement during my research, this work could not be accomplished. I learned a lot from him during the past six years and could not have asked for a better research advisor than him.

I would also like to thank the other members in my academic committee. Thank you to Prof. Jin Wang and Prof. Lisa Miller for the advice and help throughout the years, and thank you to Prof. Markus Seeliger for taking the time and serving as the outside members of my committee.

Thank you to all the great members of the Raleigh Lab, past and present, Dr. Ping Cao, Dr. Fanling Meng, Dr. Peter Marek, Dr. Wenli Meng, Dr. Vadim Patsalo, Dr. Bing Shan, Dr. Humeyra Taskent, Dr. Shifeng Xiao, Rehana Akter, Yuan Chen, Bowu Luan, Harris Noor, Ivan Peran, Zachary Ridgway, Natalie Stenzoski, Cynthia Tu, Amy Wong ,Matthew Watson, Xiaoxue Zhang. I greatly enjoyed working and interacting with them in the past several years as colleagues and friends, and I specially thank Dr. Fanling Meng for being my mentor and training me when I started my work in lab.

I also would like to thank all the scientists with whom I have collaborated: Dr. Andishen Abedini from New York University School of Medicine for her help with cytotoxicity studies, Prof. Michael Bowers from University of California, Santa Barbara and his group for the collaboration on the Mass Spectrometry studies.

Lastly, I would like to thank my parents for their continuous love and support, both morally and financially.

Publications

1. **Wang, H.**, Cao, P., and Raleigh, D. P. (2013) Amyloid formation in heterogeneous environments: islet amyloid polypeptide glycosaminoglycan interactions, *J. Mol. Biol. 425*, 492-505.

2. **Wang H.**; Raleigh, D. P. (2014) The ability of insulin to inhibit the formation of amyloid by pro-Islet amyloid polypeptide processing intermediates is significantly reduced in the presence of sulfated glycosaminoglycans, *Biochemistry 53*, 2605-2614.

3. Cao, P., Abedini, A., **Wang, H.**, Tu, L. H., Zhang, X. X., Schmidt, A. M., and Raleigh, D. P. (2013) Islet amyloid polypeptide toxicity and membrane interactions, *Proc. Natl Acad. Sci. USA 110*, 19279-19284.

4. Cao, P., Marek, P., Noor, H., Patsalo, V., Tu, L. H., **Wang, H.**, Abedini, A., and Raleigh, D. P. (2013) Islet amyloid: From fundamental biophysics to mechanisms of cytotoxicity, *FEBS Lett. 587*, 1106-1118.

5. **Wang, H.**; Raleigh, D. P., General amyloid inhibitors? A critical examination of the inhibition of IAPP amyloid formation by inositol stereoisomers. *Submitted to Plos. One*

6. Abedini, A.; Plesner, A.; Cao, P.; Zhang, J.; Meng, F.; Middleton, C. T.; Tu, L.H.; **Wang, H.**; Song, F.; Zanni, M.T.; Verchere, B.C.; Raleigh, D.P.; Schmidt, A. M., Islet amyloidosis induces β-cell death via pre-fibrillar amylin lag phase intermediates that bind RAGE. *Submitted to Cell*

7. **Wang, H.**; Cao, P.; Raleigh, D.P., Rationally designed inhibitors of amyloid formation by human amylin: A balance between optimum recognition and reduced amyloidgenicity. In preparation.

8. Wang, H.; Abedini, A.; Cao, P.; Raleigh, D. P.; Rationally designed, non-toxic, non-amyloidogenic analogs of human islet amyloid polypeptide with improved solubility. *Submitted to Biochemistry*

9. Susa A.C.; Wu, C.; Sivas, S.L.; Dupuis, N.F.; **Wang, H.**; Raleigh, D.P.; Shea, J.E.; Bowers, M.T., Defining the molecular basis of amyloid inhibitors; Human Islet Amyloid Polypeptide-insulin interactions. In preparation.

Chapter 1 Introduction

Amyloid formation refers to the aggregation of normally soluble proteins or polypeptides into partially ordered insoluble fibrils or amyloid plaques. Amyloid deposits, formed by a wide range of proteins and peptides, are associated with more than 40 human disorders including neurodegenerative diseases such as Alzheimer's and Parkinson's, and metabolic diseases such as type 2 diabetes (Table 1-1).[1] This introduction summarizes the current knowledge of the biophysical, biological, and biochemical features of amyloid deposition with the primary focus on islet amyloid polypeptide (IAPP or amylin), a peptide responsible for pancreatic islet amyloid in type 2 diabetes.

1.1 General Features of Amyloid

Amyloid formed by different proteins and polypeptides, regardless of the differences in their sequence and native secondary structure, share some common properties in terms of structure, ligand binding and polymerization pathway.

Amyloid fibrils are unbranched and 5 to 10 nm in diameter, according to transmission electron microscopy (TEM) images.[2] Individual fibrils are built from protofilaments, each of which normally contains two or more β-sheets. The β-sheet conformation extends over the length of amyloid fibrils with the individual β-strands aligned perpendicular to the fiber axis; therefore, the hydrogen bonds within a sheet are nearly parallel to the fiber axis (Figure 1.1).[2, 3] This "cross-β" motif is a defining feature of the amyloid fibrils. Amyloid fibrils are typically made up of 3 to 9 protofilaments which are left handed super-coiled (Figure 1.1).[4]

Due to their ordered structure, amyloid fibrils are able to bind histological dyes such as Congo red and thioflavin-T.[5, 6] Upon binding to amyloid fibrils, Congo red shows a characteristic green birefringence as well as a shift in absorbance maximum from 490 nm to 540 nm.[7, 8] Although the binding mode is not fully understood, a planar Congo red form may bind in grooves formed along the β-sheets in either a monomeric or supramolecular form.[9] However, Congo red does not specifically bind to amyloid fibrils; it also binds to native proteins and partially folded proteins without specific secondary structure requirement.[10] In addition, it can interfere with the kinetics of amyloid formation.[11-14]

Another dye, thioflavin-T, has been widely used as an *in vitro* fluorescent probe for characterization of amyloid fibrils and kinetics of amyloid formation. Thioflavin-T consists of a benzothiazole and an aminobenzene ring (Figure 1.2). In solutions, these two fragments rapidly rotate around the shared C-C bond, leading to non-radiative decay. Upon binding to the grooves on the surface of amyloid fibrils or protofibrils, formed by aligned side chains in ordered β-sheet structures, the excited state of thioflavin-T is stabilized due to a rigid dye environment, resulting in an increased quantum yield as well as a characteristic fluorescence signal at 482 nm when selectively excited at 450 nm.[15-20] Simulation results which model the binding of thioflavin-T to the peptide KLVFFAE protofibril are shown in Figure 1.2. The interaction of thioflavin-T with amyloid fibrils is observed with a variety of proteins and polypeptides with different size, sequence and native structures, and it has been proved that thioflavin-T, at various concentrations, does not perturb amyloid formation by IAPP.[21]

The mechanism of amyloid formation is not completely understood, but experimental evidence favors a nucleation-dependent pathway, which applies to both intrinsically disordered peptides and natively folded proteins. However, natively folded proteins need to unfold, at least

partially, prior to their aggregation into amyloid fibrils.[22-24] This step is usually facilitated by mutations in the amino acid sequence that destabilize the native structure, or by conditions that promote partial unfolding such as high temperature, high pressure, low pH, or moderate concentrations of organic solvents.[25-29]

Amyloid formation consists of three different phases.[30] The first is the lag phase in which monomers slowly associate into oligomers which then further convert to the nucleus. This is the rate limiting step. Once seeds are formed, there is a growth phase with rapid formation of protofibrils by addition of monomers to the ends of seeds and assemblies of protofibrils in order to generate mature amyloid fibrils. After the exponential growth, the fibrilization reaction reaches a plateau where amyloid fibrils and soluble species are in equilibrium (Figure 1.3). The lag phase can be partly or completely bypassed by adding preformed seeds.[31] The seeding reaction is specific to some degree since fibrils are more efficient in templating the amyloid formation by the same protein than by other amyloidgenic proteins.[32] Therefore, cross-seeding experiments, which test the ability of fibrils formed by one protein to seed the amyloid formation by another amyloidgenic protein, are conducted to investigate the structural similarity among different fibrils. Secondary nucleation is an important part of amyloid formation and refers to the catalysis of the formation of new fibrils from existing fibrils. In recent years, secondary nucleation events, which involve fragmentation of growing fibrils to generate new ends or the growth of new fibrils off existing fibrils, have been discovered, and various studies have indicated that secondary nucleation plays an important role in the kinetics of amyloid formation.[33-35]

1.2 Islet Amyloid Polypeptide (IAPP)

1.2.1 In Vivo Biosynthesis

IAPP is a 37 residue neuroendocrine hormone produced with insulin as a preform in the islet β cells of the pancreas. It is stored in the insulin secretory granule and co-secreted with insulin, a natural inhibitor of IAPP amyloid formation.[36-38] Secreted protein levels are maintained at a ~1:100 ratio of IAPP to insulin in the secretory granule of healthy β-cells, and the concentration of IAPP in the granule is in the millimolar range which is much higher than is required to promote rapid amyloid formation *in vitro*, suggesting that there are factors which inhibit its aggregation in the secretory granule.[39, 40] The low pH and interactions with insulin in the secretory granule have been proposed to play such an inhibitory role *in vivo*.[36, 41]

IAPP is synthesized as an 89 residue precursor, preproIAPP. Removal of the signal sequence generates the 67 residue prohormone, proIAPP, which is further processed by cleavage at two conserved dibasic sites (Lys-Arg) located at its N- and C-termini by the same prohormone convertases that process proinsulin.[42] The C-terminal pro-sequence is removed in either the trans-Golgi network or secretory granule, preferentially by the prohormone convertase PC(1/3). The remaining dibasic residues at the C-terminus are cleaved by carboxypeptidase E (CPE),[43] and amidation is carried out by the peptidyl amidating mono-oxygenase complex (PAM) with a conserved glycine residue acting as the nitrogen donor.[44] Cleavage of the prosequence at the N-terminus by convertase PC2 gives the 37 residue mature IAPP.[45] Additional posttranslational modifications include disulfide formation between Cys2 and Cys7 (Figure 1.4).[46] Impairment of the prohormone processing machinery leads to the secretion of an intermediate peptide with the N-terminal flanking region of proIAPP, $proIAPP_{1-48}$, which corresponds to the first 48 residues of proIAPP.[47, 48] This intermediate peptide has been conjectured to play an important role in the

initiation and progression of IAPP amyloid formation *in vivo*. [49-52] One of my research projects is to study the role of proIAPP$_{1-48}$ in islet amyloid formation. This work is summarized in chapter 2.

1.2.2 Physiological Function of IAPP

The physiological function of soluble IAPP is not completely understood due to the difficulty in distinguishing its physiological roles from its experimentally observed pharmacological effects, but hIAPP is believed to complement the effects of insulin in postprandial glycemic control by suppressing postprandial glucagon secretion, helping regulate the rate of gastric emptying, and inducing satiety to suppress food intake.[53-57] The aforementioned effects on the rate of both endogenous and exogenous glucose entry into the circulation by IAPP and its analog drug, pramlintide, has been well established in experimental animals and in humans.[58-63] Pramlintide will be discussed in more detail in section 1.2.4 and chapter 4 and 5.

IAPP was also reported to inhibit insulin-stimulated glucose uptake and glycogen synthesis in isolated incubated rat skeletal muscle.[64] Moreover, IAPP has been shown to inhibit insulin-stimulated glucose transport *in vitro*, and insulin resistance could be induced by infusion of IAPP *in vivo*.[65, 66] Thus IAPP was proposed to be related to insulin resistance mechanism in type 2 diabetes. However, these effects were observed at concentrations much higher than physiological levels.

1.2.3 IAPP Amyloid and Diabetes

IAPP has been characterized in a variety of species including mammals, birds, and teleostean fish, but *in vivo* islet amyloid has only been identified in humans, non-human primates, and cats, but notably not in rats and mice.[53, 67-73] The other species do not form islet

amyloid, and have not been reported to develop type 2 diabetes. The IAPP sequence is conserved across species, and differ most between residues 20 and 29 (Figure 1.5).[74] For example, rat IAPP (rIAPP) which does not form amyloid, differs from human IAPP (hIAPP) at only six positions out of 37, and five of them, including three Pro, are located in the 20-29 segment. Pro is a well-known β-sheet breaker, and the inability of rat IAPP to form amyloid is attributed to three Pro substitutions at positions 25, 28 and 29.[67] Due to these studies, the segment 20-29 of hIAPP, which forms amyloid on its own, was believed to form the core of IAPP amyloid and dictate the amyloidogenic properties of the peptide.[67, 75] Subsequent studies reveal that the situation is more complex. More details about the connection between primary sequence and amyloid formation are discussed in section 1.2.4.

Islet amyloid is clearly associated with type 2 diabetes, although whether it is a cause or consequence of the disease is not clear. In one study, islet amyloid has been found in up to 90% of patients with type 2 diabetes.[76] The islet amyloid deposits are also observed in nondiabetic individuals, but usually occur to a less severe degree.[77, 78] Moreover, amyloid deposition is associated with reduced islet volume due to a loss of β-cell mass, which is a hallmark feature of type 2 diabetes.[79-81] More details about the β-cell toxicity of IAPP will be discussed in the next section. Another main factor of type 2 diabetes is insulin resistance, resulting in an increased demand for insulin release, which is paralleled by an increase in IAPP and proIAPP secretion, and could lead to islet amyloid formation.[82-84]

Due to the difficulty in investigating amyloid formation in humans, studies of cultured islets and studies with animals, especially rats transgenic for human IAPP, provide more information on the effect of IAPP aggregation for the development of diabetes.[85-90] As mentioned earlier, rIAPP does not form amyloid and rats do not develop type 2 diabetes. However, in

several rat strains transgenic for human IAPP, diabetes has developed accompanying islet amyloid formation and reduction in β-cell mass, comparable to what was observed in human type 2 diabetes.[91-93] One issue with some of the animal models is that large amounts of IAPP are produced. In addition, inhibition of proIAPP expression by small interfering RNA and treatment with a peptide inhibitor of IAPP aggregation have been shown to enhance β-cell survival in cultured human islets.[89, 90]

Last but not least, IAPP also contributes to the failure of pancreatic islet transplants as a treatment for type 1 diabetes, which is featured by a lack of insulin secretion. Clinical trials carried out in the 1980's and 1990's have shown that although initially transplantation from nondiabetic donors into diabetes patients achieved an recovered insulin secretion in nearly all subjects, only 10% of them maintained normal glucose homeostasis without insulin therapy over two years.[94, 95] The failure of islet function over time is associated with the amyloid formation by IAPP in the islets.[96, 97] A recent study shows that islet amyloid deposition limits the viability of human islet grafts, but not porcine grafts since porcine IAPP is significantly less amyloidogenic than hIAPP.[98] This study also provides evidence that preventing amyloid formation promotes graft survival.

1.2.3 IAPP and β-cell Toxicity

IAPP amyloid fibrils were first thought to account for the observed cytotoxicity of IAPP to human and rat islet cells *in vitro*, but it has been generally accepted that small soluble, oligomeric IAPP aggregates formed during the lag phase of amyloid formation are the toxic species, since addition of preformed amyloid fibrils to islet cells in culture did not induce cell apoptosis, while freshly prepared solutions of IAPP did.[99-103] However, since most of the studies on oligomers are performed *in vitro*, the *in vivo* role of IAPP oligomers is still controversial and

the effects of mature IAPP amyloid fibrils on β-cell failure in type 2 diabetes cannot be ruled out.[104]

Multiple mechanisms of IAPP induced β-cell death and decrease in islet volume have been proposed including; ER stress, defects in autophagy, the enhanced production of pro-inflammatory cytokines, mitochondrial membrane damage, activation of calpain-2, receptor-mediated mechanisms linked to oxidative stress, and the activation of cell death signaling pathways.[105-112]

IAPP toxicity has also been linked to disruption of the plasma membrane. There are a number of *in vitro* studies showing that exogenously added IAPP perturbs cell membranes and leads to cell death, but the mechanism of IAPP induced membrane disruption is controversial.[103, 113, 114] Some studies support a pore formation scenario, in which prefibrillar oligomers insert into the cell membrane and form ion-channel like structures, while others argues that fibril extension on the membrane surface leads to invagination and membrane disruption (Figure 1.6).[113, 115-117] However, it is worth noting that the majority of these studies were performed *in vitro* with artificial model membranes, and the ability of IAPP to permeabilize membranes depends on the lipid composition, pH, ionic strength and lipid to peptide ratio. For example, there is a stronger interaction of IAPP with model membranes with anionic lipids, while most of the model membranes used have a much larger fraction of anionic lipids than physiological composition in the β-cell membrane.[118] Moreover, most model membranes do not contain cholesterol or gangliosides which are important components mediating hIAPP membrane interactions.[114, 119] Therefore, considerable caution should be taken when interpreting these *in vitro* results. Membrane disruption has been used in some studies to represent cell toxicity, but recent work that I have collaborated on has proven that many non-amyloidgenic peptides were effective at

inducing leakage of standard model membranes without leading to cell death. Thus there is no one-to-one correlation between membrane disruption and cell toxicity, demonstrating that more investigations needed to be conducted to reveal the role of membrane disruption in IAPP cytotoxicity.[120]

1.2.4 The Primary Sequence of IAPP and Amyloid Formation

As mentioned previously, IAPP sequences from different species differ mostly in the 20-29 region, and this segment was initially proposed to be the amyloid core. Non-amyloidgenic forms of IAPP all have one or multiple prolines, a well-known β-sheet breaker, in this region (Figure 1.5). Several designed mutants of hIAPP with single or multiple Pro substitutions in this region were also reported to be non-amyloidgenic and function as inhibitors of *in vitro* hIAPP amyloid formation, such as I26P-IAPP, G24P-IAPP and G24P, I26P-IAPP.[121, 122] Pramlintide, a non-amyloidgenic peptide that contains the same Pro substitutions as in rat IAPP, has been approved by the FDA as an adjunct drug to insulin therapy.[123] A variant of hIAPP which contains double substitutions of unnatural N-methylated amino acids in this region has been reported to be one of the most potent peptide inhibitors of hIAPP amyloid formation *in vitro*.[124] More discussions on the mechanism of these peptide inhibitors are included in section 1.2.7. In addition, the only reported mutation in the human IAPP gene, S20G IAPP, also occurs to this region. This mutation has been found in Asian populations, and has been suggested to increase the risk of developing type 2 diabetes, along with accelerating amyloid formation *in vitro*.[53, 125, 126] These findings seem to support the proposed dominant role of segment 20-29 in the amyloid formation by IAPP, but other studies have suggested that the situation is more complicated. Pro substitutions outside of the 20-29 region also abolish amyloid formation, and IAPP fragments

that do not contain the 20-29 region are also able to form amyloid.[127, 128] Thus, the 20-29 region is not the only factor governing IAPP amyloid formation *in vitro*.

The rate of IAPP amyloid formation is pH dependent, this is attributed to its N-terminus and a His at position 18. IAPP has been shown to aggregate more slowly at acidic pH when H18 is protonated. The increased charge is thought to impede initial oligomerization.[129-131] Mature IAPP is first stored in the β-cell granules at a pH of 5.5, and then secreted into the extracellular space where the pH is 7.4. His-18 is the only titratable residue over this pH range, and this could play a role in islet amyloid formation.[129] The N-terminus likely also titrates over this pH range, which will contribute to the observed pH dependent effects.[131] IAPP amyloid is rarely found in non-diabetic individuals, hence there must be other factors contributing to the islet amyloid initiation. In a research project of mine, we took advantage of the β-sheet disruption properties of Pro and the pH sensitivity of residue 18 to design non-amyloidgenic IAPP analogs with better solubility at neutral pH. These molecules may be promising drug leads for adjunct therapy with insulin for diabetes patients. That project is summarized in chapter 5.

There are three aromatic residues in the IAPP sequence: F15, F23 and Y37. Thus, aromatic-hydrophobic and aromatic-aromatic interactions have been suggested to play a role in IAPP amyloid formation.[132, 133] However, studies on peptides with aromatic to Leu substitutions of IAPP sequence demonstrated that aromatic residues are not required for amyloid formation, either by the full length polypeptide, or by the fragments originally able to form amyloid.[127, 134, 135] Even though aromatic-aromatic interactions are not necessary for IAPP amyloid formation, they might play a role in dictating the structure of the amyloid fibril since replacement of aromatic residues alters kinetics of amyloid assembly and fibril morphology.

1.2.5 Factors Other than IAPP in Islet Amyloid Formation

Amyloid formation takes places in a heterogeneous environment *in vivo* with the potential for interactions with membranes and with components of the extracellular matrix, mainly glycosaminoglycans (GAGs). Interestingly, these two components have been shown to accelerate amyloid formation *in vitro*. The mechanism of their enhancing effects are not fully understood, but electrostatic interactions of positively charged IAPP and negatively charged GAG or model lipid membranes is believed to play an important role.

Model membranes of varying lipid compositions have been used to test amyloid formation. This includes simple models only consisted of anionic lipids, mixtures of anionic lipids with zwitterionic lipids, and more complicated and physiologically relevant models containing lipid rafts. All have been shown to accelerate IAPP amyloid formation *in vitro*, and more highly charged systems have a larger effect.[118, 119, 136-138] As mentioned previously, caution should be taken when transposing these *in vitro* results into the *in vivo* situations due to the lack of resemblance of the model membranes to the β-cell membrane.

Immunohistochemical studies have shown that heparan sulfate proteoglycan (HSPG) perlecan is found in islet amyloid deposits isolated from patients with type 2 diabetes, and the glycosaminoglycan (GAG) component of HSPG, heparan sulfate (HS) accelerates amyloid formation by both IAPP and proIAPP$_{1-48}$ *in vitro*.[50, 139, 140] More specifically, it has been reported that N-terminal region of proIAPP binds to HSPG.[141] One proposed mechanism of islet amyloid formation involves HSPGs, and suggests that improperly processed N-terminal extensions of proIAPP bind to HSPG upon secretion to the extracellular space, seeding further amyloid formation by IAPP.[141] This proposal is supported by studies demonstrating that fragments corresponding to the first 22 and first 30 residues of proIAPP which, are nonamyloidogenic in

isolation form amyloid fibrils upon interaction with HS, and that amyloid fibrils formed by proIAPP$_{1-48}$ in the presence of HS are capable of seeding amyloid formation by mature IAPP.[50, 140] A schematic diagram depicting this mechanism, adapted from reference 140, is shown in Figure 1.8. One of my research projects is to investigate the effects of GAGs and the importance of GAG-peptide interaction in amyloid formation. The results are summarized in chapter 3.

1.2.6 Models of IAPP Amyloid Fibril Structure

Two atomic level models, developed separately from solid state NMR studies (Tycko model) and X-ray crystallographic studies of IAPP fragments (Eisenberg model), have been proposed for the structure of IAPP fibrils.[142-144] Some common structures are shared by both models including a parallel, in-register arrangement of the β-strands, protofibrils consisted of two columns of IAPP monomers and a U-shaped structure adopted by each monomer.[74] The U-shape of each monomer is constructed by two β-strands connected by a loop, and the β-strands form intermolecular hydrogen bonds with neighboring polypeptide chains within the same column (Figure 1.9).[74] In the Tycko model, each U-shape chain consists of one β-strand encompassing residues 8-17 and the other comprised of residues 28-37, connected by a loop involving residues 18-27.[142] Two structures disagreeing on the register of side-chain orientations were derived from the experimental NMR data, one has Arg 11 projecting into the monomer core, while the other with Arg 11 solvent-exposed. The second structure is more convincing since Arg has a charged side chain (Figure 1.9).

The Eisenberg model was derived from crystallographic studies of short fragments of IAPP that form "steric zippers". It differs from the Tycko model mainly in how the two columns of hIAPP monomers pack against each other and in the location of the C-terminal β-strand. In the Eisenberg model, two tightly interdigitated β-sheets form "steric zipper", which is proposed to be

the fundamental unit of amyloid-like fibrils.[143, 144] The N-terminal β-strand in the Eisenberg model comprises of residues 8-17, and the C-terminal β-strand is made up of residues 23 to 37. An illustration of these two models is included in Figure 1.9.

1.2.7 Inhibitors of IAPP Amyloid Formation

Due to its significant impact in type 2 diabetes, inhibition of amyloid formation by IAPP has therapeutic potential, and thus the search for IAPP amyloid inhibitors is an active area of research. Various inhibitors that slow~~er~~ or abolish IAPP amyloid information *in vitro* have been reported and several of them have been shown to reduce cell cytotoxicity, but none have been approved by FDA, and most are not drug-like, and /or require a large excess to be effective.

Most inhibitors fall into two categories~~,~~ peptide inhibitors based on the sequence of IAPP, and small-molecule inhibitors. As mentioned earlier, rIAPP and several rationally designed polypeptides with single or multiple substitutions of Pro, or unnatural amino acid within 20-29 region of IAPP sequence, have been rendered non-amyloidgenic and function as inhibitors of IAPP amyloid formation.[121, 122, 124, 145] Pramlintide, a FDA approved drug for diabetes patients, also belongs to this category. There is not a thorough understanding of the mechanism of these polypeptides, but all of them are believed to share a so-called "β-breaker" feature, that is, a molecule which combines a recognition element, usually a recognition region resembling the relevant sequence of IAPP, with an entity containing amino acids unfavored for β-sheet structure that inhibits β-sheet formation. A research project of mine investigated this design strategy using a set of polypeptide inhibitors including pramlintide and rIAPP, and helped elucidate the factors leading to optimum peptide based inhibitors. The project is summarized in chapter 4.

Several polyphenol and sulfonated triphenyl methane derivative small molecule inhibitor have also been reported.[21, 146-150] Among them, a polyphenol inhibitor epigallocatechin-3-gallate (EGCG) is one of the most potent. EGCG is a green tea-derived flavanol that has been reported to inhibit IAPP amyloid formation *in vitro*, to dissociate pre-formed fibrils into small aggregates and to protects cells from IAPP induced toxicity.[21, 146] EGCG has been proposed to bind to unaggregated polypeptides or oligomers at the early aggregation stage and remodel them to off-pathway non-toxic oligomers.[151] However, the mode of its action is not fully understood and it is not known if the effects are due to the multiple hydroxyl groups of EGCG, its polyphenolic character, or its susceptibility to spontaneous modifications.[152] In one of my research projects, a critical examination of inositol stereoisomers have been conducted, which provides clues as to the features rendering polyphenol inhibitors effective, and also helps provide information for further efforts in rational inhibitor design. The details are discussed in chapter 6.

It is also worth noting that most of the *in vitro* inhibitor studies are performed in homogeneous solutions, while *in vivo* islet amyloid formation occurs in heterogeneous solution with the potential to interact with lipid membranes or GAGs, as previously mentioned. In one of my research projects, the importance of taking GAG-peptide interaction into consideration in inhibitor screening was revealed. More details are discussed in chapter 3.

1.3 Figures

A

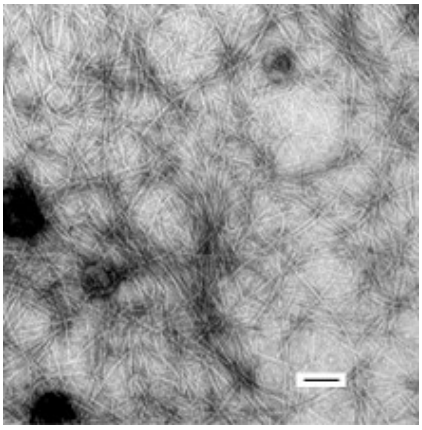

B

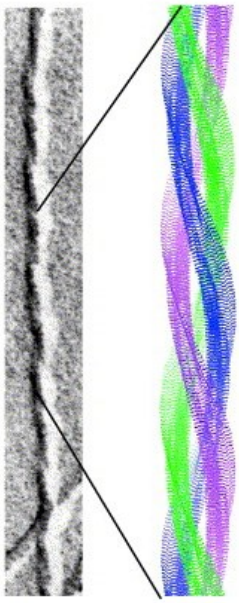

Figure 1.1 Structures of amyloid fibrils.
(A) Electron microscopy of negatively stained amyloid fibrils formed by IAPP. Scale bar represents 100 nm. (B) Electron microscopy of an IAPP amyloid fibril and a fibril model formed by three protofilaments in left handed coils. β-sheet structure is perpendicular to the fibril axis. This figure in panel B is taken from reference (4).

A

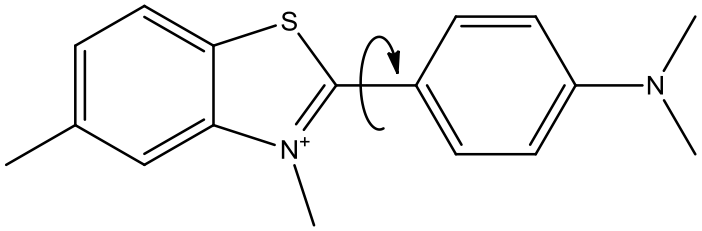

B

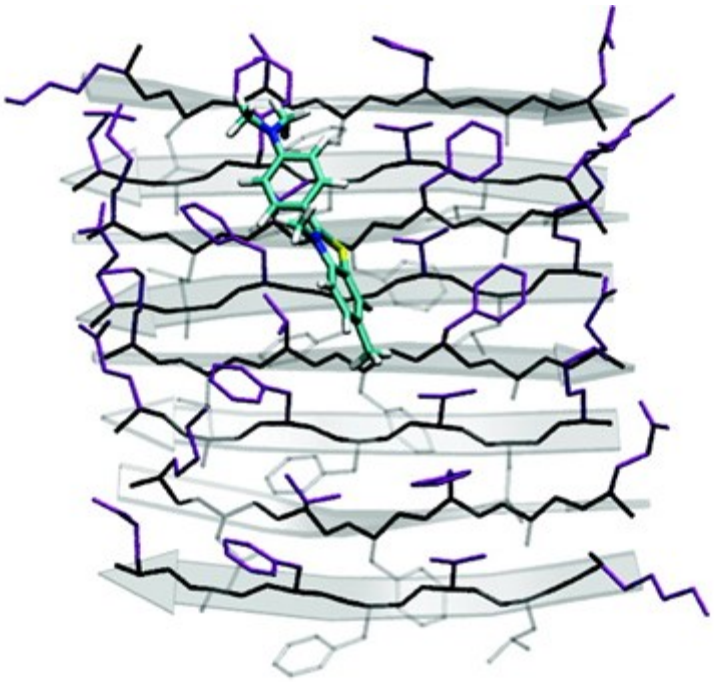

Figure 1.2 The chemical structure and binding mode of thioflavin-T.
(A) The chemical structure of thioflavin-T. (B) Representative structure that displays the binding mode of thioflavin-T and KLVFFAE, a fragment peptide of Aβ. For clarity, only the β-sheet bound to thioflavin-T is shown. The surface side-chains are colored in purple, and the buried side-chains are in silver. The backbone of each β-strand is in an arrow. Panel B is taken from reference (20).

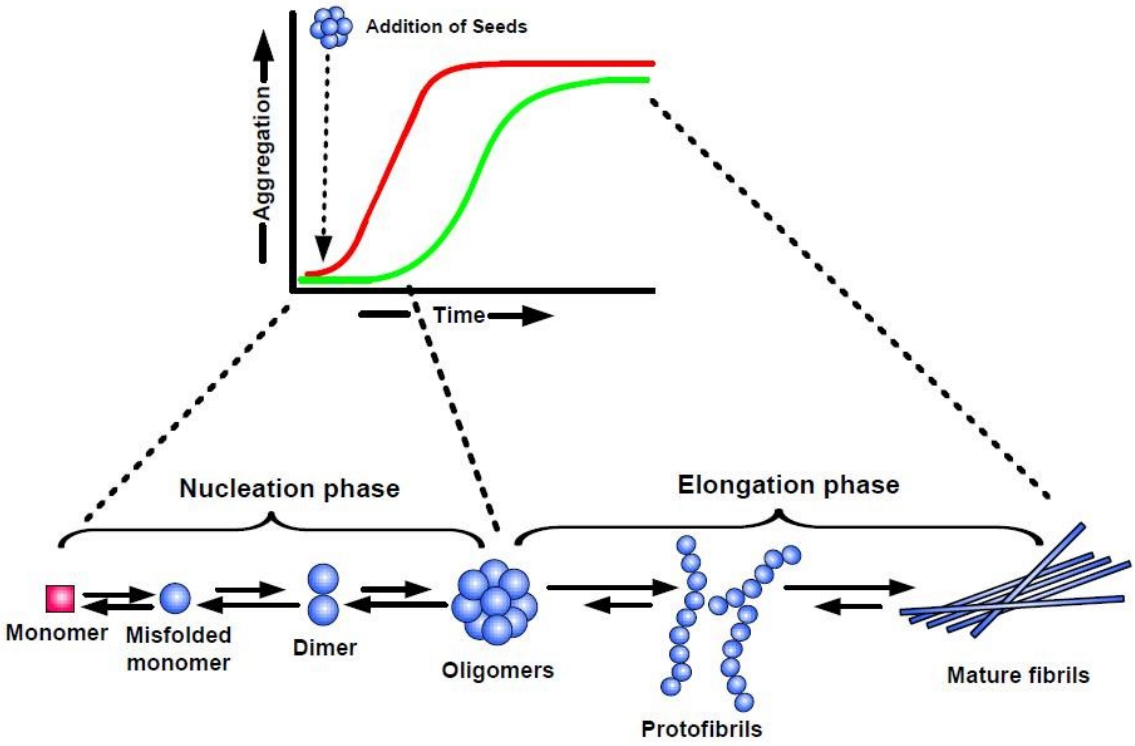

Figure 1.3 Model of nucleation-dependent pathway of amyloid formation.
Amyloid formation consists of three phases: a nucleation phase/lag phase, in which monomers associate to form nuclei and an elongation phase/ growth phase, in which protofibrils rapidly form and assembly to mature amyloid fibrils until a plateau where the reaction reaches its equilibrium (green curve). The lag phase can be partly or completely bypassed by adding preformed seeds (red curve). For natively folded proteins, an unfolding step of the native structures is required before further aggregation. This unfolding step illustrated in the figure is not relevant to intrinsically disordered peptide as IAPP. This figure is taken from reference (30). This simple diagram does not include secondary nucleation.

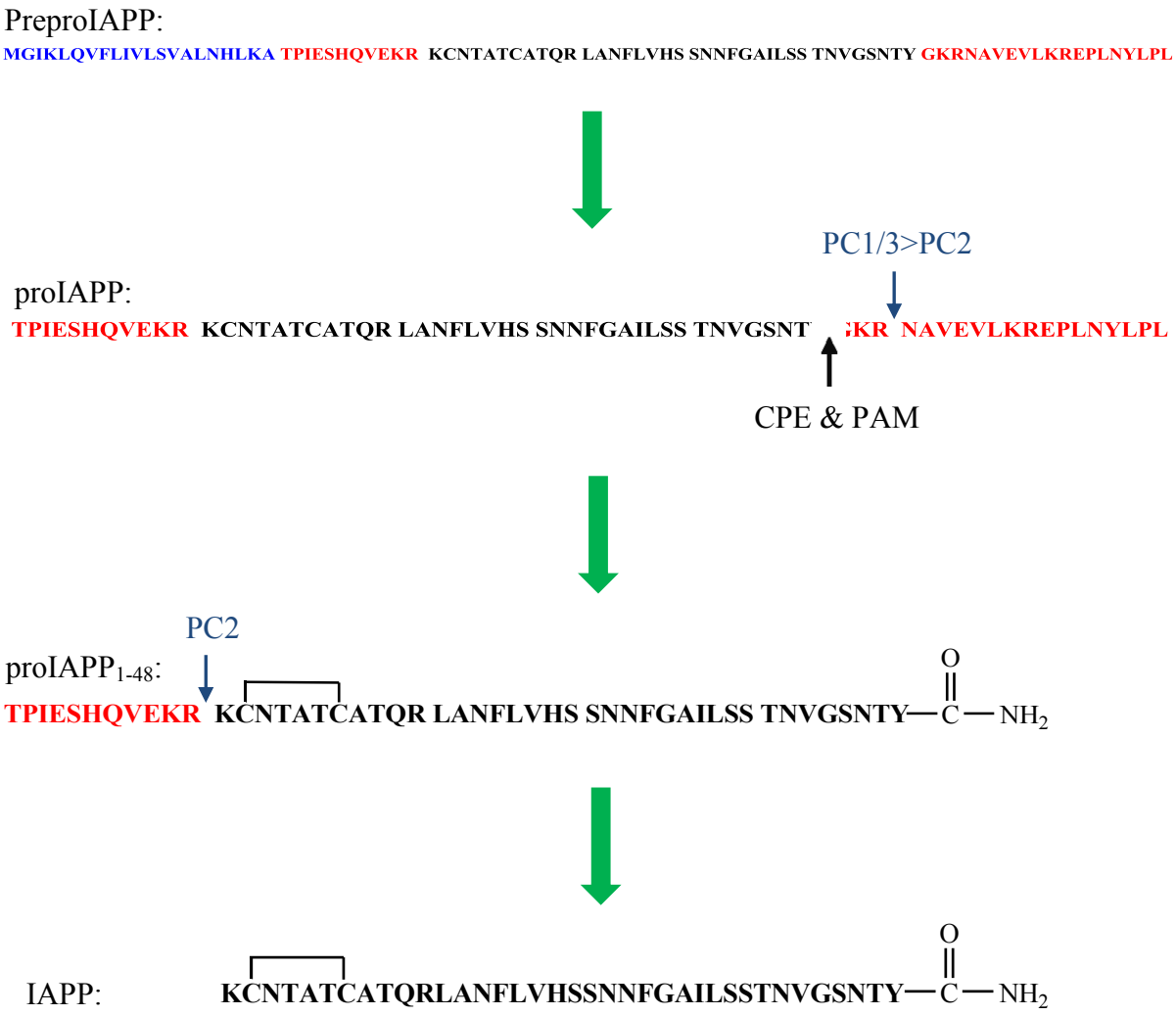

Figure 1.4 Processing pathway of human proIAPP.
The N-terminal signal sequence of preproIAPP is shown in blue. The N-terminal and C-terminal flanking regions of proIAPP are shown in red. Cleavage of proIAPP occurs at the two dibasic sites indicated by blue arrows. The C-terminal region of proIAPP is removed preferentially by PC1/3 and the remaining dibasic residues are removed by CPE. Final processing of the C-terminus includes removal of the remaining Gly and amidation of the Tyr by PAM, leading to the processing intermediate proIAPP$_{1-48}$. The N-terminal region is removed by PC2. There is an intramolecular disulfide bond in proIAPP$_{1-48}$ and in mature IAPP.

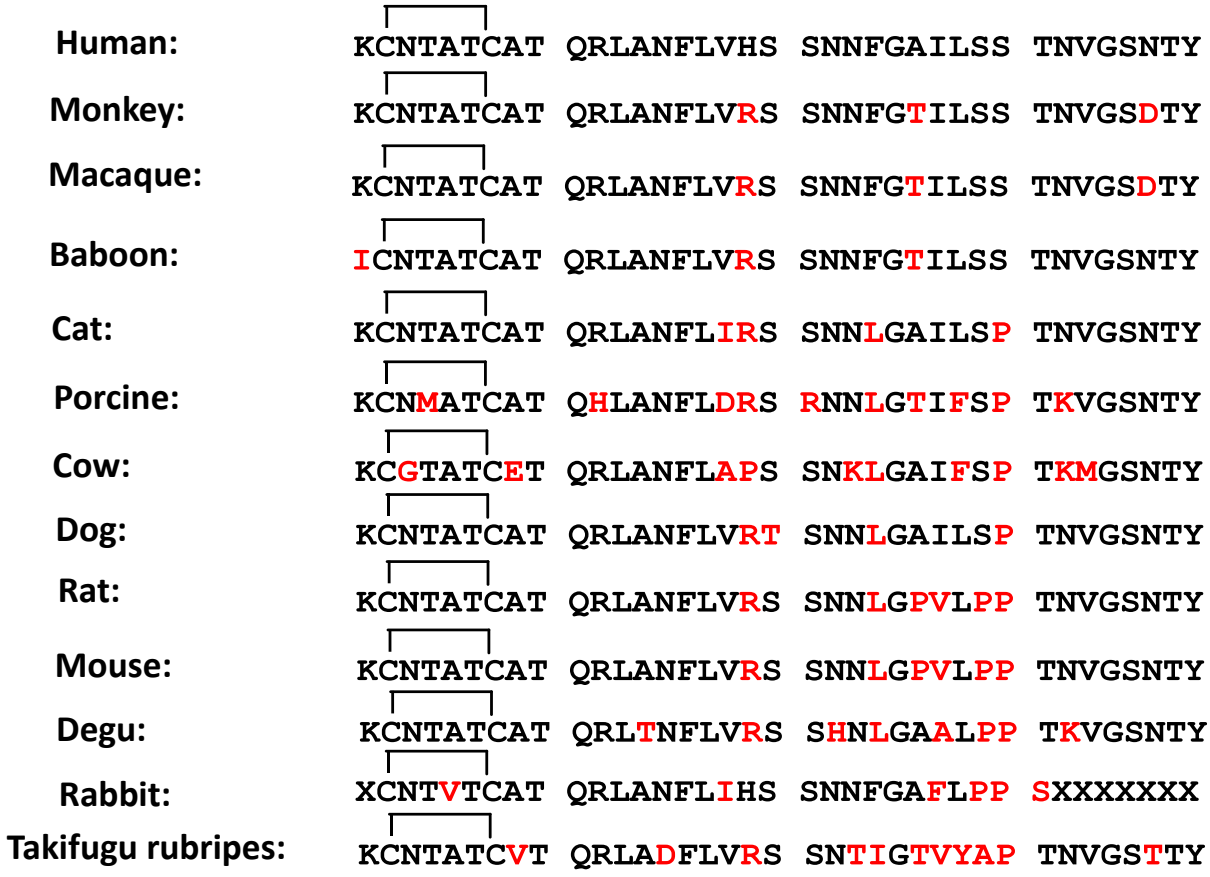

Figure 1.5 Sequences of IAPP from different species.
Different residues from the human IAPP sequence are colored in blue. Only partial sequences are available for rabbit and hare. The biologically active sequences across species all have a disulfide bond between Cys-2 and Cys-7 and an amidated C-terminus. This figure is adapted from reference (74).

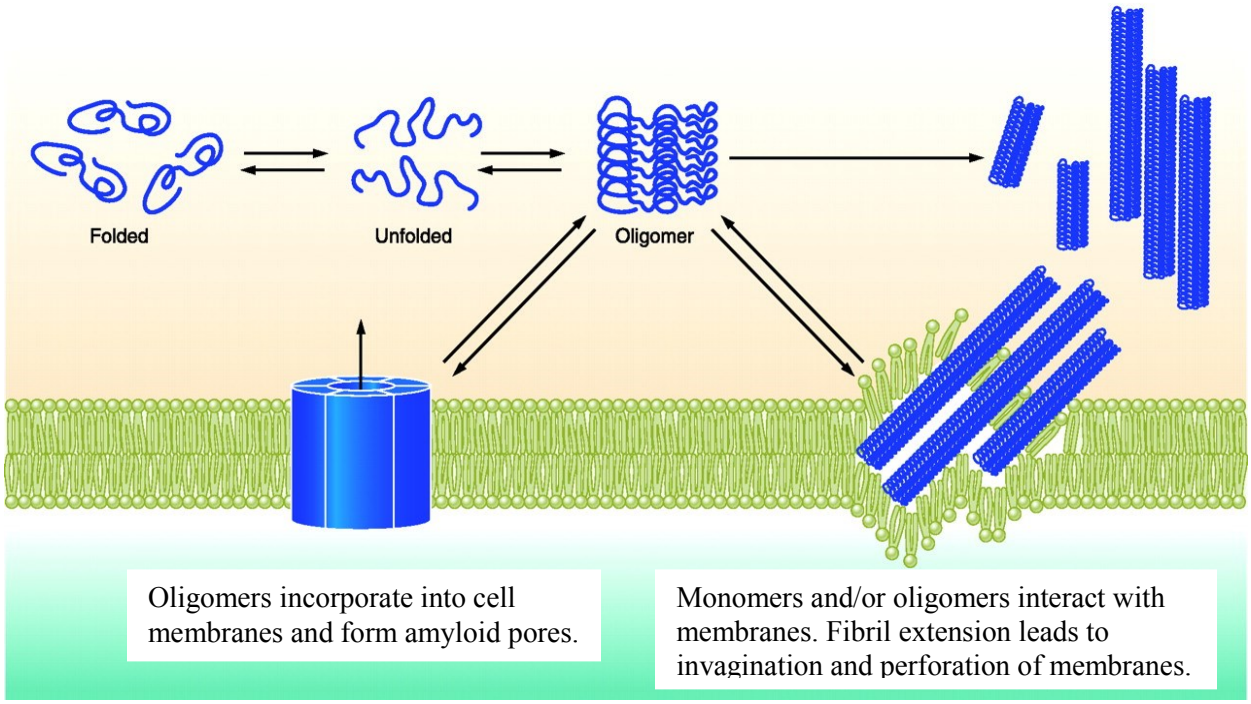

Figure 1.6 Two different mechanism of IAPP membrane disruption.
One is pore formation mechanism, in which oligomers insert into cell membranes and form amyloid pores. The other is detergent or carpeting mechanism, in which fibril extension leads to invagination and perforation of membranes. This figure is adapted from reference (53).

A

NMe-G24, NMe-I26-IAPP:

B

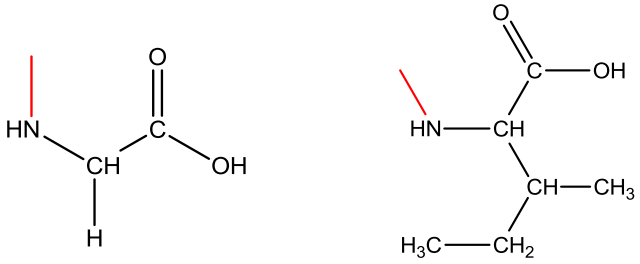

NMeG NMeI

Figure 1.7 Sequence of G24-N-methyl, I26-N-methyl-IAPP and the chemical structures of N-methylated Gly and N-methylated Ile.
(A) Sequence of G24-N-methyl, I26-N-methyl-IAPP (NMe denotes N-methylation). The peptide has an amidated C-terminus and a disulfide bond. (B) Structures of N-methylated Gly and N-methylated Ile.

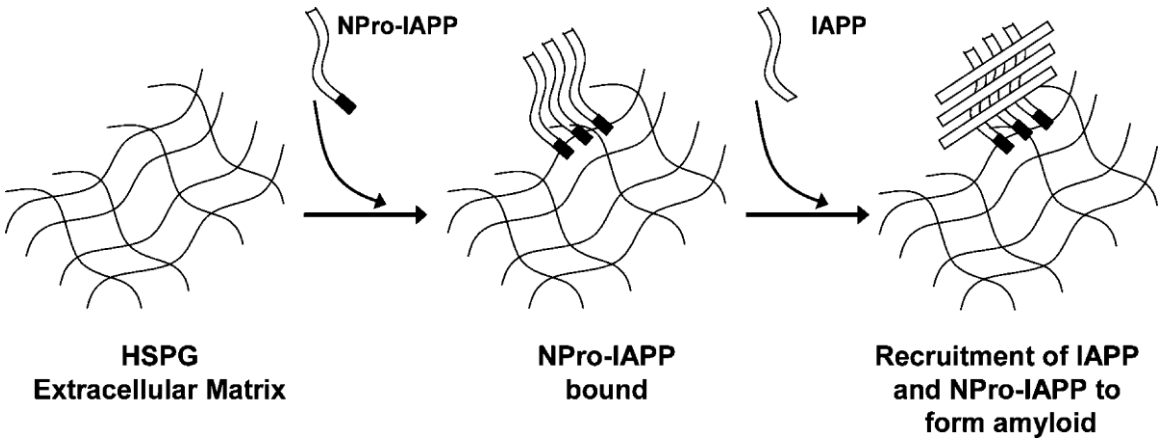

Figure 1.8 Schematic representation of how proIAPP1-48 and HSPGs contribute to islet amyloid formation.
$ProIAPP_{1-48}$ with an uncleaved N-terminal flanking region (shaded) bind to HSPGs in the extracellular matrix resulting in a high local concentration of peptides. This in turn could act as a seed for amyloid formation. This figure is taken from reference (140).

A

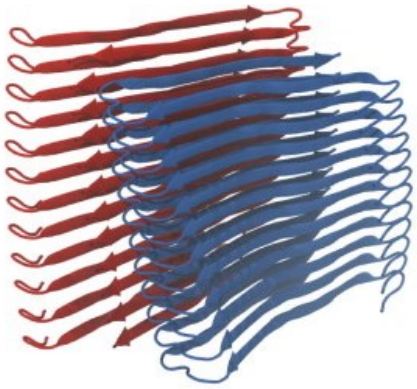

B

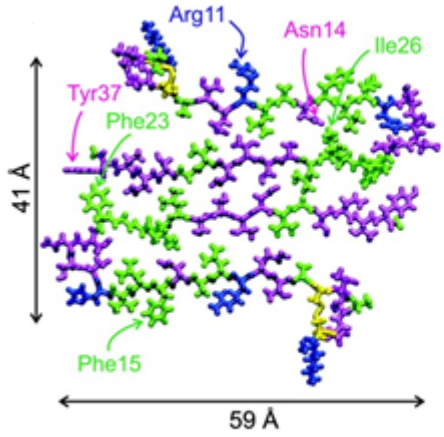
Arg11
Asn14
Ile26
Tyr37
Phe23
41 Å
Phe15
59 Å

C

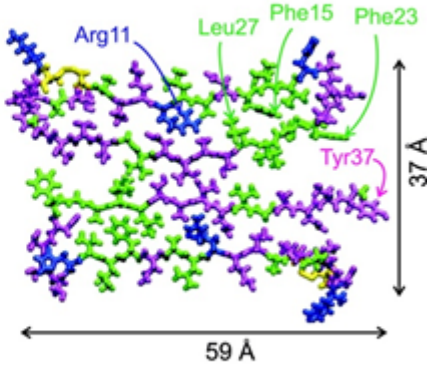
Arg11
Leu27
Phe15
Phe23
Tyr37
37 Å
59 Å

D

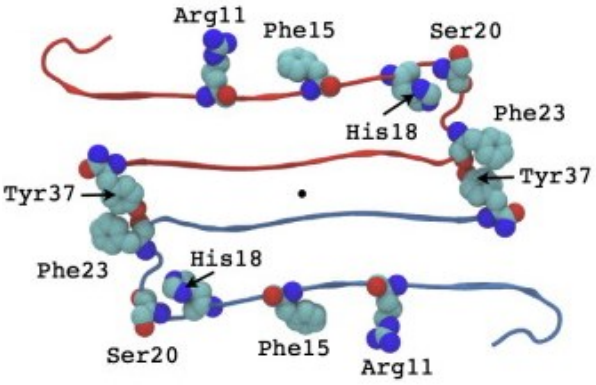
Arg11
Phe15
Ser20
His18
Phe23
Tyr37
Tyr37
Phe23
His18
Ser20
Phe15
Arg11

E

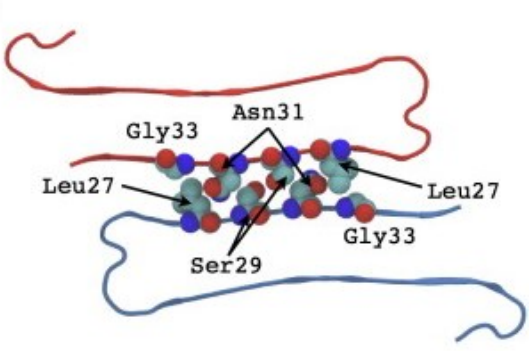
Asn31
Gly33
Leu27
Leu27
Gly33
Ser29

Figure 1.9 An illustration of different structural models of IAPP amyloid fibrils.
(A) Ribbon diagram of the fibril structure with two columns of monomers in symmetry. Panel taken from reference (74). (B & C) All-atom representation of one layer of protofibril of two possible models in Tycko model. Hydrophobic residues are labeled in green, polar residues in magenta, positively charged residues in blue, and disulfide-lined cysteine residues in yellow. These two panels are taken from reference (142). (D & E) Two representations of one layer of protofibril in Eisenberg model with emphasis on different residues. Tight "steric zipper" interface between two IAPP monomers is shown in panel E. These two panels are taken from reference (74)

1.4 Table

Amyloidgenic protein	Disease
Amylin or islet amyloid polypeptide (IAPP)	Type 2 diabetes
Amyloid β peptide	Alzheimer's disease
Prion protein	Spongiform encephalopaties
α-Synuclein	Parkinson's disease
Tau	Frontotemporal dementia
Huntingtin	Huntington's disease
Superoxide dismutase 1	Amyotrophic lateral sclerosis
ABri	Familial British dementia
ADan	Familial Danish dementia
Immunoglobulin light chains	AL amyloidosis
Serum amyloid A	AA amyloidosis
Transthyretin	Senile systemic amyloidosis
β2-microglobulin	Hemodialysis-related amyloidosis
N-terminal fragment of apolipoprotein	Apo amyloidosis
Fragments of gelsolin mutants	Finnish hereditary amyloidosis
Mutants of lysozyme	Lysozyme amyloidosis
Variants of fibrinogen α-chain	Fibrinogen amyloidosis
Mutant of cystatin C	Icelandic hereditary cerebral amyloid angiopathy
Calcitonin	Medullary carcinoma of the thyroid
Atrial natriuretic factor	Atrial amyloidosis
Prolactin	Pituitary prolactinoma
Medin	Aortic medial amyloidosis
Lactoferrin	Corneal amyloidosis associated with trichiasis
γ-Crystallins	Cataract
Lung surfactant protein C	Pulmonary alveolar proteinosis
Keratins	Cutaneous lichen amyloidosis

Table 1.1 Amyloid formation associated human diseases.[1]

Chapter 2 The Ability of Insulin to Inhibit Amyloid Formation by ProIAPP Processing Intermediates Is Significantly Reduced in the Presence of Sulfated Glycosaminoglycans.

Abstract

Islet amyloid polypeptide (IAPP) is responsible for amyloid deposition in type 2 diabetes and plays an important role in the loss of β-cell mass in the disease and in the failure of islet transplant, but the mechanism of islet amyloid formation is not understood. The incorrect processing of proIAPP to produce partially processed forms of the peptide has been proposed to play a role in the initiation of islet amyloid *in vivo* by promoting interactions with proteoglycans of the extracellular matrix. Insulin is a potent inhibitor of amyloid formation by IAPP *in vitro* in homogeneous solution, but its ability to inhibit IAPP in the presence of proteoglycans has not been tested, nor has its effect on amyloid formation by proIAPP processing intermediates been examined. Here we show that insulin is a much less effective amyloid inhibitor of both IAPP and proIAPP processing intermediates *in vitro* in the presence of model glycosaminoglycans, but does inhibit amyloid formation by proIAPP processing intermediates in homogeneous solution. This highlights another mechanism by which sulfated proteoglycans could enhance islet amyloid formation *in vivo*. Interactions with sulfated proteoglycans can directly promote amyloid formation, and can also significantly reduce the effectiveness of natural inhibitors.

The work in this chapter has been published (Wang H.; Raleigh, D. P. (2014) The ability of insulin to inhibit the formation of amyloid by pro-Islet amyloid polypeptide processing intermediates is significantly reduced in the presence of sulfated glycosaminoglycans,

Biochemistry 53, 2605-2614). This chapter contains direct excerpts from that manuscript, which was written by me with the assistance of Prof. Daniel Raleigh.

2.1 Introduction

Amyloid formation is a characteristic feature of many human diseases including Alzheimer's disease, Parkinson's disease and type 2 diabetes.[153, 154] Human islet amyloid polypeptide (IAPP or amylin), is a polypeptide hormone that forms extracellular fibrillar amyloid deposits in the pancreatic islets of Langerhans in type 2 diabetes.[155, 156] IAPP helps regulate gastric emptying, suppression of food intake and glucose homeostasis,[55, 56, 137] but formation of islet amyloid contributes to β-cell dysfunction in type 2 diabetes and is associated with the reduction in β-cell mass associated with the disease.[76, 80] Islet amyloid is also an important contributing factor to the failure of islet transplantation.[98, 157] The polypeptide is produced with insulin in the β cells as a proform, stored in the insulin secretory granule and co-secreted with insulin. Secreted Protein levels are maintained at a ~1:100 ratio of IAPP to insulin in the secretory granule of healthy β cells, but the concentration of IAPP in the granule is still much higher than required to promote rapid amyloid formation *in vitro*, suggesting that there are factors which inhibits its aggregation in the secretory granule. Interactions with insulin have been proposed to play such a role *in vivo* and have been shown to inhibit IAPP amyloid formation *in vitro*.[36-38]

The mechanisms of islet amyloid formation in type 2 diabetes are still not understood, although impairment of the prohormone processing machinery has been conjectured to play an important role in the initiation and progression of this process.[49-52] The *in vivo* biosynthesis of IAPP is described in section 1.2.1.

Unprocessed proinsulin and incompletely processed intermediates of proinsulin are present in the early phase of type 2 diabetes,[158] and the same is true for IAPP.[82] Immunohistochemical studies indicate the presence of the N-terminal prosequence of proIAPP in islet amyloid *in vivo*, but not the C-terminal region.[47, 48] This suggests that incomplete processing results in secretion of an intermediate peptide with the N-terminal flanking region of proIAPP, $proIAPP_{1-48}$, which corresponds to the first 48 residues of proIAPP (Figure 1.4).

Two models have been proposed for how incorrectly processed IAPP might contribute to islet amyloid formation. One hypothesis is that the proIAPP processing intermediate forms intragranular amyloid that causes cell death and results in the release of amyloid that can seed extracellular amyloid formation by secreted mature IAPP.[52] An alternative model is that release of $proIAPP_{1-48}$ leads to enhanced extracellular amyloid formation by promoting interactions with the glycosaminoglycan (GAG) components of heparan sulfate proteoglycans (HSPGs) of the extracellular matrix.[50, 141] The HSPG perlecan is found in islet amyloid deposits isolated from patients with type 2 diabetes,[139] and HSPGs are associated with nearly all types of amyloid plaques.[159-168] The model GAG, heparan sulfate (HS), accelerates amyloid formation by both IAPP and $proIAPP_{1-48}$ *in vitro*.[50, 140] In addition, the amyloid fibrils formed by $proIAPP_{1-48}$ in the presence of HS have been shown to seed amyloid formation by IAPP *in vitro*, supporting the hypothesis that $proIAPP_{1-48}$ may play a role in initiating amyloid formation.[140]

It is not known whether islet amyloid originates intracellularly or extracellularly and this is a controversial question. Studies with transgenic animals that overexpress IAPP suggest an intracellular origin, but other studies with islets have shown that amyloid deposition is linked with secretion.[53, 169, 170] In either case, interactions with insulin could be important for inhibiting amyloid formation *in vivo*, either in the granule or immediately after release when the local

concentration of IAPP and insulin is high. Insulin is known to be an effective inhibitor of amyloid formation by IAPP *in vitro*, but its effect on amyloid formation by proIAPP$_{1-48}$ has not been investigated and it is possible that less effective inhibition of aggregation by the pro-form could play a role in promoting islet amyloid. In addition, the effects of HSPGs or GAGs on the ability of insulin to inhibit IAPP or ProIAPP$_{1-48}$ amyloid formation have not been examined. Indeed, there are very few studies which have examined the effectiveness of IAPP inhibitors in the presence of sulfated proteoglycans or their GAG components. Here we compare the ability of insulin to inhibit amyloid formation by mature IAPP and the incompletely processed intermediate proIAPP$_{1-48}$. We also compare the effect of insulin on amyloid formation by the two peptides in the presence of the model GAG, HS.

2.2 Material and Methods

2.2.3 Peptide Synthesis and Purification

Peptides were synthesized on a 0.25 mmol scale with an Applied Biosystems 433A Peptide Synthesizer and on a 0.1 mmol scale with a CEM Microwave Peptide Synthesizer utilizing 9-fluornylmethoxycarbonyl (Fmoc) chemistry. Solvents used were ACS-grade. 5-(4'-fmoc-aminomethyl-3',5-dimethoxyphenol) valeric acid (PAL-PEG) resin was used to form an amidated C-terminus. Fmoc-protected pseudoproline (oxazolidine) dipeptide derivatives were used as previously described.[171, 172] Standard Fmoc reaction cycles were used. The first residue attached to the resin, all β-branched residues, the residues directly following a β-branched residue, all pseudoproline dipeptide derivatives and the residues directly following pseudoproline dipeptide derivatives were double-coupled for the synthesis with the Applied Biosystems 433A

Peptide Synthesizer. The microwave assisted synthesis was performed as previously described.[172] The peptides were cleaved from the resin through the use of standard trifluoroacetic acid (TFA) methods. Crude peptides were oxidized by dimethyl sulfoxide at room temperature.[173] The peptides were purified via reverse-phase high-performance liquid chromatography (RP-HPLC) using a Vydac C18 preparative column. Analytical HPLC was used to check the purity of the peptides before each experiment. The masses of the pure peptides were confirmed by ionization time-of-flight mass spectrometry. Wild type IAPP expected 3902.9, observed 3902.7; proIAPP$_{1-48}$ expected 5208.7, observed 5209.4.

2.2.4 Sample Preparation

Peptide stock solutions were dissolved in 100% hexafluoroisoproponal (HFIP) at 1.6 mM. Human insulin (recombinant, catalog No. I2643) was purchased from Sigma. Stock solutions of insulin were first prepared by dissolving insulin into 20 mM Tris-HCl buffer at pH 2 and then adding diluted NaOH to adjust the pH to 7.4. Insulin solutions were freshly made before each experiment. High molecular weight heparan sulfate (10,000-14,000 Da) was purchased from Sigma. Heparan sulfate stock solutions were prepared by dissolving HS in 20 mM Tris-HCl (pH 7.4) at 2.2 mg/ml.

2.2.5 Fluorescence Assays

Amyloid formation was monitored by thioflavin-T binding assays without stirring at 25°C. Fluorescence measurements were performed using a Beckman Coulter DTX 880 plate reader with multimode detector with 430 nm excitation and 485 nm emission. For experiments conducted in the presence of 2% HFIP, solutions were prepared by diluting filtered stock solutions of peptides (0.45 μM Acrodisc syringe filter with GHP membrane) into Tris-HCl buffer

and thioflavin-T solution immediately before the measurement. For experiments conducted without HFIP, filtered stock solutions were first lyophilized for 22 hrs and then the dry peptide was dissolved into Tris-HCl buffer and thioflavin-T solution immediately before the measurement. The inhibition experiments were performed by first diluting peptide stock solutions (assays with HFIP) or dissolving dry peptides (assays without HFIP) into the buffer, followed by the addition of insulin. HS, when present, was added last. The final conditions were 16 μM peptide and 32 μM thioflavin-T in 20 mM Tris-HCl (pH 7.4). HS, when present, was at 1.3 μM.

2.2.6 Circular Dichroism (CD)

Far-UV CD experiments were performed at 25°C on an Applied Photophysics Chirascan CD spectrophotometer. Aliquots from the kinetic experiments were removed at the end of each experiment and the spectra were recorded. Spectra were the average of three repeats recorded over a range of 190-260 nm, at 1 nm intervals. A 0.1 cm quartz cuvette was used and a background spectrum was subtracted from the data.

2.2.7 Transmission Electron Microscopy (TEM)

TEM images were collected at the Life Science Microscopy Center at the State University of New York at Stony Brook. 15 μL aliquots of the samples used for the kinetic studies were removed at the end of each experiment, placed on a carbon-coated 300-mesh copper grid for 1 min and then negatively stained with saturated uranyl acetate for 1 min.

2.3 Results and Discussion

2.3.1 Insulin Inhibits Amyloid Formation by IAPP and ProIAPP$_{1-48}$ in a Concentration Dependent Manner.

The ability of insulin to inhibit amyloid formation by IAPP and proIAPP$_{1-48}$ was tested using fluorescence detected thioflavin-T binding assays. These studies were conducted by diluting solutions of the peptides solubilized in HFIP into buffer. This is a commonly employed approach for biophysical studies of IAPP. Additional experiments were conducted in the absence of HFIP. Thioflavin-T experiences a significant increase in its quantum yield upon binding to amyloid fibrils and provides a convenient probe to monitor the time course of fibril formation. We first examined amyloid formation by different mixtures of IAPP and insulin and observed significant effects of insulin on IAPP amyloid formation at sub-stoichiometric concentrations. This is consistent with prior studies conducted in the presence of low percentages of HFIP.[37] The results, shown in Figure 2.1, confirm that insulin is an effective inhibitor of IAPP amyloid formation. The data are plotted as time normalized by T_{50} of IAPP in the absence of insulin, where T_{50} is the time required for the amyloid reaction to reach 50% of the final fluorescence intensity. The unnormalized data of this figure and some following figures are included in Figure 2.19-2.24. Insulin was still able to inhibit amyloid formation, albeit weakly, when IAPP was in 100 fold excess, as indicated by a 1.7 fold longer T_{50}. The effects of insulin became more significant as the concentration of insulin increased. In a mixture of IAPP and insulin at a 20 to 1 ratio (IAPP in 20 fold excess), T_{50} increased 23 fold under the conditions of these studies. TEM images and CD spectra confirmed the existence of fibrils with typical amyloid morphology and β-sheet structure at the end of each reaction. This excluded the possibility of false positives from the thioflavin-T binding assays (Figure 2.1, 2.10, 2.11). Control experiments conducted with

insulin alone confirm that insulin did not form amyloid in the time course of these experiments, as judged by thioflavin-T assays and TEM (Figure 2.1).

The effect of insulin on amyloid formation by proIAPP$_{1-48}$ was also studied using this approach. An increase in T_{50} was observed for all ratios of proIAPP$_{1-48}$ to insulin tested and the inhibitory effect of insulin was dose dependent. However, insulin was less effective at inhibiting amyloid formation by the processing intermediate proIAPP$_{1-48}$ than by mature IAPP under these conditions (Figure 2.2). For example, when the IAPP or proIAPP$_{1-48}$ to insulin ratio was 20 to 1, the T_{50} of proIAPP$_{1-48}$ amyloid formation was increased 8.3 fold, while the T_{50} of IAPP amyloid formation was increased by a factor of 23. TEM images and CD spectra confirmed the existence of typical fibril structure at the end of each reaction (Figure 2.2, 2.12, 2.13).

2.3.2 Insulin Is a Significantly Less Effective Inhibitor in the Presence of Heparan Sulfate.

We next conducted inhibition experiments in the presence of the model glycosaminoglycan HS. As expected, amyloid formation by IAPP was greatly enhanced in the presence of HS consistent with prior reports.[50, 140] IAPP formed amyloid immediately after the reaction was initiated in the presence of HS, and no lag time was observed (Figure 2.3A). TEM images confirmed the presence of amyloid fibrils and the fibrils formed in the presence of HS had a very similar morphology to those formed in the absence of HS (Figure 2.3). CD confirmed that β-sheet structure was formed (Figure 2.15).

Insulin was a much less effective inhibitor when HS was present, although there were modest effects on the time required to complete amyloid formation, and the effects of insulin were dose dependent. However, even at a 1:5 IAPP to insulin ratio, IAPP formed amyloid without an apparent lag phase in the presence of HS (Figure 2.3A). A rapid initial rise in

fluorescence intensity was observed followed by a more gradual rise to the final value. Although no significant lag phase was observed, even with relatively high concentrations of insulin (1:1 and 1:5 IAPP to insulin ratios), amyloid formation required several hours to reach completion after the initial rapid increase in the thioflavin-T fluorescence intensity. TEM images revealed the presence of fibrils at the end of each experiment (Figure 2.3, 2.14). Similar behavior has been observed in experiments using other inhibitors in the presence of HS, and has been proposed to be due to rapid formation of a GAG-peptide intermediate.[174] CD spectra of mixtures with a low concentration of insulin showed typical β-sheet structure, while those from samples with a higher concentration of insulin (1:1 and 1:5 IAPP to insulin ratio) exhibited a broad peak centered at 219 nm, likely due to contributions from the insulin α-helical structure (Figure 2.15). Interestingly, in the presence of HS, the CD signal of either IAPP or mixtures of IAPP and insulin appears to be more intense than in the absence of HS (Figure 2.11, 2.15). This may be caused by that HS have a solubilizing effect on the aggregates formed so they are less prone to bind to the walls of the microplates or segregate to the air water interface or pellet. The exact reason for the differencies in the intensity of the CD spectra is not clear, but the shape of the spectrum reports on the secondary structure of the soluble aggregates.

Insulin is also much less effective at inhibiting amyloid formation by proIAPP$_{1-48}$ in the presence of HS (Figure 2.4). Insulin barely showed any inhibitory effect at 20:1 and 5:1 proIAPP$_{1-48}$ to insulin ratios in the presence of HS. Increasing the amount of insulin to a ratio of 1:1 and 1:5 slightly increased the time required to complete amyloid formation, but no lag time was observed. TEM images and CD spectra confirmed the results of thioflavin-T fluorescence and showed that amyloid was formed (Figure 2.4, 2.16, 2.17).

Insulin is able to aggregate, thus, to exclude the possibility that the results discussed above were caused by interactions of insulin with HS, we monitored the thioflavin-T fluorescence of a mixture of insulin and HS. No fluorescence increase was observed during the time course of the study (Figure 2.3A), and TEM showed that no fibrils were formed (Figure 2.3E). The CD spectrum revealed helical structure that is similar to that observed from insulin samples which did not contain HS (Figure 2.18).

2.3.3 The Observed Effects Are Not Due to the Presence of Organic Co-solvents.

The results outlined above were collected using assays with 2% HFIP by volume as a co-solvent. Even this low percentage of organic solvent accelerates the kinetics of amyloid formation by IAPP significantly.[129, 175] Initial kinetic studies of the effects of insulin on IAPP amyloid formation made use of HFIP as a co-solvent,[37] and subsequent studies showed that similar relative effects were obtained in the absence of HFIP in many cases.[41] We thus compared the ability of insulin to inhibit amyloid formation by both IAPP and proIAPP$_{1-48}$ in the absence and presence of HS using a different assay which avoided the use of HFIP in order to exclude the possibility that our results were a consequence of the conditions used. Control experiments conducted on insulin in the absence of HFIP or IAPP showed that it did not form amyloid under these conditions during the time course of the experiments (Figure 2.25). The results showed that in the absence of HFIP, at a 1 to 20 ratio (IAPP is in 20 fold excess), insulin increased the T_{50} of IAPP amyloid formation by a factor of 3.3 in homogeneous solution (Figure 2.5A). For comparison, insulin at the same ratio increased T_{50} of IAPP amyloid formation by a factor of 23 in the presence of HFIP. The reason for the proportionally larger effect in HFIP is not clear, but may reflect the acquisition of structure in HFIP that facilitates interactions of IAPP with insulin.

Peptide mapping studies have suggested that the region corresponding to residue 7-19 of IAPP interacts with insulin. This segment of IAPP has been proposed to form a transient helical structure during amyloid formation,[176-180] and even low levels of HFIP can promote helical structure.

When HS was present, amyloid formation by IAPP was greatly accelerated, as indicated by the lack of a lag phase. In addition, insulin was a much less effective inhibitor of IAPP amyloid formation in the presence of HS (Figure 2.5B). At a 20 to 1 IAPP to insulin ratio, the time required to complete amyloid formation by IAPP was only increased by a factor of 1.3 when HS was in the mixture. These results are consistent with the trends observed in the presence of HFIP and indicates that the observations are not an artifact caused by residual HFIP. TEM images were collected at the end of each experiment and confirmed that amyloid were formed (Figure 2.5).

Very similar results were obtained with proIAPP$_{1-48}$. In the absence of HFIP, insulin increased the T_{50} of proIAPP$_{1-48}$ amyloid formation by 2.7 fold when proIAPP$_{1-48}$ and insulin were at a 20 to 1 ratio in homogenous solution (Figure 2.6A). In contrast, at the same proIAPP$_{1-48}$ to insulin ratio, T_{50} was increased by a factor of 8.3 in the presence of HFIP.

We also tested the ability of insulin to inhibit amyloid formation by proIAPP$_{1-48}$ in the presence of HS, but in the absence of HFIP. Insulin is a much less effective inhibitor of proIAPP$_{1-48}$ amyloid formation when HS is present. In the presence of HS, proIAPP$_{1-48}$ immediately aggregated to form amyloid fibrils without any observable lag phase. The time required to complete proIAPP$_{1-48}$ amyloid formation in the presence of insulin is nearly the same as that without insulin (Figure 2.6B). TEM images were collected at the end of each experiment and confirmed that amyloid were formed (Figure 2.6).

2.4 Conclusions

The data show that insulin is a potent amyloid inhibitor for both IAPP and the $proIAPP_{1-48}$ processing intermediate in homogeneous solutions. Figure 2.7 shows a comparison of the ability of insulin to inhibit IAPP and $proIAPP_{1-48}$ amyloid formation as judged by the T_{50} values in the presence of HFIP. Insulin, at relatively high concentrations, is more potent in slowing amyloid formation by IAPP than by $proIAPP_{1-48}$, and the inhibition of IAPP amyloid formation by insulin is more sensitive to changes in the insulin level than is the inhibition of $proIAPP_{1-48}$ amyloid formation. For example, a fivefold change of insulin concentration in the mixture (IAPP to insulin ratio ranging from 100:1 to 20:1) lead to a significant increase in the T_{50} of IAPP amyloid formation, from 1.7 to 23 fold relative to IAPP alone. In contrast, increasing the insulin ratio by the same amount had a smaller effect on $proIAPP_{1-48}$; T_{50} increased from 2.7 to 8.3 fold relative to $proIAPP_{1-48}$ alone. However, insulin is still an effective inhibitor arguing that reduced interactions between $proIAPP_{1-48}$ and insulin relative to IAPP insulin interactions are unlikely to account for islet amyloid formation *in vivo*.

The effects of insulin on amyloid formation by IAPP and $proIAPP_{1-48}$ in the presence of HS are quantitatively compared in terms of T_{50} in Figure 2.8. The ability of insulin to inhibit amyloid formation is greatly reduced in the presence of HS for both peptides. When peptide and insulin are combined at a 20 to 1 ratio, the T_{50} for amyloid formation by IAPP is increased by only a factor of 1.6, and no obvious increase in T_{50} is observed for $proIAPP_{1-48}$. Even at the highest concentrations of insulin (1:1 and 1:5 IAPP or $proIAPP_{1-48}$ to insulin ratio), T_{50} is increased by less than 3 fold for both peptides in the presence of HS. Amyloid formation by IAPP is slightly more effectively inhibited than is amyloid formation by $proIAPP_{1-48}$ in the

presence of HS. However, insulin is clearly a significantly worse inhibitor of amyloid formation by either peptide in the presence of HS.

Our control experiments show that the results are not due to the presence of HFIP. Insulin is a much less effective inhibitor of amyloid formation in the presence of HS even in the absence of HFIP. The results are summarized in Figure 2.9. The T_{50} for amyloid formation of IAPP and $proIAPP_{1-48}$ in the absence of HFIP is increased by 3.3 and 2.7 fold respectively at a 20 to 1 ratio of IAPP or $proIAPP_{1-48}$ to insulin in homogeneous solution. However, in the presence of HS, insulin, at the same ratio, only increased the time required for IAPP amyloid formation by a factor of 1.3, while the kinetics of $proIAPP_{1-48}$ amyloid formation was virtually unaltered. No lag phase was observed for the amyloid formation by either IAPP or $proIAPP_{1-48}$ even at a 20 to 1 IAPP or $proIAPP_{1-48}$ to insulin ratio.

HS is not the only factor that can accelerate IAPP amyloid formation. Anionic vesicles also catalyze amyloid formation by IAPP. Insulin still inhibits the process in the presence of anionic model membranes,[41, 181] however, it is noticeably less effective.[41] Those studies, together with the present work highlight the importance of considering the role of the heterogeneous environment in amyloid formation. The deleterious effects of HS on insulin's ability to act as an amyloid inhibitor could be due to stronger interactions of IAPP or $proIAPP_{1-48}$ with HS, than with insulin. Alternatively, HS might bind to insulin and sequester the inhibitor, or both effects could play a role. The data presented here clearly shows that HS accelerates amyloid formation by $proIAPP_{1-48}$ and IAPP, and this has been established to occur via direct interactions between the peptides and the GAG.[47,57] These observations, plus the fact that HS did not induce insulin amyloid formation under the conditions of our studies, suggest that interactions with HS of IAPP or $proIAPP_{1-48}$ out compete interactions between insulin and IAPP or $proIAPP_{1-48}$.

Our observations suggest another mechanism by which HS can promote amyloid formation. Proteoglycans can accelerate amyloid formation by direct interactions with $proIAPP_{1-48}$ or IAPP and can also significantly reduce the inhibitory effects of insulin.

2.5 Figures

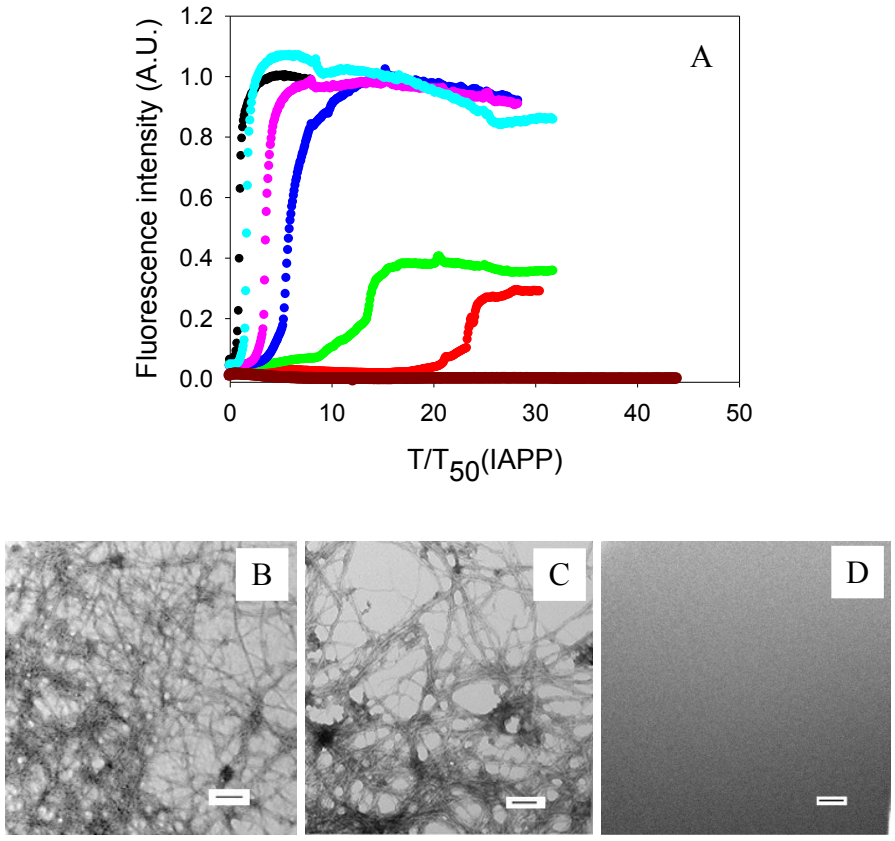

Figure 2.1 Inhibition of IAPP amyloid formation by insulin.
(A) The results of thioflavin-T binding assays are displayed. The data is plotted as time normalized by T_{50} of IAPP in the absence of insulin. Black, IAPP; red, IAPP and insulin at a 20 to 1 ratio; green, IAPP and insulin at a 40 to 1 ratio; blue, IAPP and insulin at a 60 to 1 ratio; pink, IAPP and insulin at an 80 to 1 ratio; cyan, IAPP and insulin at a 100 to 1 ratio; brown, insulin alone at 0.8 μM. (B) TEM image of IAPP. (C) TEM image of a 20:1 mixture of IAPP and insulin. IAPP is in 20 fold excess. (D) TEM image of insulin alone at 0.8 μM. Aliquots were removed at the end of each reaction for TEM analysis. Scale bars represent 100 nm. The kinetic experiments were conducted in 20 mM Tris-HCl (pH 7.4) and 2% HFIP (v/v) without stirring at 25 °C. The concentration of IAPP was 16 μM.

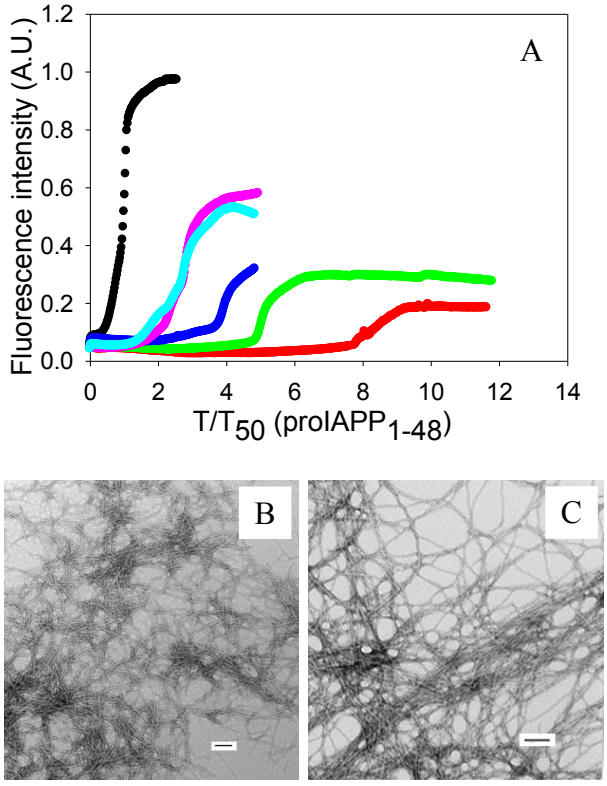

Figure 2.2 Inhibition of proIAPP$_{1-48}$ amyloid formation by insulin.
(A) The results of thioflavin-T binding assays are displayed. The data is plotted as time normalized by T_{50} of proIAPP$_{1-48}$ in the absence of insulin. Black, proIAPP$_{1-48}$; red, proIAPP$_{1-48}$ and insulin at a 20 to 1 ratio; green, proIAPP$_{1-48}$ and insulin at a 40 to 1 ratio; blue, proIAPP$_{1-48}$ and insulin at a 60 to 1 ratio; pink, proIAPP$_{1-48}$ and insulin at an 80 to 1 ratio; cyan, proIAPP$_{1-48}$ and insulin at a 100 to 1 ratio. (B) TEM image of proIAPP$_{1-48}$. (C) TEM image of a 20:1 mixture of proIAPP$_{1-48}$ and insulin. proIAPP$_{1-48}$ is in 20 fold excess. Aliquots were removed at the end of each reaction for TEM analysis. Scale bars represent 100 nm. The kinetic experiments were conducted in 20 mM Tris-HCl (pH 7.4) and 2% HFIP (v/v) without stirring at 25 °C. The concentration of proIAPP$_{1-48}$ was 16 μM.

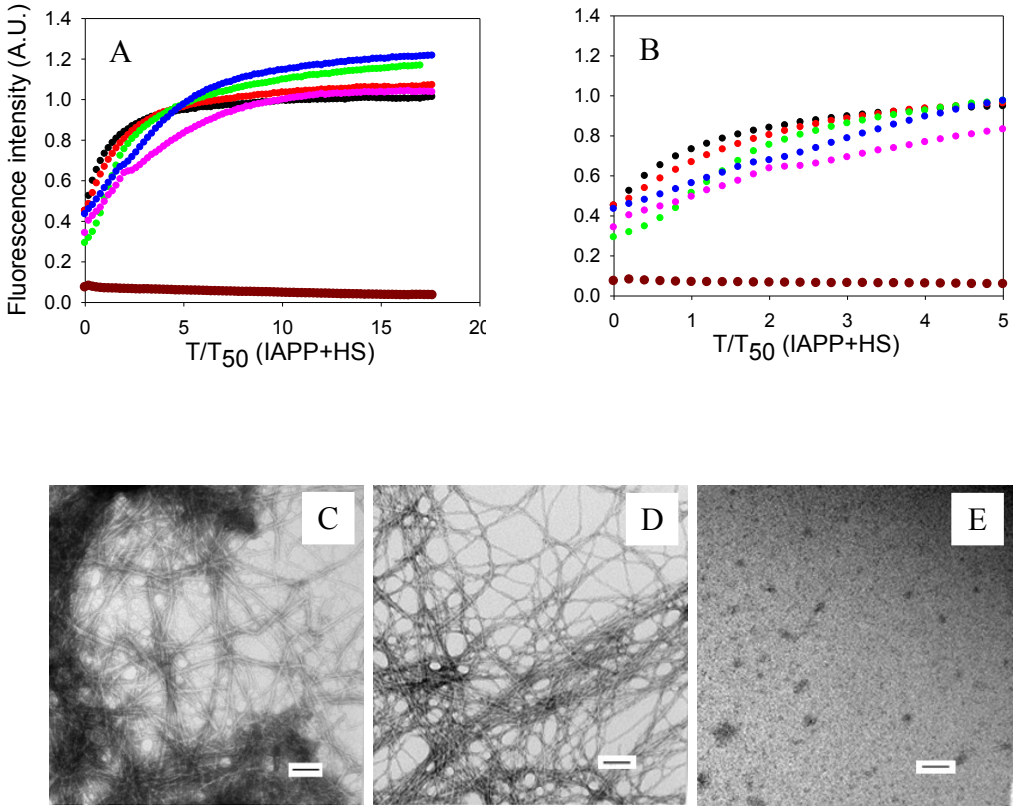

Figure 2.3 The effects of insulin on amyloid formation by IAPP in the presence of HS. (A) The results of thioflavin-T binding assays are displayed. The data is plotted as time normalized by T_{50} of IAPP in the presence of HS, but in the absence of insulin. Black, IAPP in the presence of HS; red, IAPP and insulin at a 20 to 1 ratio in the presence of HS; green, IAPP and insulin at a 5 to 1 ratio in the presence of HS; blue, IAPP and insulin at a 1 to 1 ratio in the presence of HS; pink, IAPP and insulin at a 1 to 5 ratio in the presence of HS; brown, a mixture of insulin at 80 μM and HS at 1.3 μM. (B) An expansion of the first 5 time units of panel A. The same color coding is used. (C) TEM image of IAPP in the presence of HS. (D) TEM image of a 1:5 mixture of IAPP and insulin in the presence of HS. Insulin is in 5 fold excess. (E) TEM image of the insulin HS mixture. Aliquots were removed at the end of each reaction for TEM analysis. Scale bars represent 100 nm. The kinetic experiments were conducted in 20 mM Tris-HCl (pH 7.4) and 2% HFIP (v/v) without stirring at 25 °C. The concentration of IAPP was 16 μM. HS was at 1.3 μM.

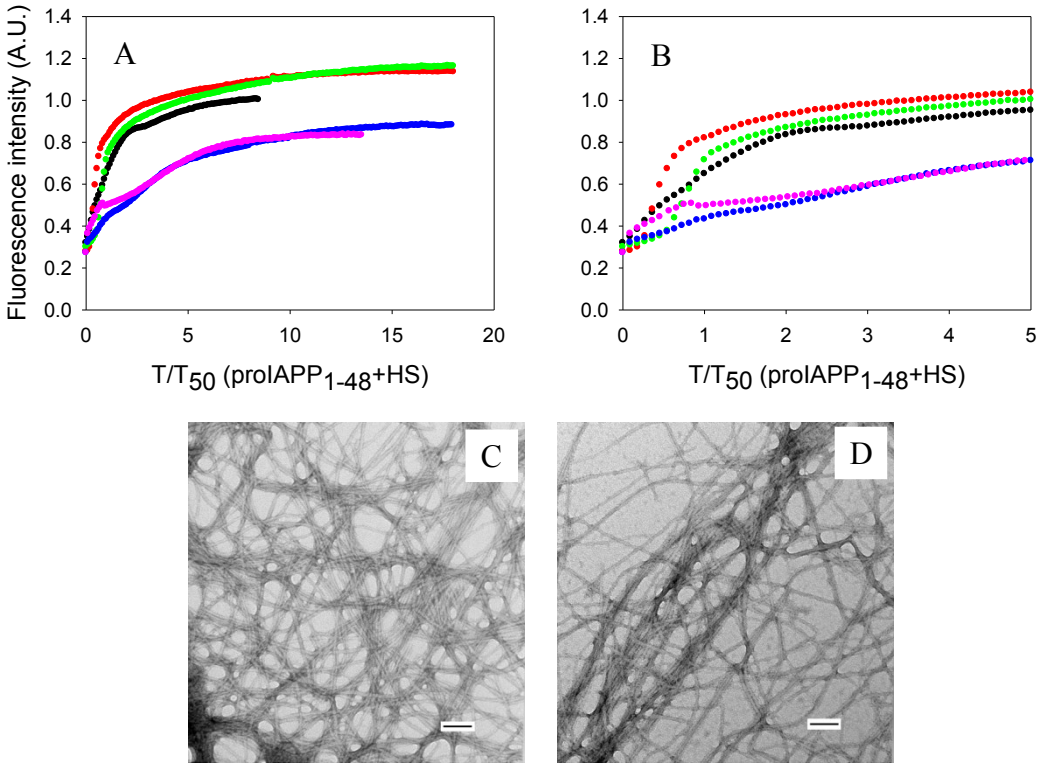

Figure 2.4 The effects of insulin on amyloid formation by proIAPP$_{1\text{-}48}$ in the presence of HS.

(A) The results of thioflavin-T binding assays are displayed. The data is plotted as time normalized by T_{50} of proIAPP$_{1\text{-}48}$ in the presence of HS, but in the absence of insulin. Black, proIAPP$_{1\text{-}48}$ in the presence of HS; red, proIAPP$_{1\text{-}48}$ and insulin at a 20 to 1 ratio in the presence of HS; green, proIAPP$_{1\text{-}48}$ and insulin at a 5 to 1 ratio in the presence of HS; blue, proIAPP$_{1\text{-}48}$ and insulin at a 1 to 1 ratio in the presence of HS; pink, proIAPP$_{1\text{-}48}$ and insulin at a 1 to 5 ratio in the presence of HS. (B) An expansion of the first 5 time units of panel A. The same color coding is used. (C) TEM image of proIAPP$_{1\text{-}48}$ in the presence of HS. (D) TEM image of a 1:5 mixture of proIAPP$_{1\text{-}48}$ and insulin in the presence of HS. Insulin is in 5 fold excess. Aliquots were removed at the end of each reaction for TEM analysis. Scale bars represent 100 nm. The kinetic experiments were conducted in 20 mM Tris-HCl (pH 7.4) and 2% HFIP (v/v) without stirring at 25 °C. The concentration of proIAPP$_{1\text{-}48}$ was 16 μM. HS was at 1.3 μM.

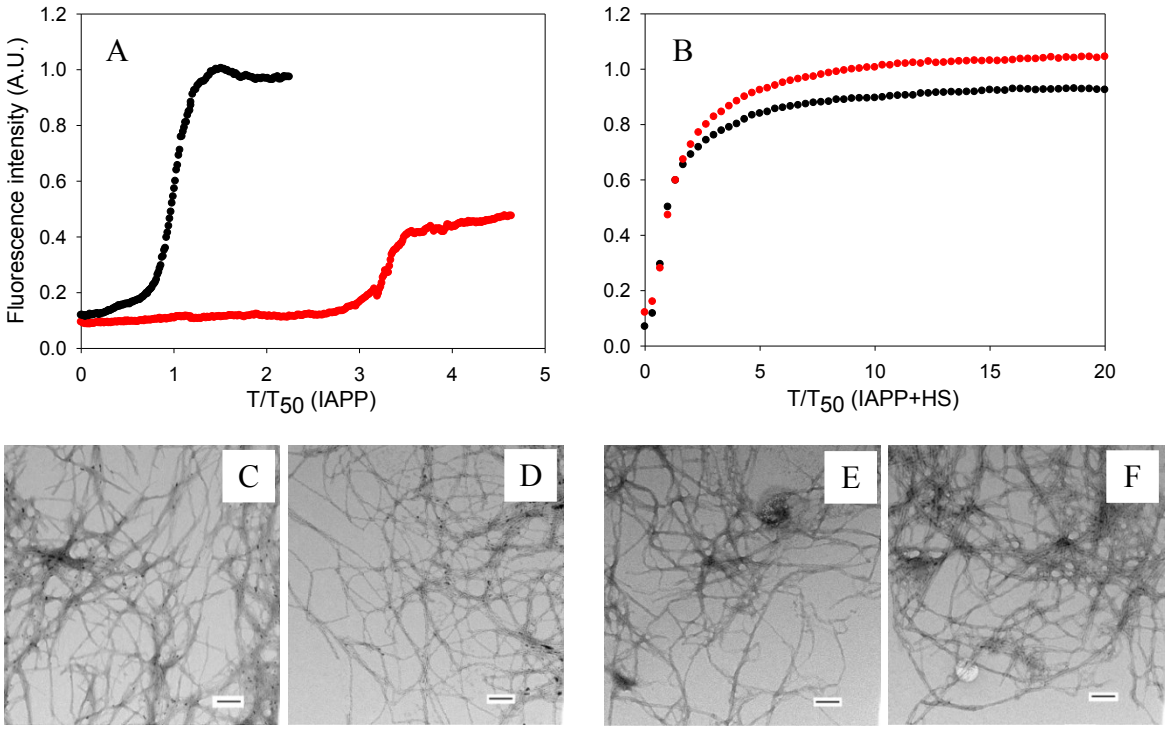

Figure 2.5 Inhibition of IAPP amyloid formation by insulin in the presence and absence of HS in buffer without HFIP.

(A) Inhibition in the absence of HS monitored by thioflavin-T assays. Black, IAPP; red, IAPP and insulin at a 20 to 1 ratio. Data is plotted as time normalized by T_{50} value of IAPP in the absence of insulin. (B) Inhibition in the presence of HS monitored by thioflavin-T assays. Data is plotted as time normalized by T_{50} value of IAPP in the presence of HS, but in the absence of insulin. The same color coding is used here as in panel A. (C) TEM image of IAPP in the absence of HS. (D) TEM image of a 20:1 mixture of IAPP and insulin in the absence of HS, IAPP was in 20 fold excess. (E) TEM image of IAPP in the presence of HS. (F) TEM image of a 20:1 mixture of IAPP and insulin in the presence of HS, IAPP was in 20 fold excess. Scale bars represent 100 nm. Aliquots were removed at the end of each experiment for TEM analysis. The kinetic experiments were conducted in 20 mM Tris-HCl (pH 7.4) without stirring at 25 °C. The concentration of IAPP was 16 μM. HS was at 1.3 μM when present.

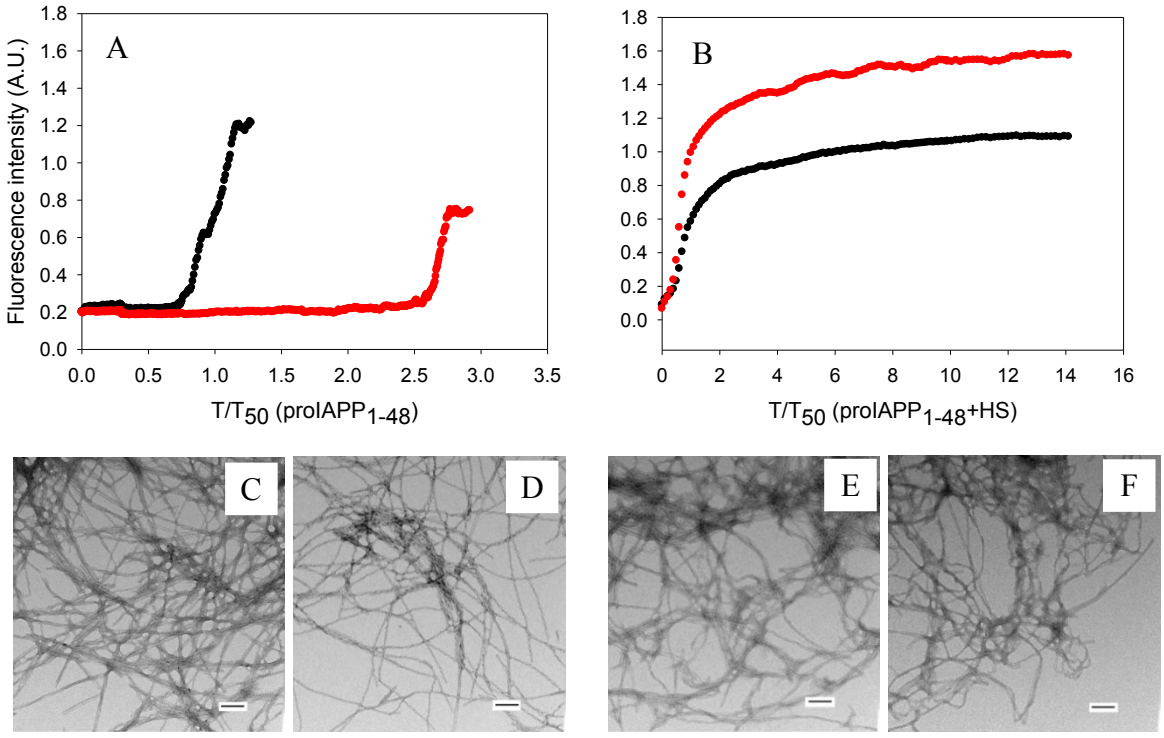

Figure 2.6 Inhibition of proIAPP$_{1-48}$ amyloid formation by insulin in the presence and absence of HS in buffer without HFIP.
(A) Inhibition in the absence of HS monitored by thioflavin-T assays. Data is plotted as time normalized by T_{50} value of proIAPP$_{1-48}$ in the absence of insulin. Black, proIAPP$_{1-48}$; red, proIAPP$_{1-48}$ and insulin at a 20 to 1 ratio. (B) Inhibition in the presence of HS monitored by thioflavin-T assays. Data is plotted as time normalized by T_{50} value of proIAPP$_{1-48}$ in the presence of HS, but in the absence of insulin. The same color coding is used here as in panel A. (C) TEM image of proIAPP$_{1-48}$ in the absence of HS. (D) TEM image of a 20:1 mixture of proIAPP$_{1-48}$ and insulin in the absence of HS. (E) TEM image of proIAPP$_{1-48}$ in the presence of HS. (F) TEM image of a 20:1 mixture of proIAPP$_{1-48}$ and insulin in the presence of HS. Scale bars represent 100 nm. Aliquots were removed at the end of each experiment for TEM analysis. The kinetic experiments were conducted in 20 mM Tris-HCl (pH 7.4) without stirring at 25 °C. The concentration of proIAPP$_{1-48}$ was 16 μM. HS was at 1.3 μM when present.

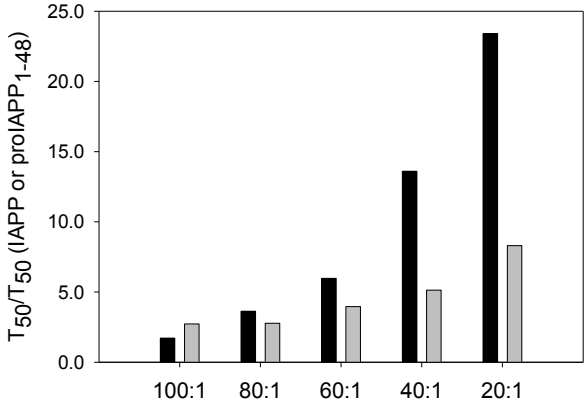

Figure 2.7 Bar graph comparing the T_{50} values for amyloid formation by IAPP and proIAPP$_{1-48}$ in the presence of 2% HFIP at different ratios of IAPP or proIAPP$_{1-48}$ to insulin.

Black bars, mixtures of IAPP and insulin; grey bars, mixtures of proIAPP$_{1-48}$ and insulin. Values of T_{50} were derived from the kinetic curves shown in Figure 2.1 and Figure 2.2. Data is plotted as T_{50} normalized by the value of T_{50} of either IAPP or proIAPP$_{1-48}$ in the absence of insulin. Experiments were conducted in 20 mM Tris-HCl (pH 7.4) and 2% HFIP (v/v) without stirring at 25 °C. The concentration of IAPP or proIAPP$_{1-48}$ was 16 μM.

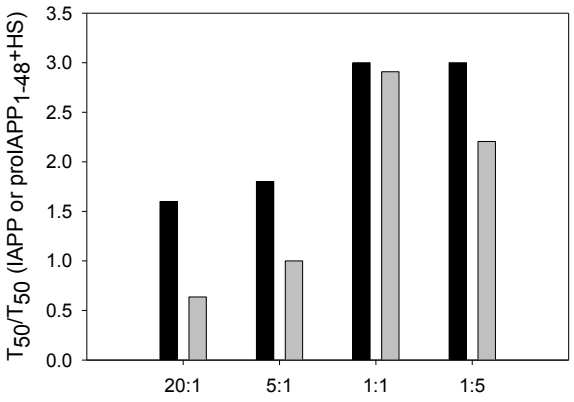

Figure 2.8 Bar graph comparing the T_{50} values for amyloid formation in buffer with HFIP for mixtures of IAPP with insulin and for mixtures of $proIAPP_{1-48}$ with insulin in the presence of HS.

Values are plotted for different IAPP, $proIAPP_{1-48}$ to insulin ratios. Black bars, mixtures of IAPP and insulin in the presence of HS; grey bars, mixtures of $proIAPP_{1-48}$ and insulin in the presence of HS. The data is plotted as T_{50} normalized by the T_{50} value of either IAPP or $proIAPP_{1-48}$ in the presence of HS, but in the absence of insulin. Values of T_{50} were derived from the kinetic curves in Figure 2.3 and Figure 2.4. Experiments were conducted in 20 mM Tris-HCl (pH 7.4) and 2% HFIP (v/v) without stirring at 25 °C. The concentration of IAPP or $proIAPP_{1-48}$ was 16 μM. HS was at 1.3 μM.

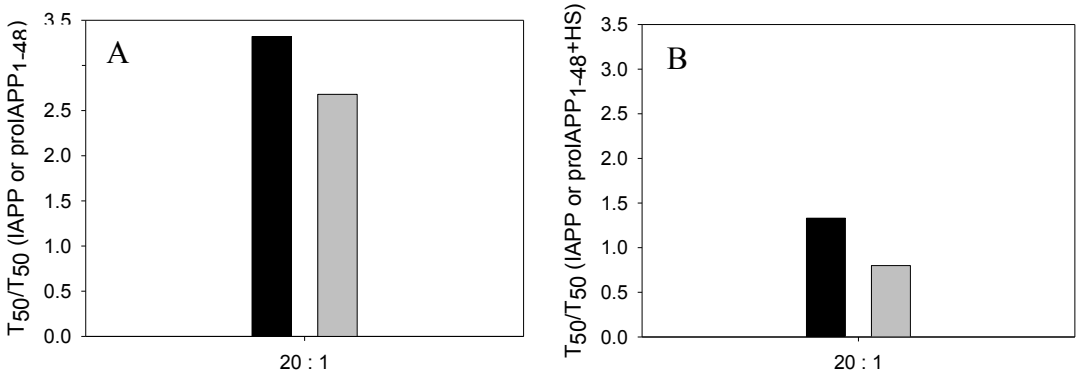

Figure 2.9 Bar graph comparing the T_{50} values for amyloid formation by mixtures of IAPP with insulin and mixtures of proIAPP$_{1-48}$ with insulin in the absence of HFIP.
(A) HS is absent in the assay. The data is plotted as T_{50} normalized by the T_{50} value of IAPP or proIAPP$_{1-48}$ in the absence of insulin. (B) HS is present in the assay. The data is plotted as T_{50} normalized by the T_{50} value of IAPP or proIAPP$_{1-48}$ in the presence of HS without insulin. IAPP or proIAPP$_{1-48}$ to insulin ratio was 20 to 1. Black bars, mixtures of IAPP and insulin; grey bars, mixtures of proIAPP$_{1-48}$ and insulin. Values of T_{50} were derived from the kinetic curves in figure 2.5 and figure 2.6. The kinetic experiments were conducted in 20 mM Tris-HCl (pH 7.4) without stirring at 25 °C. The concentration of IAPP or proIAPP$_{1-48}$ was 16 μM. HS was at 1.3 μM when present.

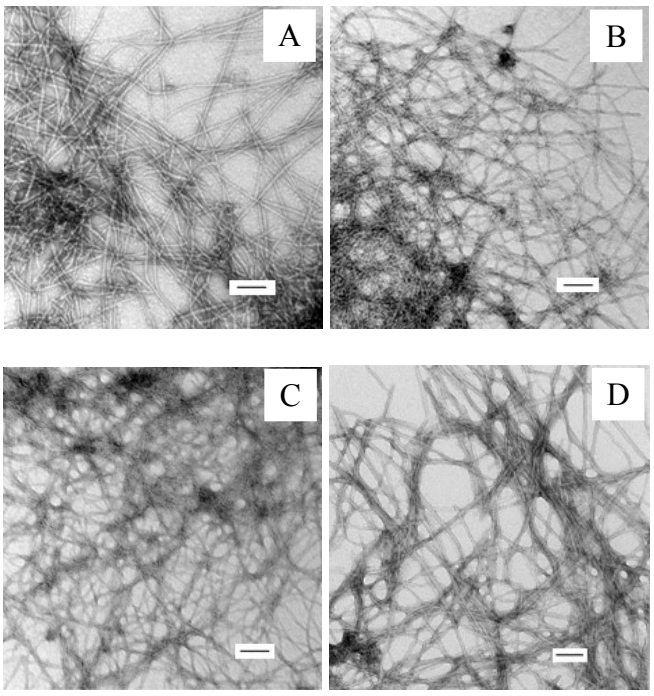

Figure 2.10 TEM images of mixtures of IAPP and insulin at different ratios of IAPP to insulin in the absence of HS.
The images correspond to time points at the end of the reactions displayed in Figure 2.1. (A) TEM image of a 100:1 mixture of IAPP and insulin, IAPP was in 100 fold excess. (B) TEM image of a 80:1 mixture of IAPP and insulin, IAPP was in 80 fold excess. (C) TEM image of a 60:1 mixture of IAPP and insulin, IAPP was in 60 fold excess. (D) TEM image of a 40:1 mixture of IAPP and insulin, IAPP was in 40 fold excess. Scale bars represent 100 nm. Aliquots were removed at the end of each experiment for TEM analysis.

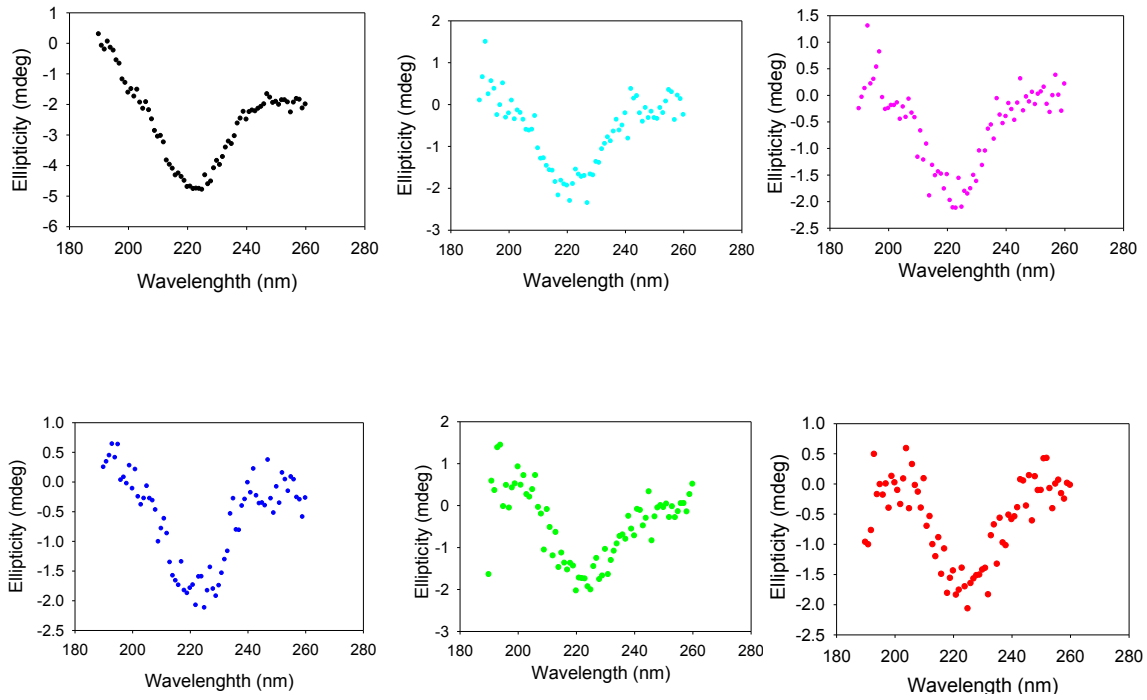

Figure 2.11 CD spectra of mixtures of IAPP and insulin at different ratios of IAPP to insulin in the absence of HS.
The spectra correspond to time points at the end of the reactions displayed in Figure 2.1. The color coding used here is the same as in Figure 2.1. Aliquots were removed at the end of each kinetic experiment.

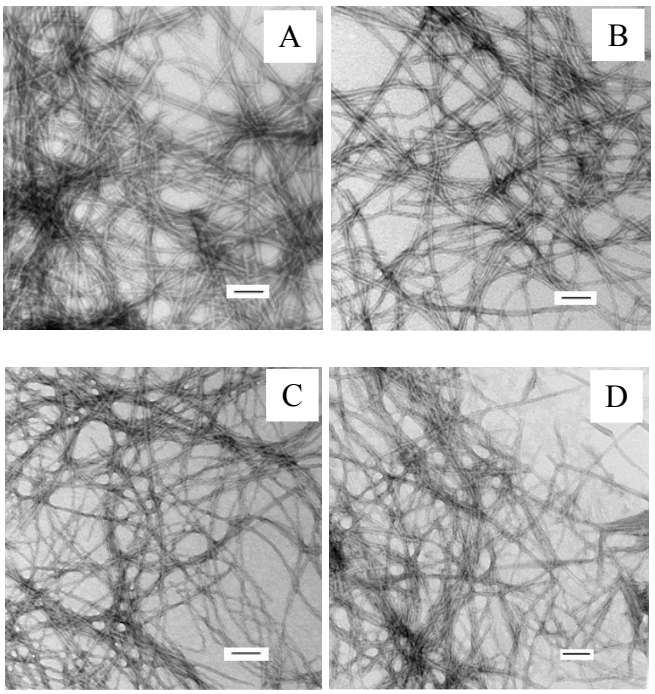

Figure 2.12 TEM images of mixtures of proIAPP1-48 and insulin mixtures at different ratios of proIAPP1-48 to insulin in the absence of HS.
The images correspond to time points at the end of the reactions displayed in Figure 2.2. (A) TEM image of a 100:1 mixture of $proIAPP_{1-48}$ and insulin, $proIAPP_{1-48}$ was in 100 fold excess. (B) TEM image of an 80:1 mixture of $proIAPP_{1-48}$ and insulin, $proIAPP_{1-48}$ was in 80 fold excess. (C) TEM image of a 60:1 mixture of $proIAPP_{1-48}$ and insulin, $proIAPP_{1-48}$ was in 60 fold excess. (D) TEM image of a 40:1 mixture of $proIAPP_{1-48}$ and insulin, $proIAPP_{1-48}$ was in 40 fold excess. Scale bars represent 100 nm. Aliquots were removed at the end of each experiment for TEM analysis.

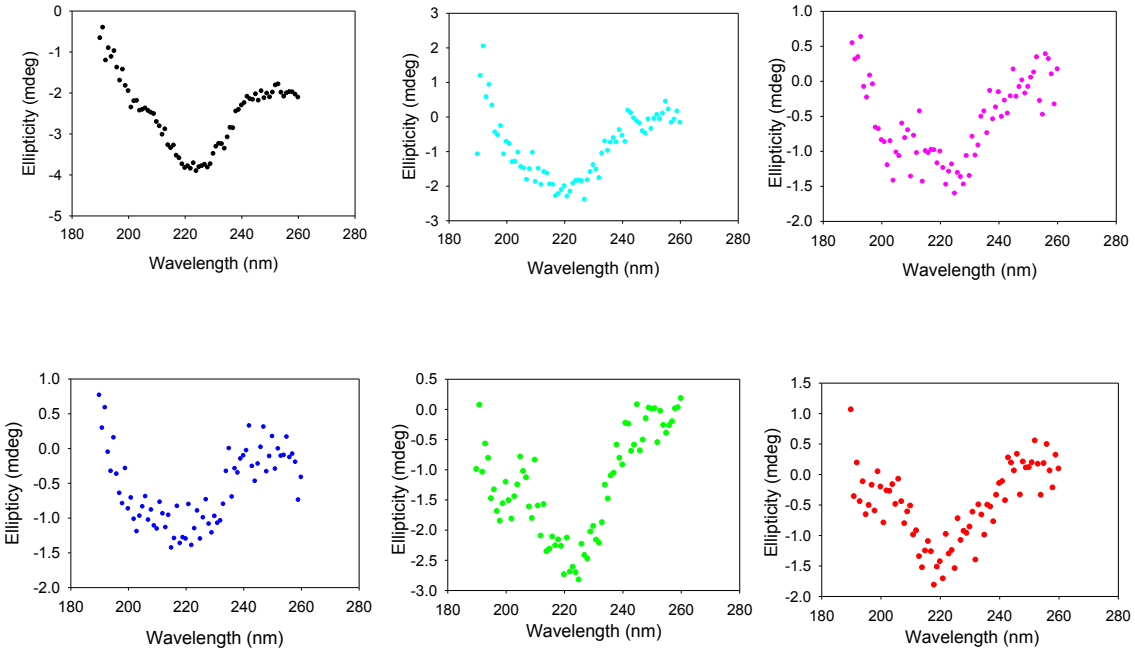

Figure 2.13 CD spectra of mixtures of proIAPP1-48 and insulin at different ratios of proIAPP1-48 to insulin in the absence of HS.
The spectra correspond to the time points at the end of the reactions displayed in Figure 2.2. The color coding used here is the same as in Figure 2.2. Aliquots were removed at the end of each kinetic experiment.

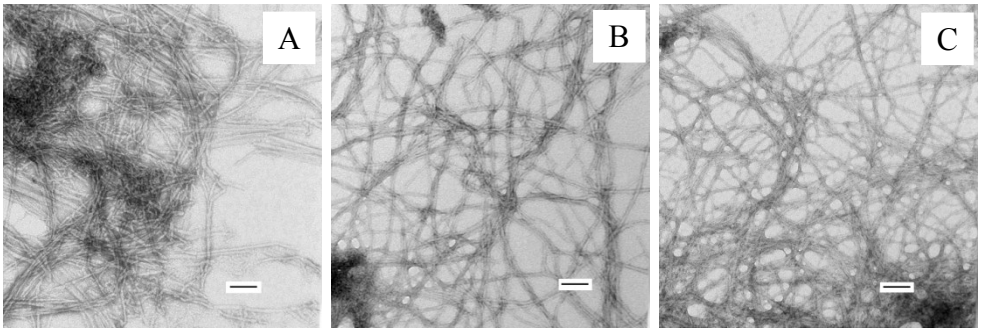

Figure 2.14 TEM images of mixtures of IAPP and insulin at different ratios of IAPP to insulin in the presence of HS.
The images correspond to the time points at the end of the reactions displayed in Figure 2.3. (A) TEM image of a 20:1 mixture of IAPP and insulin, IAPP was in 20 fold excess. (B) TEM image of a 5:1 mixture of IAPP and insulin, IAPP was in 5 fold excess. (C) TEM image of a 1:1 mixture of IAPP and insulin. Scale bars represent 100 nm. Aliquots were removed at the end of each experiment for TEM analysis.

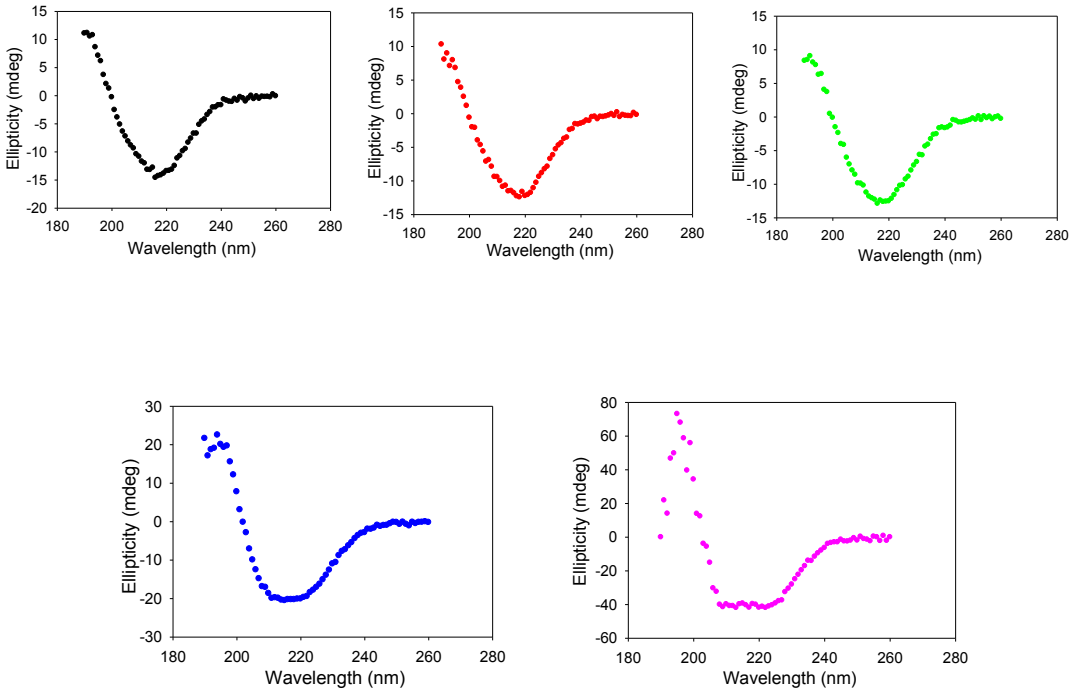

Figure 2.15 CD spectra of the mixture of IAPP and insulin at different ratios of IAPP to insulin in the presence of HS.
The spectra correspond to the time points at the end of the reactions displayed in Figure 2.3. The color coding used here is the same as in Figure 2.3. Aliquots were removed at the end of each kinetic experiment.

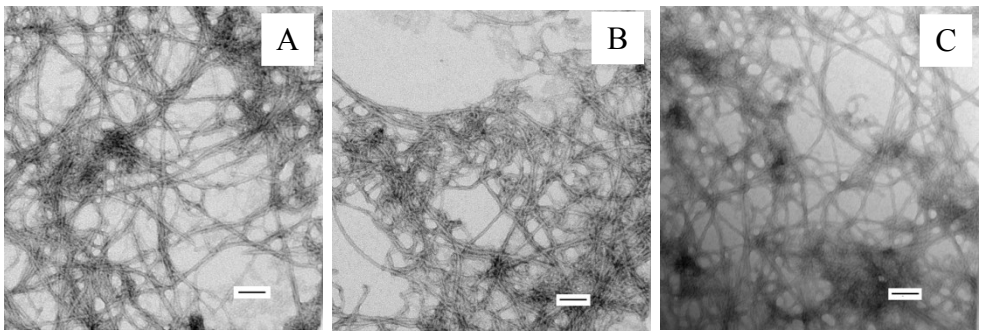

Figure 2.16 TEM images of mixtures of proIAPP1-48 and insulin at different ratios of proIAPP1-48 to insulin in the presence of HS.
The images correspond to the time points at the end of the reactions displayed in Figure 2.4. (A) TEM image of a 20:1 mixture of $proIAPP_{1-48}$ and insulin, $proIAPP_{1-48}$ was in 20 fold excess. (B) TEM image of a 5:1 mixture of $proIAPP_{1-48}$ and insulin, $proIAPP_{1-48}$ was in 5 fold excess. (C) TEM image of a 1:1 mixture of $proIAPP_{1-48}$ and insulin. Scale bars represent 100 nm. Aliquots were removed at the end of each experiment for TEM analysis.

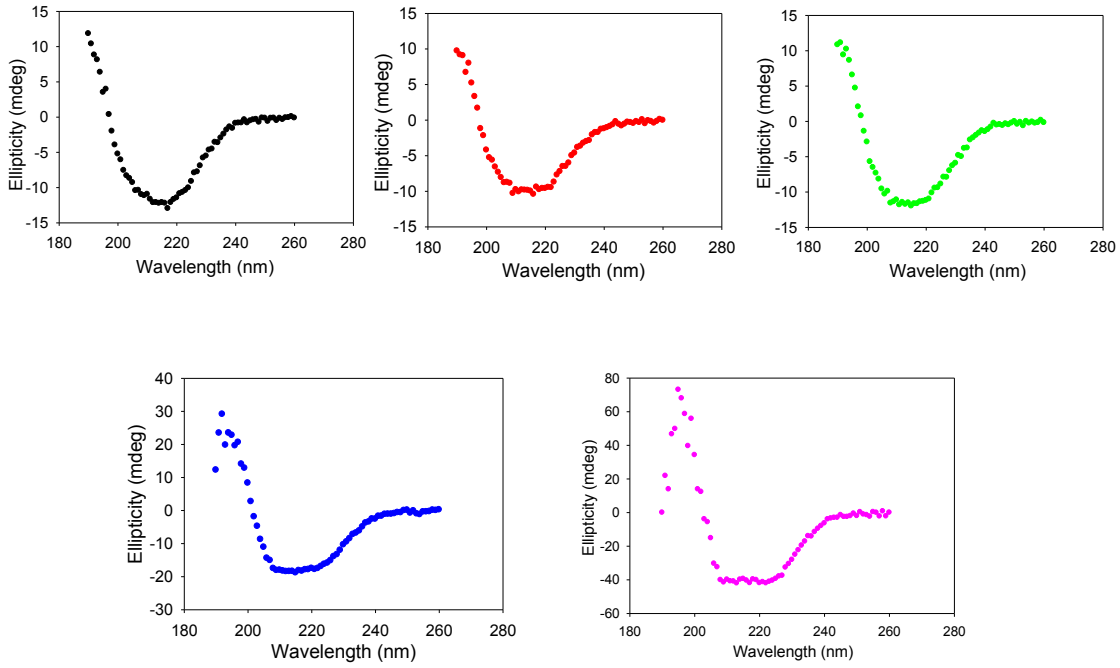

Figure 2.17 CD spectra of the mixture of proIAPP1-48 and insulin at different ratios of proIAPP1-48 to insulin in the presence of HS.
The spectra correspond to the time points at the end of the reactions displayed in Figure 2.4. The color coding used here is the same as in Figure 2.4. Aliquots were removed at the end of each kinetic experiment.

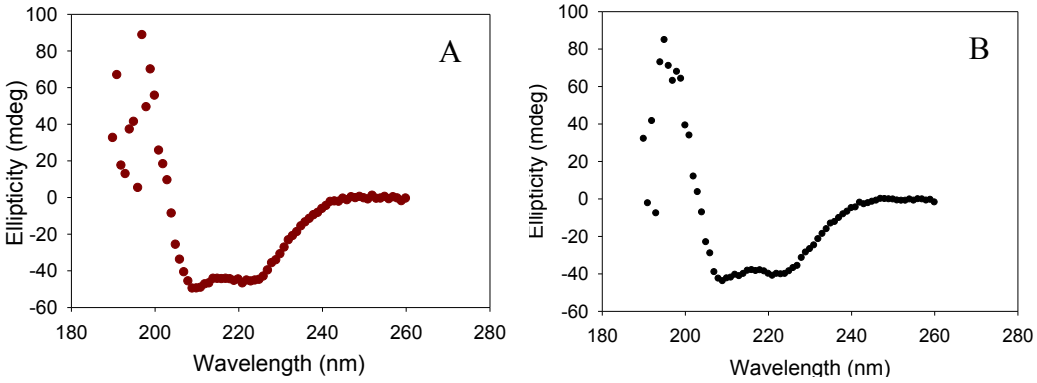

Figure 2.18 CD spectra of insulin in the absence of HS and of a mixture of insulin and HS. **(A)** The spectrum corresponds to the time point at the end of the reaction displayed as the brown curve in Figure 2.3. An aliquot was removed at the end of the kinetic experiment shown in Figure 2.3. The kinetic experiment was conducted in 20 mM Tris-HCl (pH 7.4) and 2% HFIP (v/v) without stirring at 25 °C. (B) The spectrum of insulin without HS and without any incubation. Insulin was at 80 µM and HS was at 1.3 µM, when present.

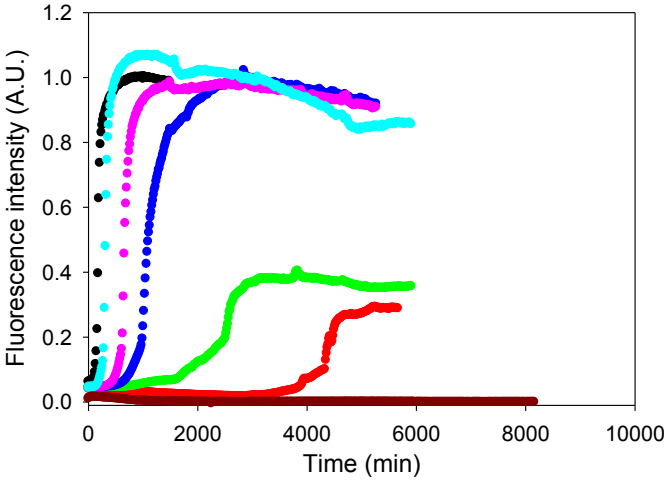

Figure 2.19 Plot of the unnormalized data displayed in Figure 2.1A.

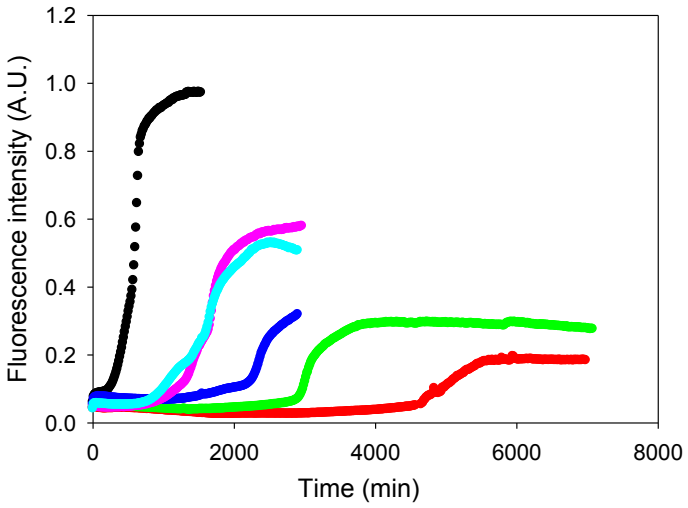

Figure 2.20 Plot of the unnormalized data displayed in Figure 2.2A.

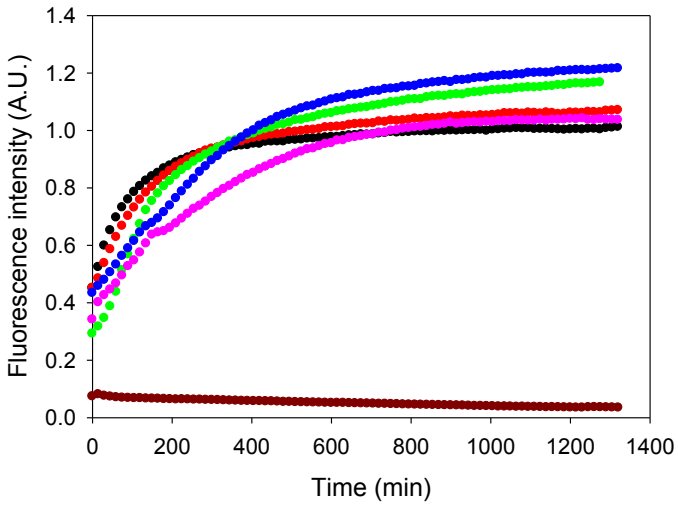

Figure 2.21 Plot of the unnormalized data displayed in figure 2.3A.

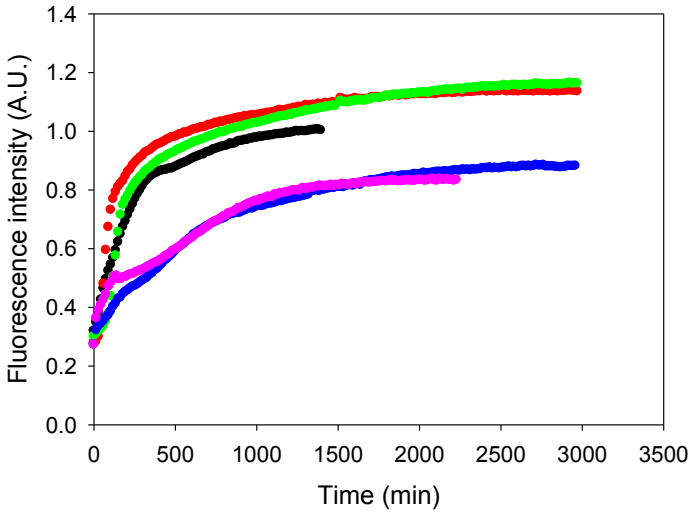

Figure 2.22 Plot of the unnormalized data displayed in Figure 2.4A.

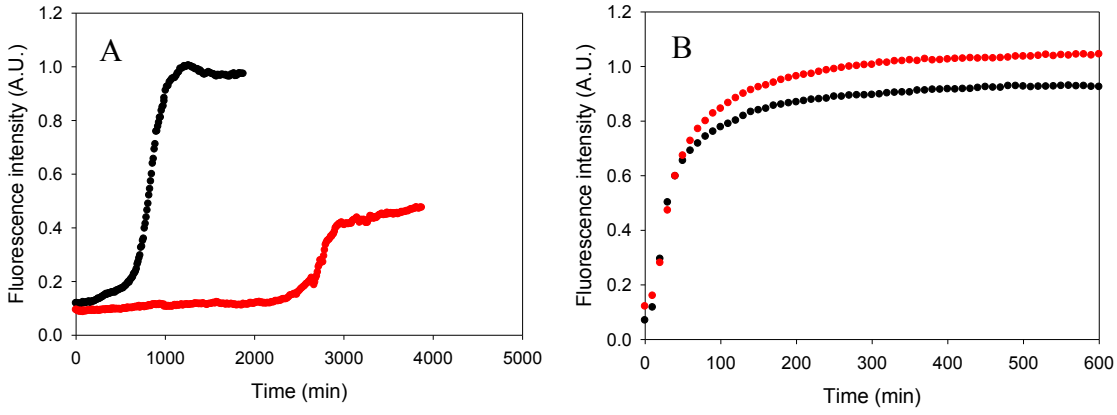

Figure 2.23 Plot of the unnormalized data displayed in (A) Figure 2.5A and (B) Figure 2.5B.

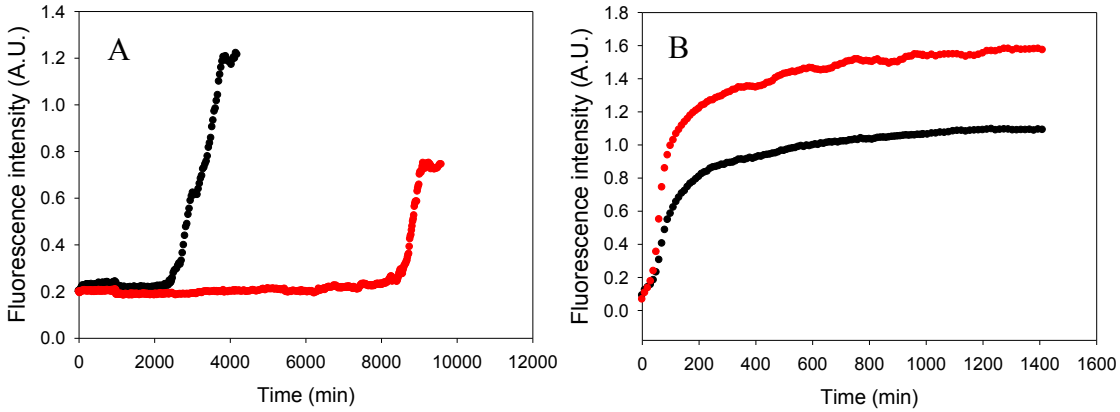

Figure 2.24 Plot of the unnormalized data displayed in (A) Figure 2.6A and (B) Figure 2.6B.

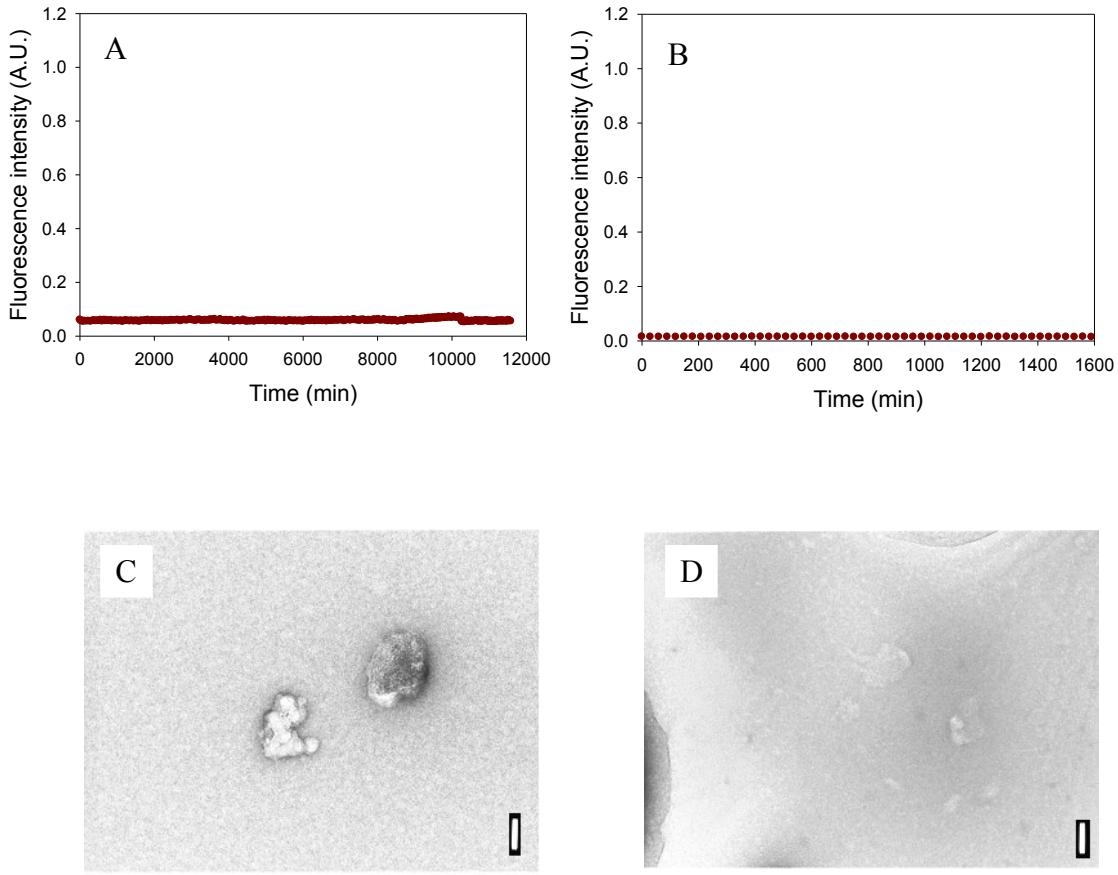

Figure 2.25 Insulin does not form amyloid during the time course of the experiments conducted in the absence of HFIP.
(A) Thioflavin-T curve recorded for a sample of insulin in the absence of IAPP, HS and HFIP. (B) Thioflavin-T curve recorded for a sample of insulin in the presence of HS, but without IAPP or HFIP. Kinetic experiments were conducted in 20 mM Tis-HCl (pH 7.4) without stirring at 25 °C. The concentration of insulin was 0.8 μM. HS, when present, was at 1.3 μM. No HFIP was present. (C) TEM image of a sample removed at the end of the curve shown in panel A. (D) TEM image of a sample removed at the end of the curve shown in panel B. Scale bars represent 50 nm.

Chapter 3 Amyloid Formation in Heterogeneous Environments: Islet Amyloid Polypeptide Glycosaminoglycan Interactions.

Abstract

Amyloid formation plays an important role in a broad range of diseases and the search for amyloid inhibitors is an active area of research. Amyloid formation takes places in a heterogeneous environment *in vivo* with the potential for interactions with membranes and with components of the extracellular matrix. Naturally occurring amyloid deposits are associated with sulfated proteoglycans and other factors. However, the vast majority of *in vitro* assays of amyloid formation and amyloid inhibition are conducted in homogeneous solution where the potential for interactions with membranes or sulfated proteoglycans is lacking and it is possible that different results may be obtained in heterogeneous environments. We show that variants of islet amyloid polypeptide, which are non-amyloidgenic in homogeneous solution, can be readily induced to form amyloid in the presence of glycosaminoglycans. Glycosaminoglycans are found to be more effective than anionic lipid vesicles at inducing amyloid formation on a per charge basis. Several known inhibitors of IAPP amyloid formation are shown to be less effective in the presence of glycosaminoglycans.

The work in this chapter has been published (Wang, H., Cao, P., and Raleigh, D. P. (2013) Amyloid formation in heterogeneous environments: islet amyloid polypeptide glycosaminoglycan interactions, *J. Mol. Biol. 425*, 492-505).
 This chapter contains direct

excerpts from that manuscript, which was written by me with the assistance of Prof. Daniel Raleigh and Dr. Ping Cao.

3.1 Introduction

Amyloid fiber formation, the aggregation of normally soluble proteins into partially ordered β-rich structures, plays a role in a broad range of diseases including type 2 diabetes and Alzhermer's disease.[153, 154] Amyloid, or the process of its formation contributes to the pathology of many diseases[99, 182, 183] and the search for inhibitors of amyloid formation is an active area of research.[121, 122, 124, 150, 184-186]

Amyloid formation takes places in a heterogeneous environment *in vivo* with the potential for interactions with membranes and with components of the extracellular matrix. All naturally occurring amyloid deposits are associated with sulfated proteoglycans and other factors.[139, 159, 160, 163, 165, 187] However, the vast majority of *in vitro* assays of amyloid formation and amyloid inhibition are conducted in homogeneous solution where the potential for interactions with membranes or sulfated proteoglycans is lacking and it is possible that different results may be obtained in heterogeneous environments. In addition, studies of proteins in buffer have been widely used to develop propensity scales for amyloid formation,[188-190] but it is not certain that these scales will have the same quantitive predictive power in heterogeneous environments.

Islet amyloid polypeptide (IAPP, also known as amylin) forms pancreatic islet amyloid deposits in type-2 diabetes. IAPP amyloid formation is toxic to cultured cells, suggesting that it contributes to the disease by leading to β-cell dysfunction and death.[76, 80, 155, 191, 192] Recent work also implicates amyloid formation as a cause of graft failure in islet cell transplantation.[98, 157] A wide range of studies have shown that model membranes which contain anionic lipids accelerate

amyloid formation by IAPP,[136, 193, 194] but less is known about the effects of glycosaminoglycans (GAGs) on IAPP amyloid formation. Immunohistochemical studies have shown that heparan sulfate proteoglycans are associated with islet amyloid isolated from patients with type 2 diabetes,[139] and GAGs can enhance amyloid formation by human proIAPP processing intermediates and by human IAPP.[50, 140] IAPP is one of the most amyloidgenic naturally occurring polypeptides, but it is not known if GAGs can induce amyloid formation in apparently non-amyloidgenic variants of IAPP, nor, with a few exceptions, have the effects of GAGs on IAPP inhibitors been generally considered. Here we examine the effects of GAGs on two apparently non-amyloidgenic variants of IAPP and study the impact of GAGs on IAPP inhibitors. The I26P point mutant of human IAPP (I26P-IAPP), renders the protein non-amyloidgenic and converts it into an inhibitor of amyloid formation by wild type IAPP.[121] The doubly N-methylated variant of human IAPP, G24-N-Methyl, I26-N-Methyl-IAPP (NMe-G24, NMe-I26-IAPP), is a potent inhibitor of IAPP amyloid formation in homogeneous solution and is itself not amyloidogenic.[124] The mode of action of these inhibitors is not known, but the substitutions are located in a region of the chain which has been highlighted as important for amyloid formation.[67, 195] We show that these two variants of IAPP can be readily induced to form amyloid by GAGs and that GAGs are more effective than model lipid micelle systems in inducing them to form amyloid. We also demonstrate that some potent inhibitors of IAPP amyloid formation are less effective in the presence of GAGs. Polypeptide-GAG interactions have been postulated to play an important role in islet amyloid formation *in vivo*,[139-141, 159, 160, 164, 165, 196-198] and our results highlight the importance of considering these effects *in vitro* and in inhibitor design.

3.2 Materials and Methods

3.2.1 Peptide Synthesis and Purification

Peptides were synthesized on a 0.25 mmol scale using a CEM Liberty Microwave Peptide Synthesizer utilizing 9-fluornylmethoxycarbonyl (Fmoc) chemistry. 5-(4'-fmoc-aminomethyl-3',5-dimethoxyphenol) valeric acid (PAL-PEG) resin was used to form an amidated C-terminus. Fmoc protected pseudoproline (oxazolidine) dipeptide derivatives were incorporated to facilitate the synthesis as previously described.[171, 172] Standard Fmoc reaction cycles were used. The first residue attached to the resin, all β-branched residues and all pseudoproline dipeptide derivatives were double-coupled. N-methylated isoleucine was triple-coupled. The alanine that directly followed the N-methylated isoleucine was coupled 5 times. N-methylated glycine, the phenylalanine and the asparagines directly following the N-methylated glycine were double coupled. The peptides were cleaved from the resin through the use of standard trifluoroacetic acid (TFA) methods. Crude peptides were oxidized by dimethyl sulfoxide (DMSO) at room temperature. The peptides were purified via reverse-phase high-performance liquid chromatography (RP-HPLC) using a Vydac C18 preparative column.[173] Analytical HPLC were used to check the purity of the peptides before each experiment. The identity of the pure peptides was confirmed by MALDI-TOF MS. Wild type IAPP expected 3902.9, observed 3902.7; I26P-IAPP expected 3888.3, observed 3888.2; NMe-G24, NMe-I26-IAPP expected, 3930.9, observed, 3930.8.

3.2.2 Sample Preparation

Peptide stock solutions were prepared in 100% hexafluoroisopropanol (HFIP) at 1.6 mM. Low molecular weight heparan sulfate (10,000-14,000 molecular weight), chondrointin sulfate

and dermatan sulfate were purchased from Sigma. Fluorescein-labeled heparin (FLH) with an average molecular weight of 18,000 was purchased from Invitrogen. All GAG stock solutions were prepared by dissolving GAG in 20 mM Tris-HCl (pH 7.4) at 2.2 mg/ml. EGCG was purchased from Sigma and dissolved in 20 mM Tris-HCl (pH 7.4) at 1.6 mM immediately before use.

3.2.3 Preparation of Large Unilamellar Vesicles (LUVs)

The LUVs were composed of 100% 1,2-dioleoyl-sn-glycero-3-phospho-(1'-rac-glycerol) (DOPG), from Avanti Polar Lipids. Stock solutions of DOPG in chloroform at a concentration of 10 mg/mL were first evaporated with a stream of nitrogen gas and then dried under a vacuum overnight to completely remove the residual organic solvent. The resulting lipid film was hydrated in 20 mM Tris-HCl, pH 7.4 buffer for 1 hour, at a lipid concentration of 8 mM. The multilamellar vesicles were subjected to 10 freeze-thaw cycles and extruded 11 times through 100 nm pore size filters (Whatman, GE). The phospholipid concentration was determined by the method of Stewart.[199] A fresh vesicle solution was used for each experiment.

3.2.4 Fluorescence Assays

Two types of ThioflavinT binding assays were utilized, one for samples with hexafluoroisopropanol (HFIP) and the other for samples which did not contain HFIP. Amyloid formations by I26P-IAPP and NMe-G24, NMe-I26-IAPP and their ability to inhibit amyloid formation by wild type human IAPP in the presence and absence of GAGs were first monitored by thioflavin-T binding assays conducted in the presence of 2% hexafluoroisopropanol (HFIP) and with continuous stirring at 25 °C. Fluorescence measurements were performed using an Applied Photon Technology fluorescence spectrophotometer with 450 nm excitation and 485 nm

emission. The slit widths for excitation and emission were set at 4 nm and a 1.0 cm cuvette was used. Each point was averaged for 1 minute. Solutions were prepared by diluting filtered stock solution (0.45 μM Acrodisc syringe filter with GHP membrane) into Tris-HCl buffer and thioflavin-T solution immediately before the measurement. The final concentration was 16 μM peptide and 32 μM thioflavinT in 20 mM Tris-HCl (pH 7.4). In the I26P-IAPP and NMe-G24, NMe-I26-IAPP amyloid formation experiments, GAGs (heparan sulfate, chondroitin sulfate and dermatan sulfate), when present, were at 1.3 μM. In the inhibition experiments, heparan sulfate, when present, was at 2.6 μM. FRET experiments involving fluorescein-labeled heparin (FLH) were also monitored using this assay in solutions which contained 2% HFIP. Fluorescence measurements were performed on the same instrument using 440 nm excitation and 510 nm emission. The final solution composition was 16 μM peptide, 1.3 μM FLH and 32 μM thioflavinT, when present.

Amyloid formation by I26P-IAPP and NMe-G24, NMe-I26-IAPP in the presence and absence of heparan sulfate were also monitored by thioflavin-T binding assays in the absence of HFIP. These assays were conducted without stirring using a Beckman Coulter DTX 880 plate reader with multimode detector using 430 nm excitation and 485 nm emission at 25°C. Fluorescence solutions were prepared by lyophilizing filtered stock solution (0.45 μM Acrodisc syringe filter with GHP membrane) for 22 hrs and then dissolving dry peptides into Tris-HCl buffer and thioflavin-T solution immediately before the measurement. The final concentration was 16 μM peptide and 32 μM thioflavin-T in 20 mM Tris-HCl (pH 7.4). Heparan sulfate, when present, was at 1.3 μM. Experiments involving high ionic strength, lipid micelle or EGCG were also monitored using this assay.

3.2.5 Circular Dichroism (CD)

Far-UV CD experiments were performed at 25°C on an Applied Photophysics Chirascan CD spectrophotometer. Aliquots from the kinetic experiments were removed at relevant time points during the experiments and the spectra were recorded. Spectra were the average of three repeats recorded over a range of 190-260 nm, at 1 nm intervals. A 0.1 cm quartz cuvette was used and a background spectrum was subtracted from the collected data.

3.2.6 Transmission Electron Microscopy (TEM)

TEM images were collected at the Life Science Microscopy Center at the State University of New York at Stony Brook. 15 μL aliquots of the samples used for the kinetic studies were removed at relevant time points, placed on a carbon-coated 300-mesh copper grid for 1 min and then negatively stained with saturated uranyl acetate for 1 min.

3.3 Results and Discussion

3.3.1 Heparan Sulfate Induces Amyloid Formation by Non-amyloidgenic Variants of IAPP.

The sequences of wild type IAPP, the I26P-IAPP and NMe-G24, NMe-I26-IAPP variants are shown in Figure 3.1. No data are available on the effects of GAGs on the ability of either of these variants to form amyloid. We first studied amyloid formation by I26P-IAPP in the presence of the model GAG heparan sulfate (HS). High molecular weight (10 to 14kd) HS was used for these studies. Alexandrescu and coworkers examined the length dependence of heparin upon amyloid formation by wild type IAPP and showed that length dependent effects leveled off above 12 monosaccharide units.[197] The high molecular weight HS used here was above the threshold observed for heparin. Figure 3.2 compares the ability of the I26P point mutant to form

amyloid in the absence and presence of HS. The peptide was not amyloidogenic in homogeneous solution over the 10 hr time course of the experiment as judged by thioflavin-T binding assays, transmission electron microscopy (TEM) and circular dichroism (CD). In contrast, wild type IAPP formed amyloid with a T_{50}, the time required for the reaction to reach 50% of the final fluorescence intensity, of 21 mins under these conditions in the absence of GAG. The mutant formed amyloid in the presence of HS. A rapid increase in thioflavin-T fluorescence was observed for I26P-IAPP in the presence of HS with a T_{50} of 20 mins. TEM confirmed the results of the thioflavin-T studies, and dense matts of amyloid fibers were observed in the presence of HS, but not in its absence (Figure 3.2). CD (Figure 3.13) revealed the presence of significant β-sheet structure in the presence of GAGs.

We analyzed a second non-amyloidgenic variant of IAPP, NMe-G24, NMe-I26-IAPP. This peptide is non-amyloidgenic and is one of the most effective inhibitors of amyloid formation by IAPP and protects against IAPP induced toxicity in cell culture.[124] Figure 3.3 compares kinetic curves collected in the presence and absence of heparan sulfate. No amyloid formation was observed in the absence of heparan sulfate, even for samples which were incubated for more than 20 times longer than the time required for wild type IAPP to form amyloid (Figure 3.3). In contrast, rapid amyloid formation was observed when heparan sulfate was present as judged by thioflavin-T assays and TEM (Figure 3.3) with a T_{50} of 30 mins. CD (Figure 3.14) confirmed the presence of β-sheet structure.

The experiments outlined above were carried out using standard protocols for biophysical studies of IAPP. These involved solubilizing the peptide in hexafluoroisopropanol (HFIP) and diluting the stock solution into buffer. This results in 2% residual HFIP by volume. Even this low percentage of organic co-solvent enhances significantly the kinetics of amyloid formation by

IAPP.[129, 175] Thus we wanted to test if our results might be a consequence of the conditions used. We repeated the experiments using a different protocol which avoids the use of HFIP. Buffer was added directly to dried peptide and the time course of amyloid formation was followed. We obtained similar results; both I26P-IAPP and NMe-G24, NMe-I26-IAPP formed amyloid in the presence of heparan sulfate, but not in its absence (Figure 3.15, 3.16). The T_{50} of I26P-IAPP in the presence of heparan sulfate under this condition was 465 mins and was 2010 mins for the NMe-G24, NMe-I26-IAPP, wild type IAPP formed amyloid with a T_{50} of 60 mins in the presence of heparan sulfate under these conditions.

3.3.2 FRET Experiments Reveal the Co-localization of Amyloid Fibrils and GAGs.

To further investigate the mechanism of the amyloid inducing effects of GAGs on I26P-IAPP and NMe-G24, NMe-I26-IAPP, we tested if GAGs are associated with amyloid fibrils. This is important because GAGs might exert their effects by binding to the IAPP variants or through non-specific polyanion effects. We used a recently developed assay based on FRET from thioflavin-T to fluorescein labeled heparin (FLH).[197] Labeled heparin with one fluorescein conjugated per heparin was used as a model GAG. The excitation maximum of thioflavin-T when bound to amyloid fibrils is near 450 nm and its emission maximum is near 485 nm. The excitation maximum of fluorescein is 488 nm and its emission maximum is 515 nm. Thus, the two dyes form a convenient FRET pair to monitor the proximity of GAG and amyloid fibrils. Figure 3.4 shows the kinetic profile of I26P-IAPP amyloid formation induced by FLH, monitored at an excitation wavelength of 440 nm and an emission wavelength of 510 nm. This pair of wavelengths was chosen to detect just the fluorescent signal due to FRET between fluorescein and thioflavin-T bound to fibrils by avoiding signal from direct excitation of bound thioflavin-T. FRET to fluorescein from fibril bound thioflavin-T was detected as amyloid

formation by I26P-IAPP proceeds (Figure 3.4, red curve). CD (Figure 3.17) and TEM images (Figure 3.4) confirmed the existence of fibrils. In a control experiment containing I26P-IAPP and FLH without thioflavin-T, no significant increase in fluorescence intensity was detected (Figure 3.4, black curve), although CD (Figure 3.17) and TEM (Figure 3.4) confirmed the presence of fibrils. We also studied the co-localization of FLH and NMe-G24, NMe-I26-IAPP using FRET. The results were very similar to those observed with I26P-IAPP. (Figure 3.18) The observation of FRET between FLH and thioflavin-T in both cases demonstrates an association of GAG with the peptides. The association may occur during the process of amyloid formation or might result from the IAPP peptides forming amyloid fibers in solution and then binding to GAG. We conducted additional experiments to test these possibilities. We simultaneously monitored direct thioflavin-T fluorescence and thioflavin-T to FLH FRET for the same sample. (Figure 3.19) The two curves showed identical time courses; the simplest explanation is that the peptides bind GAGs before amyloid formation is complete.

3.3.3 The effect of Heparan Sulfate on I26P-IAPP Amyloid Formation Can Be Screened by High Ionic Strength.

IAPP and the two variants studied here all have a net charge between +2 and +4 at physiologically relevant pH, depending upon the exact pKa of the N-terminus and His-18, thus all are capable of making electrostatic interactions with heparan sulfate. In order to study the potential role of electrostatic interactions between I26P-IAPP and heparan sulfate, we examined amyloid formation kinetics in buffers with high concentrations of salt. Amyloid formation by wild type IAPP is very sensitive to salt.[200] Thioflavin-T fluorescence assays without HFIP were used to follow amyloid formation as a function of added salt. Figure 3.5 compares the ability of I26P-IAPP to form amyloid in the presence and absence of heparan sulfate as a function of NaCl

in the assay. I26P-IAPP was still non-amyloidgenic in homogeneous solution when 150 mM NaCl was added to the buffer (Figure 3.5, black curve). Heparan sulfate still induced amyloid formation under these conditions (Figure 3.5, blue curve), but with a lower efficiency as indicated by a 3.3 fold longer lag phase (990 mins), compared to the kinetic profile without NaCl. (Figure 3.15). At higher NaCl, 500 mM, I26P-IAPP did form amyloid in the presence and in the absence of heparan sulfate (Figure 3.5). Similar kinetic profiles were obtained with and without heparan sulfate, although slightly higher final fluorescence intensity was observed in the presence of heparan sulfate. TEM images collected at the end of each experiment (Figure 3.5) are consistent with the thioflavin-T fluorescence measurements. The observation that heparan sulfate no longer accelerates IAPP amyloid formation by I26P-IAPP at high salt relative to control suggests that electrostatic interactions make a significant contribution to GAG-peptide interactions.

3.3.4 GAGs are More Effective than Anionic Vesicles at Inducing Amyloid Formation by I26P-IAPP.

A wide range of studies have shown that lipid membranes containing negatively charged lipids promote the formation of IAPP amyloid.[193, 194, 201, 202] Although the mechanism of the effect is not completely clear, it is believed that electrostatic interactions between positively charged peptides and negatively charged lipids play an important role. If the effects of GAGs and lipid vesicles depended only on the concentration of negative charges rather than on their spatial distribution, then we would expect similar effects when the total number of negatively charged sites were matched. To test if this is the case, we compared the effects of lipid vesicles and heparan sulfate on amyloid formation by I26P-IAPP. Anionic dioleoylphosphatidylglycerol

(DOPG) which contains a single negative charge was chosen as a model lipid. DOPG has been widely used in model studies of IAPP membrane interactions.[136, 203, 204]

DOPG induces amyloid formation by I26P-IAPP, but much less efficiently on a per negative charge basis than heparan sulfate. The concentration of heparan sulfate (0.97 μM) and DOPG (48 μM) used here correspond to a concentration of 48 μM negative charges. The lag phase of I26P-IAPP amyloid formation in the presence of DOPG (675 mins) was almost 10 fold longer than observed with heparan sulfate (68 mins). (Figure 3.6) Peptide-lipid binding and lipid induced fiber formation are highly dependent on the concentration of lipids and on the lipid to peptide ratio. A 5 fold increase in the concentration of DOPG increased T_{50} two fold. (Figure 3.20) This dependence was weaker for HS. A 10 fold increase in HS concentration led to only a 1.5 fold increase in rate. (Figure 3.21) These results demonstrate that heparan sulfate is more efficient than DOPG in inducing amyloid formation by I26P-IAPP at the same net total charge under the conditions used. Moreover, the effects of HS are less dependent on its concentration.

3.3.5 I26P-IAPP and NMe-G24, I26-IAPP Can Be Induced to Form Amyloid by Other GAGs.

It is natural to inquire if the effect of heparan sulfate is specific to the structure of the GAG used. We studied amyloid formation by the IAPP variants in the presence of two other GAGs, chondroitin sulfate and dermatan sulfate. All three of these GAGs are composed of repeating disaccharide units. The most common unit of heparan sulfate is glucuronic acid (GlcA) linked to N-acetylglucosamine (GlcNAc). Chondrointin sulfate is composed mainly of alternating D-glucuronic acid (GlcA) and N-acetyl-D-galactosamine (GalNAc). When the GlcA is epimerized into L-iduronic acid (IdoA), the resulting GAG is denoted dermatan sulfate.

Figure 3.7 compares I26P-IAPP amyloid formation induced by the three GAGs. Chondroitin sulfate and dermatan sulfate also promoted amyloid formation by I26P-IAPP. A

slightly shorter lag phase and lower final fluorescence intensity was observed in the presence of chondroitin sulfate (Figure 3.7, red curve) than with heparan sulfate (Figure 3.7, black curve), while the lag phase for dermatan sulfate induced amyloid formation was between that observed for chondroitin sulfate and heparan sulfate. TEM (Figure 3.7) and CD (Figure 3.22) confirmed that fibrils had formed at the end of each experiment. Similar results were observed with NMe-G24, NMe-I26-IAPP. The peptide was amyloidgenic in the presence of each of the three GAGs and the trend in the efficiency in inducing amyloid formation was the same as observed for I26P-IAPP as judged by the lag times (Figure 3.23). The results show that the amyloid inducing effect of GAGs on non-amyloidgenic IAPP variants is not specific to heparan sulfate. The difference in GAGs' structures and the arrangement of the charges are likely responsible for the slight variations in the kinetic parameters.

3.3.6 IAPP Amyloid Inhibitors Are Less Effective in the Presence of GAGs.

I26P-IAPP and NMe-G24, NMe-I26-IAPP are both inhibitors of IAPP amyloid formation in homogeneous solution. We tested their efficiency in the presence of heparan sulfate. Figure 3.8 displays the results of an inhibition experiment using I26P-IAPP. In the absence of GAG, the lag phase of amyloid formation by IAPP was a factor of 3 times longer when the inhibitor was present, consistent with previous reports.[122] Quite different results were obtained when GAG was present in the mixture; an initial, rapid increase in the thioflavin fluorescence was observed followed by an intermediate plateau. Similar biphasic behavior has been observed during GAG catalyzed amyloid formation by proIAPP processing intermediates and is thought to be due to the rapid formation of a GAG bound intermediate.[140] This was followed by a second growth phase leading to a final plateau. TEM analysis of aliquots removed during the first plateau revealed the presence of thin fibers as well as shorter fibril like objects (Figure 3.8). Numerous fibers were

observed in the final plateau (Figure 3.8). The results of the thioflavin-T assays are difficult to unambiguously interpret since both polypeptides can form amyloid in the presence of GAGs. Thus the final thioflavin-T signal could arise from amyloid formation by one or both of the polypeptides. None the less, it is clear that mixtures of wild type IAPP with I26P-IAPP or with NMe-G24, NMe-I26-IAPP behave very differently in the presence of GAGs than in their absence.

This experiment was conducted by mixing IAPP, inhibitor and HS at the beginning of the experiment. The effect of the GAG could arise from sequestration of the inhibitor by HS. We conducted an additional experiment to test whether GAGs accelerated amyloid formation if they were added in the lag phase of the I26P-IAPP: IAPP mixture. In this experiment, IAPP and inhibitor were allowed to form a complex before addition of HS. HS still accelerated amyloid formation (Figure 3.9), suggesting that simple sequestration of the inhibitor is not the only cause of the HS induced effects. This is reasonable since both IAPP and I26P-IAPP can bind HS and there is no reason that HS should selectively remove I26P-IAPP from solution.

We next examined the ability of NMe-G24, NMe-I26-IAPP to inhibit amyloid formation. Figure 3.10 compares thioflavin-T kinetic curves for wild type IAPP in the absence of heparan sulfate, a 1:1 mixture of wild type IAPP and inhibitor without heparan sulfate and a 1:1 mixture of wild type IAPP and inhibitor in the presence of heparan sulfate. NMe-G24, NMe-I26-IAPP is, as expected, an effective inhibitor in the absence of heparan sulfate. Under our conditions wild type IAPP forms amyloid with a lag time of 17 mins, in contrast, no significant increase in thioflavin-T fluorescence is observed for 150 mins in the presence of inhibitor although eventually a significant increase is detected around 400 mins. The inhibitor is less effective when heparan sulfate is present. A rapid increase in thioflavin-T fluorescence is observed, which is

followed, quickly, by a second transition to a final plateau. TEM reveals some fibril like aggregates in the first plateau (Figure 3.10). Dense matts of fibers were observed at the end of the reaction (Figure 3.10).

We also analyzed the ability of the small molecule (−)-epigallocatechin 3-gallate (EGCG) to inhibit amyloid formation in the presence of heparan sulfate in order to test if GAGs can affect small molecule inhibitors as well as peptide-based inhibitors. EGCG is a green tea-derived flavanol that has been reported to inhibit amyloid formation by a wide range of natively unfolded polypeptides including IAPP.[21, 146, 151, 205, 206] Previous work from our laboratory has shown that EGCG effectively inhibits *in vitro* IAPP amyloid formation and dissociates pre-formed fibrils into small aggregates.[21, 146] In the presence of heparan sulfate without EGCG, IAPP amyloid formation is greatly accelerated compared to the same reaction in homogeneous solution (Figure 3.11). No increase of thioflavin-T fluorescence is observed for the 1:1 mixture of IAPP with EGCG without heparan sulfate (Figure 3.11). However, when heparan sulfate and EGCG are present, an initial rapid increase of thioflavin-T fluorescence was observed followed by a slow decrease, which may indicate that aggregates formed immediately and then gradually dissociated into small aggregates or were restructured (Figure 3.11, red curve). The initial increase of fluorescence was lower for higher concentrations of added EGCG (Figure 3.24), but the effect was still observable even when EGCG was in 20 fold excess. TEM images confirmed the existence of small aggregates at the end of each experiment. (Figure 3.11, Figure 3.25) The aggregates did not show any obvious change in morphology as the concentration of EGCG is increased (Figure 3.25).

EGCG was still able to dissociate amyloid fibrils formed by IAPP in the presence of heparan sulfate (Figure 3.12). The structures of the aggregates formed were similar to those

formed when EGCG is added at the beginning of the reaction as judged by TEM images (Figure 3.12, Figure 3.28). CD confirmed that all of the aggregates contain β-sheet structure (Figure 3.26, 3.27). These results indicate that EGCG is still able to inhibit IAPP amyloid formation and dissociate mature amyloid fibrils into small aggregates in the presence of heparan sulfate, but is less effective than in a homogeneous environment.

3.4 Conclusions

The analysis presented here reveals that IAPP amyloid formation in heterogeneous environment is very different than in homogeneous solutions: Apparently non-amyloidgenic variants can be readily induced to form amyloid in the presence of GAGs and some peptide based and small molecule amyloid inhibitors are less effective. The GAGs tested here are more effective at inducing amyloid formation than are anionic lipid vesicles on a per net charge basis even when the total number of anionic sites is the same, suggesting that the spatial arrangement of negatively charged sites is important. This conjecture is supported by a recent study of the effects of varying the number of sulfated saccharide monomers in heparin on amyloid formation by wild type human IAPP.[197] Small fragments were less effective than large ones, but the length dependence leveled off beyond 12 sulfated saccharide units. Control experiments showed that the dependence was due to a length effect rather than an increase in the number of monomer units. The length dependent effects are believed to arise from the ability of the longer heparin fragments to adopt specific structures. Solution NMR studies have shown that heparin forms a left-handed helix structure with four saccharides per turn[207] and the length dependence studies imply that heparin exerts its most potent effects on IAPP amyloid formation when it can form helix structures.[197] IAPP contains a positively charged N-terminus, a Lys at position 1, an Arg at

position-11 and a His at position 18. All of these groups have been shown to be important for IAPP GAG interactions and the charge arrangement in helical heparin fragments is complimentary to the arrangement of positive charges in models of IAPP amyloid fibers.[140, 142, 197] Modeling of Aβ GAG interactions also suggests a role for complimentary charged interfaces in the catalytic effects of GAGs on Aβ amyloid formation.[208]

HSPGs are associated with *in vivo* islet amyloid and the interaction of proIAPP processing intermediates with HSPGs of the extracellular has been postulated to play a role in inducing amyloid formation.[50, 141] Studies with inhibitors of GAG synthesis show that decreasing GAG synthesis and protein glycosylation in islets results in reduced islet amyloid formation *in vitro*.[209] This result is consistent with earlier *in vivo* findings that these inhibitors reduce amyloid formation in mouse models of Amyloid A amyloidosis.[210] These *in vitro* and *in vivo* studies suggest that limiting IAPP GAG interaction might be a therapeutic method for amyloid related diseases.

Relatively little attention has been paid to the role of IAPP GAG interactions. The results presented here show they can strongly impact amyloid formation and the efficiency of amyloid inhibitors. Thus potential interactions with GAGs should be considered in inhibitor design and in the analysis of amyloidgenicity. GAGs have also been shown to induce amyloid formation by other polypeptides which appear to be non-amyloidgenic in homogeneous solution.[211] Thus the effects observed with IAPP may be one example of a broader role for GAGs in amyloid formation.

3.5 Figures

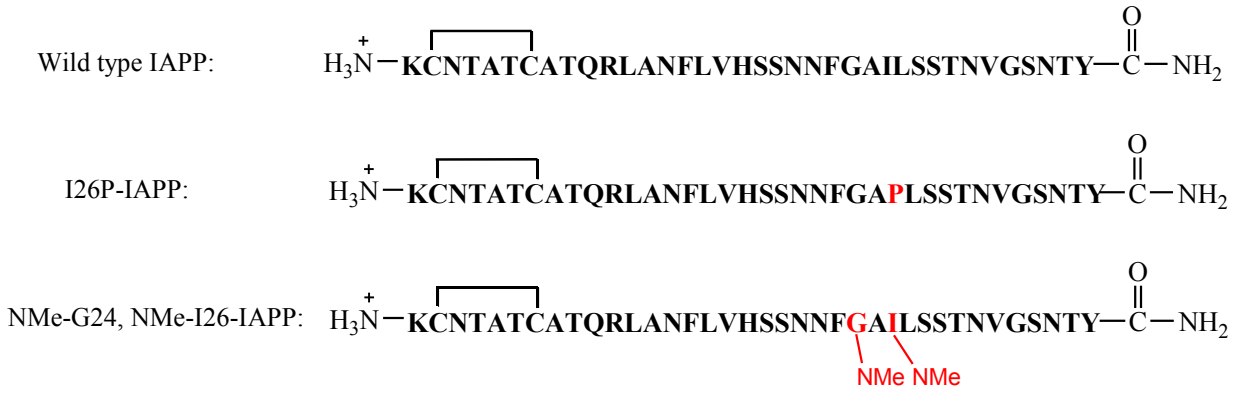

Figure 3.1 Sequence of wild type IAPP, I26P-IAPP and G24-N-methyl, I26-N-methyl-IAPP (NMe denotes N-methylation).
Each peptide has an amidated C-terminus and a disulfide bond.

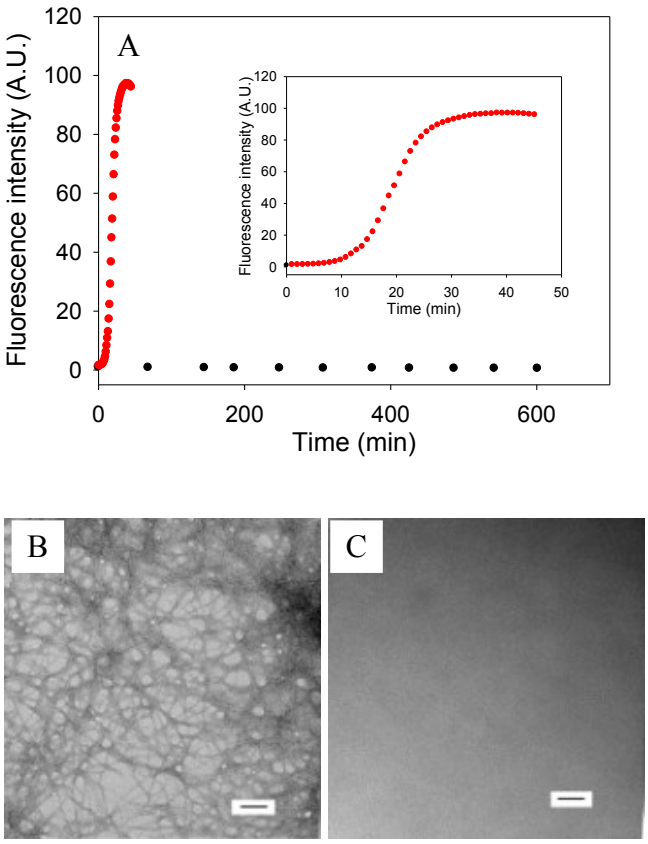

Figure 3.2 Amyloid formation by I26P-IAPP in the absence and presence of heparan sulfate.
(A) Results of fluorescence-monitored thioflavin-T binding assays are displayed. Black, I26P-IAPP in the absence of heparan sulfate; red, I26P-IAPP in the presence of heparan sulfate. The insert shows an expanded plot of the first 50 mins. (B) TEM image of I26P-IAPP in the presence of heparan sulfate. (C) TEM image of I26P-IAPP in the absence of heparan sulfate. Aliquots were removed at the end of each kinetic experiment for TEM analysis. Scale bars represent 100 nm. The kinetic experiments were conducted in 20 mM Tris-HCl (pH 7.4), 2% HFIP (v/v) with continuous stirring at 25 °C. The concentration of I26P-IAPP was 16 μM. Heparan sulfate, when present, was at 1.3 μM.

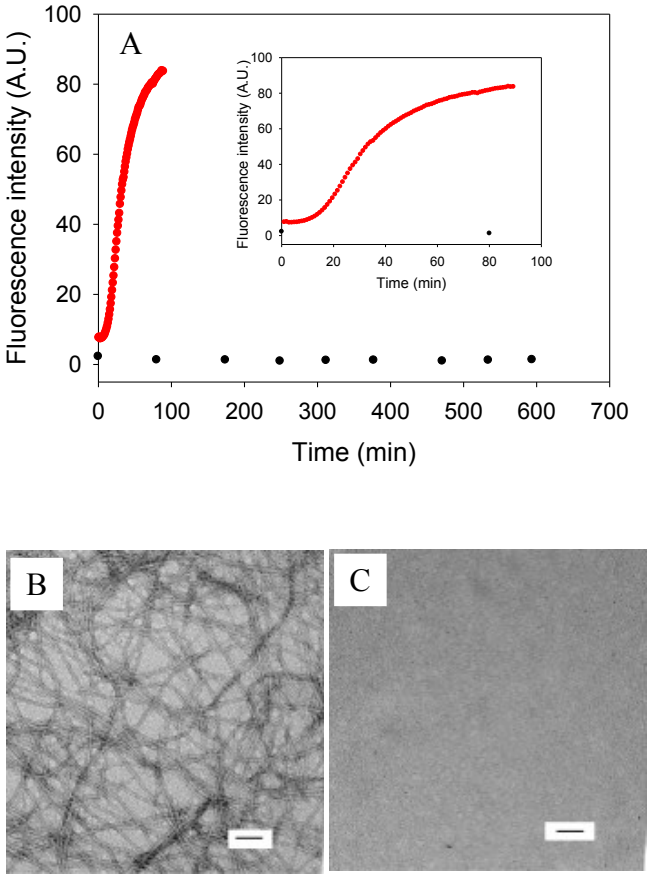

Figure 3.3 Amyloid formation by NMe-G24, NMe-I26-IAPP in the absence and presence of heparan sulfate.

(A) Results of fluorescence-monitored thioflavin-T binding assays are displayed. Black, NMe-G24, NMe-I26-IAPP in the absence of heparan sulfate; red, NMe-G24, NMe-I26-IAPP in the presence of heparan sulfate. The insert shows an expanded plot of the first 100 mins. (B) TEM image of NMe-G24, NMe-I26-IAPP in the presence of heparan sulfate. (C) TEM image of NMe-G24, NMe-I26-IAPP in the absence of heparan sulfate. Aliquots were removed at the end of each kinetic experiment for TEM analysis. Scale bars represent 100 nm. The kinetic experiments were conducted in 20 mM Tris-HCl (pH 7.4), 2% HFIP (v/v) with continuous stirring at 25 °C. The concentration of NMe-G24, NMe-I26-IAPP was 16 μM. Heparan sulfate, when present, was at 1.3 μM.

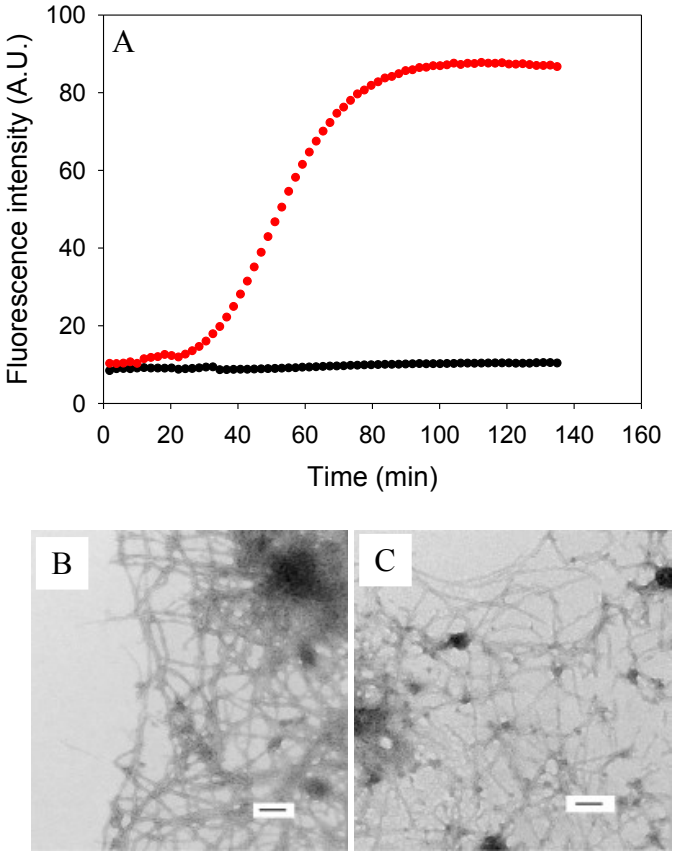

Figure 3.4 Heparan sulfate is associated with amyloid fibrils.
FRET between fluorescein labeled heparin (FLH) and thioflavin-T bound to amyloid fibrils formed by I26P-IAPP. (A) Kinetic profile of I26P-IAPP in the presence of FLH monitored by FRET between FLH and thioflavin-T bound to amyloid fibrils. The fluorescence was measured using an excitation wavelength of 440 nm and an emission wavelegnth of 510 nm. Black, control experiment, I26P-IAPP in the presence of FLH, no thioflavin-T; red, I26P-IAPP in the presence of FLH and thioflavin-T. (B) TEM image of I26P-IAPP in the presence of FLH and thioflavin-T. An aliquot was removed at the end of the reaction for TEM analysis. (C) TEM image of I26P-IAPP in the presence of FLH, no thioflavin-T. An aliquot was removed at the end of the reaction for TEM analysis. Scale bars represent 100 nm. The kinetic experiments were conducted in 20 mM Tris-HCl (pH 7.4), 2% HFIP (v/v) with continuous stirring at 25 °C. The concentration of I26P-IAPP was 16 μM. FLH was at 1.3 μM.

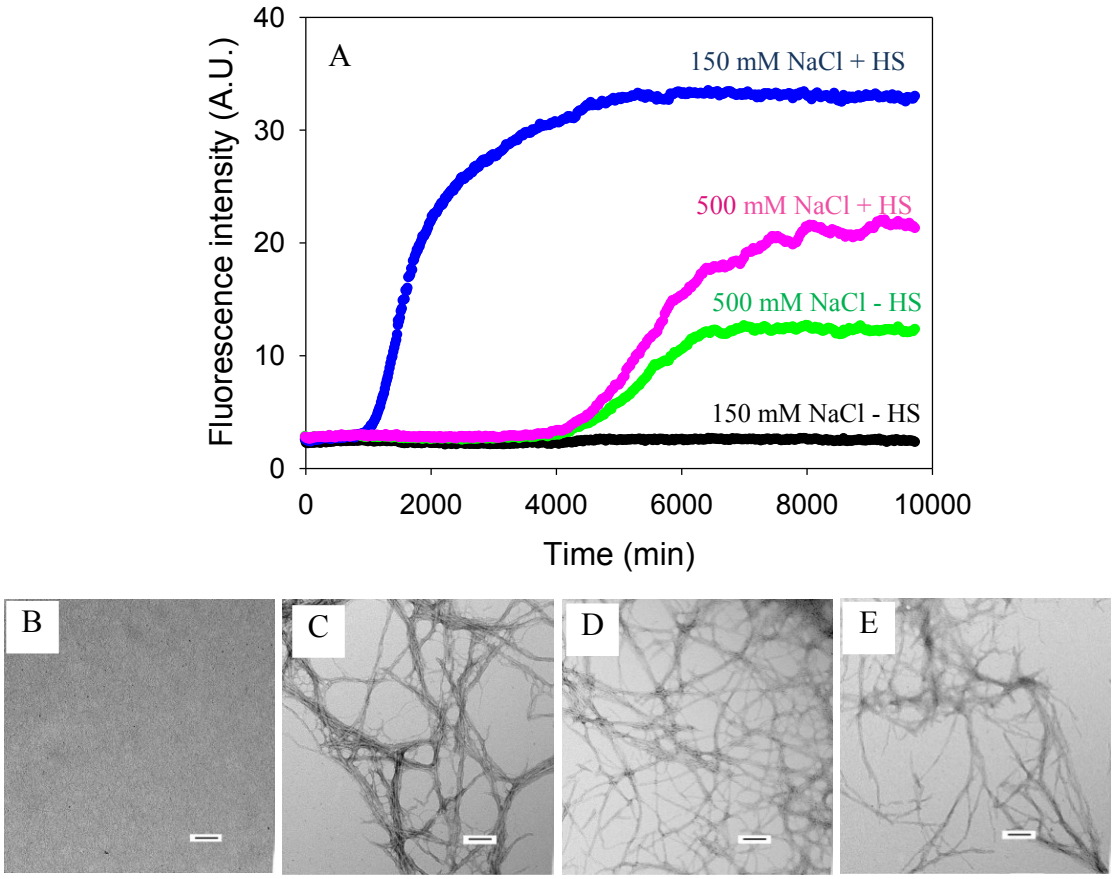

Figure 3.5 I26P-IAPP amyloid formation in the presence and absence of heparan sulfate at different NaCl concentrations.
(A) Results of fluorescence-monitored thioflavin-T binding assays are displayed. The kinetic profiles were collected with 20 mM Tris-HCl and either 150 mM or 500 mM NaCl at pH 7.4, no HFIP, without stirring at 25 °C. Black and blue curves were collected in a buffer with 170 mM total salt concentration (20 mM Tris+150 mM NaCl). Black, I26P-IAPP in the absence of heparan sulfate; blue, I26P-IAPP in the presence of heparan sulfate. Green and pink curves were collected in a buffer with 520 mM salt concentration (20 mM Tris+500 mM NaCl). Green, I26P-IAPP in the absence of heparan sulfate; pink, I26P-IAPP in the presence of heparan sulfate. (B) TEM image of I26P-IAPP in the absence of heparan sulfate with 150 mM NaCl in the buffer. (C) TEM image of I26P-IAPP in the presence of heparan sulfate with 150 mM NaCl in the buffer. (D) TEM image of I26P-IAPP in the absence of heparan sulfate with 500 mM NaCl in the buffer. (E) TEM image of I26P-IAPP in the presence of heparan sulfate with 500 mM NaCl in the buffer. Aliquots were removed at the end of each experiment for TEM analysis. Scale bars represent 100 nm. The concentration of I26P-IAPP was 16 μM. Heparan sulfate, when present, was at 1.3 μM.

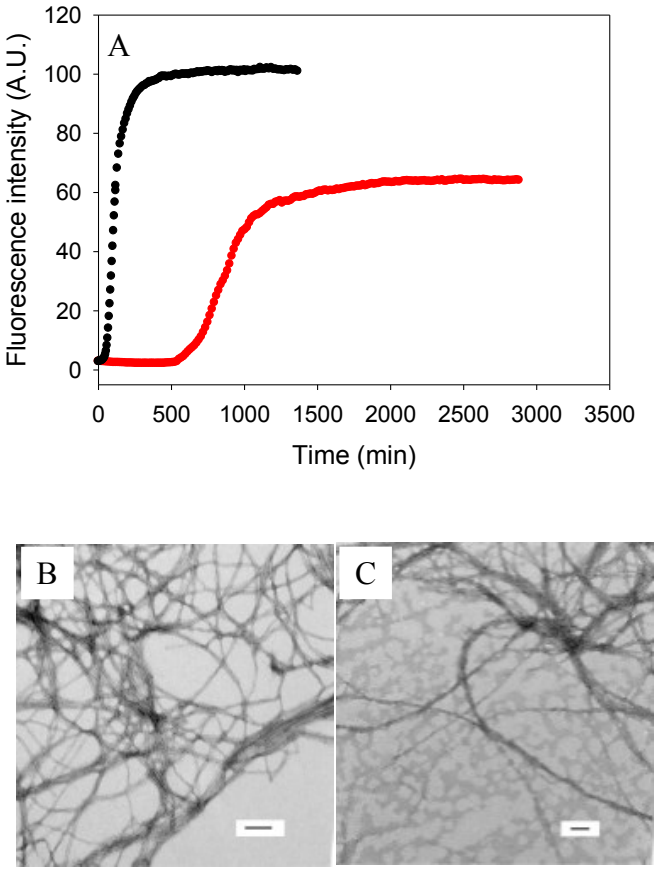

Figure 3.6 Comparison of amyloid formation by I26P-IAPP in the presence of GAG and lipids.
(A) Results of fluorescence-monitored thioflavin-T binding assays are displayed. Black, I26P-IAPP in the presence of heparan sulafte; red, I26P-IAPP in the presence of 100 nm DOPG vesicles. (B) TEM image of I26P-IAPP in the presence of heparan sulfate. (C) TEM image of I26P-IAPP in the presence of 100 nm DOPG vesicles. Aliquots were removed at the end of each reaction for TEM analysis. Scale bars represent 100 nm. The kinetic profiles were collected with 20 mM Tris at pH 7.4, no HFIP, no stirring at 25°C. The concentration of IAPP is 16 μM. Heparan sulfate, when present was at 0.97 μM. DOPG, when present, was at 48 μM. The concentration of heparan sulfate and DOPG were chosen so that the samples would contain the same number of negatively charged sites.

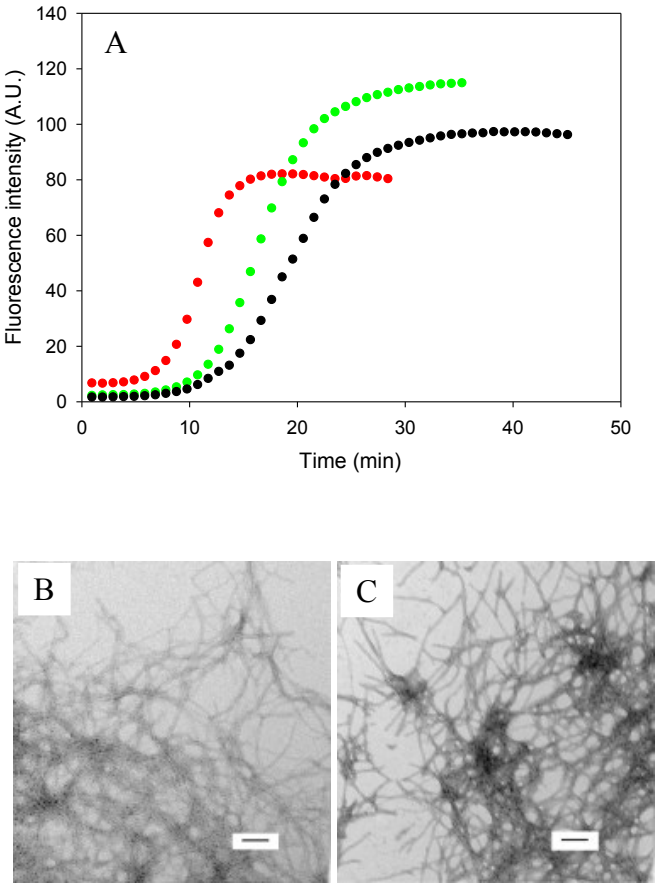

Figure 3.7 Comparison of I26P-IAPP amyloid formation in the presence of different GAGs. (A) Kinetic profiles. Black, I26P-IAPP in the presence of heparan sulfate; red, I26P-IAPP in the presence of chondroitin sulfate; green, I26P-IAPP in the presence of dermatan sulfate. (B) TEM image of I26P-IAPP in the presence of chondroitin sulfate. (C) TEM image of I26P-IAPP in the presence of dermatan sulfate. Aliquots were removed at the end of each reaction for TEM analysis. Scale bars represent 100 nm. The kinetic experiments were conducted in 20 mM Tris-HCl (pH 7.4), 2% HFIP (v/v) with continuous stirring at 25 °C. The concentration of I26P-IAPP was 16 μM, and the concentration of GAG was 1.3 μM.

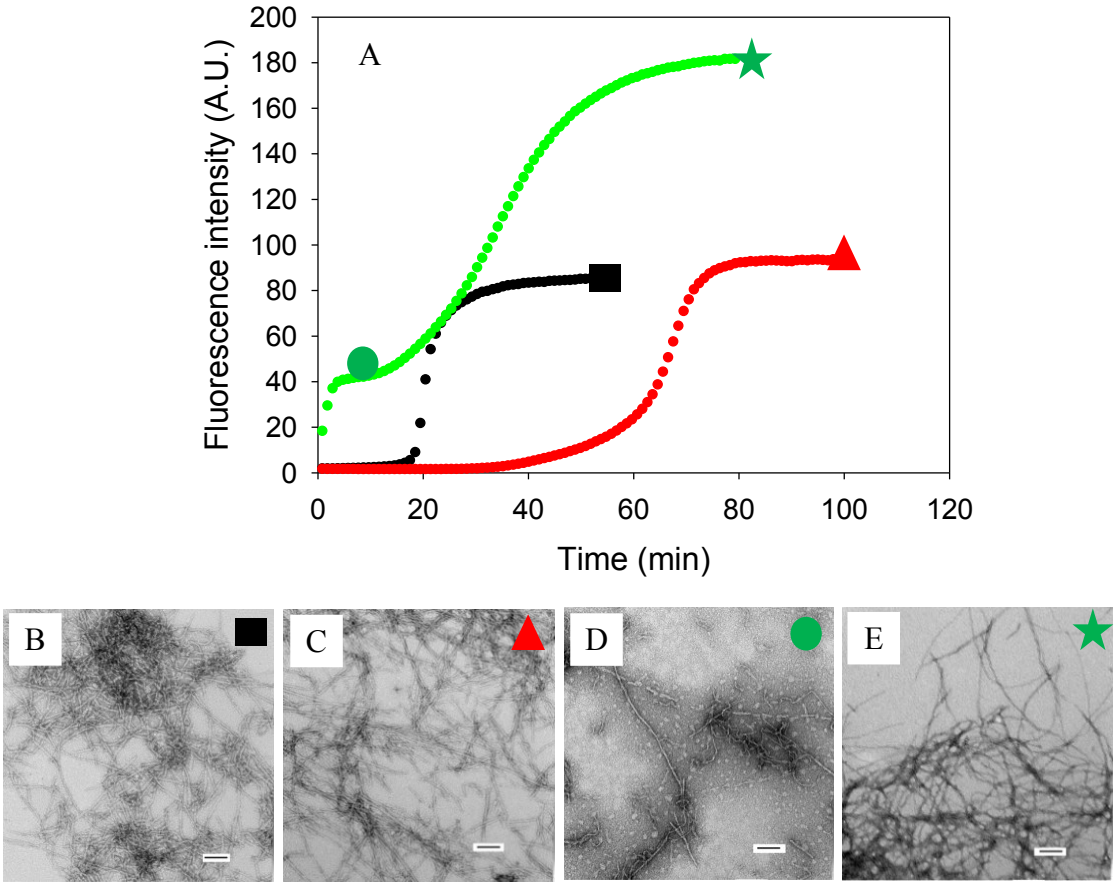

Figure 3.8 Inhibition of IAPP amyloid formation by I26P-IAPP in the absence and presence of heparan sulfate.
(A) The results of thioflavin-T binding assays are plotted. Black, wild type IAPP in the absence of heparan sulfate; red, a 1:1 mixture of wild type IAPP and I26P-IAPP in the absence of heparan sulfate; green, a 1:1 mixture of wild type IAPP and I26P-IAPP in the presence of heparan sulfate. (B) TEM image of wild type IAPP in the absence of heparan sulfate. An aliquot was removed at the end of the reaction for TEM analysis as indicated by the black rectangle in panel A. (C) TEM image of a 1:1 mixture of wild type IAPP and I26P-IAPP in the absence of heparan sulfate. An aliquot was removed at the end of the reaction for TEM analysis as indicated by the red triangle in panel A. (D) TEM image of a 1:1 mixture of wild type IAPP and I26P-IAPP in the presence of heparan sulfate in the first plateau. An aliquot was removed in the middle of the first plateau (10 mins) for TEM analysis as indicated by the green circle in panel A. (E) TEM image of a 1:1 mixture of wild type IAPP and I26P-IAPP in the presence of heparan sulfate. An aliquot was removed at the end of the reaction for TEM analysis as indicated by the green star in panel A. Scale bars represent 100 nm. The kinetic experiments were conducted in 20 mM Tris-HCl (pH 7.4), 2% HFIP (v/v) with continuous stirring at 25 °C. The concentration of wild type IAPP was 16 μM. Heparan sulfate, when present, was at 2.6 μM.

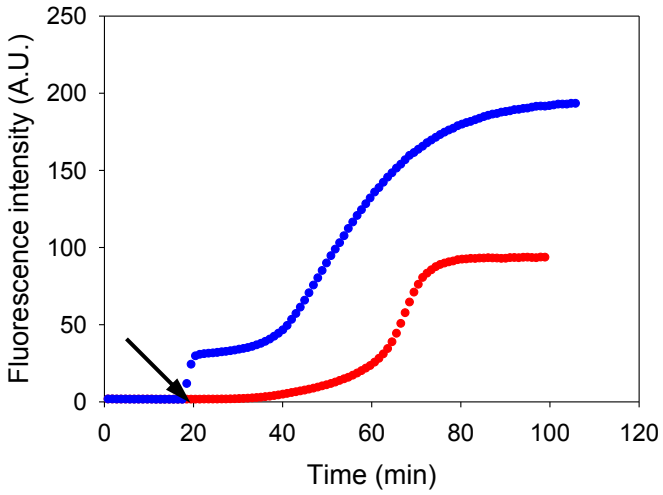

Figure 3.9 Heparan sulfate can induce amyloid formation by a mixture of IAPP and I26P-IAPP.
The results of thioflavin-T binding assays are plotted. Red, a 1:1 mixture of wild type IAPP and I26P-IAPP in the absence of heparan sulfate; blue, a 1:1 mixture of wild type IAPP and I26P-IAPP in the presence of heparan sulfate, heparan sulfate was added at the time point as indicated by the black arrow.

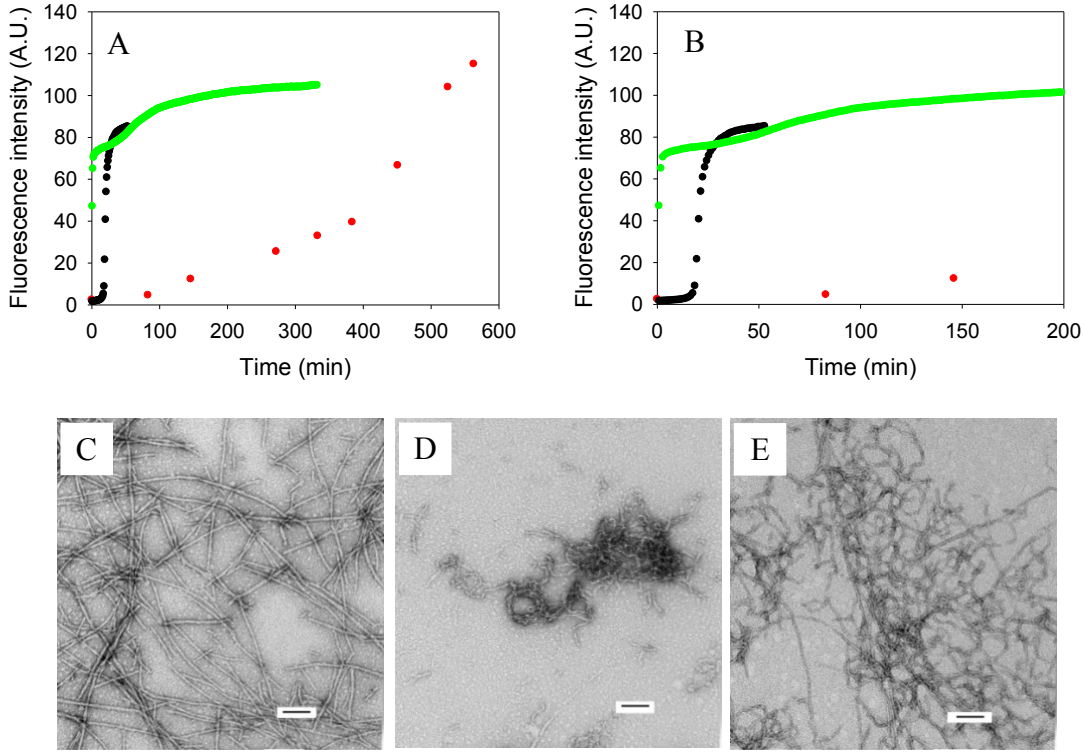

Figure 3.10 Inhibition of IAPP amyloid formation by NMe-G24, NMe-I26-IAPP in the absence and presence of heparan sulfate.
(A) The results of thioflavin-T binding assays are plotted. Black, wild type IAPP; red, a 1:1 mixture of wild type IAPP and NMe-G24, NMe-I26-IAPP in the absence of heparan sulfate; green, a 1:1 mixture of wild type IAPP and NMe-G24, NMe-I26-IAPP in the presence of heparan sulfate. (B) An expansion of the first 200 mins of panel A. The same color coding is used. (C) TEM image of a 1:1 mixture of wild type IAPP and NMe-G24, NMe-I26-IAPP in the absence of heparan sulfate. An aliquot was removed at the end of the reaction (563 min) for TEM analysis. (D) TEM image of a 1:1 mixture of wild type IAPP and NMe-G24, NMe-I26-IAPP in the presence of heparan sulfate in the first plateau. An aliquot was removed in the middle of the first plateau (17 min) for TEM analysis. (E) TEM image of a 1:1 mixture of wild type IAPP and NMe-G24, NMe-I26-IAPP in the presence of heparan sulfate. An aliquot was removed at the end of the reaction (333 min) for TEM analysis. Scale bars represent 100 nm. The kinetic experiments were conducted in 20 mM Tris-HCl (pH 7.4), 2% HFIP (v/v) with continuous stirring at 25 °C. The concentration of wild type IAPP was 16 μM. Heparan sulfate, when present, was at 2.6 μM.

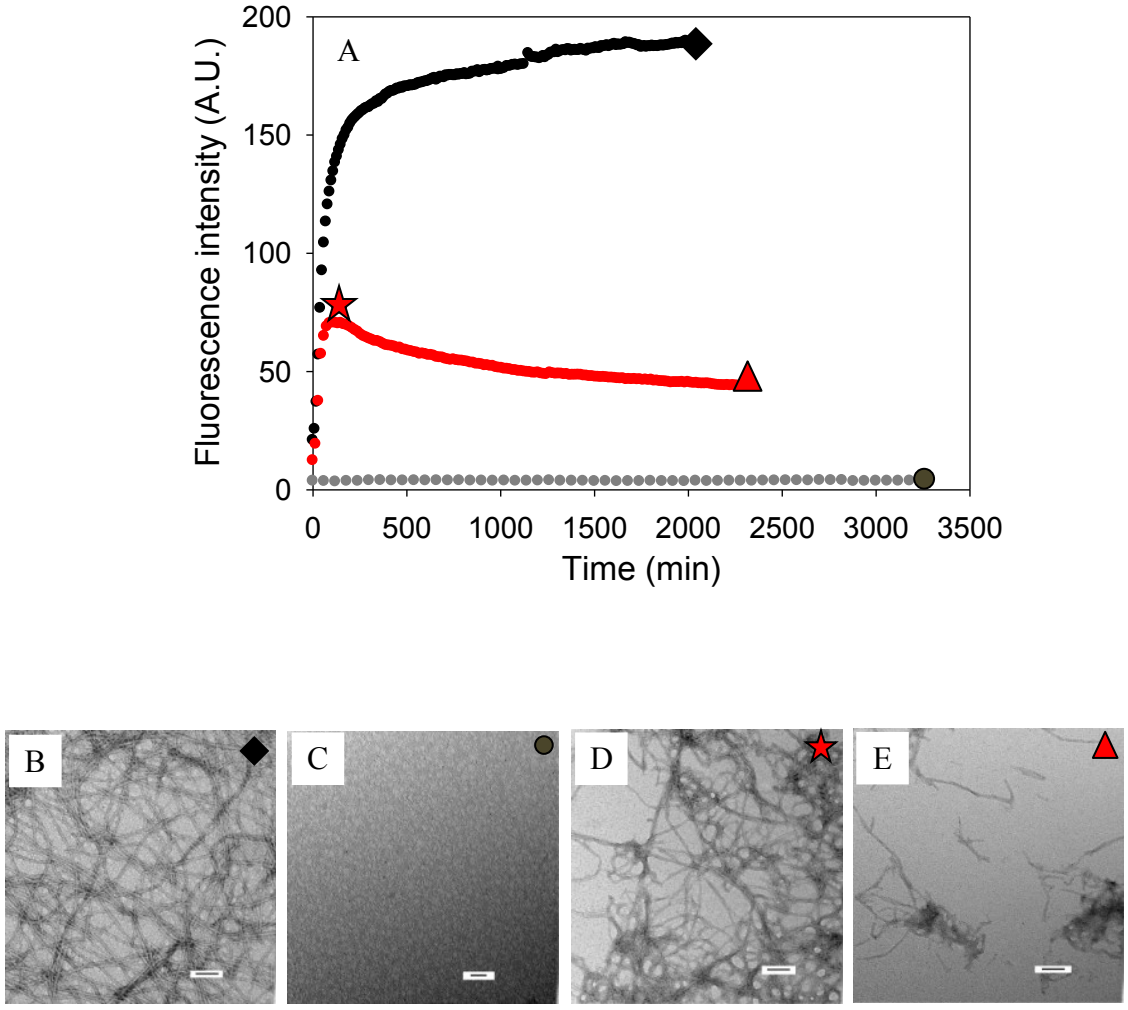

Figure 3.11 Heparan sulfate interferes with the ability of EGCG to inhibit IAPP amyloid formation.
(A) Results of fluorescence-monitored thioflavin-T binding assays are displayed. Black, IAPP in the presence of heparan sulfate; grey, a 1:1 mixture of IAPP and EGCG in the absence of heparan sulfate; red, a 1:1 mixture of IAPP and EGCG in the presence of heparan sulfate. (B) TEM image of an aliquot removed at the end of the experiment represented by the black curve in panel A, at the time point corresponding to the black diamond. (C) TEM image of an aliquot removed at the end of the experiment represented by the grey curve in panel A, at the time point corresponding to the grey circle. (D) TEM image of an aliquot removed from the sample represented by the red curve in panel A, at the time point corresponding to the red star. (E) TEM image of an aliquot removed at the end of the experiment represented by the red curve in panel A, at the time point corresponding to the red triangle. Scale bar represent 100 nm. Kinetic experiments were conducted under experimental conditions with 20 mM Tris-HCl, no HFIP and no stirring at 25 °C. The concentration of IAPP was 16 μM. Heparan sulfate, when present, was at 1.3 μM.

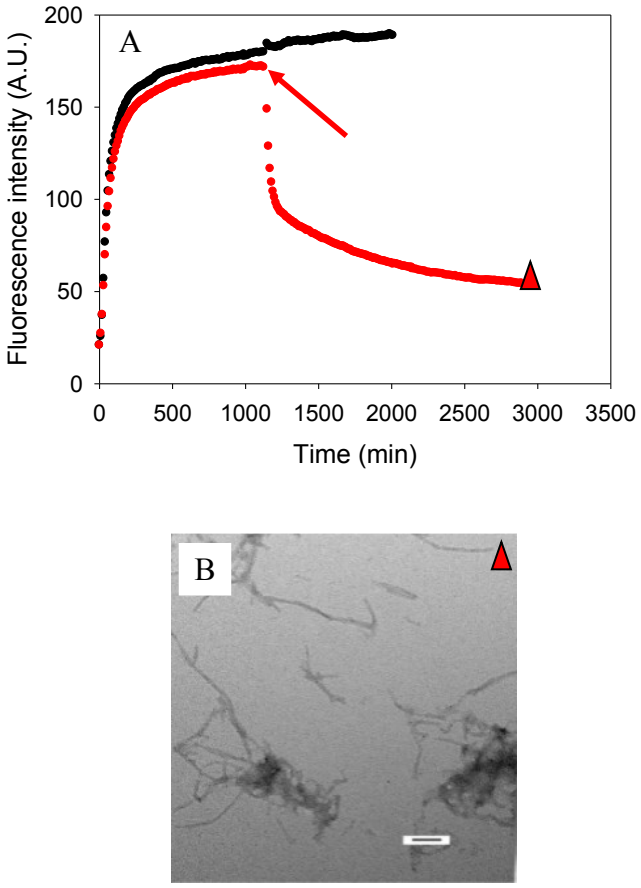

Figure 3.12 EGCG can dissociate amyloid fibrils formed by IAPP in the presence of heparan sulfate.
(A) Results of fluorescence-monitored thioflavin-T binding assays are displayed. Black, IAPP in the presence of heparan sulfate; red, a 1:1 mixture of IAPP and EGCG in the presence of heparan sulfate, EGCG was added at the time point indicated by the red arrow. (B) TEM image of an aliquot taken at the end of the experiment represented by the red curve in panel A, at the time point corresponding to the red triangle. Scale bar represent 100 nm. Kinetic experiments were conducted under experimental conditions with 20 mM Tris-HCl, no HFIP and no stirring at 25 °C. The concentration of IAPP was 16 μM. Heparan sulfate was at 1.3 μM.

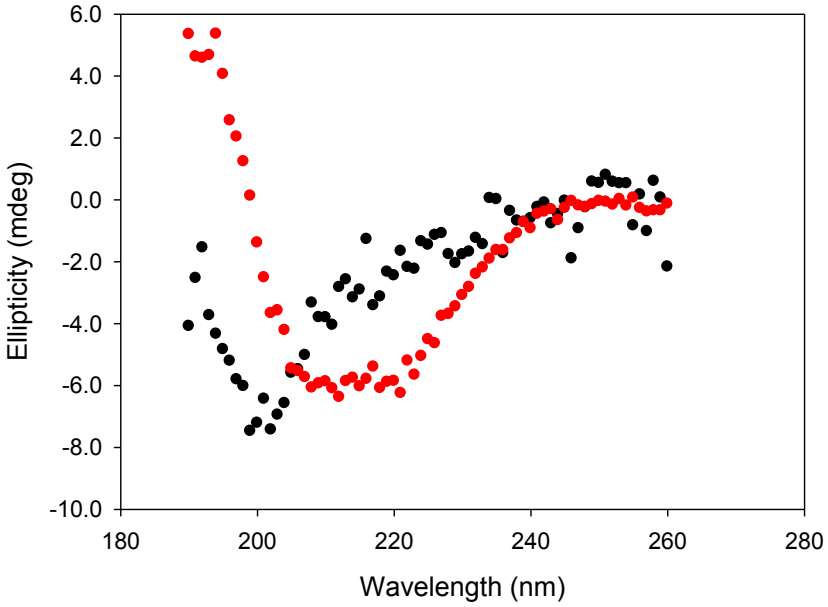

Figure 3.13 CD spectra of I26P-IAPP in the absence and presence of heparan sulfate. Aliquots were removed at the end of thioflavin-T monitored kinetic experiments displayed in Figure 3.2 and CD spectra were recorded. Black, I26P-IAPP in the absence of heparan sulfate; red, I26P-IAPP in the presence of heparan sulfate.

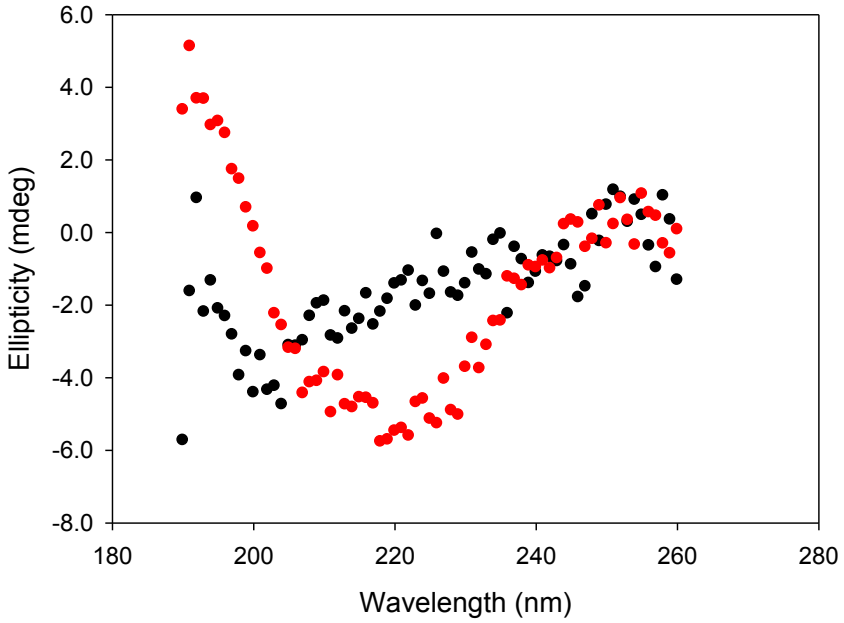

Figure 3.14 CD spectra of NMe-G24, NMe-I26-IAPP in the absence and presence of heparan sulfate.
Aliquots were removed at the end of thioflavin-T monitored kinetic experiments displayed in Figure 3.3 and CD spectra were recorded. Black, NMe-G24, NMe-I26-IAPP in the absence of heparan sulfate; red, NMe-G24, NMe-I26-IAPP in the presence of heparan sulfate.

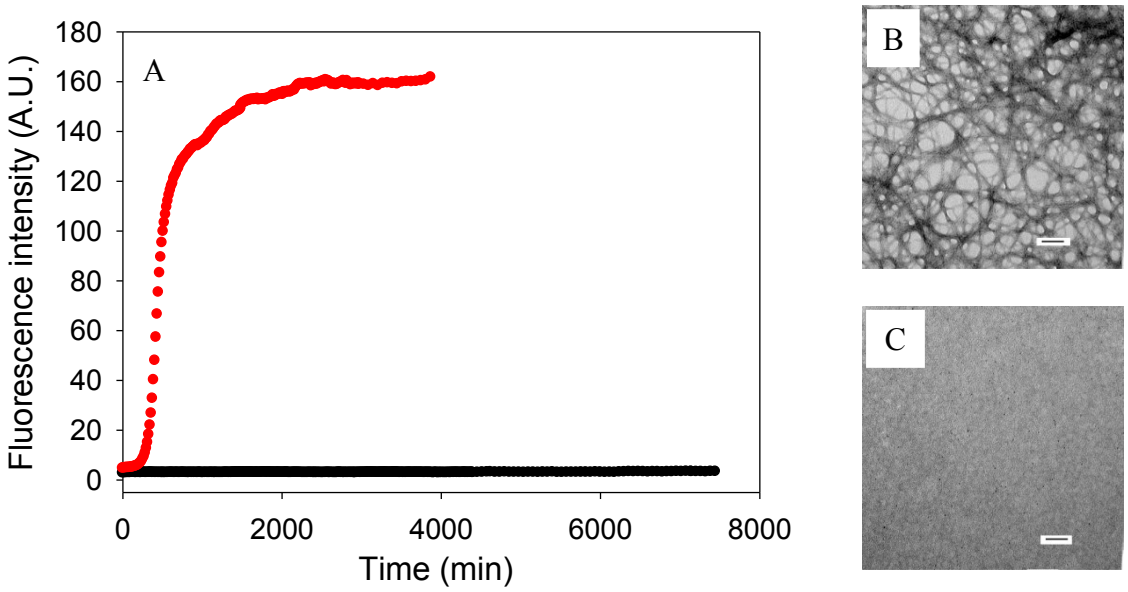

Figure 3.15 Amyloid formation by I26P-IAPP in the absence and presence of heparan sulfate monitored by thioflavin-T assays without HFIP.
(A) Black, I26P-IAPP in the absence of heparan sulfate; red, I26P-IAPP in the presence of heparan sulfate. (B) TEM image of I26P-IAPP in the presence of heparan sulfate. An aliquot was removed for TEM analysis at the end of the reaction. (C) TEM image of I26P-IAPP in the absence of heparan sulfate. An aliquot was removed for TEM analysis at the end of the reaction. Scale bars represent 100 nm. Experiments were conducted with 20 mM Tris at pH 7.4, 25°C, without stirring.

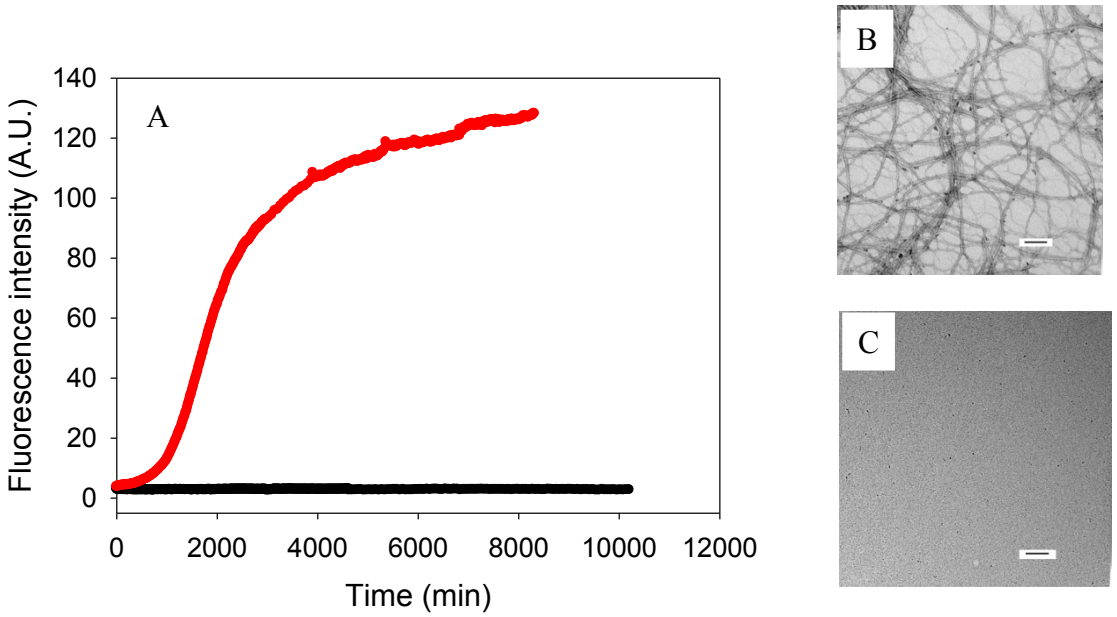

Figure 3.16 Amyloid formation by NMe-G24, NMe-I26-IAPP in the absence and presence of heparan sulfate monitored by thioflavin-T assays without HFIP.
(A) Black, NMe-G24, NMe-I26-IAPP in the absence of heparan sulfate; red, NMe-G24, NMe-I26-IAPP in the presence of heparan sulfate. (B) TEM image of NMe-G24, NMe-I26-IAPP in the presence of heparan sulfate. An aliquot was removed at the end of the reaction for TEM analysis. (C) TEM image of NMe-G24, NMe-I26-IAPP in the absence of heparan sulfate. An aliquot was removed at the end of the reaction for TEM analysis. Scale bars represent 100 nm. Experiments were conducted with 20 mM Tris at pH 7.4, 25°C, without stirring.

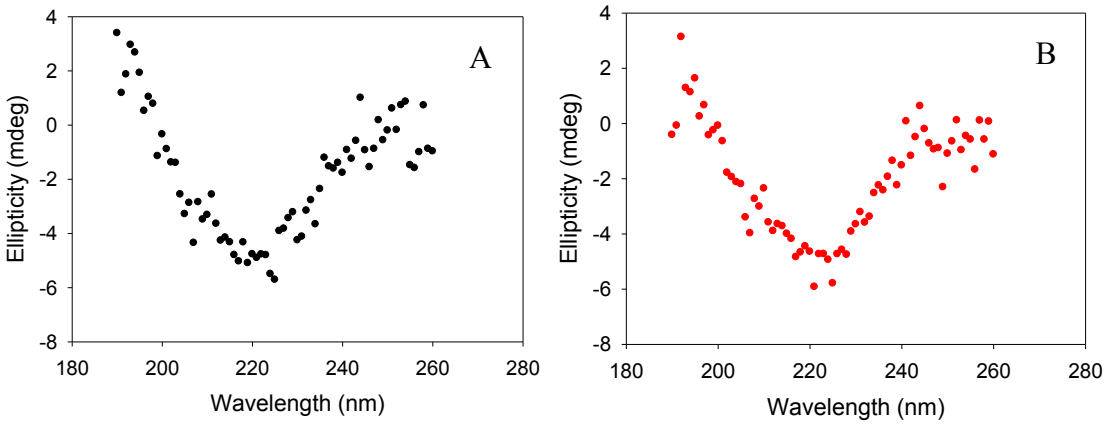

Figure 3.17 CD spectra of samples used for the FRET experiments displayed in Figure 3.4. (A) I26P-IAPP in the presence of fluorescein labeled heparin. (B) I26P-IAPP in the presence of fluorescein labeled heparin and thioflavin-T. Aliquots were removed at the end of each kinetic experiment displayed in Figure 3.4 and CD spectra were recorded.

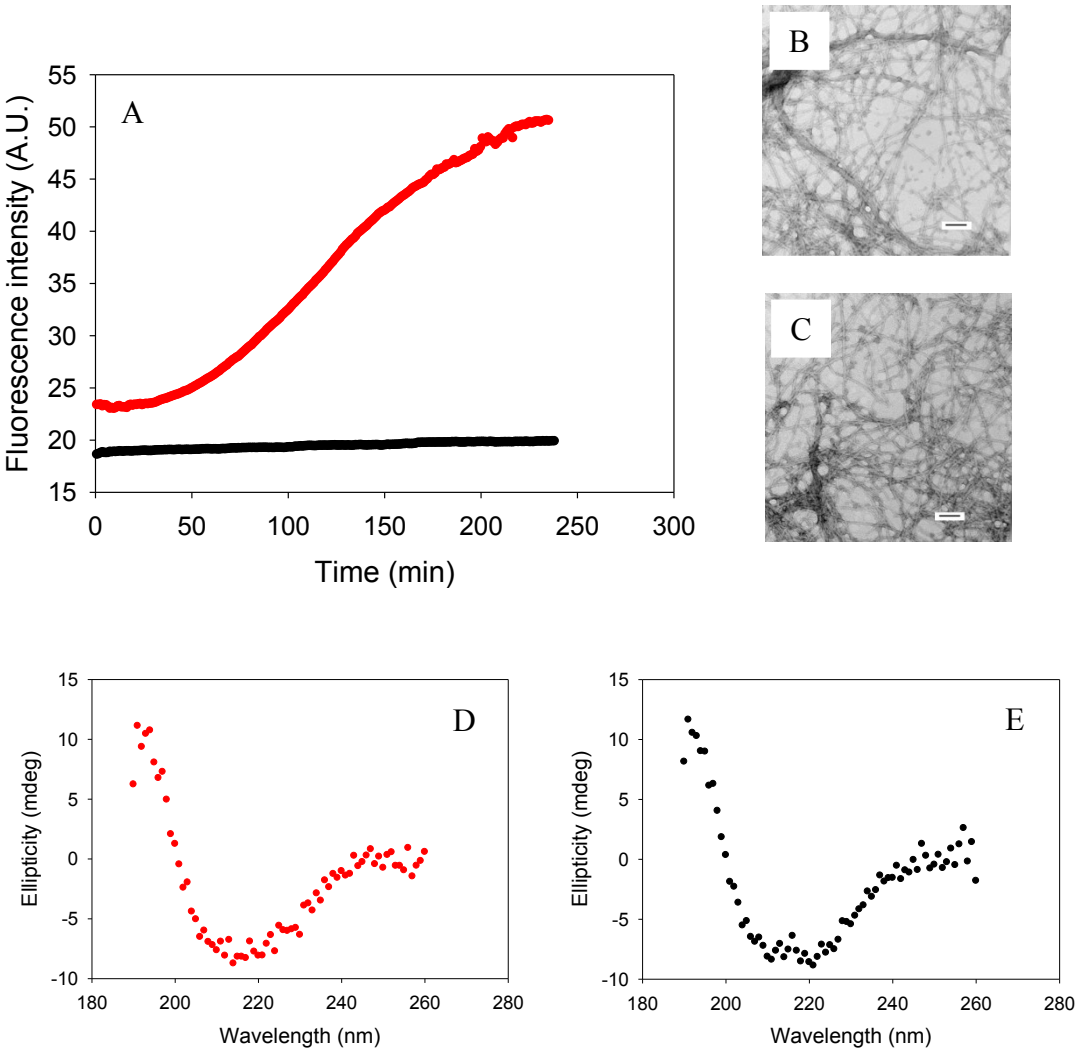

Figure 3.18 Heparan sulfate forms a complex with NMe-G24, NMe-G26-IAPP amyloid fibrils.

FRET between fluorescein labeled heparin (FLH) and thioflavin-T bound to NMe-G24, NMe-I26-IAPP amyloid fibers. (A) Kinetic profile of NMe-G24, NMe-I26-IAPP in the presence of FLH monitored by FRET between Thioflavin-T bound to amyloid fibrils and FLH. The fluorescence was measured using an excitation wavelength of 440 nm and an emission wavelegnth of 510 nm. Black, control experiment, NMe-G24. NMe-I26-IAPP in the presence of FLH without thioflavin-T; red, NMe-G24. NMe-I26-IAPP in the presence of FLH and thioflavin-T. (B) TEM image of NMe-G24, NMe-I26-IAPP in the presence of FLH and thioflavin-T. (C) TEM image of NMe-G24, NMe-I26-IAPP in the presence of FLH. (D) CD spectrum of NMe-G24, NMe-I26-IAPP in the presence of FLH and Thioflavin-T. (E) CD spectrum of NMe-G24, NMe-I26-IAPP in the presence of FLH. Aliquots were removed at the end of each reaction and used for TEM and CD. Scale bars represent 100 nm. The kinetic experiments were conducted in 20 mM Tris-HCl (pH 7.4), 2% HFIP (v/v) with continuous stirring at 25 °C. The concentration of NMe-G24, NMe-I26-IAPP was 16 μM. FLH was at 1.3 μM.

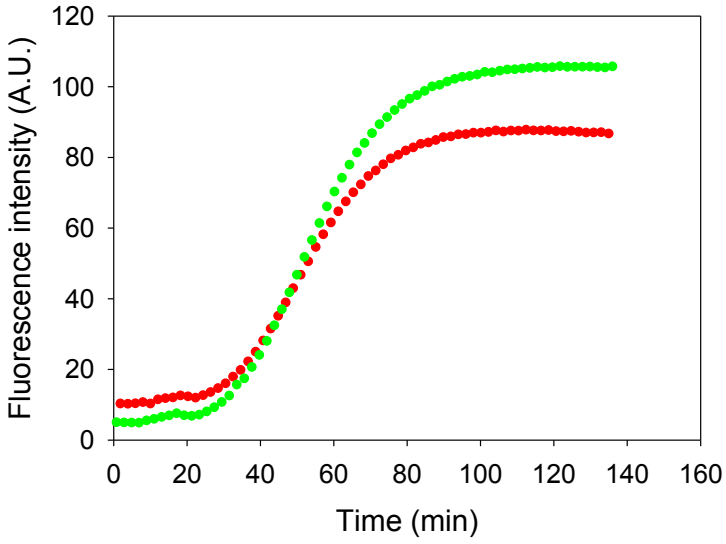

Figure 3.19 Amyloid formation of I26P-IAPP in the presence of fluorescein labeled heparin.
Comparison of kinetic profiles monitored by direct thioflavin-T fluorescence and by FRET from thioflavin-T to FLH. Red, I26P-IAPP in the presence of FLH monitored by the FRET signal, λ_{ex} = 440 nm, λ_{em} = 510nm; green, I26p-IAPP in the presence of FLH monitored by thioflavin-T fluorescence, λ_{ex} = 450 nm, λ_{em} = 485nm.

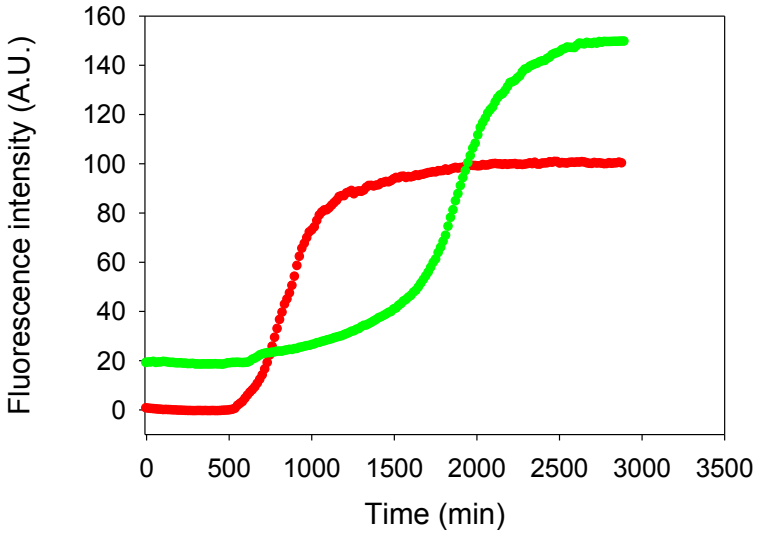

Figure 3.20 The dependence of amyloid formation by I26P-IAPP on the concentration of lipids.
Red, I26P-IAPP in the presence of 48 μM DOPG corresponding to 48 μM anionic sites; green, I26P-IAPP in the presence of 256 μM DOPG corresponding to 256 μM anionic sites in the assay. The kinetic experiments were conducted with 20 mM Tris-HCl (pH 7.4), no HFIP, no stirring at 25 °C. The concentration of I26P-IAPP was 16 μM.

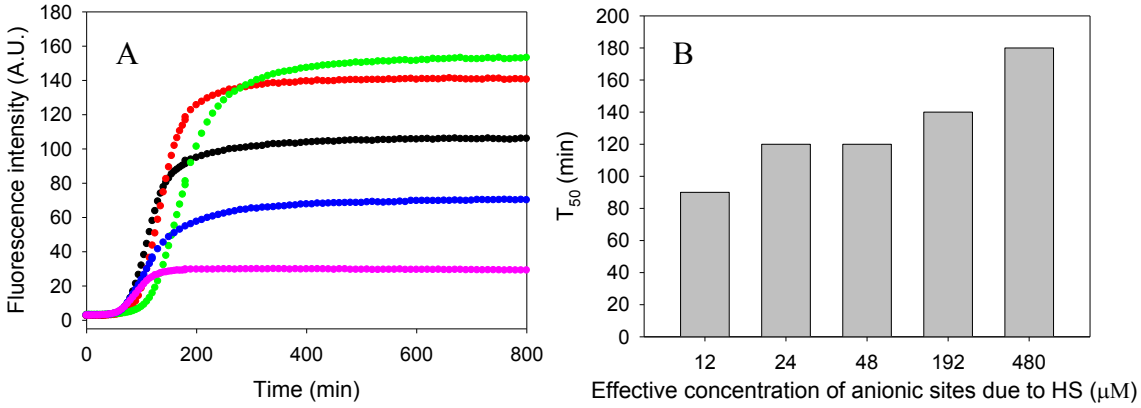

Figure 3.21 The dependence of I26P-IAPP amyloid formation on the concentration of heparan sulfate.
(A) Kinetic profiles of I26P-IAPP in the presence of heparan sulfate over the range of 0.24 μM to 9.7 μM corresponding to a total concentration of negatively charged sites of 12 μM to 480 μM. Experiments were conducted in 20 mM Tris-HCl (pH 7.4), no HFIP, no stirring at 25 °C. Black, I26P-IAPP in the presence of heparan sulfate at 0.97 μM; red, I26P-IAPP in the presence of heparan sulfate at 3.9 μM; green, I26P-IAPP in the presence of heparan sulfate at 9.7 μM; blue, I26P-IAPP in the presence of heparan sulfate at 0.49 μM; pink, I26P-IAPP in the presence of heparan sulfate at 0.24 μM. (B) Comparison of T_{50} for amyloid formation by I26P-IAPP at different concentrations of heparan sulfate.

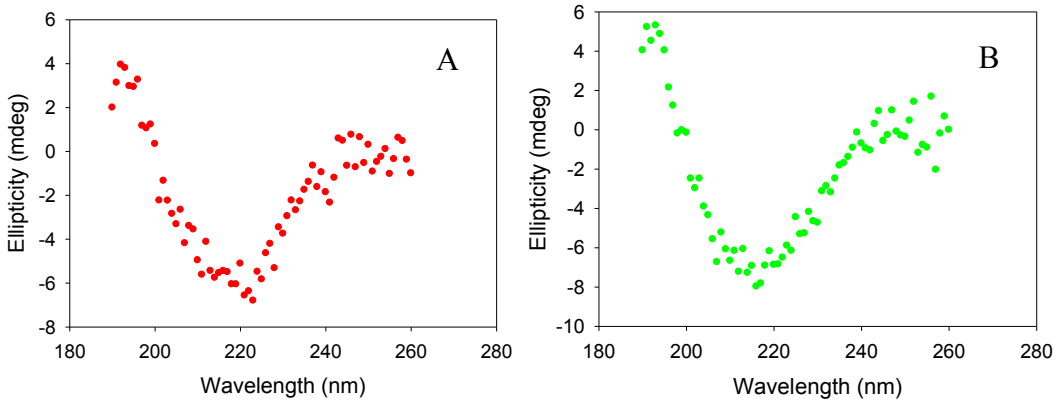

Figure 3.22 CD spectra of I26P-IAPP in the presence of chondroitin sulfate and dermatan sulfate.
(A) I26P-IAPP in the presence of chondroitin sulfate. (B) I26P-IAPP in the presence of dermatan sulfate. Aliquots were removed at the end of each thioflavin-T monitored kinetic experiment displayed in Figure 3.7 and the CD spectra were recorded.

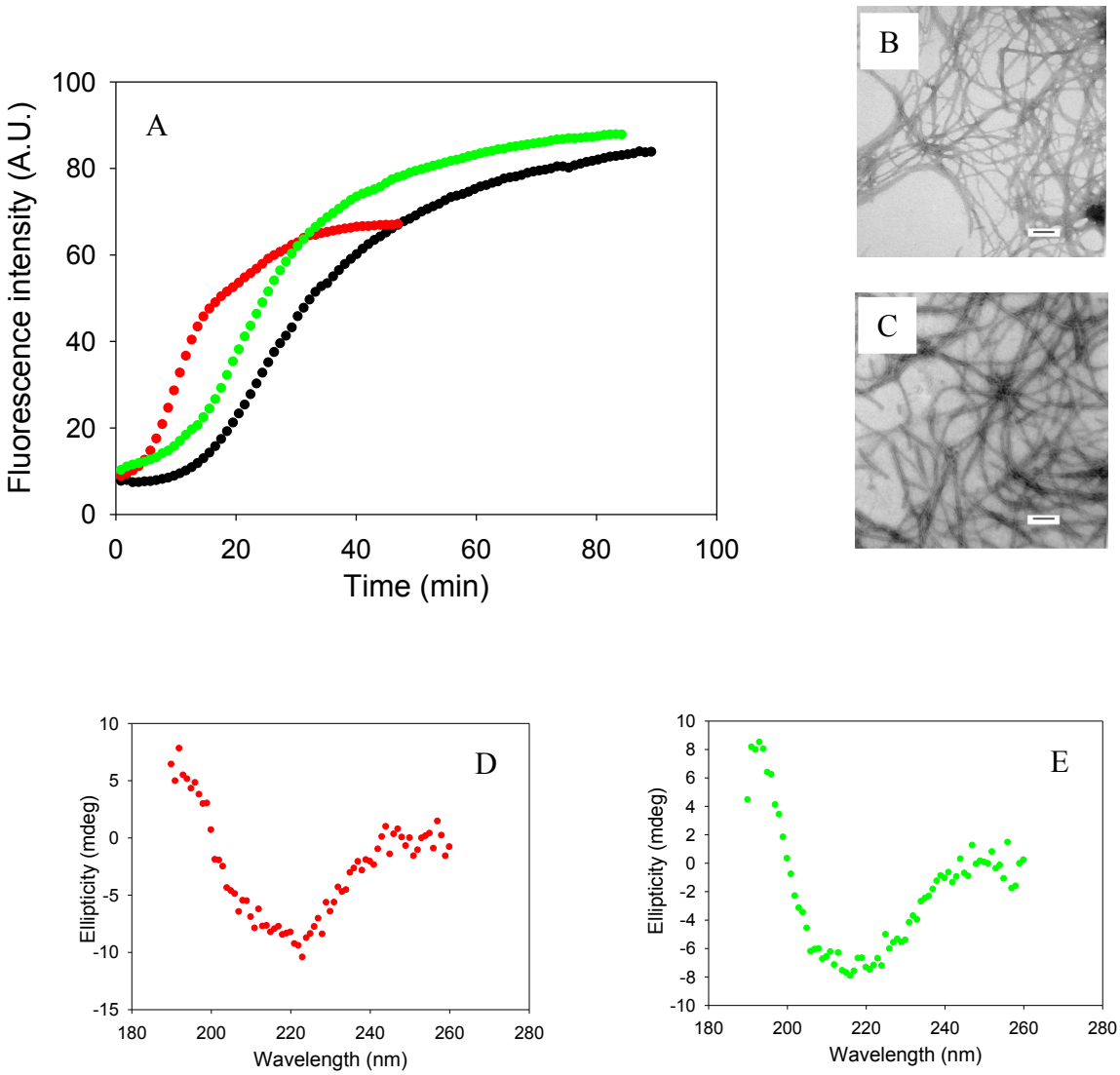

Figure 3.23 Comparison of amyloid formation by NMe-G24, NMe-I26-IAPP in the presence of different GAGs.
(A) Kinetic profiles. Black, NMe-G24, NMe-I26-IAPP in the presence of heparan sulfate; red, NMe-G24, NMe-I26-IAPP in the presence of chondroitin sulfate; green, NMe-G24, NMe-I26-IAPP in the presence of dermatan sulfate. (B) TEM image of NMe-G24, NMe-I26-IAPP in the presence of chondroitin sulfate. (C) TEM image of NMe-G24, NMe-I26-IAPP in the presence of dermatan sulfate. Scale bars represent 100 nm. (D) CD spectrum of NMe-G24, NMe-I26-IAPP in the presence of chondroitin sulfate. (E) CD spectra of NMe-G24, NMe-I26-IAPP in the presence of dermatan sulfate. Aliquots were removed at the end of each reaction for TEM and CD analysis. The kinetic experiments were conducted in 20 mM Tris-HCl (pH 7.4), 2% HFIP (v/v) with continuous stirring at 25 °C. The concentration of NMe-G24, NMe-I26-IAPP was 16 μM. The concentration of GAG was 1.3 μM.

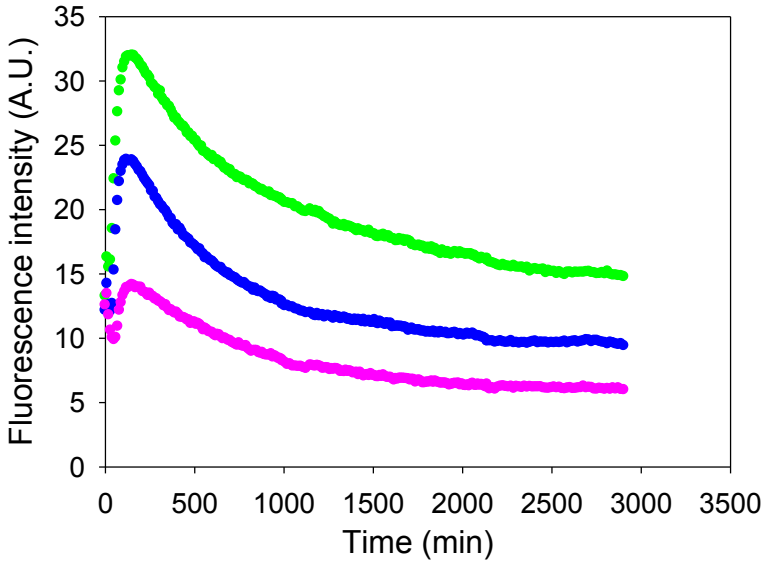

Figure 3.24 Heparan sulfate interferes with EGCG's ability to inhibit IAPP amyloid formation.
Green, a 1:5 mixture of IAPP and EGCG in the presence of heparan sulfate, EGCG was in 5 fold excess; blue, a 1:10 mixture of IAPP and EGCG in the presence of heparan sulfate, EGCG was in 10 fold excess; pink, a 1:20 mixture of IAPP and EGCG in the presence of heparan sulfate, EGCG was in 20 fold excess. EGCG was added at the beginning of each reaction. The same experimental conditions were used here as described in Figure 3.11.

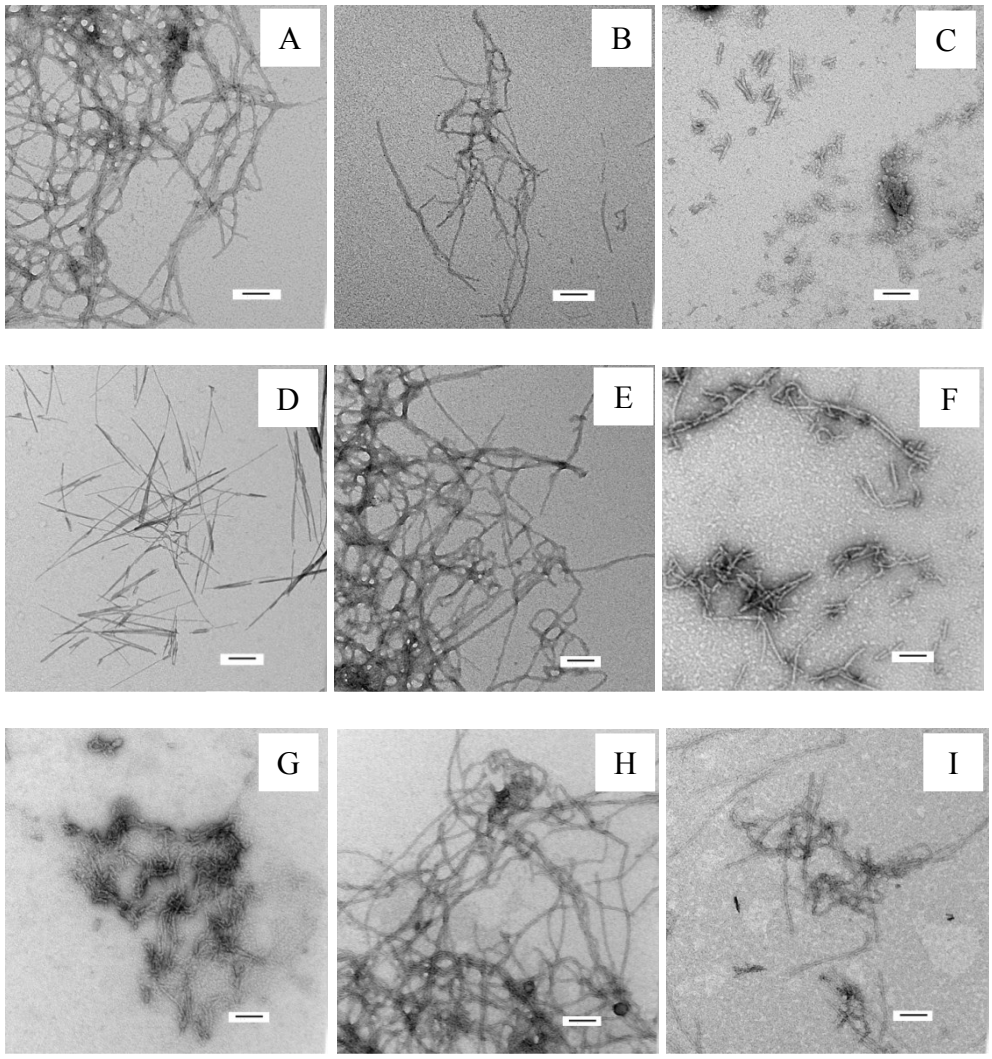

Figure 3.25 TEM images of IAPP amyloid inhibition experiments with high concentrations of EGCG in the presence of heparan sulfate.
The images are from samples removed at the end of the kinetic curves displayed in Figure 3.24. (A & B & C) TEM images of a 1:5 mixture of IAPP and EGCG in the presence of heparan sulfate, EGCG was in 5 fold excess. (D & E & F) TEM images of a 1:10 mixture of IAPP and EGCG in the presence of heparan sulfate, EGCG was in 10 fold excess. (G & H & I) TEM images of a 1:20 mixture of IAPP and EGCG in the presence of heparan sulfate, EGCG was in 20 fold excess. Scale bars represent 100 nm. Aliquots were removed at the end of each experiment for TEM analysis. Kinetic experiments were conducted with 20 mM Tris-HCl, no HFIP and no stirring at 25 °C. The concentration of IAPP was 16 μM. Heparan sulfate, when present, was at 1.3 μM. EGCG was added at the beginning of each experiment.

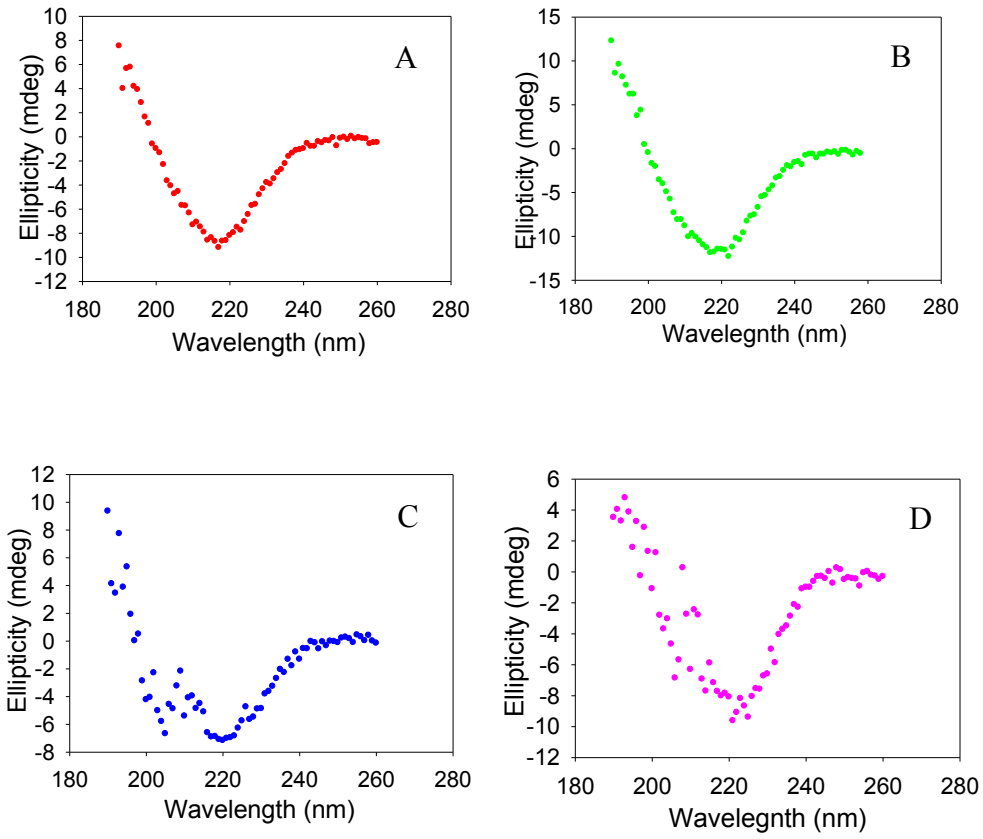

Figure 3.26 CD spectra of EGCG inhibition experiments displayed in Figure 3.11 and Figure 3.24.

(A) 1:1 mixture of IAPP and EGCG in the presence of heparan sulfate. (B) 1:5 mixture of IAPP and EGCG in the presence of heparan sulfate. (C) 1:10 mixture of IAPP and EGCG in the presence of heparan sulfate. (D) 1:20 mixture of IAPP and EGCG in the presence of heparan sulfate. EGCG was added at the beginning of each experiment. Aliquots were removed at the end of each reaction displayed in Figure 3.11 and Figure 3.24 and CD spectra were recorded.

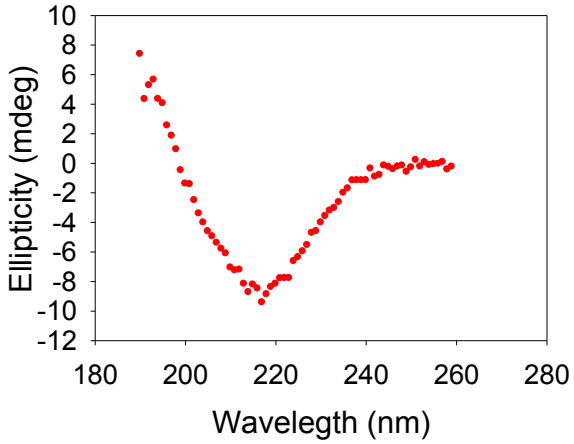

Figure 3.27 CD spectrum of the sample corresponding to the red curve displayed in Figure 3.12, the result of adding EGCG to a mixture of IAPP and HS.
An aliquot was removed at the end of the reaction and the CD spectrum was recorded.

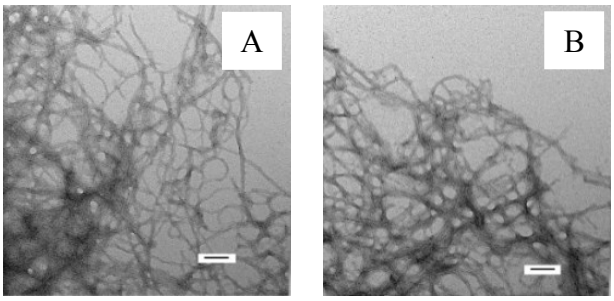

Figure 3.28 Additional TEM images for Figure 3.11 and Figure 3.12.
(A) TEM image of an aliquot removed at the end of the experiment represented by the red curve in Figure 3.11A. (B) TEM image of an aliquot removed at the end of the experiment represented by the red curve in figure 3.12A.

Chapter 4 Rationally Designed Inhibitors of Amyloid Formation by Human Amylin: A Balance Between Optimum Recognition and Reduced Amyloidgenicity

Abstract

Human islet amyloid polypeptide (hIAPP or amylin), a polypeptide hormone, forms fibrillar amyloid deposits in the pancreatic islets of Langerhans in type 2 diabetes (T2D). Islet amyloid is associated with reduced β-cell mass and is believed to contribute to T2D, and to the failure of islet transplantation. Thus inhibitors of hIAPP amyloid formation have therapeutic potential. However, there are no clinically approved inhibitors of islet amyloid and the mode of action of existing inhibitors is not well understood. The rat form of IAPP (rIAPP), does not form amyloid and is an inhibitor of hIAPP amyloid formation. Five of the six different residues in the sequence of rIAPP relative to hIAPP are located in the region of residues 20-29, and three of them are Pro residues, which are well know β-sheet breakers. rIAPP has been thought of as a natural example of a so-called "β-breaker" inhibitor; a molecule which combines a recognition element with an entity that inhibits β-sheet formation. Pramlintide (PM) is a peptide drug approved by the FDA as an adjunct to insulin therapy for both type 1 diabetes and T2D. PM was designed by introducing the three Pro substitutions found in rIAPP into hIAPP. The inhititory effects of PM on hIAPP amyloid formation have not been investigated. Here we examine the ability of a set of designed polypeptide analogs of hIAPP, including rIAPP and PM, in order to elucidate the factors which lead to effective peptide based inhibitors. Our results reveal, for this class of molecules, a balance between the amyloidogenicity of the inhibitory sequence on the one hand and its ability to recognize hIAPP on the other.

The work in this chapter has been written in a manuscript in preparation for Journal of the American Chemical Society. This chapter contains direct excerpts from that manuscript, which was written by me with the assistance of Prof. Daniel Raleigh, Dr. Ping Cao and Dr. Bela Ruzsicska.

4.1 Introduction

Amyloid formation plays a role in over 25 different human diseases including Alzheimer's disease, Parkinson's disease and type 2 diabetes (T2D).[153, 154] Islet amyloid polypeptide (IAPP or amylin) forms fibrillar amyloid deposits in the pancreatic islets of Langerhans in T2D.[155, 156] Islet amyloid is associated with reduced β-cell mass, and is believed to contribute to T2D,[80, 81, 212] and to the failure of islet transplantation.[98, 157] There are no clinically approved inhibitors of islet amyloid and the mode of action of existing inhibitors is not well understood. Here we examine the ability of a set of designed polypeptide analogs of human IAPP (hIAPP) in order to help elucidate the factors which lead to optimum peptide based inhibitors. Our work reveals, for this class of molecules, a balance between the amyloidogenicity of the inhibitory sequence on the one hand and its ability to recognize hIAPP on the other.

Mature hIAPP is a 37 residue hormone with a disulfide bond between Cys-2 and Cys-7 and an amidated C-terminus (Figure 4.1). It aggressively forms amyloid *in vitro* and is toxic to cultured pancreatic islet β-cells.[99] Rat IAPP (rIAPP) differs from hIAPP at six positions, does not form amyloid, is not toxic to cultured cells and is a moderately effective inhibitor of hIAPP amyloid formation *in vitro*.[145] Five of the six differences relative to hIAPP are located in the region of residues 20-29, which is believed to be an important amyloidgenic segment. rIAPP contains three prolines in this region (Pro-25, Pro-28 and Pro-29), which are well known β-sheet

breakers. The other differences between rIAPP and hIAPP involve the replacement of His-18, Phe-23 and Ile-26 in hIAPP with Arg-18, Leu-23 and Val-26 in rIAPP respectively (Figure 4.1). Thus rIAPP can be thought of as a natural example of a so-called "β-breaker" inhibitor; a molecule which combines a recognition element, in this case the N-terminal half to two thirds of the molecule, with an entity that inhibits β-sheet formation.

hIAPP normally functions as a complement to insulin in glucose homeostasis by suppressing postprandial glucagon secretion, helping regulate the rate of gastric emptying and suppressing food intake.[54-56, 137, 213] hIAPP is thus an attractive adjunct to insulin therapy, however, hIAPP aggregates in solution leading to difficulty in its formulation and storage. A soluble analog of hIAPP, Pramlintide (PM), is approved by the FDA as an adjunct to insulin therapy for both type 1 diabetes and T2D. PM was designed based on the sequence of hIAPP and rIAPP. The rationale was to substitute the proline residues found in rIAPP to render the human peptide non-amyloidgenic, but to retain its activity.[58] Therefore, Ala-25, Ser-28 and Ser-29 in hIAPP were replaced with prolines to generate PM (Figure 4.1).

rIAPP has been proposed to inhibit hIAPP amyloid formation by binding to early, potentially partially helical intermediates, through the N-terminal half to two thirds of the peptide and then preventing propagation of intermolecular β-sheet structure.[145] Peptide mapping studies have provided evidence that the initial hIAPP-hIAPP interaction occurs in the region centered near residue 15, and this region could be critical for hIAPP-rIAPP interactions, given their high sequence identity from residue 1 through 22.[214] Structural studies indirectly support a helical model, although other experiments suggest different initial modes of oligomerization of hIAPP.[177, 215, 216] PM is expected to be a better inhibitor of hIAPP than rIAPP if this model is correct since PM is more "human like" in the recognition region, but still contains the same β-

sheet breaker residues. Limited biophysical studies have been done on PM. Nonoyama et al have reported that PM is disordered as a monomer and that its aggregation is sensitive to pH.[217] There are no reported studies of the potential inhibition effects of PM on amyloid formation by hIAPP. Here, we compare the ability of PM and rIAPP as well as two mutants of PM, His18Arg pramlintide (H18R PM) and Phe23Leu pramlintide (F23L PM) to inhibit amyloid formation by the human peptide. The latter two mutations are chosen because they are the least conservative non-proline mutations between rIAPP and hIAPP. Our results also provide some clues as to the mechanism of hIAPP amyloid inhibitors, which should be useful for future rational peptide inhibitor design.

4.2 Material and methods

4.2.1 Peptide Synthesis

All peptides were synthesized using a CEM microwave peptide synthesizer on a 0.25 mmol scale utilizing 9-fluornylmethoxycarbonyl (Fmoc) chemistry. Solvents used were ACS-grade. The 5-(4'-fmoc-aminomethyl-3',5-dimethoxyphenol) valeric acid (PAL-PEG) resin was used to afford an amidated c-terminus. Fmoc-protected pseudoproline (oxazolidine) dipeptide derivatives were incorporated to improve the yield as previously described.[171] Standard Fmoc reaction cycles were used.[172] The first residue attached to the resin, all β-branched residues, all pseudoproline dipeptide derivatives and the residues directly following pseudoproline dipeptide derivatives were double-coupled. The peptides were cleaved from the resin through the use of standard trifluoroacetic acid (TFA) methods.

4.2.2 Peptide Oxidation and Purification

After cleavage, crude peptides were dissolved into 20% (v/v) acetic acid and then lyophilized. This was repeated several times before oxidation and purification to improve their solubility. The peptides were oxidized by 100% dimethyl sulfoxide at room temperature and then were purified via reverse-phase high-performance liquid chromatography (RP-HPLC) using a Vydac C18 preparative column.[173] Analytical HPLC was used to check the purity of the peptides before each experiment. The mass of the pure peptides was confirmed by ionization time-of-flight mass spectrometry. hIAPP, expected 3903.6, observed 3904.6; rIAPP, expected 3921.3, observed 3921.6; PM, expected 3949.4, observed 3949.2; H18R PM, expected 3969.4, observed 3967.1; F23L PM, expected 3916.4, observed 3915.4.

4.2.3 Sample Preparation

Stock solutions of each peptide were prepared by dissolving into 100% hexafluoroisoproponal (HFIP) at 1.6 mM. Stock solutions were filtered using 0.45 μM Acrodisc syringe filter with a GHP membrane and the required amount was lyophilized overnight to remove HFIP. Dry peptide was then dissolved into Tris-buffer for the fluorescence assays.

4.2.4 Fluorescence Assays

The kinetics of amyloid formation were monitored using thioflavin-T binding assays conducted with no cosolvent and no stirring at 25°C. Fluorescence measurements were performed using a Beckman Coulter DTX 880 plate reader with a multimode detector using an excitation wavelength of 430 nm and an emission wavelength of 485 nm. Solutions were prepared by dissolving dry peptide into Tris-HCl buffer and thioflavin-T solution immediately

before the measurement. The final concentrations were 16 μM hIAPP, 32 μM thioflavin-T in 20 mM Tris-HCl (pH 7.4) and various amounts of the inhibitors.

4.2.5 Transmission Electron Microscopy (TEM)

TEM images were collected at the Life Science Microscopy Center at the State University of New York at Stony Brook. 15 μL aliquots of the samples used for the kinetic studies were removed at the end of each experiment, blotted on a carbon-coated 300-mesh copper grid for 1 min and then negatively stained with saturated uranyl acetate for 1 min.

4.2.6 Mass Spectroscopy Experiments

Peptides were incubated in 20 mM Tris-HCl buffer at pH 7.4 until amyloid formed. Samples were then centrifuged at 17500g for 45 min. Pellets were collected and rinsed with DDI water twice. In each rinse, samples in DDI water were centrifuged at 17500g for 30 min. Final pellets collected were depolymerized in 100% (v/v) HFIP and then lyophilized for 20 hours.

The peptide solutions are analyzed by LC-MS-UV using an Agilent 1260 HPLC and an Agilent G6224A oaTOF mass spectrometer. The HPLC method uses a Kinetex C18 column; 100Å, 2.6μm, 100x2.1mm, (Phenomenex) at 35°C and 0.55mℓ/min. The HPLC solvents were A – H_2O(0.05%AceticAcid, 0.05%TFA) and B – CH_3CN(0.05%AceticAcid, 0.05%TFA). The HPLC solvent gradient method consisted of the following: t=0-1', B=10%; t=1-5', B=10-30%; t=5-45', B=30-50%; t=45-52', B=50-95%.

The mass spectrometer was tuned and calibrated in the 2GHZ ExtDynRange 3200 state. The ionization source was electrospray ionization in the positive mode. The ESI source was operated at 325°C with N_2 flow at 12ℓ/min and nebulizer pressure at 55psi. Mass spectra were

acquired at 4Hz profile mode, in the range m/*z* = 300-3200 with internal calibration using 4 calibration standards.

UV chromatograms were acquired with a diode array detector operating with 5Hz acquisition rate, 2nm bandwidth in the range 210-500nm. Specific channels used were 215 and 280nm.

The ESI positive mass chromatograms were integrated and averaged mass spectra were acquired from the integrated peaks with background subtraction. The mass spectra of the target peptides were observed in predominantly the +3 and +4 charge states. The resolution of the mass spectrometer in the described state and in this m/*z* range is ~13,000. This resolution allows the isotopic distribution of the peptide m/*z* peaks in these charge states to be fully resolved. These mass spectra are deconvoluted using the Agilent Resolved Isotope Deconvolution algorithm. In this way, the monoisotopic, neutral masses of the peptides are determined with an accuracy of 20ppm.

4.3 Results and Discussion

4.3.1 PM is a Better Inhibitor than rIAPP, But Has Less Effect on the Final Fibril Structure.

The ability of rIAPP and PM to inhibit amyloid formation by hIAPP were compared using thioflavin-T fluorescence assays. Thioflavin-T is a dye whose quantum yield is increased upon binding to amyloid fibrils, and it provides a convenient probe to monitor amyloid formation. The dye does not perturb the kinetics of hIAPP amyloid formation under the conditions used here. We first tested mixtures of hIAPP and rIAPP. The kinetic curves measured at different ratios of the two peptides are shown in Figure 4.2 The X-axis is presented as reduced time; time divided by T_{50} of hIAPP, where T_{50} is the time required to reach half of the maximum fluorescence

intensity in the assay. No increase in fluorescence intensity of a sample of rIAPP was detected during the time course of the experiment. The effects of rIAPP amyloid formation are dose dependent, as previously reported.[145] At low concentrations of rIAPP (where hIAPP and rIAPP are at a 1 to 1, or a 1 to 2 ratio), rIAPP shows a slight inhibitory effect on amyloid formation by hIAPP, in agreement with earlier studies.[145] T_{50} was increased by a factor of only 1.2 for the 1 to 1 ratio and by a factor of 1.4 for the 1 to 2 ratio (rIAPP is in 2 fold excess). When the concentration of rIAPP is increased to a 5 fold excess, a more significant effect was observed as indicated by a 2.2 fold longer T_{50}. This parameter increased by a factor of 3.5 when the concentration of rIAPP is increased to give a 10 fold excess of hIAPP in the mixture. A decrease in the final fluorescence was observed as the concentration of rIAPP was increased. This is consistent with fewer fibrils being formed by hIAPP, or with the formation of fibrils with reduced capacity to bind thioflavin-T, or with a lower quantum yield of the bound thioflavin-T. Since the fluorescence results come from fibril bound thioflavin-T, instead of an intrinsic probe of the fibrils, the values are dependent on how well the dye binds, and this can sometimes give misleading results. Therefore, we collected TEM images at the end of each kinetic experiment. As shown in Figure 4.3 and Figure 4.9, TEM confirmed that rIAPP does not aggregate during the time course of the experiment. Images of mixtures of hIAPP and rIAPP showed changes in morphology as the concentration of rIAPP increased. At 1 to 1 ratio, fibrils with typical hIAPP amyloid morphology were observed, while thinner and shorter fibrils were observed in the presence of 10 fold excess rIAPP. These results confirm the conclusion of prior studies that rIAPP increases the T_{50} of hIAPP amyloid formation, and also reduces the amounts of amyloid fibrils formed and/or changes their morphology. Our results are consistent with previous findings conducted in buffers which contain 2% HFIP, that rIAPP does not form amyloid under these

conditions, inhibits amyloid formation by hIAPP, and modifies fibril morphology.[145] The results shown here confirm that the behavior of rIAPP is not a consequence of the presence of the organic cosolvent.

We next tested the effect of PM using this assay. PM did not form amyloid during the time course of the study under the conditions used, as indicated by a flat fluorescence curve (Figure 4.2) and TEM (Figure 4.9). Inhibition of hIAPP amyloid formation was observed at all ratios tested and the inhibition efficiency of PM was dose dependent. PM is more effective at inhibiting the aggregation of hIAPP than rIAPP. An equimolar amount of PM increased T_{50} of hIAPP amyloid formation by a factor of 1.9, compared to the more modest factor of 1.2 observed for rIAPP. T_{50} was further increased to a factor of 2.7 when PM was in 2 fold excess and to 3.9 when PM was in 5 fold excess. When the ratio of hIAPP and PM was 1 to 10, the T_{50} of hIAPP amyloid formation was increased by 5.6 fold. For comparison, rIAPP increases T_{50} by a factor of 3.5 at this ratio.

The final fluorescence intensity of the PM hIAPP mixtures did not change significantly, even in the presence of 10 fold excess of PM. In addition, the fibrils formed at all ratios showed typical IAPP amyloid fibril structure, and no PM induced morphology change was observed in contrast to the effects detected with rIAPP (Figure 4.3). These results demonstrate that PM is more efficient than rIAPP at inhibiting amyloid formation by hIAPP in terms of the kinetics, but it does not cause any detectable change in the fibril morphology at this level of resolution.

There are several possible explanations for the lack of a detectable effect of PM on fibril morphology. PM could have a higher amyloidgenic potential than rIAPP due to its higher sequence similarity to hIAPP. In particular, the replacement of R18 in rIAPP by the human residue should increase the tendency to aggregate at pHs above the pKa of His.[129, 131] Thus, it is

possible that the amyloid fibrils formed in the mixture of hIAPP and PM are a combination of hIAPP and PM. It is also possible that hIAPP fibrils induce the formation of PM fibrils and any fibrils that may be formed by PM have a morphology similar to hIAPP amyloid fibrils. Alternatively, PM could transiently interact with hIAPP and ultimately end up in the soluble phase. Either of these scenarios might contribute to the different effects observed between rIAPP and PM on the morphology of the amyloid formed.

To test if rIAPP or PM are incorporated in the fibrils formed by mixtures of rIAPP or PM with hIAPP, we conduct mass spectrum experiments. We centrifuged the aggregates formed by mixtures of rIAPP or PM with hIAPP respectively and identified the peptides in the pellets by redissolving them and conducting LC-MS studies. Control experiments were conducted, in which samples of pure hIAPP, pure rIAPP and pure PM were incubated. A much stronger peak was observed from the pellet formed in the hIAPP control experiments than from PM or rIAPP control studies, consistent with the fact that hIAPP forms amyloid during the time course of the experiments while the other two peptides do not. Weak peaks were detected for PM and rIAPP which are probably due to residual supernatant in the "pelleted" samples. For 1 to 1 mixtures of hIAPP with the other peptides, we observed only weak peaks due to PM and rIAPP from the pellets with intensities similar to that observed in control experiments, suggesting that neither PM nor rIAPP was incorporated into the fibrils formed and suggesting that the fibrils observed were mainly made up of hIAPP. When PM or rIAPP were in 10 fold excess, only a weak peak due to rIAPP was detected from the pellet in the mixture with hIAPP, but a strong peak was observed for PM in the pellet formed by the hIAPP PM mixture. The PM peak had a similar intensity to the hIAPP peak for this case (Figure 4.4). There are several plausible explanations for this result. hIAPP and PM might coaggregate into mixted fibrils and thus both be found in the

pellet. Alternatively, the two might independently aggregate and be sedimented into a pellet. The fact that samples of pure PM do not show appreciable pelletable material argues against this scenario, but does not formally rule out situations where human fibrils promote aggregation of PM into fibrils that are largely composed of PM. Seeding experiments show that hIAPP fibrils do not seed amyloid formation by PM, indicating that it is unlikely that hIAPP fibrils directly promote formation of independent PM fibrils under these conditions (Figure 4.10).

4.3.2 Mutations of PM Make its Behavior More rIAPP-like.

We next examined two point mutants of PM, chosen to make their sequences more rIAPP-like, in order to study the contribution of these sites to the difference in the ability of rIAPP and PM to inhibit hIAPP amyloid formation.

There are three differences between rIAPP and hIAPP, in addition to the three prolines. His-18 and Phe-23 in hIAPP are replaced by Arg and Leu respectively in rIAPP (Figure 4.1). These are less conservative changes than the third substitution which is an Ile-26 to Val mutation. We focused on the least conservative replacements, H18R and F23L. Arg is protonated and charged at pH 7.4 while His is largely deprotonated, thus a H18R replacement changes the charge distribution of the peptide. Electrostatic interactions are believed to play an important role in amyloid formation,[200] and hIAPP amyloid formation is pH dependent.[129, 131] The F23L substitution replaces an aromatic residue with an aliphatic sidechain and this substitution has been shown to increase the lag time of hIAPP by a factor of two.[135] In contrast, the Ile to Val substitution is more conservative, replacing one β-branched hydrophobic amino acid with another. Green et al studied mutants of rIAPP with substitution of residues from hIAPP by using variants with a free C-teimini. They did not test the ability of these molecules to inhibit hIAPP amyloid formation, but they reported that all mutants of rIAPP including PM*, H18R PM* and

F23L PM* were able to form amyloid with a slightly different morphology than hIAPP. Here we use a star to denote the variants with free C-termini. PM* was reported to form amyloid in 10 days, faster than F23L PM* and H18R PM* which formed amyloid after two weeks and three or four weeks respectively.[218] The peptides they used are not C-terminally amidated and variants with this modification have been shown to behave differently than the physiologically relevant amidated form.[131, 219] Never the less, their results indicate that a higher sequence similarity to the human analog leads to higher amyloidgenic potential.

The kinetics of amyloid formation by mixtures of hIAPP with the two mutants are shown in Figure 4.5. Both H18R PM and F23L PM did not aggregate during the time course of the study, as indicated by their flat fluorescence time courses and by TEM (Figure 4.5, 4.6 and 4.7). Dose dependent inhibition effects were observed for both mutants. Both PM mutants behaved more like rIAPP than like PM in the sense that they were less effective inhibitors than PM. The inhibitory effects of H18R PM and F23L PM were almost the same in terms of their effects on the value of T_{50} (Figure 4.8). As the concentration of peptide was increased, H18R PM showed a more obvious effect on the final thioflavin-T fluorescence intensity than F23L PM (Figure 4.5) and less dense matts of fibrils were observed in the TEM images (Figure 4.6, 4.7). However, neither of the mutants changed the fibril morphology as drastically as rIAPP did as judged by TEM. All of the TEM images collected with either mutant, at different ratios, showed typical hIAPP amyloid fibril structure (Figure 4.6, 4.7).

4.4 Conclusions

The effects of the four peptide inhibitors on the value of T_{50} for hIAPP amyloid formation are summarized in Figure 4.8. Our results showed that PM is more efficient than rIAPP in

inhibiting amyloid formation by hIAPP, however, in contrast to rIAPP, it does not affect the morphology of fibrils at a level detectable by TEM. Our mass spectroscopy analysis of the amyloid fibrils formed by mixtures of PM with hIAPP and rIAPP with hIAPP argues that PM interacts more strongly with hIAPP than rIAPP does. One possible explanation is that PM is incorporated into the fibrils under these conditions while rIAPP is not.

These results argue that a higher sequence similarity to hIAPP leads to a non-amyloidgenic peptide being a better inhibitor of hIAPP amyloid formation, likely due to more efficient sequence recognition. rIAPP and the two mutants of PM, H18R PM and F23L PM, are less effective inhibitors than PM, consistent with this hypothesis, however, the correlation is not perfect since the two PM single mutants do not outperform rIAPP even though they have a higher sequence identity to hIAPP. This suggests that the two positions, residue 18 and 23, play important roles in the inhibitor hIAPP interaction.

Middleton et al has constructed a model of how rIAPP inhibits hIAPP amyloid formation based on 2DIR studies conducted under different conditions where both peptides were present at higher concentrations. They reported that rIAPP first blocks the formation of the C-terminal β-sheet which explains the increased lag time. rIAPP then loses this effect and the recognition sequence in rIAPP forms its own β-sheet.[220] The resolution of the methods employed here does not allow one to determine if PM forms its own fibrils or is incorporated into the hIAPP fibrils.

A trade-off exists between more efficient recognition of the target protein and the higher amyloidgenicity attributed to higher sequence similarity. An optimum balance should lead to the best inhibition efficiency. Having a too low sequence identity may prevent the peptide from effectively interacting with the target peptide, while having too high a similarity may lead to mixed fibrils formed by the designed inhibitor and the target peptide. PM appears to be nearly

balanced between these effects. This does not mean than PM is the optimum inhibitor. Other variants of hIAPP which target different residues can have larger effects on hIAPP amyloid formation presumably because the other sites are more important.

Data with other sets of peptides support the notation of a trade-off between recognition and β-sheet inhibition. For example, data on a set of G24P, I26P analogs support this conjecture.[121, 122, 124] The double mutant is a moderately effective inhibitor, but each single mutant is more effective. In this case, the single site mutations are sufficient to reduce amyloidogenicity and the higher sequence identity presumably leads to better recognition of the human sequence. The fact that the double proline mutant is a less effective inhibitor of wild type amyloid formation than either single mutant suggests that they may interact with hIAPP in a more complicated manner than simply through the region with helical propensity. All these peptides in this family are identical between residues 1 to 23 which encompasses the region from residues 5-19 that NMR has identified as having a tendency to preferentially sample the helical region of the Ramachandran plot.[180] Hence, they should have similar abilities to target the helical region.

4.5 Figures

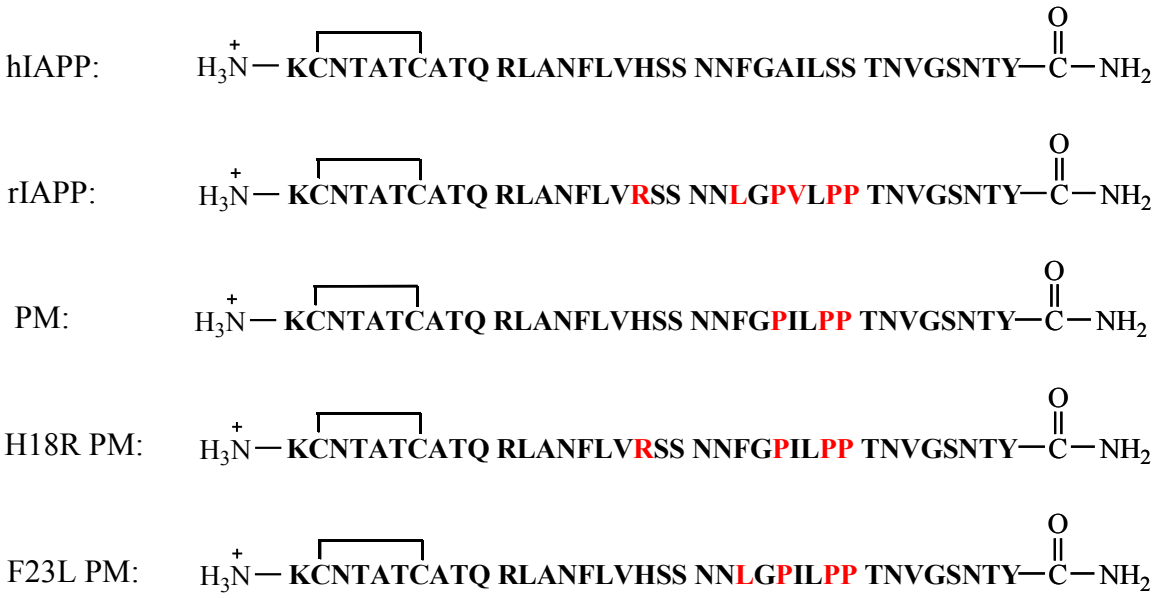

Figure 4.1 Sequence of hIAPP, rIAPP, PM, H18R PM and F23L PM.
Each peptide contains a disulfide bond connecting Cys 2 and Cys 7 and has an amidated C-terminus. Residues which differ from hIAPP are colored red.

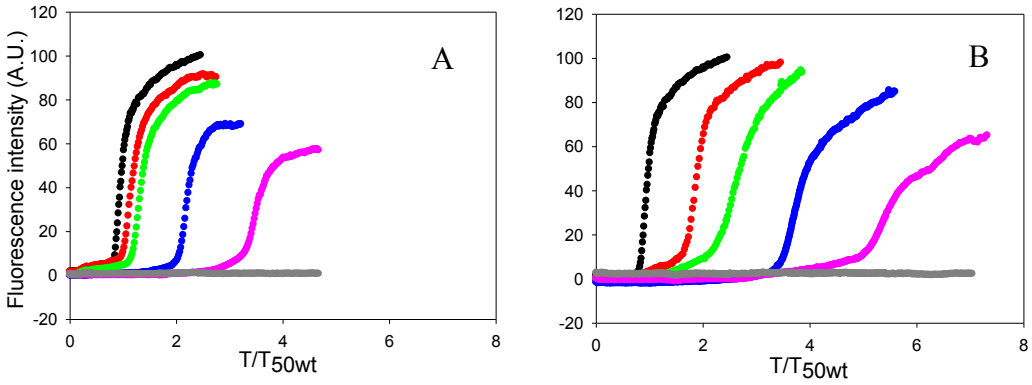

Figure 4.2 Pramlintide (PM) is a more effective inhibitor than rIAPP.
(A) The kinetics of hIAPP amyloid formation in the presence of rIAPP monitored by thioflavin-T fluorescence assays. Black, hIAPP; red, a 1:1 mixture of hIAPP and rIAPP; green, a mixture of hIAPP and rIAPP at a 1 to 2 ratio; blue, a mixture of hIAPP and rIAPP at a 1 to 5 ratio; pink, a mixture of hIAPP and rIAPP at a 1 to 10 ratio; grey, 160 μM rIAPP. (B) The kinectics of hIAPP amyloid formation in the presence of PM monitored by thioflavin-T fluorescence essays. The same color coding is used as in panel A. Experiments were conducted in 20 mM Tris-HCl (pH 7.4), without stirring at 25 °C. The concentration of hIAPP was 16 μM.

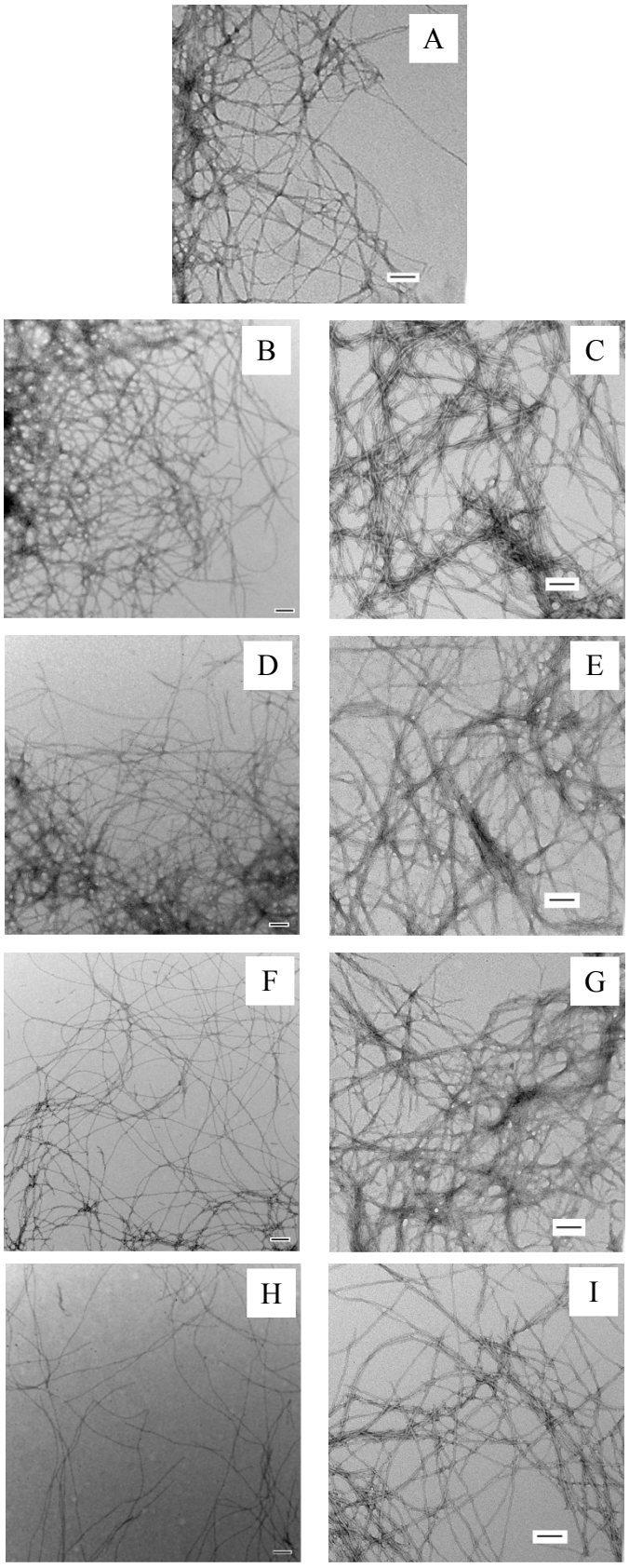
A
B
C
D
E
F
G
H
I

Figure 4.3 Comparison of the final products of the reaction shown in Figure 4.2.
(A) TEM image of hIAPP. (B) TEM image of a 1:1 mixture of hIAPP and rIAPP. (C) TEM image of a 1:1 mixture of hIAPP and PM. (D) TEM image of a 1:2 mixture of hIAPP and rIAPP. (E) TEM image of a 1:2 mixture of hIAPP and PM. (F) TEM image of a 1:5 mixture of hIAPP and rIAPP. (G) TEM image of a 1:5 mixture of hIAPP and PM. (H) TEM image of a 1:10 mixture of hIAPP and rIAPP. (I) TEM image of a 1:10 mixture of hIAPP and PM. All images were collected at the end of corresponding experiments shown in Figure 4.2. Scale bars represent 100 nm.

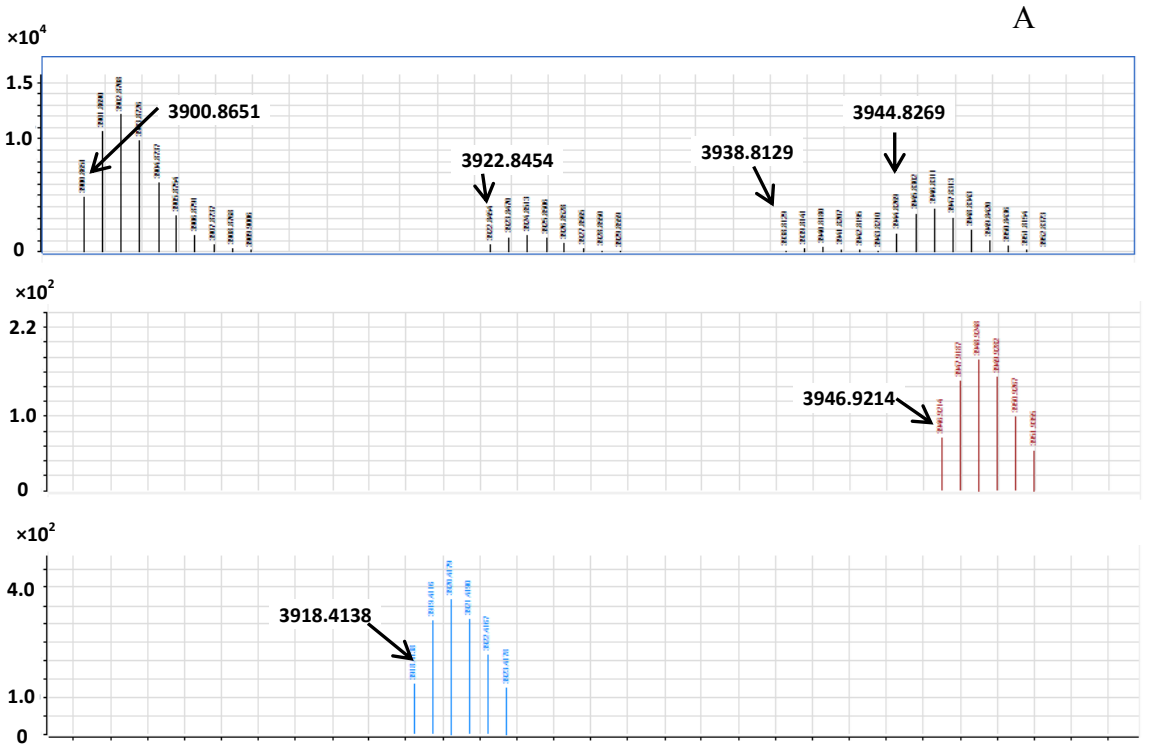
A
×10^4
1.5
1.0
0
3900.8651
3922.8454
3938.8129
3944.8269
×10^2
2.2
1.0
0
3946.9214
×10^2
4.0
1.0
0
3918.4138

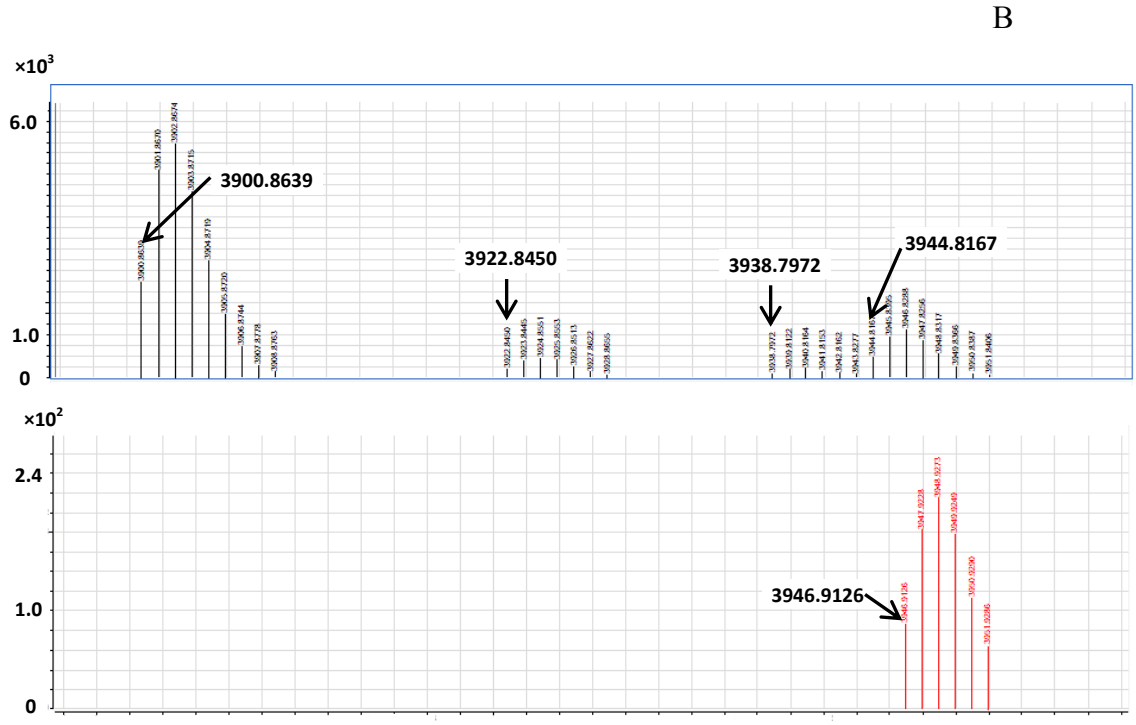
B
×10^3
6.0
1.0
0
3900.8639
3922.8450
3938.7972
3944.8167
×10^2
2.4
1.0
0
3946.9126

C

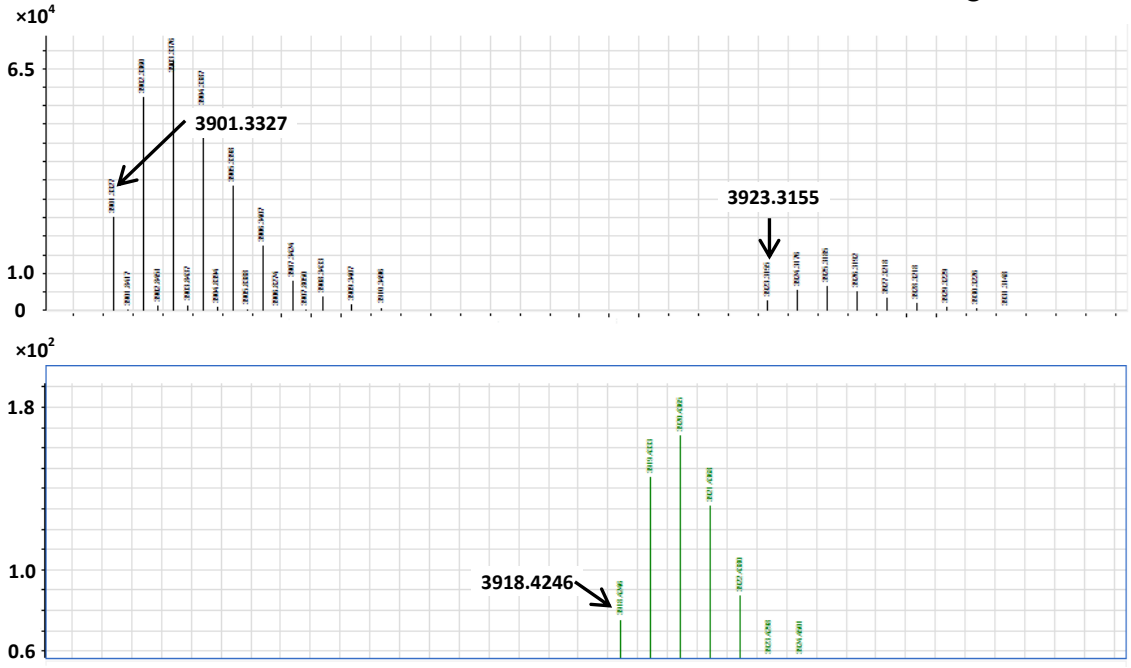
×10^4
6.5
1.0
0
3901.3327
3923.3155
×10^2
1.8
1.0
0.6
3918.4246

D

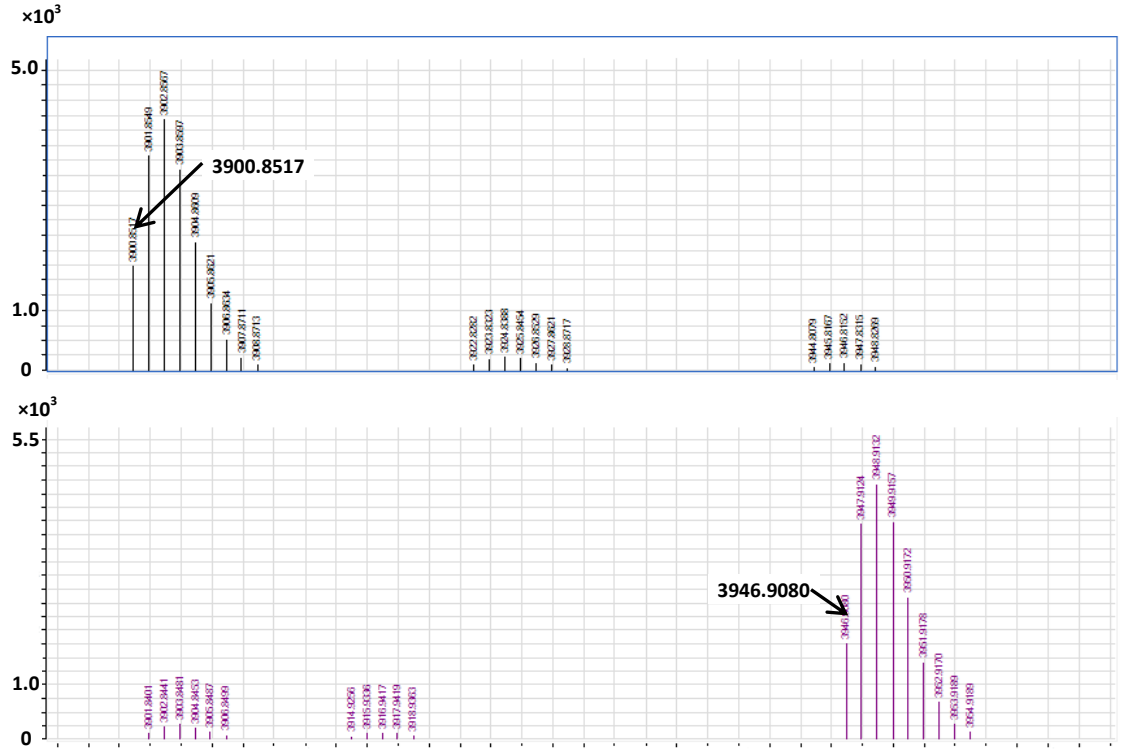
×10^3
5.0
1.0
0
3900.8517
×10^3
5.5
1.0
0
3946.9080

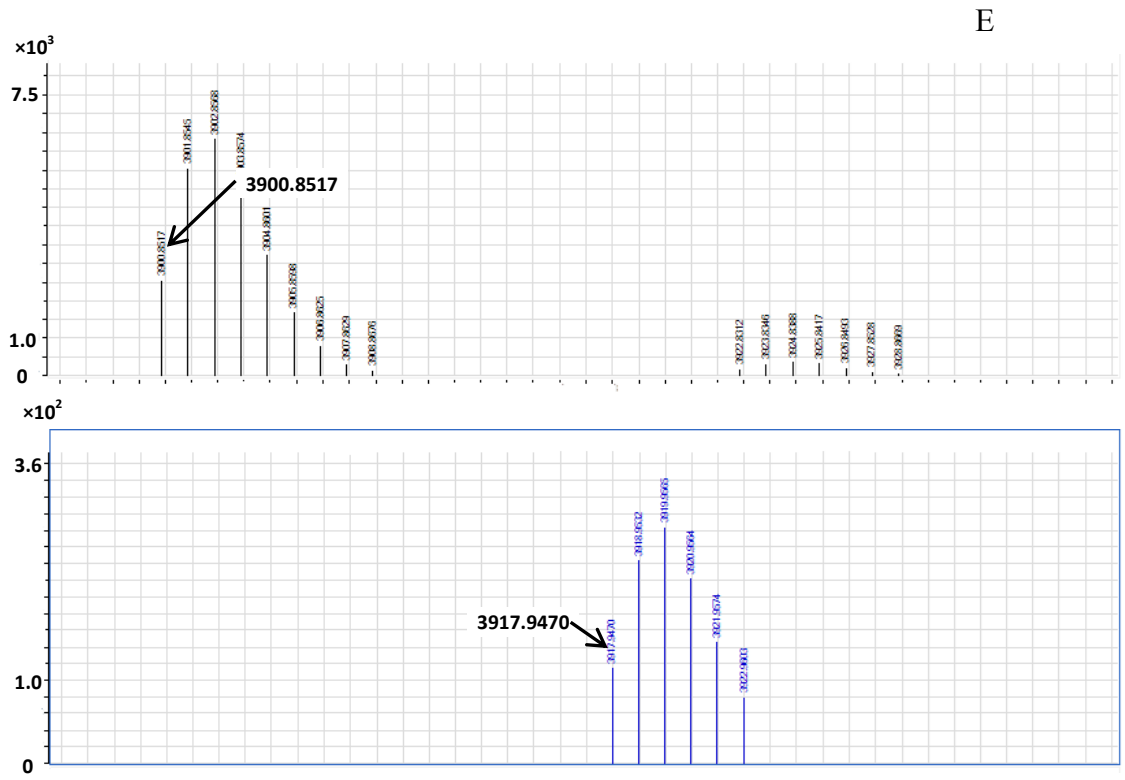

Figure 4.4 Results of mass spec experiments.
(A) Results of control experiments. hIAPP, PM and rIAPP were incubated separately. Black, hIAPP; brown, PM; light blue, rIAPP. (B) Results of a 1 to 1 mixture of hIAPP and PM. Black, hIAPP; red, PM. (C) Results of a 1 to 1 mixture of hIAPP and rIAPP. Black, hIAPP; green, rIAPP. (D) Results of a 1 to 10 mixture of hIAPP and PM. PM was in 10 fold excess. Black, hIAPP; pink, PM. (E) Results of a 1 to 10 mixture of hIAPP and rIAPP. rIAPP was in 10 fold excess. Black, hIAPP; dark blue, rIAPP.

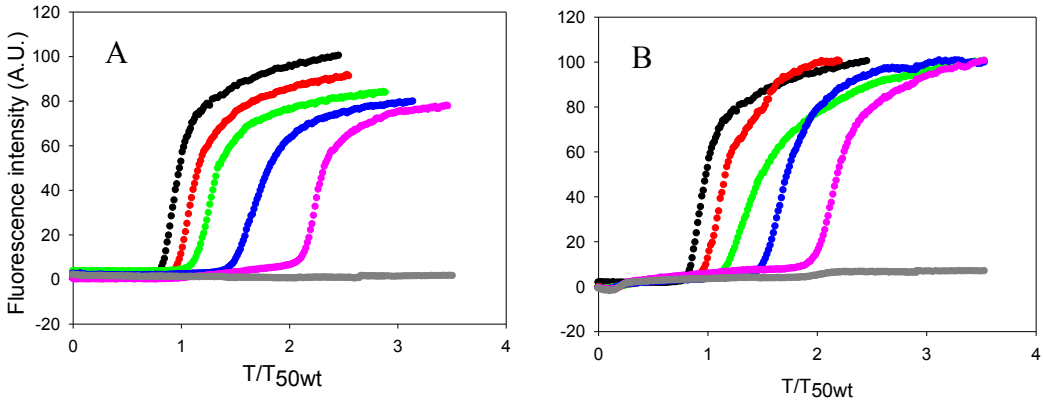

Figure 4.5 Effects of replacing His-18 and Phe-23 in PM by the corresponding residues of rIAPP.
(A) The kinetics of hIAPP amyloid formation in the presence of H18R PM monitored by thioflavin-T fluorescence assays. Black, hIAPP; red, a 1:1 mixture of hIAPP and H18R PM; green, a mixture of hIAPP and H18R PM at a 1 to 2 ratio; blue, a mixture of hIAPP and H18R PM at a 1 to 5 ratio; pink, a mixture of hIAPP and H18R PM at a 1 to 10 ratio; grey, 160 μM H18R PM. (B) The kinetics of hIAPP amyloid formation in the presence of F23L PM monitored by thioflavin-T fluorescence essays. The same color coding is used here as in panel A. The kinetic experiments were conducted in 20 mM Tris-HCl (pH 7.4), without stirring at 25 °C. The concentration of hIAPP was 16 μM.

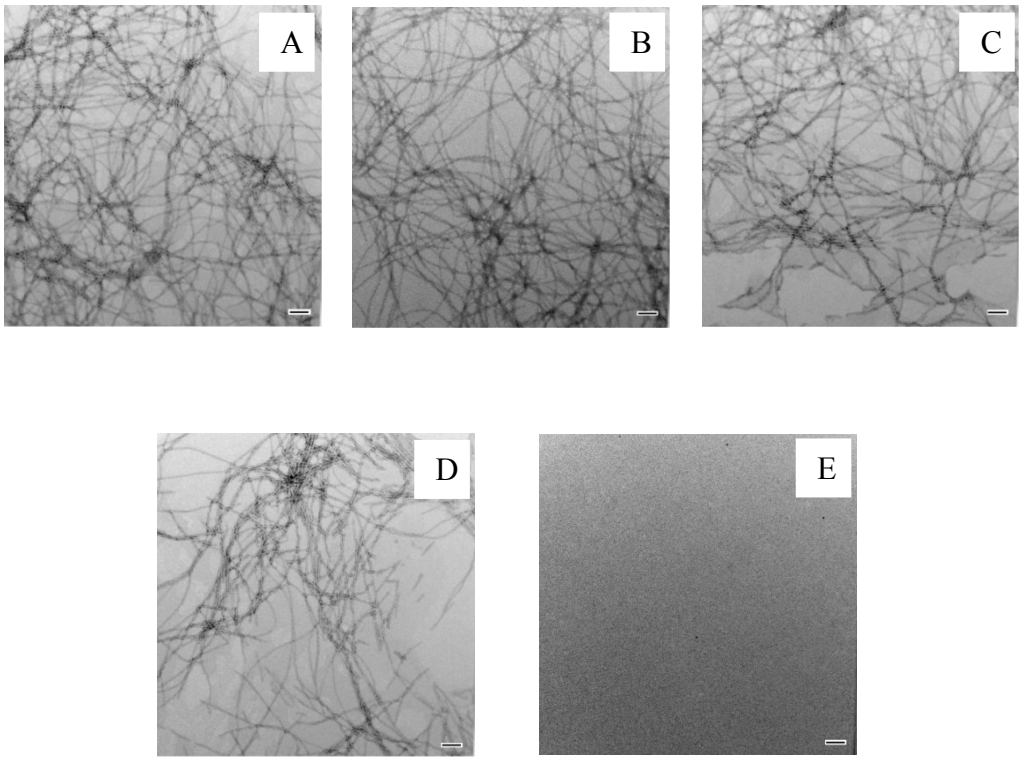

Figure 4.6 TEM of mixtures of hIAPP and H18R PM at different ratios.
(A) TEM image of a 1:1 mixture of hIAPP and H18R PM. (B) TEM image of a 1:2 mixture of hIAPP and H18R PM. (C) TEM image of a 1:5 mixture of hIAPP and H18R PM. (D) TEM image of a 1:10 mixture of hIAPP and H18R PM. (E) TEM image of H18R PM at 160 μM. All images were collected at the end of each kinetic experiment shown in Figure 4.5A. Scale bars represent 100 nm.

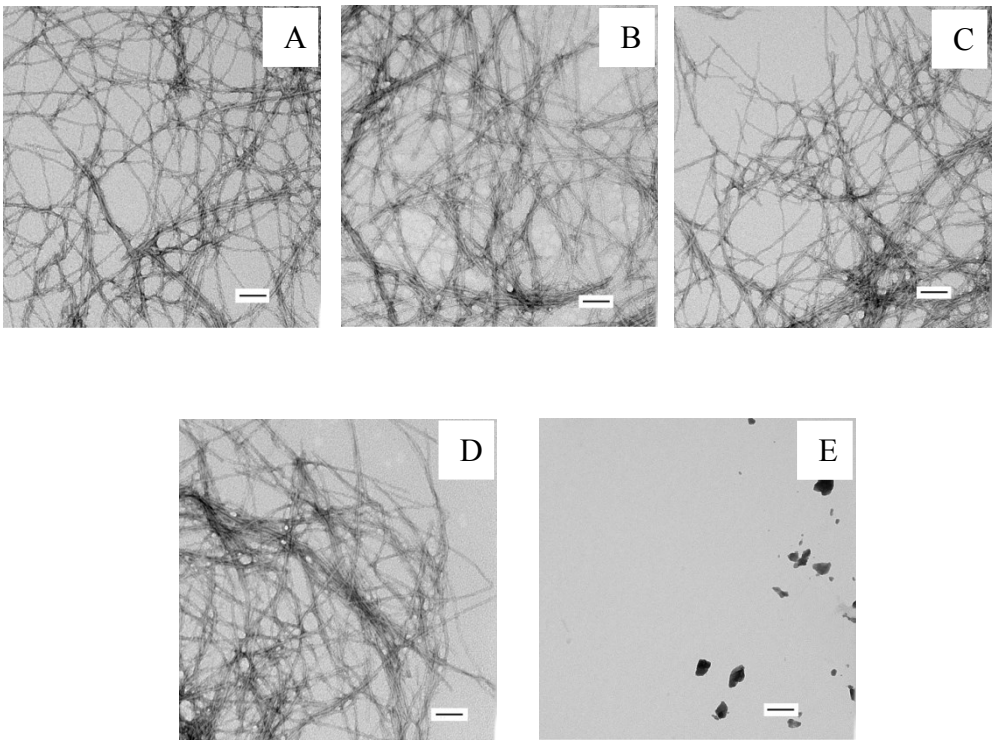

Figure 4.7 TEM of mixtures of hIAPP and F23L PM at different ratios.
(A) TEM image of a 1:1 mixture of hIAPP and F23L PM. (C) TEM image of a 1:2 mixture of hIAPP and F23L PM. (D) TEM image of a 1:5 mixture of hIAPP and F23L PM. (E) TEM image of a 1:10 mixture of hIAPP and F23L PM. (F) TEM image of F23L PM at 160 μM. All images were collected at the end of each kinetic experiment shown in Figure 4.5B. Scale bars represent 100 nm.

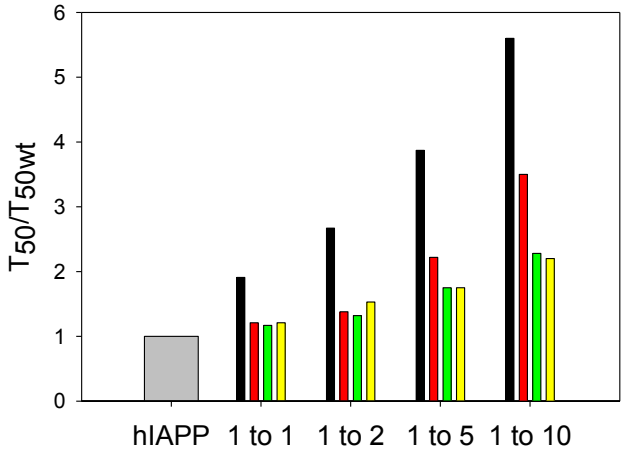

Figure 4.8 Summary of the effect of the different inhibitors on amyloid formation by hIAPP.
The factors by which the T_{50} for hIAPP amyloid formation was increased were plotted as; grey, hIAPP; black, mixtures of hIAPP and PM at different ratios; red, mixtures of hIAPP and rIAPP at different ratios; green, mixtures of hIAPP and H18R PM at different ratios; yellow, mixtures of hIAPP and F23L PM at different ratios. Values were determined from the kinetic curves shown in Figure 4.2 and Figure 4.5.

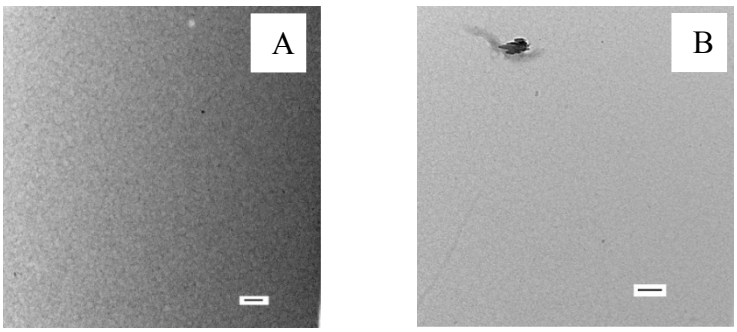

Figure 4.9 TEM image of (A) rIAPP and (B) PM.
Aliquots were taken at the end of corresponding kinetic experiments shown in Figure 4.2. Scale bars represent 100 nm. Kinetic experiments were carried out in 20 mM Tris-HCl (pH 7.4), without stirring at 25 °C. The concentration of rIAPP or PM was 160 μM.

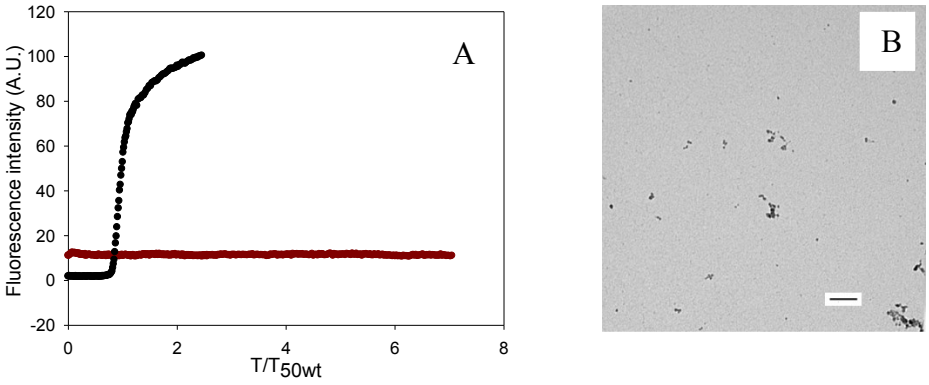

Figure 4.10 hIAPP fibrils do not seed amyloid formation by PM.
(A) Thioflain-T fluorescence results. Black, hIAPP; brown, PM seeded by 10% (by concentration) hIAPP fibrils. An aliquot was taken at the end of the experiment indicated by the black curve and used as seeds. Experiments were conducted in 20 mM Tris-HCl (pH 7.4), without stirring at 25 °C. The concentration of hIAPP and PM was 16 μM. Seeds used in the experiment shown by the brown curve included 1.6 μM hIAPP amyloid fibrils. (B) TEM image of a sample of seeding experiments. An aliquot was taken at the end of the experiment indicated by the brown curve in panel A for the TEM image. Scale bar represents 100 nm.

Chapter 5 Rationally Designed, Non-Toxic, Non-Amyloidogenic Analogs of Human Islet Amyloid Polypeptide with Improved Solubility.

Abstract.

Human islet amyloid polypeptide (hIAPP or amylin) is a hormone produced in the pancreatic β cells which normally plays a complementary role with insulin in glycemic control. hIAPP is deficient in both type 1 and type 2 diabetes patients and is thus a promising adjunct to insulin therapy. However, hIAPP rapidly forms amyloid and its strong tendency to aggregate limits its usefulness. hIAPP Amyloid formation is toxic to cultured β-cells and islets, and islet amyloid formation *in vivo* has been linked to β-cell death and to islet graft failure. An analog of hIAPP with reduced tendency to aggregate, denoted Pramlintide, has been approved by the FDA. Pramlintide suffers from solubility issues, particularly at physiological pH, and its unfavorable solubility profile prevents co-formulation with insulin. We describe rationally designed analogs of hIAPP, developed using the strategy of mutating select residues to proline and making substitutions to increase the net charge on the molecule, that have improved properties. An H18R G24P I26P triple mutant and an H18R, Ala-25, Ser-28, Ser-29 quadruple mutant are significantly more solubility at neutral pH than hIAPP and PM, are non-amyloidogenic and are not toxic to INS β-cells. The approach is not limited to these two examples; additional analogs can be designed using this strategy. To illustrate this point we show that a S20R G24P I26P triple mutant and a H18R I26P double mutant are non-amyloidogenic and significantly more soluble than human IAPP or PM. These analogs and second generation derivatives are potential candidates for the co-formulation of IAPP with insulin and other polypeptides.

The work in this chapter has been submitted to Biochemistry. This chapter contains direct excerpts from that manuscript, which was written by me with the assistance of Prof. Daniel Raleigh and Dr. Andishen Abedini.

5.1 Introduction

Insulin therapy is the most widely used clinical treatment for type 1 and type 2 diabetes. Despite improvements in insulin therapy over the past few decades, the goal of reinstating complete physiological glucose homeostasis in diabetes patients is far from achieved. In particular, postprandial hyperglycemia remains an obstacle even with aggressive insulin therapy, likely in part because diabetes is a multihormonal disease which involves the disturbed secretion of several hormones that physiologically work in concert to achieve normal glycemic control.[58]

Human islet amyloid polypeptide (hIAPP or amylin) is a neuropancreatic hormone produced in the pancreatic β-cells, that is stored in the insulin secretory granule and co-secreted with insulin.[155, 221] Mature hIAPP is 37 residues in length with an amidated C-terminus and a disulfide bond between Cys-2 and Cys-7 (Figure 5.1). hIAPP normally complements the effects of insulin by suppressing postprandial glucagon secretion, helping regulate the rate of gastric emptying, and inducing satiety to suppress food intake.[54-57] The polypeptide forms amyloid in the pancreatic islets of Langerhans in type 2 diabetes by an unknown mechanism. IAPP amyloid deposits are associated with reduced β-cell mass and are believed to contribute to type 2 diabetes.[80, 81, 155, 156, 212] Recent studies have revealed that islet amyloid contributes to the failure of islet transplantation and have shown the prevention of islet amyloid enhances graft survival.[98, 157] hIAPP is also prone to aggregate *in vitro*, indeed it is one of the most aggregation prone naturally occurring sequences known, and aggregates more aggressively than Aβ.

hIAPP is deficient in both type 1 and type 2 diabetes patients,[222-224] and is hence a promising adjunct to insulin therapy. However, clinical use of hIAPP is not practical because of its aggressive tendency to aggregate *in vitro*, leading to difficulties in formulation and storage. Furthermore, hIAPP aggregates are toxic to β-cells. Rat IAPP (rIAPP) differs from the human polypeptide at six positions, is not toxic, does not form amyloid and is more soluble than hIAPP,[145] owing, in part, to three prolines found in the rat sequence at positions 25, 28 and 29. These residues are Ala, Ser and Ser respectively in the human polypeptide (Figure 5.1). The sequence differences between rat and human IAPP have been exploited to develop a more soluble analog of hIAPP, pramlintide (PM), that has been approved by the FDA, in which residues 25, 28, and 29 of hIAPP were substituted with proline (Figure 5.1). The substitution of the three prolines renders the human peptide non-amyloidgenic. Clinical studies show that PM retains the activity of hIAPP and the addition of PM to insulin therapy improves postprandial glycemic control in patients with type 1 and type 2 diabetes.[58-63]

PM still has solubility issues particularly at physiological pH. PM is more soluble at acidic pH where the N-terminus and His-18 will be fully protonated and is formulated under these conditions, while insulin is formulated at near neutral pH. This prevents the co-formulation of insulin and PM, and requires separate injections of the drugs, leading to increased cost. There is also interest in the co-formulation of IAPP or PM with other proteins, and IAPP analogs with improved solubility could be useful in this context as well. [225-227]

Here, we describe rationally designed analogs of hIAPP developed using the strategy of mutating select residues to proline and making substitutions to increase the net charge on the molecule, that have improved properties. We illustrate the approach with an H18R G24P I26P

triple mutant (TM-a) and an H18R, Ala-25, Ser-28, Ser-29 quadruple mutant (QM). Both are significantly more soluble than hIAPP or PM, and both are non-amyloidogenic and are not toxic to INS β-cells. The approach is not limited to these two cases and additional analogs can be designed using this strategy (Figure 5.1). We tested a S20R G24P I26P triple mutant (TM-b) and a H18R I26P double mutant (DM) as an example for the second generation of derivatives.

5.2 Material and Methods

5.2.1 Peptide Synthesis

All peptides were synthesized on a 0.1 mmol scale using a CEM microwave peptide synthesizer. 9-fluornylmethoxycarbonyl (Fmoc) chemistry was utilized. 5-(4'-fmoc-aminomethyl-3'5-dimethoxyphenol) valeric acid (PAL-PEG) resin was used to afford an amidated C-terminus. For hIAPP, TM-a, TM-b, and DM, Fmoc-protected pseudoproline (oxazolidine) dipeptide derivatives were incorporated to improve the yield as previously described.[171] For PM and QM, only Fmoc-Ala-Thr($\Psi^{Me,\ Me}$pro)-OH and Fmoc-Leu-Ser($\Psi^{Me,\ Me}$pro)-OH were utilized. Standard Fmoc reaction cycles were used as previously described.[172] The first residue attached to the resin, all β-branched residues, all pseudoproline dipeptide derivatives were double-coupled. The peptides were cleaved from the resin through the use of standard trifluoroacetic acid (TFA) methods.

5.2.2 Oxidation and Purification of Peptides

Crude peptides collected after cleavage were dissolved into 20% (v/v) acetic acid and then lyophilized. This step was repeated several times before oxidation and purification to improve the solubility of the peptides. The peptides were oxidized in 100% dimethyl sulfoxide at room

temperature and were then purified via reverse-phase high-performance liquid chromatography (RP-HPLC) using a Vydac C18 preparative column.[173] The purity of the peptides was checked by analytical HPLC before each experiment. The mass of the pure peptides was confirmed by ionization time-of-flight mass spectrometry. hIAPP, expected 3903.6, observed 3904.6; PM, expected 3949.3, observed 3949.2; QM, expected 3969.4, observed 3968.1; TM-a, expected 3946.9, observed 3945.7; TM-b, expected 3997.4, observed, 3997.1; DM, expected 3907.3, observed, 3908.1.

5.2.3 Sample Preparation

Each peptide was dissolved into 100% hexafluoroisoproponal (HFIP) to make a 1.6 mM stock solution. Stock solutions were filtered using 0.45 μM Acrodisc syringe filter with a GHP membrane and the required amount of peptide was lyophilized overnight to remove HFIP. Dry peptide was dissolved into the appropriate buffer for the fluorescence assays.

5.2.4 Fluorescence Assays

Thioflavin-T binding assays, conducted without HFIP or stirring at 25 °C, were utilized to monitor amyloid formation kinetics. Fluorescence measurements were performed using a Beckman Coulter DTX 880 plate reader with a multimode detector using an excitation wavelength of 430 nm and an emission wavelength of 485 nm. Samples were prepared by dissolving dry peptide into Tris-HCl buffer and thioflavin-T solution immediately before the measurement. The final concentrations were 16 μM hIAPP or 160 μM of each analog and 32μM thioflavin-T in 20 mM Tris-HCl (pH 7.4).

5.2.5 Solubility Measurements

Dry peptides were dissolved into PBS buffer at pH 7.4 at different initial concentrations, and were incubated for 7 days at 25 °C without stirring. Each sample was then centrifuged using a Beckman Coulter Microfuge 22R Centrifuge at 24 °C for 20 min. The relative centrifugal force used was 1.75×10^4g. The solubility of each sample was approximated by measuring the absorbance of the corresponding supernatant at 280 nm measured using a Beckman Coulter DU 730 UV/Vis Spectrophotometer. All of the peptides contain a single Tyr, three Phe and a disulfide bond and no Trp, thus their extinction coefficients at 280 nm are very similar.

5.2.6 Transmission Electron Microscopy (TEM)

TEM images were collected at the Life Science Microscopy Center at the State University of New York at Stony Brook. 15 µL aliquots of the samples used for fluorescence assays were removed at the end of each kinetic experiment, blotted on a carbon-coated 200-mesh copper grid for 1 min and then negatively stained with saturated uranyl acetate for 1min.

5.2.7 Circular Dichroism (CD)

Far-UV CD experiments were performed on an Applied Photophysics Chirascan CD spectrophotometer at 25°C. Aliquots from the kinetic experiments were removed at the end of each experiment and the spectra were recorded as the average of three repeats over a range of 190-260 nm, at 1 nm intervals. A 0.1 cm quartz cuvette was used and a background spectrum was subtracted from the data.

5.2.8 Cell Culture

Transformed rat insulinoma-1 (INS-1) pancreatic β-cells were grown in RPMI 1640 supplemented with 10% fetal bovine serum (FBS), 11 mM glucose, 10 mM Hepes, 2 mM L-glutamine, 1 mM sodium pyruvate, 50 μM β-mercaptoethanol, 100 U/ml penicillin, and 100 U/ml streptomycin. Cells were maintained at 37 ºC under 5% CO_2.

5.2.9 AlamarBlue Cell Viability Assays

Cytotoxicity was measured by AlamarBlue reduction assays. INS-1 β-cells were seeded at a density of 25,000 cells per well in 96-well plates and cultured for 24 hours prior to stimulation with wild type human IAPP, and mutant IAPP peptides. Peptides dissolved in RPMI were added directly to cells and incubated on cells for 24 hrs and 48 hrs, AlamarBlue was diluted ten-fold in culture media and incubated on cells for another 5 hours at 37 °C. Fluorescence (excitation 530; emission 590 nm) was measured on a Beckman Coulter DTX880 fluorescent plate reader. Values were calculated relative to those of control cells treated with buffer only. All values represent means ± SEM (n=4).

5.3 Results and Discussion

5.3.1 Design of Soluble Analogs

The rate of amylin formation by hIAPP is strongly pH dependent and is significantly faster above neutral pH, reflecting changes in the ionization state of the N-terminus and His-18.[129, 131, 228, 229] PM and hIAPP both contain a His residue at position 18. These observations lead us to suspect that the solubility of PM could be significantly increased by ensuring that residue 18 remained positively charged in the pH range of interest. The two choices for substitution are

either Lys or Arg. Either would accomplish this goal, but the Arg replacement is found in a number of IAPP sequences while Lys is not, in addition the amino group in Lys is generally more reactive than the guanidino group of Arg owning to its lower pKa, thus we choose to replace His-18 in the human peptide with Arg to generate the quadruple mutant.

It is natural to inquire if three proline substitutions are required and if the proline substitutions need to be located at positions 25, 28, 29 thus we designed a second analog that contain only two prolines in addition to the H18R substitution. Single proline mutations at position 24 or 26 of hIAPP significantly reduced the tendency of the human peptide to aggregate and actually convert the peptide into moderately effective inhibitors of amyloid formation by wild type hIAPP.[121, 122] The motivation for choosing these sites was that substitutions with proline were shown to have large effects on amyloid formation by a set of ten residue fragments of hIAPP.[230] However each of the single mutants can still aggregate to form non-amyloid aggregates at neutral pH, thus we prepared an analog (TM-a), in which both residues 24 and 26 were mutated to proline and which include the H18R mutation.

5.3.2 The Analogs Do Not Form Amyloid

We first tested the propensity of the different analogs to form amyloid at pH 7.4 using thioflavin-T fluorescence assays. Thioflavin-T is a small dye that undergoes an increase in quantum yield upon binding to amyloid fibrils, and thus provides a convenient probe to monitor the kinetics of amyloid formation. The dye does not perturb the kinetics of hIAPP formation under the conditions used here. Amyloid formation follows a sigmoidal time course consisting of a lag phase in which few or no fibrils are formed followed by a growth phase and a saturation phase in which amyloid fibrils are in equilibrium with soluble peptide. Amyloid formation by hIAPP reaches the saturation phase within 40 hours, while none of the analogs tested (PM, TM-a

and QM) formed any amyloid during the time course of the experiments (about 140 hrs.) as indicated by flat fluorescence curves, even though they were examined at a 10 fold higher concentration than hIAPP (Figure 5.2). The thioflavin-T fluorescence derives from the fibril bound dye, and the intensity is highly dependent on how well the dye binds, hence the thioflavin-T studies can sometimes be misleading.[231] Therefore, we conducted TEM and CD measurement on the samples collected at the end of each kinetic experiment. The TEM image of hIAPP showed typical amyloid fibril morphology, while no fibrils were found in the TEM images of the three analogs (PM, TM-a and QM) (Figure 5.3). The CD results are consistent with the fluorescence experiments and the TEM studies; the spectrum of hIAPP showed β-sheet structure, while the spectra of the three analogs all indicated random structures (Figure 5.11).

5.3.3 The Analogs Are Significantly More Soluble Than PM at Neutral pH.

We next compared the apparent solubility of PM and TM-a and QM at pH 7.4. Each peptide was incubated in buffer for 7 days at three different concentrations (100 μM, 500 μM and 1 mM) and the solution was then centrifuged. The apparent solubility was represented by the absorbance of the supernatant of each sample measured at 280 nm. The extinction coefficients of all polypeptides are very similar at 280 nm since they all contain the same aromatic residues and each contains a disulfide bond. A sample of hIAPP at 1 mM was used as a control. At 100 μM, there is a detectable difference in apparent solubility. The supernatant of the QM sample has a higher absorbance, 0.162, than that of TM-a and PM, 0.103 and 0.112 respectively (Figure 5.4). At higher concentrations (500 μM and 1 mM), the amount of peptide remaining in solution was significantly higher for both analogs compared to PM. At 1 mM, the absorbance of the soluble fraction of TM-a and QM were 1.23 and 1.33 respectively, while that value of PM was only 0.354. In comparison, the absorbance of the supernatant of the 1 mM hIAPP was 0.109 (Figure

5.4). At 500 μM, the absorbance of the supernatant of TM-a and QM were 0.609 and 0.716 respectively, and both were still significantly higher than that of PM, 0.330 (Figure 5.4).

5.3.4 Neither TM-a Nor QM Are Toxic to β-cells.

We tested the effects of the analogs on cell viability using rat INS-1 β-cells, a pancreatic cell line that is commonly employed in studies of hIAPP toxicity. Cell viability was monitored by AlamarBlue assays conducted at both 30 μM and 60 μM. hIAPP was used as a positive control. Incubating INS-1 β-cells with 30 μM hIAPP lead to clearly distinguishable toxicity; cell viability was reduced to 62±4% relative to the media alone control after 24 hr incubation and 54±5% after 48 hr incubation. In contrast, incubation of cells with either TM-a or QM at 30 μM barely decreased cell viability (Figure 5.5). Increasing the hIAPP concentration to 60 μM resulted in even more significant cell toxicity; cell viability was reduced to only 14±9% after 24 hr incubation and 9±9% after 48 hr incubation. In striking contrast, no obvious cytotoxicity was observed for TM-a or QM at 60 μM (Figure 5.6). These results demonstrated that, unlike hIAPP, TM-a and QM are not toxic to cells at the concentrations examined.

5.3.5 The Strategy Can Be Extended to Include Charged Substitutions at Different Sites.

We wanted to test if a charge substitution at a different site would also lead to an enhanced solubility and reduced amyloidogenicity. We chose to target Ser-20. Substitution of a glycine at this site leads to accelerated amyloid formation while replacement with a Lys has been shown to slow significantly, but not prevent amyloid formation.[126]

We prepared a S20R, G24P, I26P triple mutant (TM-b), and tested both its ability to form amyloid and its apparent solubility at neutral pH. Thioflavin-T fluorescence experiments and the TEM images both showed that TM-b did not form amyloid fibrils during the time course of the

experiments, even at 160 μM peptide concentration (Figure 5.7). We then compared the apparent solubility of TM-b with PM and TM-a at pH 7.4 using the same method as mentioned earlier (Figure 5.8). TM-b is somewhat more soluble than PM and TM-a at 100 μM. The absorbance of the soluble fraction of TM-b, TM-a and PM sample is 0.155, 0.103 and 0.112, respectively. However, TM-b is much more soluble than PM and somewhat more soluble than TM-a at 500 μM and 1 mM. The absorbance of the supernatant of samples of TM-b prepared at a concentration of 500 μM and 1 mM were 0.785 and 1.49, respectively, while the values for PM were 0.330, and 0.354 respectively.

5.3.6 Multiple proline substitutions are not necessary in this strategy.

Single proline substitution have been reported to reduce the amyloidgenicity of hIAPP.[121] To test if multiple proline substitutions are required to accompany the charged mutations in order to improve the solubility at neutral pH, we tested a H18R, I26P double mutant of hIAPP (DM). This peptide did not form amyloid during the time course of the experiments, as demonstrated by a flat thioflavin-T fluorescence curve and by TEM images (Figure 5.9). DM showed a much better solubility at neutral pH than PM, similar to the behavior of TM-a and TM-b, each of which has one more Pro substitution in the sequence (Figure 5.10). The absorbance of the soluble fraction of 1 mM, 500 μM, and 100 μM samples of DM measured after one week incubation is 1.18 for the 1 mM sample, 0.673 for the 500 μM sample, and 0.104 for the 100 μM sample.

5.4 Conclusions

In this work, we developed a simple strategy to design non-amyloidgenic, non-toxic analogs of hIAPP with significantly better solubility at neutral pH. The strategy includes a combination of mutations that increase the net charge of the peptide and single or multiple

proline substitutions. Our results demonstrate that the strategy is not limited to a specific site and there is no strict requirement for the number of proline substitutions. In the present case, we have localized the proline substitutions within the region of residue 20 to 29, however, it is known that multiple proline substitutions outside this segment can reduce amyloidogenicity, thus the approach may be even more general.[128] It is likely that N-methylated amino acids could also be used, since they, like proline, are β-sheet breakers. Analogs such as the ones described here, and next generation variants, could prove useful as potential adjunct to insulin therapy and allow co-formulation.

5.5 Figures

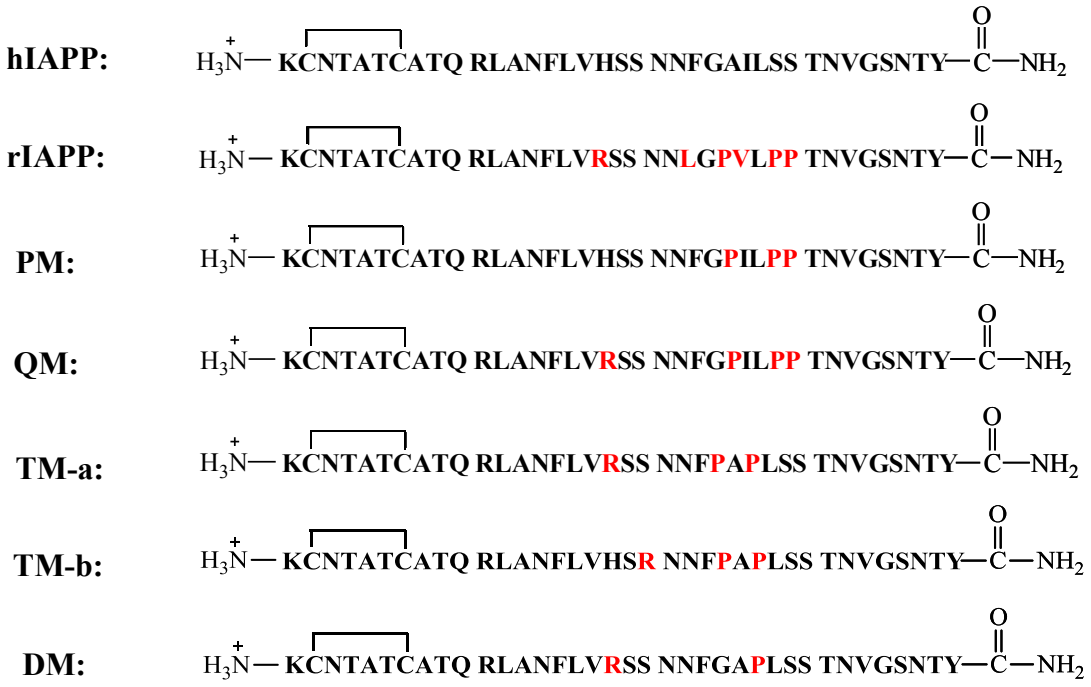

Figure 5.1 Peptide sequence.
Sequence of human-IAPP (hIAPP), rat-IAPP (rIAPP), Pramlintide (PM), H18R Pramlintide (QM), H18R, G24P, I26P-IAPP (TM-a), S20R, G24P, I26P-IAPP (TM-b), and H18R, I26P-IAPP (DM). Each peptide has a disulfide bond connecting Cys 2 and Cys 7 and an amidated C-terminus. Residues which differ from human IAPP are colored red.

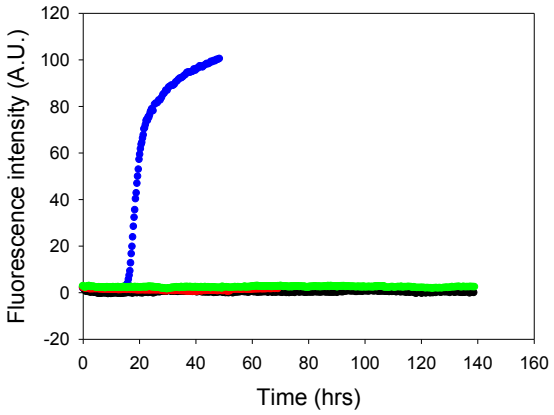

Figure 5.2 The kinetics of amyloid formation by hIAPP, TM-a, QM and PM monitored by thioflavin-T fluorescence assays.
Blue, hIAPP; black, TM-a; red, QM; green, PM. The black, red, and green curves overlap. The kinetic experiments were conducted in 20 mM Tris-HCl (pH 7.4), without stirring at 25 °C. The concentration of hIAPP was 16 μM. The concentration of the other three peptides was 160 μM.

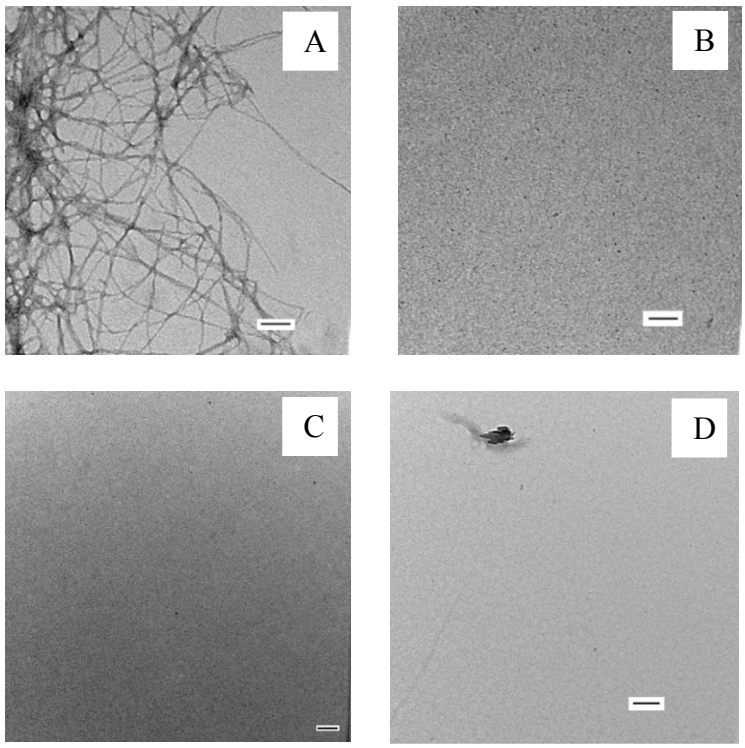

Figure 5.3 TEM images of (A) hIAPP, (B) TM-a, (C) QM and (D) PM.
TEM images were recorded from samples that were collected at the end of each kinetic experiment shown in Figure 5.2. Scale bars represent 100 nm.

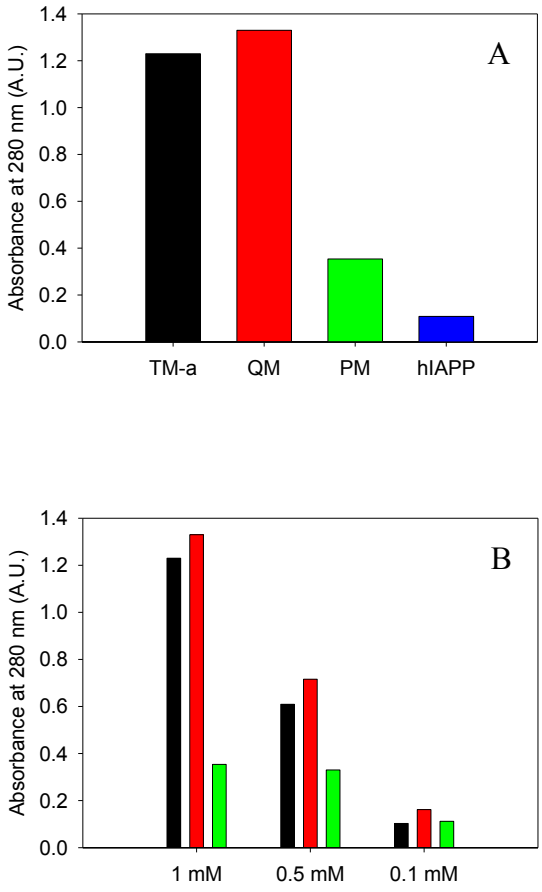

Figure 5.4 Comparison of the apparent solubility of TM-a, QM, PM and hIAPP.
The apparent solubility of the different peptides in PBS buffer at pH 7.4 is represented by absorbance at 280 nm and was measured after 7 days. (A) Amount of peptide remaining in the supernatant of samples of TM-a (black), QM (red), PM (green) and hIAPP (blue) samples prepared at an initial concentration of 1 mM. (B) Amount of peptide remaining in the supernatant of samples of TM-a, QM and PM measured for different initial concentrations. The same color coding is used here as in panel A. The absorbance was measured after centrifugation at 24°C for 20 min. The relative centrifugal force used was 1.75×10^4g.

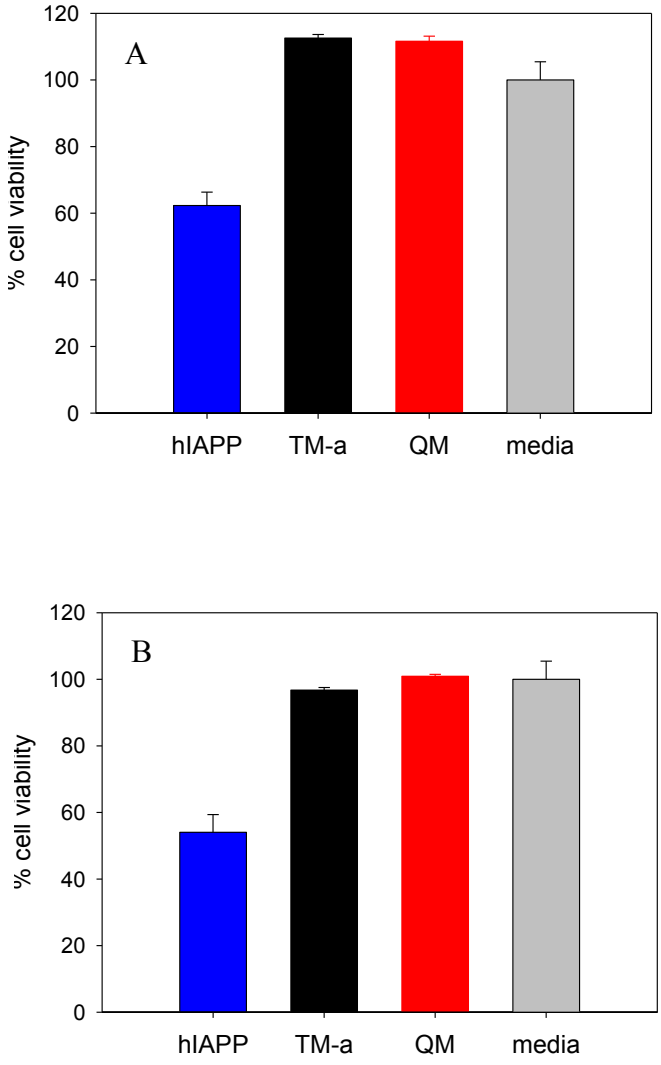

Figure 5.5 Comparison of the cell toxicity induced by hIAPP, TM-a and QM at 30 μM peptide concentration.
(A) Cell viability measured after 24 hr incubation of the peptides with the cells as judged by AlmarBlue Assays. (B) Cell viability measured after 48 hr incubation of the peptides with the cells as judged by AlmarBlue assays. The error bars represent the standard deviation determined from 4 repeated measurements. The data presented here were collected by our collaborators in New York University.

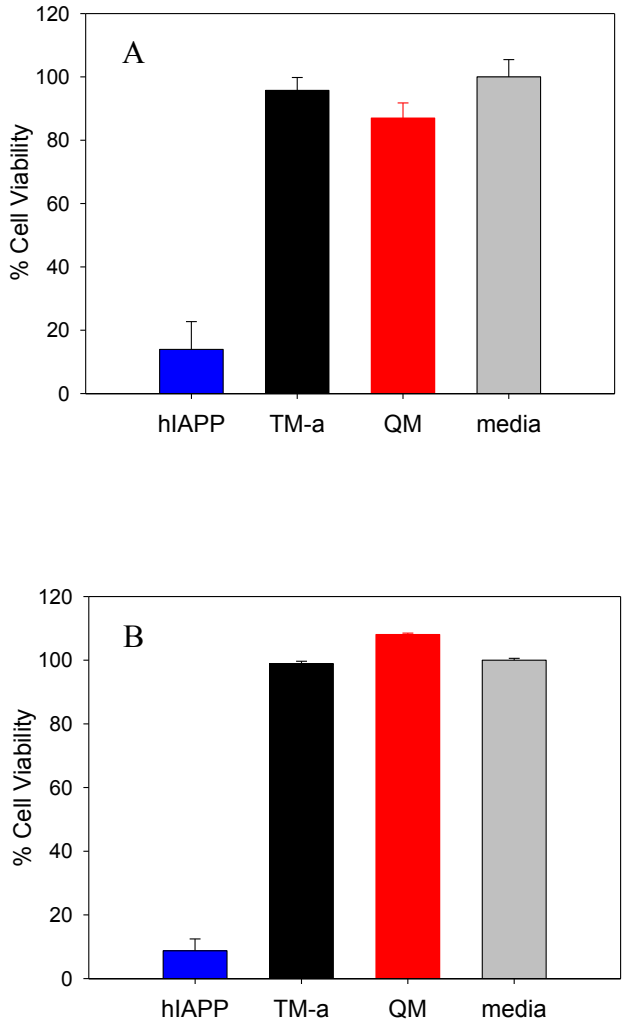

Figure 5.6 Comparison of cell toxicity induced by hIAPP, TM-a and QM at a peptide concentration of 60 µM.
(A) Cell viability measured after 24 hr incubation of the peptides with the cells as judged by AlmarBlue Assays. (B) Cell viability measured after 48 hr incubation of the peptides with the cells as judged by AlmarBlue assays. The error bars represent the standard deviation determined from 4 repeated measurements. The data presented here were collected by our collaborators in New York University.

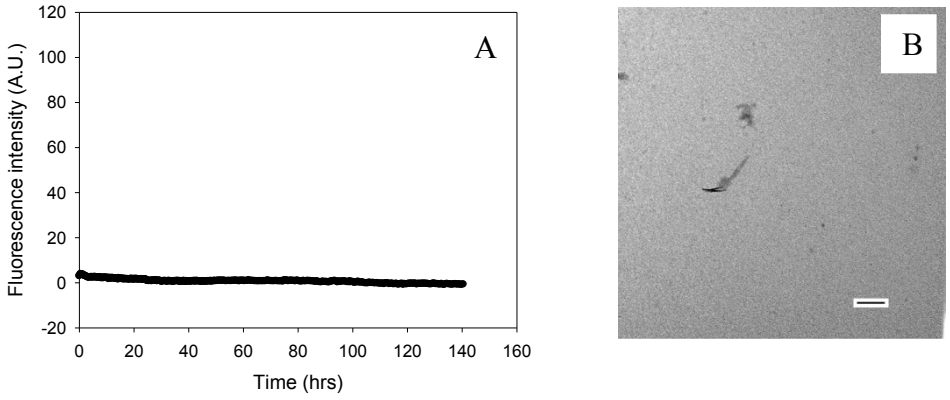

Figure 5.7 TM-b does not form amyloid during the time course of the experiments.
(A) The kinetics of amyloid formation by TM-b monitored by thioflavin-T fluorescence assays. The kinetic experiments were conducted in 20 mM Tris-HCl (pH 7.4), without stirring at 25 °C. The concentration of TM-b was 160 μM. (B) A TEM image of a sample collected at the end of the experiment shown in panel A. The scale bar represents 100 nm.

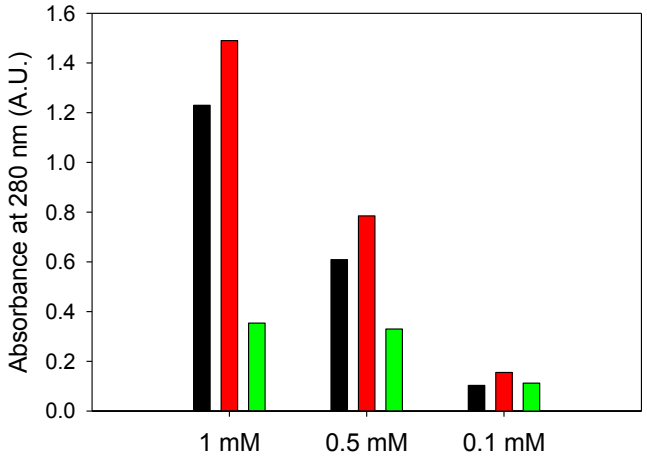

Figure 5.8 Comparison of the apparent solubility of samples of TM-a, TM-b and PM prepared at different initial concentrations.
The apparent solubility of the peptides in PBS buffer at pH 7.4 is represented by absorbance at 280 nm and was measured after 7 days. Black, TM-a; red, TM-b; green; PM. The absorbance was measured after centrifugation at 24°C for 20 min. The relative centrifugal force used was 1.75×10^4g.

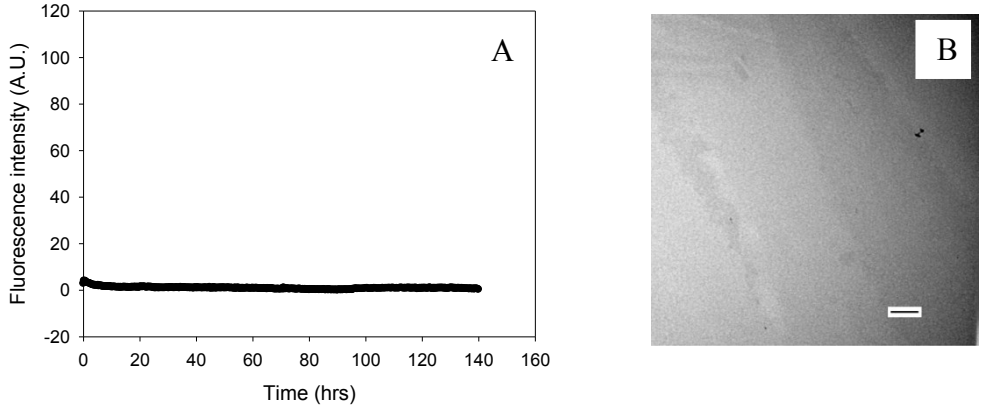

Figure 5.9 DM does not form amyloid during the time course of the experiments.
(A) The kinetics of amyloid formation by DM monitored by thioflavin-T fluorescence assays. The kinetic experiments were conducted in 20 mM Tris-HCl (pH 7.4), without stirring at 25 °C. The concentration of DM was 160 μM. (B) A TEM image of a sample collected at the end of the experiments shown in panel A. The scale bar represents 100 nm.

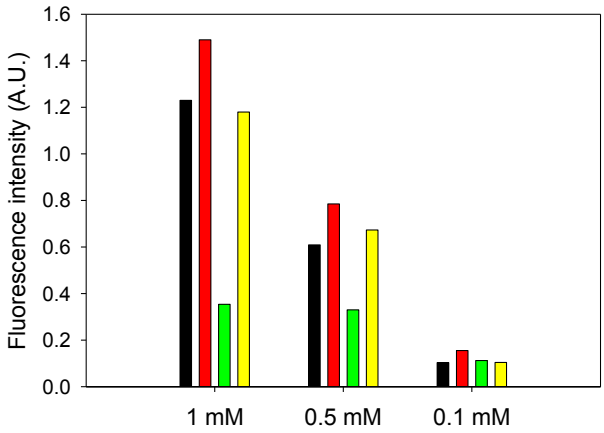

Figure 5.10 Comparison of the apparent solubility of samples of TM-a, TM-b, PM and DM prepared at different initial concentrations.
The apparent solubility of the peptides in PBS buffer at pH 7.4 is represented by absorbance at 280 nm and was measured after 7 days. Black, TM-a; red, TM-b, green; PM, yellow, DM. The absorbance was measured after centrifugation at 24°C for 20 min. The relative centrifugal force used was 1.75×10^4g.

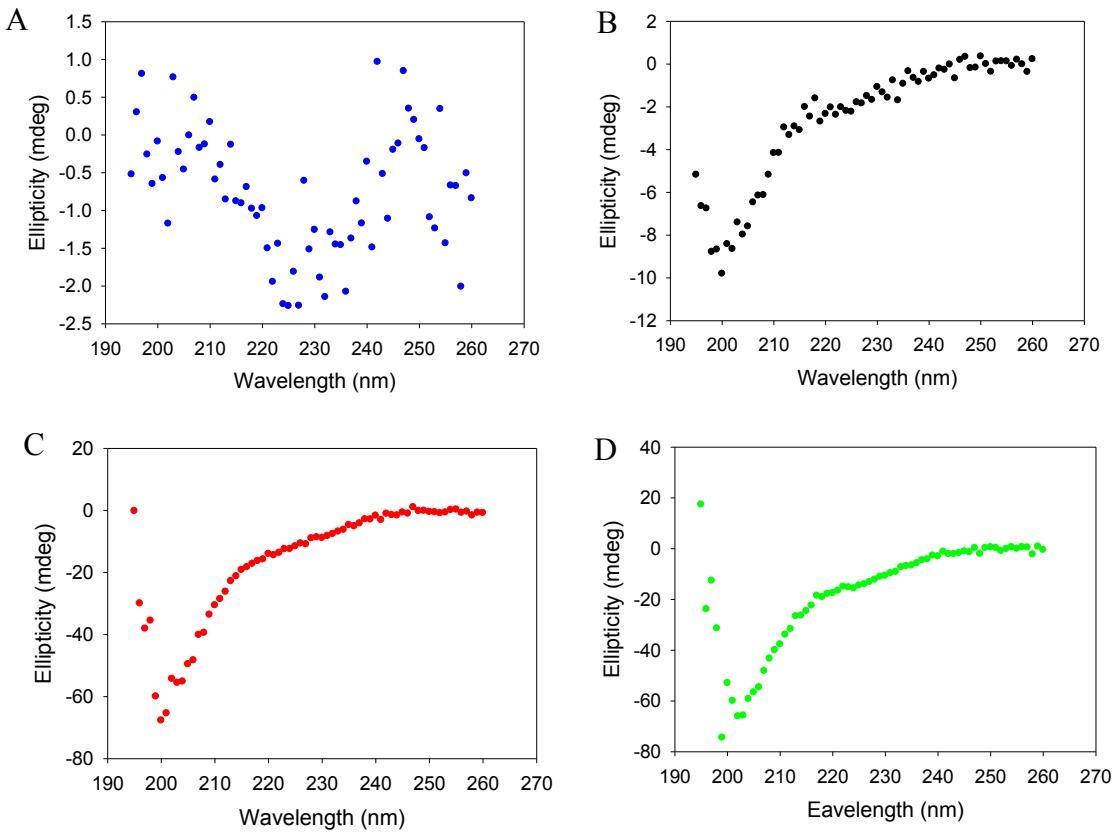

Figure 5.11 CD spectra of aliquots of hIAPP (A), TM-a (B), QM (C) and PM (D) taken at the end of each kinetic experiment shown in Figure 5.2.
The scatter and the low intensity of the spectrum shown in panel A reflect the fact that hIAPP formed amyloid.

Chapter 6 General Amyloid Inhibitors? A Critical Examination of the Inhibition of IAPP Amyloid Formation by Inositol Stereoisomers

Abstract

Islet amyloid polypeptide (IAPP or amylin) forms amyloid deposits in type 2 diabetes; a process that is believed to contribute to the progression of the disease and to the failure of islet transplants. An emerging theme in amyloid research is the hypothesis that the toxic species produced during amyloid formation by different polypeptides share common features and exert their effects by common mechanisms. If correct, this suggests that inhibitors of amyloid formation by one polypeptide might be effective against other amyloidogenic sequences. IAPP and Aβ, the peptide responsible for amyloid formation in Alzheimer's disease, are particularly interesting in this regard as they are both natively unfolded in their monomeric states and share some common characteristics. Comparatively little effort has been expended on the design of IAPP amyloid inhibitors, thus it is natural to inquire if Aβ inhibitors are effective against IAPP, especially since no IAPP inhibitors have been clinically approved. A range of compounds inhibit Aβ amyloid formation, including various stereoisomers of inositol. Myo-, scyllo-, and epi-inositol have been shown to induce conformational changes in Aβ and prevent Aβ amyloid fibril formation by stabilizing non-fibrillar, β-sheet structures. We investigate the activity of inositol stereoisomers to inhibit amyloid formation by IAPP. The compounds do not induce a conformational change in IAPP and are ineffective inhibitors of IAPP amyloid formation, although some do lead to modest, apparent changes in IAPP amyloid fibril morphology. Thus not all classes of Aβ inhibitors are effective against IAPP. The study provides a basis of comparison to work on polyphenol based inhibitors of IAPP amyloid formation and helps provide clues as to

the features which render them effective. The study also helps provide information for further efforts in rational inhibitor design.

The work in this chapter has been submitted to Plos One. This chapter contains direct excerpts from that manuscript, which was written by me with the assistance of Prof. Daniel Raleigh.

6.1 Introduction

Amyloid formation plays a role in a range of human diseases including Alzheimer's disease, Parkinson's disease and type 2 diabetes (T2D).[153, 154] Islet amyloid polypeptide (IAPP or amylin) is a neuroendocrine hormone that forms amyloid deposits in the pancreatic islets of Langerhans in T2D.[155, 156] The peptide normally suppresses postprandial glucagon secretion, helps regulate gastric emptying, and induces satiety, thereby complementing the effects of insulin in glycemic control, but IAPP forms islet amyloid in T2D for an unknown reason. [54-57] Islet amyloid formation is associated with the reduction of β cell mass in T2D and is believed to contribute to the progression of the disease.[79-81] Recent investigations have revealed that islet amyloid also contributes to graft failure in islet transplantation.[98, 157] IAPP is produced as a prohormone and is processed in the Golgi as well as the insulin secretory granule, where it is stored. Mature IAPP is 37 residues in length with a disulfide bond in its N-terminus and an amidated C-terminus (Figure 6.1). The peptide aggregates aggressively *in vitro* and is toxic to cultured pancreatic islet β cells and islets.[99]

An emerging theme in amyloid research is the hypothesis that the toxic species produced during amyloid formation share common physio-chemical features and exert their deleterious effects by common modes.[232-236] If correct, this suggests that inhibitors of amyloid formation by

one polypeptide might be effective against other amyloidogenic sequences. IAPP and Aβ are particularly interesting in this regard as both are natively unfolded in their monomeric states, and although they have little direct sequence identity, they do share some common characteristics (Figure 6.1).[32] Comparatively little effort has been expended on the design and development of islet amyloid inhibitors compared to that invested in studies of Aβ inhibitors. Thus it is natural to inquire if Aβ inhibitors are effective against IAPP, especially since none of the existing IAPP inhibitors have been clinically approved and the mechanism of their action is not well understood.[21, 121, 122, 124, 149, 237-239]

Some peptide inhibitors, based on the full sequence of IAPP, have been derived that are also effective against Aβ *in vitro*.[122, 240] The polyphenol epigallocatechin-3-gallate (EGCG) also inhibits amyloid formation by a wide range of natively unfolded polypeptides, but its mode of action is not clear, and in some cases might involve chemical modification of the target peptide.[21, 151, 152, 205] However, neither EGCG nor the long peptide based inhibitors are "drug like" and it is not clear if the results with these compounds are generalizable.

A range of compounds have been reported to inhibit Aβ amyloid formation, including various stereoisomers of inositol. Inositols are a class of cyclohexylpolyols with eight naturally occurring stereoisomers, the physiologically active four of which are: myo-, chiro-, epi- and scyllo-inositol (Figure 6.1).[241] Both myo- and scyllo-inositol are found in the human central nervous system, and myo-inositol, the most abundant stereoisomer, is the head group of phosphotidylinositol and plays a role in a range of physiological processes.[241, 242] *In vitro* studies have shown that inositol stereoisomers inhibit amyloid formation by Aβ42 in a stereochemistry-dependent manner. Myo-, scyllo-, and epi-inositol prevent Aβ amyloid fibril formation by stabilizing non-fibrillar, β-sheet structures and have been shown to protect cultured neuronal

cells from Aβ-induced toxicity, while chiro-inositol does not have these effects.[243, 244] These studies were conducted with the inositol stereoisomers in large excess, at a peptide to inositol ratio of 1 to 20 by weight (~ 1 to 500 by molar). A more recent study of the interaction of Aβ42 and scyllo-inositol used thioflavin-T fluorescence assays to show that the compound, when added in a 10-fold molar excess, only slightly slowed the rate of Aβ42 amyloid formation and did not abolish fibril formation.[245] The two studies argue that the capability of inositol to inhibit Aβ42 amyloid formation is dose dependent. This conclusion is supported by a recent ion mobility spectrometry study conducted at a peptide to scyllo-inositol ratio of 1 to 1, which revealed that scyllo-inositol reduced the extent of oligomer formation by a fragment of Aβ, Aβ(25-35), but did not prevent the formation of oligomers with β-sheet fibrillar structure.[246] Collectively, the *in vitro* data indicate that scyllo-inositol inhibits Aβ amyloid formation in a dose dependent manner and protects cultured neurons. Scyllo-inositol has also been reported to prevent and reverse the Alzheimer phenotype in a mouse model.[247]

However, this class of compounds has not been investigated as IAPP inhibitors, and the most effective small molecule anti-IAPP compounds *in vitro*, polyphenols and sulfated triphenyl methyl compounds are undesirable as drug leads. Thus, it is important to expand the chemical diversity of potential IAPP inhibitors. Here we investigate the activity of four inositol stereoisomers to inhibit amyloid formation by IAPP. Myo-, scyllo-, and epi-inositol have been shown to induce conformational changes in Aβ and prevent Aβ amyloid fibril formation by stabilizing non-fibrillar, β-sheet structures. The compounds do not induce a conformational change in IAPP and are ineffective inhibitors of IAPP amyloid formation, although some do lead to changes in IAPP amyloid fibril morphology. Thus not all classes of Aβ inhibitors are effective against IAPP.

The study is also of interest as a basis of comparison to work on polyphenol based inhibitors of IAPP amyloid formation. EGCG and other polyphenols inhibit IAPP amyloid formation, but the mechanism is not fully understood and it is not known if the effects are due to their multiple hydroxyl functionalities, the polyphenolic character, or other features.[21, 149, 152, 239] The results also help provide clues about the features important in polyol and polyphenol based IAPP amyloid inhibitors and help provide a basis for further rational inhibitor design.

6.2 Material and Methods

6.2.1 Peptide Synthesis

IAPP was synthesized using a CEM microwave peptide synthesizer on a 0.1 mmol scale, utilizing 9-fluorenylmethyloxycarbonyl (Fmoc) chemistry. The 5-(4'-Fmoc-aminomethyl-3'5-dimethoxyphenol) valeric acid (PAL-PEG) resin was used in order to afford an amidated C-terminus. To improve the yield, Fmoc-protected pseudoproline (oxazolidine) dipeptide derivatives were incorporated as previously described.[171] Standard Fmoc reaction cycles were used as previously described.[172] The first residue attached to the resin, all β-branched residues and all pseudoproline dipeptide derivatives were double-coupled. Standard trifluoroacetic acid (TFA) methods were employed to cleave the peptides from the resin.

6.2.2 Peptide Oxidation and Purification

After cleavage, crude peptides were dissolved into 20% (v/v) acetic acid and then lyophilized. This step was repeated several times before oxidation to improve the solubility of the peptides. The dry peptides were dissolved into 100% dimethyl sulfoxide at room temperature to promote disulfide formation and then were purified via reverse-phase high-performance liquid

chromatography using a Vydac C18 preparative column.[173] The purity of the peptide was checked by analytical HPLC before each experiment, and the mass of the peptide was identified by ionization time-of-flight mass spectrometry; IAPP, expected 3903.6, observed 3904.6.

6.2.3 Sample Preparation

Myo-, Scyllo-, and chiro-inositol were purchased from Sigma. Epi-inositol was purchased from TCI America. They were used without further purification. They were dissolved in 20 mM Tris-HCl buffer at pH 7.4 to make 50 mM stock solutions before each experiment. IAPP was dissolved in 100% hexafluoroisoproponal (HFIP) to make a 1.6 mM stock solution. Stock solutions of the peptide were filtered using 0.45 μM Acrodisc syringe filter with a GHP membrane and the required amount of peptide was lyophilized overnight to remove HFIP. Dry peptide was dissolved into Tris-HCl buffer for the fluorescence experiments.

6.2.4 Thioflavin-T Detected Fluorescence Assays

Amyloid formation was monitored by thioflavin-T binding assays conducted without stirring at 25 °C. A Beckman Coulter DTX 880 plate reader with a multimode detector was used to measure the fluorescence, using an excitation wavelength of 430 nm and an emission wavelength of 485 nm. Immediately before the measurement, dry peptide was dissolved into Tris-HCl buffer and thioflavin-T solution, followed by the addition of inositol from stock solutions when inositol was used. The final concentrations were 16 μM IAPP and 32 μM thioflavin-T in 20 mM Tris-HCl (pH 7.4) When inositol was present, the IAPP to inositol ratio was at 1 to 20 by weight.

6.2.5 Circular Dichroism (CD)

Far-UV CD experiments were performed on an Applied Photophysics Chirascan CD spectrophotometer at 25 °C. Aliquots from the kinetic experiments were removed at the time points of interest and the spectra were recorded as the average of three repeats over a range of 190-260 nm, at 1 nm intervals. A 0.1 cm quartz cuvette was used and a background spectrum was subtracted from each measurement.

6.2.6 Transmission Electron Microscopy (TEM)

TEM images were collected at the Life Science Microscopy Center at Stony Brook University. 15 μL aliquots were removed from the solution, blotted on a carbon-coated 200-mesh copper grid for 1 min and then negatively stained with saturated uranyl acetate for 1 min.

6.3 Results and Discussion

6.3.1 Inositols Do Not Induce a Conformational Change in IAPP, Unlike Their Effect on Aβ.

Previous studies showed that myo-, epi- and scyllo-inositol immediately induce Aβ42 to form β-structure, while chiro-inositol does not.[243, 244] To test if inositol exerts similar effects on IAPP, we incubated the polypeptide with each stereoisomer separately at a peptide to inositol ratio of 1 to 20 by weight, chosen to mimic the conditions used for the Aβ studies. CD was used to monitor the conformation of IAPP. Immediately after mixing, all of the samples showed typical random coil structure CD spectra which were indistinguishable from the spectrum of IAPP alone (Figure 6.2), indicating that the compounds exert different effects on IAPP compared to Aβ. TEM images of all of the mixtures were similar to images recorded of freshly dissolved IAPP alone and only showed a few amorphous aggregates (Figure 6.3). Under the conditions of

our experiments, IAPP forms amyloid with a lag time of about 10 hours. We collected the CD spectra again after 5 hours incubation, a time chosen to be in the middle of the lag phase, but did not observe any obvious conformational change induced by any of the four stereoisomers (Figure 6.2).

6.3.2 Inositol Is a Modest Inhibitor of IAPP Aggregation, But Does Not Abolish Amyloid Fibril Formation.

In the case of Aβ42, three of the isomers proved to be effective at inhibiting amyloid formation. No fibrils were detected during the time course of the experiments conducted in the presence of myo-, epi-, and scyllo-inositol, but fibrils with typical Aβ42 amyloid fibril morphology were reported in the presence of chiro-inositol. We measured the kinetics of amyloid formation by IAPP in the presence of each inositol stereoisomer using fluorescence detected thioflavin-T binding assays. Thioflavin-T is a small dye that undergoes an increase in its quantum yield upon binding to amyloid fibrils and is widely used to monitor the kinetics of amyloid formation. Prior work has shown that the dye does not perturb the kinetics of IAPP amyloid formation under the conditions used here. As shown in Figure 6.4, the four stereoisomers have modest inhibitory effects on IAPP amyloid formation. Myo-inositol, the most potent inhibitor among the four against IAPP, increased the lag phase of IAPP amyloid formation by a factor of 2, compared to a factor of 1.7 for epi-inositol and 1.4 for scyllo-inositol. Comparison to the published data on the ability of these three stereoisomers to inhibit amyloid formation by Aβ shows that the compounds are far less effective at inhibiting IAPP amyloid formation. Chiro-inositol barely changed the lag time of IAPP in our studies, which is generally consistent with the results of the earlier work on Aβ. We collected TEM images at the end of each reaction to examine the effects of different inositol stereoisomers on fibril morphology. The

fibrils formed by IAPP in the presence of chiro- or epi-inositol had a typical fibril morphology which was indistinguishable from that observed for fibrils formed by IAPP alone. In contrast, in the presence of myo- or scyllo-inositol, shorter fibrils were observed (Figure 6.5).

6.3.3 The Potential Molecular Basis for the Different Effects of Inositols on Aβ and IAPP.

The mechanism of inositol-Aβ42 interaction is not fully understood. Molecular dynamics (MD) simulations have led to the hypothesis that scyllo- and chiro-inositol exhibit similar weak binding to a seven residue core fragment of Aβ, Aβ(16-22), which contains a di-phenylalanine sequence. This work suggested that a stereospecific face-to-face stacking mode of scyllo-inositol with the Phe side chains in Aβ plays a role in the ability of the compound to inhibit amyloid formation. The stacking is postulated to result from the interaction of the two hydrophobic planar surfaces in the compound with Aβ. The equatorial position of the hydroxyls in scyllo-inositol leads to two hydrophobic faces, and this combined with a higher propensity for hydrogen bonding was proposed to contribute to the stereochemistry-dependent activity observed.[248, 249] The simulations also suggested that inositol inhibits Aβ amyloid formation by preventing the lateral association or stacking of protofibrillar β-sheet oligomers.[249] IAPP contains three aromatic residues, F15, F23 and Y37, but lacks a di-aromatic sequence. The prior results together with a sequence comparison of IAPP and Aβ suggest that inositol peptide interactions are sequence specific and may depend on the aromatic sequence in Aβ.

6.4 Conclusions

We have characterized the ability of four stereoisomers, myo-, scyllo-, epi- and chiro-inositol to inhibit amyloid formation by IAPP. Their efficacy is stereo-chemically dependent. Chiro-inositol does not affect IAPP amyloid formation, consistent with prior studies on Aβ.

However, the remaining three inositol stereoisomers clearly have much less effect upon IAPP amyloid formation than they do on Aβ amyloid formation. Myo-inositol, the most potent inhibitor among the four under our experimental conditions, still had only very modest effects, and increased the lag time of IAPP amyloid formation by just 2 fold. In sharp contrast, according to published reports, myo-, epi-, and scyllo-inositol totally abolish amyloid fibril formation by Aβ when added at the same concentration used here.[243, 244] Moreover, these inositol stereoisomers stabilized non-fibrillar β-structure in Aβ, an effect that was proposed to contribute to the inhibition of fibril formation.[243, 244] In contrast, none of the stereoisomers tested were capable of inducing an initial conformational change in IAPP, similar to that seen for Aβ. These observations clearly indicate that the design of amyloid inhibitors is likely to be specific for the protein of interest, and show that, while some compounds can inhibit multiple amyloidogenic proteins, not all inhibitors of one protein will be effective against a similar amyloidogenic peptide.

Myo- and scyllo-inositol did have a modest effect on IAPP fibril morphology and shorter fibrils were observed in their presence. The effects of the inositol stereoisomers on fibril morphology are modest, but are dependent on the spatial distribution of the hydroxyl groups. IAPP contains a large fraction of residues with hydrogen bonding functionalities in their side chains (Figure 6.1), including ten Thr or Ser residues and seven Asn or Gln residues, and these provide multiple potential sites for hydrogen bonding interactions with the inositols.

A range of polyphenols have been proven to be potent *in vitro* inhibitors of amyloid formation. EGCG is particularly effective and abolishes IAPP amyloid formation when added at a 1 to 1 ratio.[239] It is not clear if the effects are due to the multiple hydroxyl groups of EGCG, its polyphenolic character, or its susceptibility to spontaneous modifications.[152] The fact that the

inhibitory ability of inositol stereoisomers are stereochemistry-dependent and are much less effective on IAPP amyloid formation than EGCG,[21, 239] suggests that factors other than simply multiple hydroxyl groups are important on polyphenol IAPP interaction. These likely include the aromatic character of the polyphenols, the spatial distribution of their hydroxyl groups and, at least in the case of EGCG, their ability to form covalent linkages with polypeptides.

6.5 Figures

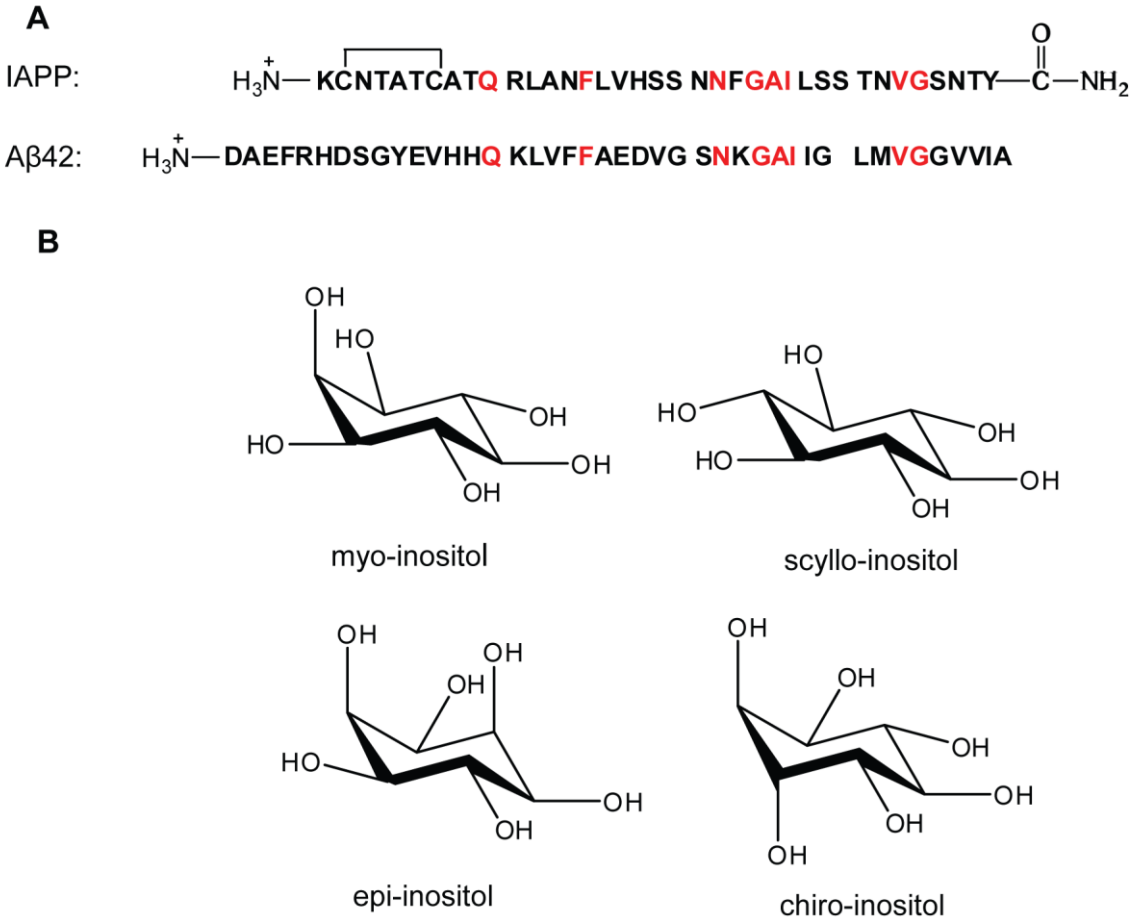

Figure 6.1 Peptide sequence and inositol structures.
(A) Sequence of IAPP and Aβ42. The molecules are aligned according to reference 32. Residues which are identical in both sequences are labeled in red. IAPP has a disulfide bond between Cys 2 and Cys 7 and an amidated C-terminus. (B) Structures of the inositol stereoisomers examined in this work.

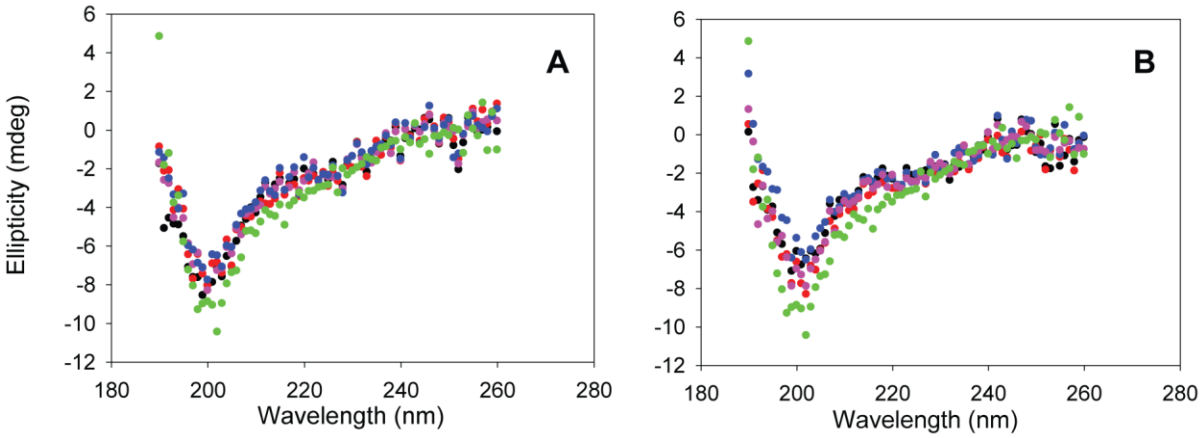

Figure 6.2 Inositols do not induce a conformational change in IAPP.
CD spectra of IAPP in the presence of different inositol stereoisomers at the beginning of the reaction (A) and after 300 min incubation (B). Black, IAPP; red, IAPP+myo-inositol; green, IAPP+epi-inositol; purple, IAPP+scyllo-inositol; blue, IAPP+chiro-inositol. The concentration of IAPP was 16 μM. The IAPP to inositol ratio was 1 to 20 by weight in each mixture. The experiments were conducted in 20 mM Tris-HCl (pH 7.4), without stirring at 25 °C.

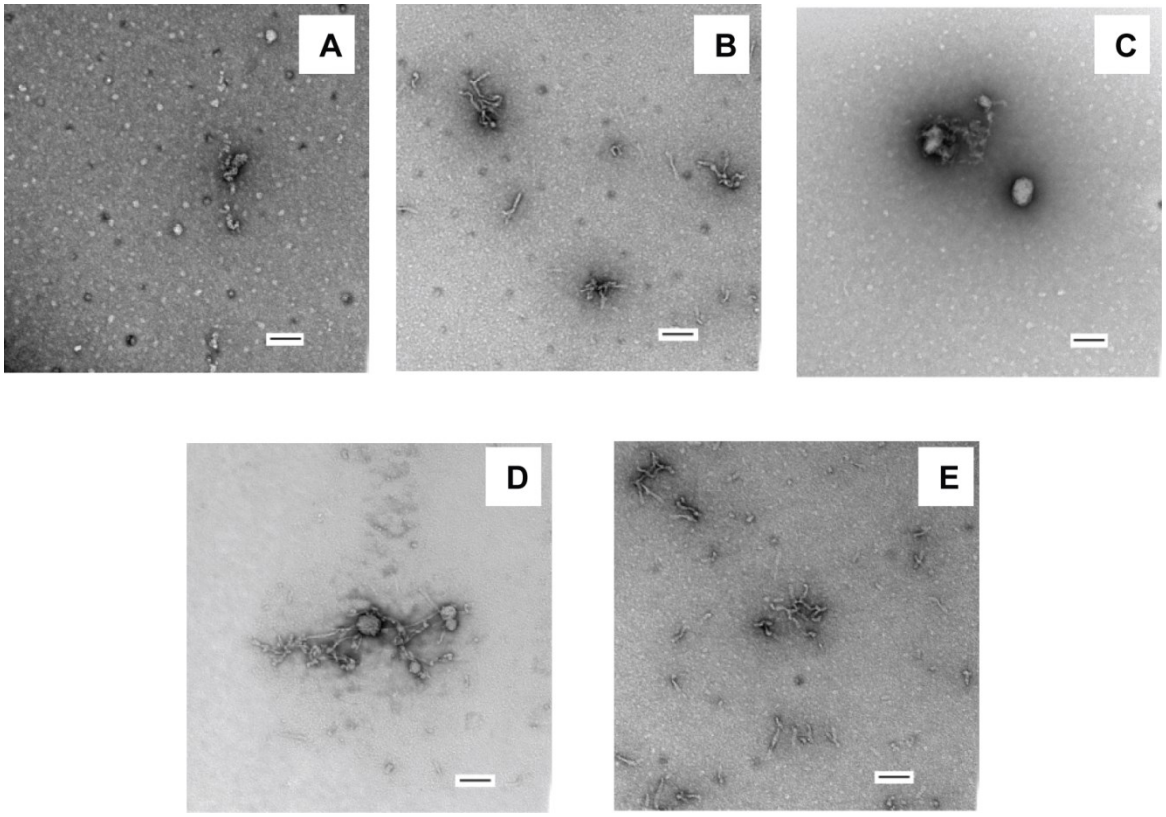

Figure 6.3 TEM images at the beginning of the reaction.
(A) IAPP (B) IAPP+myo-inositol (C) IAPP+epi-inositol (D) IAPP+scyllo-inositol (E) IAPP+chiro-inositol. Scale bars represent 100 nm. The concentration of IAPP was 16 μM. The IAPP to inositol ratio was 1 to 20 by weight in each mixture. The experiments were conducted in 20 mM Tris-HCl (pH 7.4), without stirring at 25 °C.

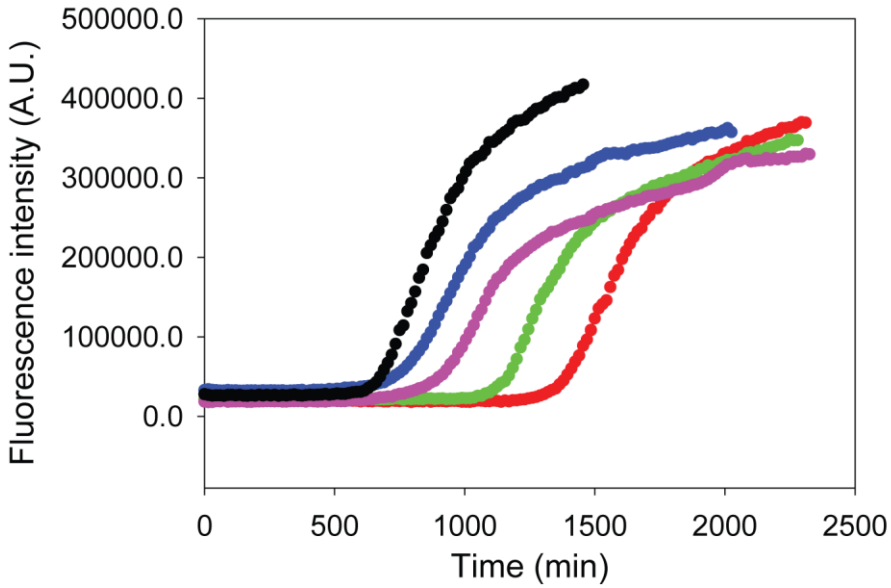

Figure 6.4 The effect of inositols on IAPP amyloid formation depends on their stereochemistry.
Kinetic curves of amyloid formation by IAPP and mixtures of IAPP with inositol stereoisomers monitored by thioflavin-T fluorescence assays are displayed. Black, IAPP; red, IAPP+myo-inositol; green, IAPP+epi-inositol; purple, IAPP+scyllo-inositol; blue, IAPP+chiro-inositol. The concentration of IAPP was 16 μM. The IAPP to inositol ratio was 1 to 20 by weight in each mixture. The experiments were conducted in 20 mM Tris-HCl (pH 7.4), without stirring at 25 °C.

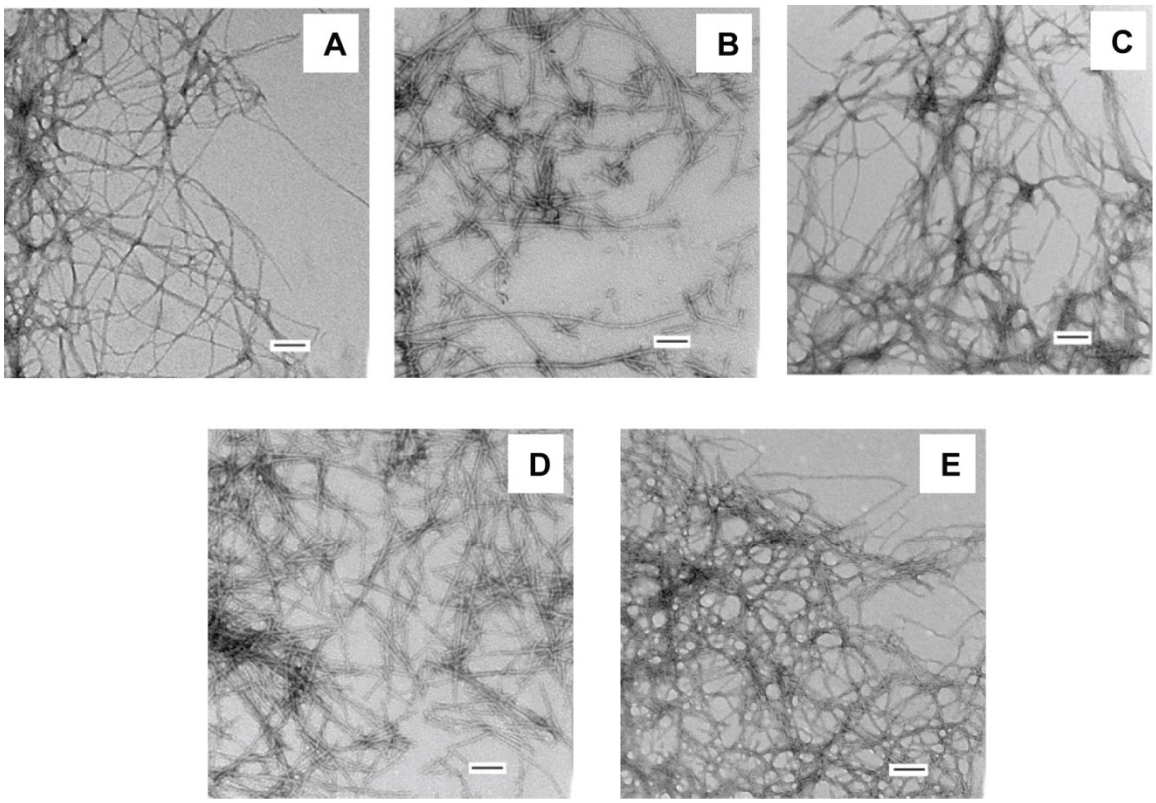

Figure 6.5 Inositols do not prevent IAPP amyloid formation.
TEM images of (A) IAPP, (B) IAPP+myo-inositol, (C) IAPP+epi-inositol, (D) IAPP+scyllo-inositol and (E) IAPP+chiro-inositol were recorded at the end of the reaction. Scale bars represent 100 nm. An aliquot was removed at the end of each experiment for TEM analysis. The concentration of hIAPP was 16 μM. The IAPP to inositol ratio was 1 to 20 by weight in each mixture. The experiments were conducted in 20 mM Tris-HCl (pH 7.4), without stirring at 25 °C.

References

1. Chiti, F., and Dobson, C. M. (2006) Protein misfolding, functional amyloid, and human disease, *Annu Rev Biochem 75*, 333-366.
2. Makin, O. S., and Serpell, L. C. (2005) Structures for amyloid fibrils, *Febs J. 272*, 5950-5961.
3. Sunde, M., Serpell, L. C., Bartlam, M., Fraser, P. E., Pepys, M. B., and Blake, C. C. F. (1997) Common core structure of amyloid fibrils by synchrotron X-ray diffraction, *J Mol Biol 273*, 729-739.
4. Kajava, A. V., Aebi, U., and Steven, A. C. (2005) The parallel superpleated beta-structure as a model for amyloid fibrils of human amylin, *J Mol Biol 348*, 247-252.
5. Puchtler, H., Sweat, F., and Levine, M. (1962) On binding of congo red by amyloid, *J Histochem Cytochem 10*, 355-364.
6. LeVine, H. (1995) Thioflavine T interaction with amyloid β-sheet structures, *Amyloid 2*, 1-6.
7. Howie, A. J., and Brewer, D. B. (2009) Optical properties of amyloid stained by Congo red: History and mechanisms, *Micron 40*, 285-301.
8. Demaimay, R., Harper, J., Gordon, H., Weaver, D., Chesebro, B., and Caughey, B. (1998) Structural aspects of congo red as an inhibitor of protease-resistant prion protein formation, *J Neurochem 71*, 2534-2541.
9. Groenning, M. (2010) Binding mode of Thioflavin T and other molecular probes in the context of amyloid fibrils—current status, *J Chem Biol 3*, 1-18.
10. Khurana, R., Uversky, V. N., Nielsen, L., and Fink, A. L. (2001) Is congo red an amyloid-specific dye?, *J Biol Chem. 276*, 22715-22721.
11. Klunk, W. E., Pettegrew, J. W., and Abraham, D. J. (1989) Quantitative-evaluation of congo red binding to amyloid-like proteins with a beta-pleated sheet conformation, *J Histochem Cytochem 37*, 1273-1281.
12. Lorenzo, A., and Yankner, B. A. (1994) Beta-amyloid neurotoxicity requires fibril formation and is inhibited by congo red., *Proc Natl Acad Sci USA 91*, 12243-12247.
13. Caughey, B., Ernst, D., and Race, R. E. (1993) Congo red inhibition of scrapie agent replication, *J Virol 67*, 6270-6272.
14. Kim, Y. S., Randolph, T. W., Manning, M. C., Stevens, F. J., and Carpenter, J. F. (2003) Congo red populates partially unfolded states of an amyloidogenic protein to enhance aggregation and amyloid fibril formation, *J Biol Chem 278*, 10842-10850.
15. Sulatskaya, A. I., Maskevich, A. A., Kuznetsova, I. M., Uversky, V. N., and Turoverov, K. K. (2010) Fluorescence quantum yield of thioflavin T in rigid isotropic solution and incorporated into the amyloid fibrils, *Plos One 5*.
16. Stsiapura, V. I., Maskevich, A. A., Kuzmitsky, V. A., Uversky, V. N., Kuznetsova, I. M., and Turoverov, K. K. (2008) Thioflavin T as a molecular rotor: fluorescent properties of thioflavin T in solvents with different viscosity, *J Phys Chem B 112*, 15893-15902.
17. Rodriguez-Rodriguez, C., Rimola, A., Rodriguez-Santiago, L., Ugliengo, P., Alvarez-Larena, A., Gutierrez-de-Teran, H., Sodupe, M., and Gonzalez-Duarte, P. (2010) Crystal structure of thioflavin-T and its binding to amyloid fibrils: insights at the molecular level, *Chem Commun 46*, 1156-1158.

18. Khurana, R., Coleman, C., Ionescu-Zanetti, C., Carter, S. A., Krishna, V., Grover, R. K., Roy, R., and Singh, S. (2005) Mechanism of thioflavin T binding to amyloid fibrils, *J Struct Biol 151*, 229-238.
19. Levine, H. (1993) Thioflavine-T interaction with synthetic Alzheimers-Disease beta-amyloid peptides - detection of amyloid aggregation in solution, *Protein Sci 2*, 404-410.
20. Wu, C., Wang, Z. X., Lei, H. X., Zhang, W., and Duan, Y. (2007) Dual binding modes of Congo red to amyloid protofibril surface observed in molecular dynamics simulations, *J Am Chem Soc 129*, 1225-1232.
21. Cao, P., and Raleigh, D. P. (2012) Analysis of the inhibition and remodeling of islet amyloid polypeptide amyloid fibers by flavanols, *Biochemistry 51*, 2670-2683.
22. Uversky, V. N., and Fink, A. L. (2004) Conformational constraints for amyloid fibrillation: the importance of being unfolded, *Biochimica et Biophysica Acta (BBA) - Proteins and Proteomics 1698*, 131-153.
23. Kelly, J. W. (1998) The alternative conformations of amyloidogenic proteins and their multi-step assembly pathways, *Curr Opin Chem Biol 8*, 101-106.
24. Dobson, C. M. (1999) Protein misfolding, evolution and disease, *Trends in Biochemical Sciences 24*, 329-332.
25. Gosal, W. S., Morten, I. J., Hewitt, E. W., Smith, D. A., Thomson, N. H., and Radford, S. E. (2005) Competing pathways determine fibril morphology in the self-assembly of β2-microglobulin into amyloid, *J Mol Biol 351*, 850-864.
26. Guijarro, J. I., Sunde, M., Jones, J. A., Campbell, I. D., and Dobson, C. M. (1998) Amyloid fibril formation by an SH3 domain, *Proc Natl Acad Sci 95*, 4224-4228.
27. Chiti, F., Taddei, N., Bucciantini, M., White, P., Ramponi, G., and Dobson, C. M. (2000) Mutational analysis of the propensity for amyloid formation by a globular protein, *The EMBO Journal 19*, 1441-1449.
28. Villegas, V., Zurdo, J., Filimonov, V. V., Aviles, F. X., Dobson, C. M., and Serrano, L. (2000) Protein engineering as a strategy to avoid formation of amyloid fibrils, *Protein Sci 9*, 1700-1708.
29. Ferrão-Gonzales, A. D., Souto, S. O., Silva, J. L., and Foguel, D. (2000) The preaggregated state of an amyloidogenic protein: Hydrostatic pressure converts native transthyretin into the amyloidogenic state, *Proc Natl Acad Sci 97*, 6445-6450.
30. Kumar, S., and Walter, J. (2011) Phosphorylation of amyloid beta (A beta) peptides - A trigger for formation of toxic aggregates in Alzheimer's disease, *Aging-Us 3*, 803-812.
31. Harper, J. D., and Lansbury, P. T. (1997) Models of amyloid seeding in Alzheimer's disease and scrapie: mechanistic truths and physiological consequences of the time-dependent solubility of amyloid proteins, *Annu Rev Biochem 66*, 385-407.
32. O'Nuallain, B., Williams, A. D., Westermark, P., and Wetzel, R. (2004) Seeding specificity in amyloid growth induced by heterologous fibrils, *J Biol Chem 279*, 17490-17499.
33. Xue, W. F., Homans, S. W., and Radford, S. E. (2008) Systematic analysis of nucleation-dependent polymerization reveals new insights into the mechanism of amyloid self-assembly, *Proc Natl Acad Sci USA 105*, 8926-8931.
34. Knowles, T. P. J., Waudby, C. A., Devlin, G. L., Cohen, S. I. A., Aguzzi, A., Vendruscolo, M., Terentjev, E. M., Welland, M. E., and Dobson, C. M. (2009) An analytical solution to the kinetics of breakable filament assembly, *Science 326*, 1533-1537.

35. Knowles, T. P. J., White, D. A., Abate, A. R., Agresti, J. J., Cohen, S. I. A., Sperling, R. A., De Genst, E. J., Dobson, C. M., and Weitz, D. A. (2011) Observation of spatial propagation of amyloid assembly from single nuclei, *Proc Natl Acad Sci USA 108*, 14746-14751.
36. Jaikaran, E., Nilsson, M. R., and Clark, A. (2004) Pancreatic beta-cell granule peptides form heteromolecular complexes which inhibit islet amyloid polypeptide fibril formation, *Biochem J 377*, 709-716.
37. Larson, J. L., and Miranker, A. D. (2004) The mechanism of insulin action on islet amyloid polypeptide fiber formation, *J Mol Biol 335*, 221-231.
38. Westermark, P., Li, Z. C., Westermark, G. T., Leckstrom, A., and Steiner, D. F. (1996) Effects of beta cell granule components on human islet amyloid polypeptide fibril formation, *FEBS Lett. 379*, 203-206.
39. Butler, P. C., Chou, J., Carter, W. B., Wang, Y.-N., Bu, B.-H., Chang, D., Chang, J.-K., and Rizza, R. A. (1990) Effects of meal ingestion on plasma amylin concentration in NIDDM and nondiabetic humans, *Diabetes 39*, 752-756.
40. Sanke, T., Hanabusa, T., Nakano, Y., Oki, C., Okai, K., Nishimura, S., Kondo, M., and Nanjo, K. (1991) Plasma islet amyloid polypeptide (Amylin) levels and their responses to oral glucose in type-2 (non-insulin-dependent) diabetic-patients, *Diabetologia 34*, 129-132.
41. Knight, J. D., Williamson, J. A., and Miranker, A. D. (2008) Interaction of membrane-bound islet amyloid polypeptide with soluble and crystalline insulin, *Protein Sci 17*, 1850-1856.
42. Sanke, T., Bell, G. I., Sample, C., Rubenstein, A. H., and Steiner, D. F. (1988) An islet amyloid peptide is derived from an 89-amino acid precursor by proteolytic processing, *J Biol Chem 263*, 17243-17246.
43. Marzban, L., Trigo-Gonzales, G., Zhu, X. R., Rhodes, C. J., Halban, P. A., Steiner, D. F., and Verchere, C. B. (2004) Role of beta-cell prohormone convertase (PC) 1/3 in processing of pro-islet antyloid polypeptide, *Diabetes 53*, 141-148.
44. Marzban, L., Soukhatcheva, G., and Verchere, C. B. (2005) Role of carboxypeptidase E in processing of pro-islet amyloid polypeptide in beta-cells, *Endocrinology 146*, 1808-1817.
45. Badman, M. K., Shennan, K. I. J., Jermany, J. L., Docherty, K., and Clark, A. (1996) Processing of pro-islet amyloid polypeptide (proIAPP) by the prohormone convertase PC2, *FEBS Lett 378*, 227-231.
46. Roberts, A. N., Leighton, B., Todd, J. A., Cockburn, D., Schofield, P. N., Sutton, R., Holt, S., Boyd, Y., Day, A. J., Foot, E. A., and et al. (1989) Molecular and functional characterization of amylin, a peptide associated with type 2 diabetes mellitus, *Proc Natl Acad Sci 86*, 9662-9666.
47. Westermark, G. T., Steiner, D. F., Gebre-Medhin, S., Engstrom, U., and Westermark, P. (2000) Pro islet amyloid polypeptide (ProIAPP) immunoreactivity in the islets of langerhans, *Ups J Med Sci 105*, 97-106.
48. Westermark, P., Engstrom, U., Westermark, G. T., Johnson, K. H., Permerth, J., and Betsholtz, C. (1989) Islet amyloid polypeptide (Iapp) and Pro-Iapp immunoreactivity in human islets of Langerhans, *Diabetes Res Clin Pr 7*, 219-226.
49. Paulsson, J. F., and Westermark, G. T. (2005) Aberrant processing of human proislet amyloid polypeptide results in increased amyloid formation, *Diabetes 54*, 2117-2125.

50. Abedini, A., Tracz, S. M., Cho, J. H., and Raleigh, D. P. (2006) Characterization of the heparin binding site in the N-terminus of human pro-islet amyloid polypeptide: Implications for amyloid formation, *Biochemistry 45*, 9228-9237.
51. Marzban, L., Rhodes, C. J., Steiner, D. F., Haataja, L., Halban, P. A., and Verchere, C. B. (2006) Impaired NH2-terminal processing of human proislet amyloid polypeptide by the prohormone convertase PC2 leads to amyloid formation and cell death, *Diabetes 55*, 2192-2201.
52. Paulsson, J. F., Andersson, A., Westermark, P., and Westermark, G. T. (2006) Intracellular amyloid-like deposits contain unprocessed pro-islet amyloid polypeptide (proIAPP) in beta cells of transgenic mice overexpressing the gene for human IAPP and transplanted human islets, *Diabetologia 49*, 1237-1246.
53. Westermark, P., Andersson, A., and Westermark, G. T. (2011) Islet amyloid polypeptide, islet amyloid, and diabetes mellitus, *Physiol Rev 91*, 795-826.
54. Gedulin, B. R., Rink, T. J., and Young, A. A. (1997) Dose-response for glucagonostatic effect of amylin in rats, *Metabolism 46*, 67-70.
55. Rushing, P. A., Hagan, M. M., Seeley, R. J., Lutz, T. A., D'Alessio, D. A., Air, E. L., and Woods, S. C. (2001) Inhibition of central amylin signaling increases food intake and body adiposity in rats, *Endocrinology 142*, 5035-5038.
56. Clementi, G., Caruso, A., Cutuli, V. M. C., deBernardis, E., Prato, A., and AmicoRoxas, M. (1996) Amylin given by central or peripheral routes decreases gastric emptying and intestinal transit in the rat, *Experientia 52*, 677-679.
57. Scherbaum, W. A. (1998) The role of amylin in the physiology of glycemic control, *Exp Clin Endocr Diab 106*, 97-102.
58. Kruger, D. F., and Gloster, M. A. (2004) Pramlintide for the treatment of insulin-requiring diabetes mellitus - Rationale and review of clinical data, *Drugs 64*, 1419-1432.
59. Weyer, C., Maggs, D. G., Young, A. A., and Kolterman, O. G. (2001) Amylin replacement with pramlintide as an adjunct to insulin therapy in type 1 and type 2 diabetes mellitus: A physiological approach toward improved metabolic control, *Curr. Pharm Design 7*, 1353-1373.
60. Fineman, M., Weyer, C., Maggs, D. G., Strobel, S., and Kolterman, O. G. (2002) The human amylin analog, pramlintide, reduces postprandial hyperglucagonemia in patients with type 2 diabetes mellitus, *Horm Metab Res 34*, 504-508.
61. Fineman, M. S., Koda, J. E., Shen, L. Z., Strobel, S. A., Maggs, D. G., Weyer, C., and Kolterman, O. G. (2002) The human amylin analog, pramlintide, corrects postprandial hyperglucagonemia in patients with type I diabetes, *Metabolism 51*, 636-641.
62. Kleppinger, E. L., and Vivian, E. M. (2003) Pramlintide for the treatment of diabetes mellitus, *Ann Pharmacother 37*, 1082-1089.
63. Schmitz, O., and Brock, B. (2004) Amylin agonists: A novel approach in the treatment of diabetes, *Diabetes 53*, S233-S238.
64. Cooper, G. J. S., Leighton, B., Dimitriadis, G. D., Parrybillings, M., Kowalchuk, J. M., Howland, K., Rothbard, J. B., Willis, A. C., and Reid, K. B. M. (1988) Amylin found in amyloid deposits in human type-2 diabetes-mellitus may be a hormone that regulates glycogen-metabolism in skeletal-muscle, *Proc Natl Acad Sci USA 85*, 7763-7766.
65. Zierath, J. R., Galuska, D., Engstrom, A., Johnson, K. H., Betsholtz, C., Westermark, P., and Wallberghenriksson, H. (1992) Human islet amyloid polypeptide at pharmacological

levels inhibits insulin and phorbol ester-stimulated glucose-transport in in vitro incubated human muscle strips, *Diabetologia 35*, 26-31.
66. Johnson, K. H., Obrien, T. D., Jordan, K., Betsholtz, C., and Westermark, P. (1990) The putative hormone islet amyloid polypeptide (IAPP) induces impaired glucose-tolerance in cats, *Biochem Bioph Res Co 167*, 507-513.
67. Westermark, P., Engstrom, U., Johnson, K. H., Westermark, G. T., and Betsholtz, C. (1990) Islet amyloid polypeptide - pinpointing amino-acid-residues linked to amyloid fibril formation, *Proc Natl Acad Sci USA 87*, 5036-5040.
68. Betsholtz, C., Christmansson, L., Engstrom, U., Rorsman, F., Svensson, V., Johnson, K. H., and Westermark, P. (1989) Sequence divergence in a specific region of islet amyloid polypeptide (IAPP) explains differences in islet amyloid formation between species *FEBS Lett. 251*, 261-264.
69. Johnson, K. H., Wernstedt, C., Obrien, T. D., and Westermark, P. (1991) Amyloid in the pancreatic-islets of the cougar (Felis concolor) is derived from islet amyloid polypeptide (IAPP), *Comp Biochem Phys B 98*, 115-119.
70. Martinez-Alvarez, R. M., Volkoff, H., Cueto, J. A. M., and Delgado, M. J. (2008) Molecular characterization of calcitonin gene-related peptide (CGRP) related peptides (CGRP, amylin, adrenomedullin and adrenomedullin-2/intermedin) in goldfish (Carassius auratus): Cloning and distribution, *Peptides 29*, 1534-1543.
71. Miyazato, M., Nakazato, M., Shiomi, K., Aburaya, J., Kangawa, K., Matsuo, H., and Matsukura, S. (1992) Molecular forms of islet amyloid polypeptide (IAPP/amylin) in 4 mammals, *Diabetes Res Clin Pr 15*, 31-36.
72. Nishi, M., Chan, S. J., Nagamatsu, S., Bell, G. I., and Steiner, D. F. (1989) Conservation of the sequence of islet amyloid polypeptide in 5 mammals is consistent with its putative role as an islet hormone, *Proc Natl Acad Sci USA 86*, 5738-5742.
73. Westermark, G. T., Falkmer, S., Steiner, D. F., Chan, S. J., Engstrom, U., and Westermark, P. (2002) Islet amyloid polypeptide is expressed in the pancreatic islet parenchyma of the teleostean fish, Myoxocephalus (cottus) scorpius, *Comp Biochem Phys B 133*, 119-125.
74. Cao, P., Marek, P., Noor, H., Patsalo, V., Tu, L. H., Wang, H., Abedini, A., and Raleigh, D. P. (2013) Islet amyloid: From fundamental biophysics to mechanisms of cytotoxicity, *FEBS Lett. 587*, 1106-1118.
75. Tenidis, K., Waldner, M., Bernhagen, J., Fischle, W., Bergmann, M., Weber, M., Merkle, M. L., Voelter, W., Brunner, H., and Kapurniotu, A. (2000) Identification of a penta- and hexapeptide of islet amyloid polypeptide (IAPP) with amyloidogenic and cytotoxic properties, *J Mol Biol 295*, 1055-1071.
76. Kahn, S. E., Andrikopoulos, S., and Verchere, C. B. (1999) Islet amyloid: A long-recognized but underappreciated pathological feature of type 2 diabetes, *Diabetes 48*, 241-253.
77. Bell, E. T. (1959) Hyalinization of the islets of Langerhans in nondiabetic individuals, *Am J Pathol 35*, 801-805.
78. Westerma.P. (1972) Quantitative studies of amyloid in islets of Langerhans, *Ups J Med Sci 77*, 91-94.
79. Westermark, P., and Grimelius, L. (1973) The pancreatic islet cells in insular amyloidosis in human diabetic and non-diabetic adults, *Acta Pathologica Microbiologica Scandinavica Section A Pathology 81A*, 291-300.

80. Clark, A., Wells, C. A., Buley, I. D., Cruickshank, J. K., Vanhegan, R. I., Matthews, D. R., Cooper, G. J., Holman, R. R., and Turner, R. C. (1988) Islet amyloid, increased A-cells, reduced B-cells and exocrine fibrosis: quantitative changes in the pancreas in type 2 diabetes, *Diabetes Res Clin Pract 9*, 151-159.
81. Westermark, P., and Wilander, E. (1978) The influence of amyloid deposits on the islet volume in maturity onset diabetes mellitus, *Diabetologia 15*, 417-421.
82. Zheng, X. Y., Ren, W., Zhang, S. H., Liu, J. J., Li, S. F., Li, J. C., Yang, P., He, J., Su, S. C., and Li, P. (2010) Serum levels of proamylin and amylin in normal subjects and patients with impaired glucose regulation and type 2 diabetes mellitus, *Acta Diabetologica 47*, 265-270.
83. Mulder, H., Ahren, B., and Sundler, F. (1996) Islet amyloid polypeptide and insulin gene expression are regulated in parallel by glucose in vivo in rats, *Am J Physiol-Endoc M 271*, E1008-E1014.
84. Hanabusa, T., Kubo, K., Oki, C., Nakano, Y., Okai, K., Sanke, T., and Nanjo, K. (1992) Islet amyloid polypeptide (IAPP) secretion from islet cells and its plasma-concentration in patients with non-insulin-dependent diabetes-mellitus, *Diabetes Res Clin Pr 15*, 89-96.
85. Koning, E. J. P., Bodkin, N. L., Hansen, B. C., and Clark, A. (1993) Diabetes mellitus in Macaca mulatta monkeys is characterised by islet amyloidosis and reduction in beta-cell population, *Diabetologia 36*, 378-384.
86. Howard, C. F. (1978) Insular amyloidosis and diabetes-mellitus in Macaca nigra, *Diabetes 27*, 357-364.
87. Johnson, K. H., and Stevens, J. B. (1973) Light and electron-microscopic studies of islet amyloid in diabetic cats, *Diabetes 22*, 81-90.
88. Johnson, K. H., Obrien, T. D., Betsholtz, C., and Westermark, P. (1989) Islet amyloid, islet-amyloid polypeptide, and diabetes-mellitus, *New Engl J Med 321*, 513-519.
89. Marzban, L., Tomas, A., Becker, T. C., Rosenberg, L., Oberholzer, J., Fraser, P. E., Halban, P. A., and Verchere, C. B. (2008) Small interfering RNA–mediated suppression of proislet amyloid polypeptide expression inhibits Islet amyloid formation and enhances survival of human islets in culture, *Diabetes 57*, 3045-3055.
90. Potter, K. J., Scrocchi, L. A., Warnock, G. L., Ao, Z., Younker, M. A., Rosenberg, L., Lipsett, M., Verchere, C. B., and Fraser, P. E. (2009) Amyloid inhibitors enhance survival of cultured human islets, *Biochimica et Biophysica Acta (BBA) - General Subjects 1790*, 566-574.
91. Janson, J., Soeller, W. C., Roche, P. C., Nelson, R. T., Torchia, A. J., Kreutter, D. K., and Butler, P. C. (1996) Spontaneous diabetes mellitus in transgenic mice expressing human islet amyloid polypeptide, *Proc Natl Acad Sci USA 93*, 7283-7288.
92. Matveyenko, A. V., and Butler, P. C. (2006) Beta-cell deficit due to increased apoptosis in the human islet amyloid polypeptide transgenic (HIP) rat recapitulates the metabolic defects present in type 2 diabetes, *Diabetes 55*, 2106-2114.
93. Soeller, W. C., Janson, J., Hart, S. E., Parker, J. C., Carty, M. D., Stevenson, R. W., Kreutter, D. K., and Butler, P. C. (1998) Islet amyloid-associated diabetes in obese A(vy)/a mice expressing human islet amyloid polypeptide, *Diabetes 47*, 743-750.
94. Swift, S. M., Clayton, H. A., London, N. J. M., and James, R. F. L. (1998) The potential contribution of rejection to survival of transplanted human islets, *Cell Transplant 7*, 599-606.

95. Ryan, E. A., Paty, B. W., Senior, P. A., Bigam, D., Alfadhli, E., Kneteman, N. M., Lakey, J. R. T., and Shapir, A. M. J. (2005) Five-year follow-up after clinical islet transplantation, *Diabetes 54*, 2060-2069.
96. Westermark, P., Andersson, A., and Westermark, G. (2005) Is aggregated IAPP a cause of beta-cell failure in transplanted human pancreatic islets?, *Current Diabetes Reports 5*, 184-188.
97. Davalli, A. M., Maffi, P., Socci, C., Sanvito, F., Freschi, M., Bertuzzi, F., Falqui, L., Di Carlo, V., Pozza, G., and Secchi, A. (2000) Insights from a successful case of intrahepatic islet transplantation into a type 1 diabetic patient, *J Clin Endocrinol Metab 85*, 3847-3852.
98. Potter, K. J., Abedini, A., Marek, P., Klimek, A. M., Butterworth, S., Driscoll, M., Baker, R., Nilsson, M. R., Warnock, G. L., Oberholzer, J., Bertera, S., Trucco, M., Korbutt, G. S., Fraser, P. E., Raleigh, D. P., and Verchere, C. B. (2010) Islet amyloid deposition limits the viability of human islet grafts but not porcine islet grafts, *Proc Natl Acad Sci USA 107*, 4305-4310.
99. Lorenzo, A., Razzaboni, B., Weir, G. C., and Yankner, B. A. (1994) Pancreatic-islet cell toxicity of amylin associated with type-2 diabetes-mellitus, *Nature 368*, 756-760.
100. Glabe, C. G. (2008) Structural classification of toxic amyloid oligomers, *J Biol Chem 283*, 29639-29643.
101. Kayed, R., Pensalfini, A., Margol, L., Sokolov, Y., Sarsoza, F., Head, E., Hall, J., and Glabe, C. (2009) Annular protofibrils are a structurally and functionally distinct type of amyloid oligomer, *J Biol Chem 284*, 4230-4237.
102. Mizushima, N., Yamamoto, A., Matsui, M., Yoshimori, T., and Ohsumi, Y. (2004) In vivo analysis of autophagy in response to nutrient starvation using transgenic mice expressing a fluorescent autophagosome marker, *Mol Biol Cell 15*, 1101-1111.
103. Janson, J., Ashley, R. H., Harrison, D., McIntyre, S., and Butler, P. C. (1999) The mechanism of islet amyloid polypeptide toxicity is membrane disruption by intermediate-sized toxic amyloid particles, *Diabetes 48*, 491-498.
104. Zraika, S., Hull, R. L., Verchere, C. B., Clark, A., Potter, K. J., Fraser, P. E., Raleigh, D. P., and Kahn, S. E. (2010) Toxic oligomers and islet beta cell death: guilty by association or convicted by circumstantial evidence?, *Diabetologia 53*, 1046-1056.
105. Zhang, S. P., Liu, J. X., Dragunow, M., and Cooper, G. J. S. (2003) Fibrillogenic amylin evokes islet beta-cell apoptosis through linked activation of a caspase cascade and JNK1, *J Biol Chem 278*, 52810-52819.
106. Subramanian, S. L., Hull, R. L., Zraika, S., Aston-Mourney, K., Udayasankar, J., and Kahn, S. E. (2012) cJUN N-terminal kinase (JNK) activation mediates islet amyloid-induced beta cell apoptosis in cultured human islet amyloid polypeptide transgenic mouse islets, *Diabetologia 55*, 166-174.
107. Park, Y. J., Lee, S., Kieffer, T. J., Warnock, G. L., Safikhan, N., Speck, M., Hao, Z., Woo, M., and Marzban, L. (2012) Deletion of Fas protects islet beta cells from cytotoxic effects of human islet amyloid polypeptide, *Diabetologia 55*, 1035-1047.
108. Rivera, J. F., Gurlo, T., Daval, M., Huang, C. J., Matveyenko, A. V., Butler, P. C., and Costes, S. (2011) Human-IAPP disrupts the autophagy/lysosomal pathway in pancreatic beta-cells: protective role of p62-positive cytoplasmic inclusions, *Cell Death Differ. 18*, 415-426.

109. Masters, S. L., Dunne, A., Subramanian, S. L., Hull, R. L., Tannahill, G. M., Sharp, F. A., Becker, C., Franchi, L., Yoshihara, E., Chen, Z., Mullooly, N., Mielke, L. A., Harris, J., Coll, R. C., Mills, K. H. G., Mok, K. H., Newsholme, P., Nunez, G., Yodoi, J., Kahn, S. E., Lavelle, E. C., and O'Neill, L. A. J. (2010) Activation of the NLRP3 inflammasome by islet amyloid polypeptide provides a mechanism for enhanced IL-1 beta in type 2 diabetes, *Nat Immunol 11*, 897-U1501.
110. Zraika, S., Hull, R. L., Udayasankar, J., Aston-Mourney, K., Subramanian, S. L., Kisilevsky, R., Szarek, W. A., and Kahn, S. E. (2009) Oxidative stress is induced by islet amyloid formation and time-dependently mediates amyloid-induced beta cell apoptosis, *Diabetologia 52*, 626-635.
111. Westwell-Roper, C., Dai, D. L., Soukhatcheva, G., Potter, K. J., van Rooijen, N., Ehses, J. A., and Verchere, C. B. (2011) IL-1 blockade attenuates islet amyloid polypeptide-induced proinflammatory cytokine release and pancreatic islet graft dysfunction, *J Immunol 187*, 2755-2765.
112. Huang, C. J., Gurlo, T., Haataja, L., Costes, S., Daval, M., Ryazantsev, S., Wu, X. J., Butler, A. E., and Butler, P. C. (2010) Calcium-activated calpain-2 is a mediator of beta cell dysfunction and apoptosis in type 2 diabetes, *J Biol Chem 285*, 339-348.
113. Mirzabekov, T. A., Lin, M. C., and Kagan, B. L. (1996) Pore formation by the cytotoxic islet amyloid peptide amylin, *J Biol Chem 271*, 1988-1992.
114. Trikha, S., and Jeremic, A. M. (2011) Clustering and internalization of toxic amylin oligomers in pancreatic cells require plasma membrane cholesterol, *J Biol Chem 286*, 36086-36097.
115. Anguiano, M., Nowak, R. J., and Lansbury, P. T. (2002) Protofibrillar islet amyloid polypeptide permeabilizes synthetic vesicles by a pore-like mechanism that may be relevant to type II diabetes, *Biochemistry 41*, 11338-11343.
116. Porat, Y., Kolusheva, S., Jelinek, R., and Gazit, E. (2003) The human islet amyloid polypeptide forms transient membrane-active prefibrillar assemblies, *Biochemistry 42*, 10971-10977.
117. Smith, P. E. S., Brender, J. R., and Ramamoorthy, A. (2009) Induction of negative curvature as a mechanism of cell toxicity by amyloidogenic peptides: The case of islet amyloid polypeptide, *J Am Chem Soc 131*, 4470-4478.
118. Seeliger, J., Weise, K., Opitz, N., and Winter, R. (2012) The effect of A beta on IAPP aggregation in the presence of an isolated beta-cell membrane, *J Mol Biol 421*, 348-363.
119. Wakabayashi, M., and Matsuzaki, K. (2009) Ganglioside-induced amyloid formation by human islet amyloid polypeptide in lipid rafts, *FEBS Lett. 583*, 2854-2858.
120. Cao, P., Abedini, A., Wang, H., Tu, L. H., Zhang, X. X., Schmidt, A. M., and Raleigh, D. P. (2013) Islet amyloid polypeptide toxicity and membrane interactions, *Proc Natl Acad Sci USA 110*, 19279-19284.
121. Abedini, A., Meng, F. L., and Raleigh, D. P. (2007) A single-point mutation converts the highly amyloidogenic human islet amyloid polypeptide into a potent fibrillization inhibitor, *J Am Chem Soc 129*, 11300-11301.
122. Meng, F. L., Raleigh, D. P., and Abedini, A. (2010) Combination of kinetically selected inhibitors in trans leads to highly effective inhibition of amyloid formation, *J Am Chem Soc 132*, 14340-14342.
123. Ratner, R. E., Dickey, R., Fineman, M., Maggs, D. G., Shen, L., Strobel, S. A., Weyer, C., and Kolterman, O. G. (2004) Amylin replacement with pramlintide as an adjunct to

insulin therapy improves long-term glycaemic and weight control in Type 1 diabetes mellitus: a 1-year, randomized controlled trial, *Diabetic Med 21*, 1204-1212.
124. Yan, L. M., Tatarek-Nossol, M., Velkova, A., Kazantzis, A., and Kapurniotu, A. (2006) Design of a mimic of nonamyloidogenic and bioactive human islet amyloid polypeptide (IAPP) as nanomolar affinity inhibitor of IAPP cytotoxic fibrillogenesis, *Proc Natl Acad Sci USA 103*, 2046-2051.
125. Sakagashira, S., Sanke, T., Hanabusa, T., Shimomura, H., Ohagi, S., Kumagaye, K. Y., Nakajima, K., and Nanjo, K. (1996) Missense mutation of amylin gene (S20G) in Japanese NIDDM patients, *Diabetes 45*, 1279-1281.
126. Cao, P., Tu, L. H., Abedini, A., Levsh, O., Akter, R., Patsalo, V., Schmidt, A. M., and Raleigh, D. P. (2012) Sensitivity of amyloid formation by human islet amyloid polypeptide to mutations at residue 20, *J Mol Biol 421*, 282-295.
127. Tracz, S. M., Abedini, A., Driscoll, M., and Raleigh, D. P. (2004) Role of aromatic interactions in amyloid formation by peptides derived from human amylin, *Biochemistry 43*, 15901-15908.
128. Abedini, A., and Raleigh, D. P. (2006) Destabilization of human IAPP amyloid fibrils by proline mutations outside of the putative amyloidogenic domain: Is there a critical amyloidogenic domain in human IAPP?, *J Mol Biol 355*, 274-281.
129. Abedini, A., and Raleigh, D. P. (2005) The role of His-18 in amyloid formation by human islet amyloid polypeptide, *Biochemistry 44*, 16284-16291.
130. Schmittschmitt, J. P., and Scholtz, J. M. (2003) The role of protein stability, solubility, and net charge in amyloid fibril formation, *Protein Sci 12*, 2374-2378.
131. Tu, L.-H., Serrano, Arnaldo L., Zanni, Martin T., and Raleigh, Daniel P. (2014) Mutational analysis of preamyloid intermediates: The role of His-Tyr interactions in islet amyloid formation, *Biophys J 106*, 1520-1527.
132. Gazit, E. (2002) A possible role for pi-stacking in the self-assembly of amyloid fibrils, *Faseb J. 16*, 77-83.
133. Azriel, R., and Gazit, E. (2001) Analysis of the structural and functional elements of the minimal active fragment of islet amyloid polypeptide (IAPP) - An experimental support for the key role of the phenylalanine residue in amyloid formation, *J Biol Chem 276*, 34156-34161.
134. Marek, P., Abedini, A., Song, B. B., Kanungo, M., Johnson, M. E., Gupta, R., Zaman, W., Wong, S. S., and Raleigh, D. P. (2007) Aromatic interactions are not required for amyloid fibril formation by islet amyloid polypeptide but do influence the rate of fibril formation and fibril morphology, *Biochemistry 46*, 3255-3261.
135. Tu, L. H., and Raleigh, D. P. (2013) Role of Aromatic Interactions in Amyloid Formation by Islet Amyloid Polypeptide, *Biochemistry 52*, 333-342.
136. Knight, J. D., Hebda, J. A., and Miranker, A. D. (2006) Conserved and cooperative assembly of membrane-bound alpha-helical states of islet amyloid polypeptide, *Biochemistry 45*, 9496-9508.
137. Hebda, J. A., and Miranker, A. D. (2009) The interplay of catalysis and toxicity by amyloid intermediates on lipid bilayers: Insights from type II diabetes, *Ann Rev Biophys 38*, 125-152.
138. Weise, K., Radovan, D., Gohlke, A., Opitz, N., and Winter, R. (2010) Interaction of hIAPP with model raft membranes and pancreatic β-cells: Cytotoxicity of hIAPP oligomers, *ChemBioChem 11*, 1280-1290.

139. Young, I. D., Ailles, L., Narindrasorasak, S., Tan, R., and Kisilevsky, R. (1992) Localization of the basement membrane heparan sulfate proteoglycan in islet amyloid deposits in type II diabetes mellitus, *Arch Pathol Lab Med 116*, 951-954.
140. Meng, F., Abedini, A., Song, B., and Raleigh, D. P. (2007) Amyloid formation by pro-islet amyloid polypeptide processing intermediates: Examination of the role of protein heparan sulfate interactions and implications for islet amyloid formation in type 2 diabetes, *Biochemistry 46*, 12091-12099.
141. Park, K., and Verchere, C. B. (2001) Identification of a heparin binding domain in the N-terminal cleavage site of pro-islet amyloid polypeptide - Implications for islet amyloid formation, *J Biol Chem 276*, 16611-16616.
142. Luca, S., Yau, W. M., Leapman, R., and Tycko, R. (2007) Peptide conformation and supramolecular organization in amylin fibrils: constraints from solid-state NMR, *Biochemistry 46*, 13505-13522.
143. Wiltzius, J. J. W., Sievers, S. A., Sawaya, M. R., Cascio, D., Popov, D., Riekel, C., and Eisenberg, D. (2008) Atomic structure of the cross-beta spine of islet amyloid polypeptide (amylin), *Protein Sci 17*, 1467-1474.
144. Sawaya, M. R., Sambashivan, S., Nelson, R., Ivanova, M. I., Sievers, S. A., Apostol, M. I., Thompson, M. J., Balbirnie, M., Wiltzius, J. J. W., McFarlane, H. T., Madsen, A. O., Riekel, C., and Eisenberg, D. (2007) Atomic structures of amyloid cross-beta spines reveal varied steric zippers, *Nature 447*, 453-457.
145. Cao, P., Meng, F., Abedini, A., and Raleigh, D. P. (2010) The ability of rodent islet amyloid polypeptide to inhibit amyloid formation by human islet amyloid polypeptide has important implications for the mechanism of amyloid formation and the design of inhibitors, *Biochemistry 49*, 872-881.
146. Meng, F. L., Abedini, A., Plesner, A., Verchere, C. B., and Raleigh, D. P. (2010) The flavanol (-)-epigallocatechin 3-gallate inhibits amyloid formation by islet amyloid polypeptide, disaggregates amyloid fibrils, and protects cultured cells against IAPP-induced toxicity, *Biochemistry 49*, 8127-8133.
147. Mishra, R., Sellin, D., Radovan, D., Gohlke, A., and Winter, R. (2009) Inhibiting islet amyloid polypeptide fibril formation by the red wine compound resveratrol, *ChemBioChem 10*, 445-449.
148. Sinha, S., Lopes, D. H. J., Du, Z. M., Pang, E. S., Shanmugam, A., Lomakin, A., Talbiersky, P., Tennstaedt, A., McDaniel, K., Bakshi, R., Kuo, P. Y., Ehrmann, M., Benedek, G. B., Loo, J. A., Klarner, F. G., Schrader, T., Wang, C. Y., and Bitan, G. (2011) Lysine-specific molecular tweezers are broad-spectrum inhibitors of assembly and toxicity of amyloid proteins, *J Am Chem Soc 133*, 16958-16969.
149. Noor, H., Cao, P., and Raleigh, D. P. (2012) Morin hydrate inhibits amyloid formation by islet amyloid polypeptide and disaggregates amyloid fibers, *Protein Sci 21*, 373-382.
150. Meng, F., Abedini, A., Plesner, A., Middleton, C. T., Potter, K. J., Zanni, M. T., Verchere, C. B., and Raleigh, D. P. (2010) The sulfated triphenyl methane derivative acid fuchsin is a potent inhibitor of amyloid formation by human islet amyloid polypeptide and protects against the toxic effects of amyloid formation, *J Mol Biol 400*, 555-566.
151. Ehrnhoefer, D. E., Bieschke, J., Boeddrich, A., Herbst, M., Masino, L., Lurz, R., Engemann, S., Pastore, A., and Wanker, E. E. (2008) EGCG redirects amyloidogenic polypeptides into unstructured, off-pathway oligomers, *Nat Struct Mol Biol 15*, 558-566.

152. Palhano, F. L., Lee, J., Grimster, N. P., and Kelly, J. W. (2013) Toward the molecular mechanism(s) by which EGCG treatment remodels mature amyloid fibrils, *J Am Chem Soc 135*, 7503-7510.
153. Sipe, J. D. (1994) Amyloidosis, *Crit Rev Clin Lab Sci 31*, 325-354.
154. Vendruscolo, M., Zurdo, J., MacPhee, C. E., and Dobson, C. M. (2003) Protein folding and misfolding: a paradigm of self-assembly and regulation in complex biological systems, *Philos Trans A Math Phys Eng Sci 361*, 1205-1222.
155. Cooper, G. J., Willis, A. C., Clark, A., Turner, R. C., Sim, R. B., and Reid, K. B. (1987) Purification and characterization of a peptide from amyloid-rich pancreases of type 2 diabetic patients, *Proc Natl Acad Sci 84*, 8628-8632.
156. Westermark, P., Wernstedt, C., O'Brien, T. D., Hayden, D. W., and Johnson, K. H. (1987) Islet amyloid in type 2 human diabetes mellitus and adult diabetic cats contains a novel putative polypeptide hormone, *Am J Pathol 127*, 414-417.
157. Andersson, A., Bohman, S., Borg, L. A., Paulsson, J. F., Schultz, S. W., Westermark, G. T., and Westermark, P. (2008) Amyloid deposition in transplanted human pancreatic islets: a conceivable cause of their long-term failure, *Exp Diabetes Res 2008*, 562985.
158. Ward, W. K., Lacava, E. C., Paquette, T. L., Beard, J. C., Wallum, B. J., and Porte, D. (1987) Disproportionate elevation of immunoreactive proinsulin in type-2 (non-insulin-dependent) diabetes-mellitus and in experimental insulin resistance, *Diabetologia 30*, 698-702.
159. Snow, A. D., and Wight, T. N. (1989) Proteoglycans in the pathogenesis of Alzheimer's disease and other amyloidoses, *Neurobiol Aging 10*, 481-497.
160. Ancsin, J. B. (2003) Amyloidogenesis: historical and modern observations point to heparan sulfate proteoglycans as a major culprit, *Amyloid 10*, 67-79.
161. Watson, D. J., Lander, A. D., and Selkoe, D. J. (1997) Heparin-binding properties of the amyloidogenic peptides A beta and amylin - Dependence on aggregation state and inhibition by Congo red, *J Biol Chem 272*, 31617-31624.
162. Castillo, G. M., Ngo, C., Cummings, J., Wight, T. N., and Snow, A. D. (1997) Perlecan binds to the beta-amyloid proteins (A beta) of Alzheimer's disease, accelerates A beta fibril formation, and maintains A beta fibril stability, *J Neurochem 69*, 2452-2465.
163. Inoue, S. (2001) Basement membrane and beta amyloid fibrillogenesis in Alzheimer's disease, *Int Rev Cytol 210*, 121-161.
164. Castillo, G. M., Cummings, J. A., Yang, W. H., Judge, M. E., Sheardown, M. J., Rimvall, K., Hansen, J. B., and Snow, A. D. (1998) Sulfate content and specific glycosaminoglycan backbone of perlecan are critical for perlecan's enhancement of islet amyloid polypeptide (amylin) fibril formation, *Diabetes 47*, 612-620.
165. Potter-Perigo, S., Hull, R. L., Tsoi, C., Braun, K. R., Andrikopoulos, S., Teague, J., Verchere, C. B., Kahn, S. E., and Wight, T. N. (2003) Proteoglycans synthesized and secreted by pancreatic islet beta-cells bind amylin, *Arch Biochem Biophys 413*, 182-190.
166. Yamamoto, S., Yamaguchi, I., Hasegawa, K., Tsutsumi, S., Goto, Y., Gejyo, F., and Naiki, H. (2004) Glycosaminoglycans enhance the trifluoroethanol-induced extensionof beta(2)-microglobulin-related amyloid fibrils at a neutral pH, *J Am Soc Nephrol 15*, 126-133.
167. Suk, J. Y., Zhang, F. M., Balch, W. E., Linhardt, R. J., and Kelly, J. W. (2006) Heparin accelerates gelsolin amyloidogenesis, *Biochemistry 45*, 2234-2242.

168. Blancas-Mejía, L. M., and Ramirez-Alvarado, M. (2013) Systemic amyloidoses, *Annu Rev Biochem 82*, 745-774.
169. Gurlo, T., Ryazantsev, S., Huang, C. J., Yeh, M. W., Reber, H. A., Hines, O. J., O'Brien, T. D., Glabe, C. G., and Butler, P. C. (2010) Evidence for proteotoxicity in beta cells in type 2 diabetes toxic islet amyloid polypeptide oligomers form intracellularly in the secretory pathway, *Am J Pathol 176*, 861-869.
170. Aston-Mourney, K., Hull, R. L., Zraika, S., Udayasankar, J., Subramanian, S. L., and Kahn, S. E. (2011) Exendin-4 increases islet amyloid deposition but offsets the resultant beta cell toxicity in human islet amyloid polypeptide transgenic mouse islets, *Diabetologia 54*, 1756-1765.
171. Abedini, A., and Raleigh, D. P. (2005) Incorporation of pseudoproline derivatives allows the facile synthesis of human IAPP, a highly amyloidogenic and aggregation-prone polypeptide, *Org Lett 7*, 693-696.
172. Marek, P., Woys, A. M., Sutton, K., Zanni, M. T., and Raleigh, D. P. (2010) Efficient microwave-assisted synthesis of human islet amyloid polypeptide designed to facilitate the specific incorporation of labeled amino acids, *Org Lett 12*, 4848-4851.
173. Abedini, A., Singh, G., and Raleigh, D. P. (2006) Recovery and purification of highly aggregation-prone disulfide-containing peptides: Application to islet amyloid polypeptide, *Anal Biochem 351*, 181-186.
174. Wang, H., Cao, P., and Raleigh, D. P. (2013) Amyloid formation in heterogeneous environments: islet amyloid polypeptide glycosaminoglycan interactions, *J Mol Biol. 425*, 492-505.
175. Padrick, S. B., and Miranker, A. D. (2002) Islet amyloid: Phase partitioning and secondary nucleation are central to the mechanism of fibrillogenesis, *Biochemistry 41*, 4694-4703.
176. Gilead, S., Wolfenson, H., and Gazit, E. (2006) Molecular mapping of the recognition interface between the islet amyloid polypeptide and insulin, *Angew Chem-Int Edit 45*, 6476-6480.
177. Wiltzius, J. J. W., Sievers, S. A., Sawaya, M. R., and Eisenberg, D. (2009) Atomic structures of IAPP (amylin) fusions suggest a mechanism for fibrillation and the role of insulin in the process, *Protein Sci 18*, 1521-1530.
178. Abedini, A., and Raleigh, D. P. (2009) A critical assessment of the role of helical intermediates in amyloid formation by natively unfolded proteins and polypeptides, *Protein Eng Des Sel 22*, 453-459.
179. Abedini, A., and Raleigh, D. P. (2009) A role for helical intermediates in amyloid formation by natively unfolded polypeptides?, *Phys Biol 6*, 015005.
180. Williamson, J. A., and Miranker, A. D. (2007) Direct detection of transient alpha-helical states in islet amyloid polypeptide, *Protein Sci 16*, 110-117.
181. Sellin, D., Yan, L. M., Kapurniotu, A., and Winter, R. (2010) Suppression of IAPP fibrillation at anionic lipid membranes via IAPP-derived amyloid inhibitors and insulin, *Biophys Chem 150*, 73-79.
182. Kirkitadze, M. D., Bitan, G., and Teplow, D. B. (2002) Paradigm shifts in Alzheimer's disease and other neuro degenerative disorders: The emerging role of oligomeric assemblies, *J Neurosci Res 69*, 567-577.
183. Silveira, J. R., Raymond, G. J., Hughson, A. G., Race, R. E., Sim, V. L., Hayes, S. F., and Caughey, B. (2005) The most infectious prion protein particles, *Nature 437*, 257-261.

184. Blazer, L. L., and Neubig, R. R. (2009) Small molecule protein-protein interaction inhibitors as CNS therapeutic agents: Current progress and future hurdles, *Neuropsychopharmacology 34*, 126-141.
185. Takahashi, T., and Mihara, H. (2008) Peptide and protein mimetics inhibiting amyloid beta-peptide aggregation, *Acc Chem Res 41*, 1309-1318.
186. Chafekar, S. M., Malda, H., Merkx, M., Meijer, E. W., Viertl, D., Lashuel, H. A., Baas, F., and Scheper, W. (2007) Branched KLVFF tetramers strongly potentiate inhibition of beta-amyloid aggregation, *ChemBioChem 8*, 1857-1864.
187. van Horssen, J., Wesseling, P., van den Heuvel, L. P., de Waal, R. M., and Verbeek, M. M. (2003) Heparan sulphate proteoglycans in Alzheimer's disease and amyloid-related disorders, *Lancet Neurol 2*, 482-492.
188. Bonifacio, M. J., Sakaki, Y., and Saraiva, M. J. (1996) 'In vitro' amyloid fibril formation from transthyretin: The influence of ions and the amyloidogenicity of TTR variants, *BBA-Mol Basis Dis 1316*, 35-42.
189. McParland, V. J., Kad, N. M., Kalverda, A. P., Brown, A., Kirwin-Jones, P., Hunter, M. G., Sunde, M., and Radford, S. E. (2000) Partially unfolded states of beta(2)-microglobulin and amyloid formation in vitro, *Biochemistry 39*, 8735-8746.
190. Kayed, R., Bernhagen, J., Greenfield, N., Sweimeh, K., Brunner, H., Voelter, W., and Kapurniotu, A. (1999) Conformational transitions of islet amyloid polypeptide (IAPP) in amyloid formation in vitro, *J Mol Biol 287*, 781-796.
191. Westermark, P., Wernstedt, C., Wilander, E., Hayden, D. W., Obrien, T. D., and Johnson, K. H. (1987) Amyloid fibrils in human insulinoma and islets of Langerhans of the diabetic cat are derived from a neuropeptide-like protein also present in normal islet cells, *Proc Natl Acad Sci USA 84*, 3881-3885.
192. Clark, A., and Nilsson, M. R. (2004) Islet amyloid: a complication of islet dysfunction or an aetiological factor in Type 2 diabetes?, *Diabetologia 47*, 157-169.
193. Knight, J. D., and Miranker, A. D. (2004) Phospholipid catalysis of diabetic amyloid assembly, *J Mol Biol 341*, 1175-1187.
194. Jayasinghe, S. A., and Langen, R. (2005) Lipid membranes modulate the structure of islet amyloid polypeptide, *Biochemistry 44*, 12113-12119.
195. Shim, S. H., Gupta, R., Ling, Y. L., Strasfeld, D. B., Raleigh, D. P., and Zanni, M. T. (2009) Two-dimensional IR spectroscopy and isotope labeling defines the pathway of amyloid formation with residue-specific resolution, *Proc Natl Acad Sci. USA 106*, 6614-6619.
196. Inoue, S. (2001) Basement membrane and beta amyloid fibrillogenesis in Alzheimer's disease, *Int Rev Cytol*, pp 121-161, Academic Press Inc, San Diego.
197. Jha, S., Patil, S. M., Gibson, J., Nelson, C. E., Alder, N. N., and Alexandrescu, A. T. (2011) Mechanism of amylin fibrillization enhancement by heparin, *J Biol Chem 286*, 22894-22904.
198. Solomon, J. P., Bourgault, S., Powers, E. T., and Kelly, J. W. (2011) Heparin binds 8 kDa gelsolin cross-beta-sheet oligomers and accelerates amyloidogenesis by hastening fibril extension, *Biochemistry 50*, 2486-2498.
199. Stewart, J. C. (1980) Colorimetric determination of phospholipids with ammonium ferrothiocyanate, *Anal Biochem 104*, 10-14.

200. Marek, P. J., Patsalo, V., Green, D. F., and Raleigh, D. P. (2012) Ionic strength effects on amyloid formation by amylin are a complicated interplay among Debye screening, ion selectivity, and Hofmeister effects, *Biochemistry 51*, 8478-8490.
201. Lopes, D. H. J., Meister, A., Gohlke, A., Hauser, A., Blume, A., and Winter, R. (2007) Mechanism of islet amyloid polypeptide fibrillation at lipid interfaces studied by infrared reflection absorption spectroscopy, *Biophys J 93*, 3132-3141.
202. Brender, J. R., Lee, E. L., Cavitt, M. A., Gafni, A., Steel, D. G., and Ramamoorthy, A. (2008) Amyloid fiber formation and membrane disruption are separate processes localized in two distinct regions of IAPP, the type-2-diabetes-related peptide, *J Am Chem Soc 130*, 6424-6429.
203. Domanov, Y. A., and Kinnunen, P. K. J. (2008) Islet amyloid polypeptide forms rigid lipid-protein amyloid fibrils on supported phospholipid bilayers, *J Mol Biol 376*, 42-54.
204. Evers, F., Jeworrek, C., Tiemeyer, S., Weise, K., Sellin, D., Paulus, M., Struth, B., Tolan, M., and Winter, R. (2009) Elucidating the mechanism of lipid membrane-induced IAPP fibrillogenesis and its inhibition by the red wine compound resveratrol: a synchrotron X-ray reflectivity study, *J Am Chem Soc 131*, 9516-9521.
205. Bieschke, J., Russ, J., Friedrich, R. P., Ehrnhoefer, D. E., Wobst, H., Neugebauer, K., and Wanker, E. E. (2010) EGCG remodels mature alpha-synuclein and amyloid-beta fibrils and reduces cellular toxicity, *Proc Natl Acad Sci USA 107*, 7710-7715.
206. Ehrnhoefer, D. E., Duennwald, M., Markovic, P., Wacker, J. L., Engemann, S., Roark, M., Legleiter, J., Marsh, J. L., Thompson, L. M., Lindquist, S., Muchowski, P. J., and Wanker, E. E. (2006) Green tea (-)-epigallocatechin-gallate modulates early events in huntingtin misfolding and reduces toxicity in Huntington's disease models, *Hum Mol Genet 15*, 2743-2751.
207. Zhang, Z., McCallum, S. A., Xie, J., Nieto, L., Corzana, F., Jimenez-Barbero, J., Chen, M., Liu, J., and Linhardt, R. J. (2008) Solution structures of chemoenzymatically synthesized heparin and its precursors, *J Am Chem Soc 130*, 12998-13007.
208. Valle-Delgado, J. J., Alfonso-Prieto, M., de Groot, N. S., Ventura, S., Samitier, J., Rovira, C., and Fernandez-Busquets, X. (2010) Modulation of A beta(42) fibrillogenesis by glycosaminoglycan structure, *Faseb J. 24*, 4250-4261.
209. Hull, R. L., Zraika, S., Udayasankar, J., Kisilevsky, R., Szarek, W. A., Wight, T. N., and Kahn, S. E. (2007) Inhibition of glycosaminoglycan synthesis and protein glycosylation with WAS-406 and azaserine result in reduced islet amyloid formation in vitro, *Am. J. Physiol.-Cell Physiol 293*, C1586-C1593.
210. Kisilevsky, R., Szarek, W. A., Ancsin, J. B., Elimova, E., Marone, S., Bhat, S., and Berkin, A. (2004) Inhibition of amyloid A amyloidogenesis in vivo and in tissue culture by 4-deoxy analogues of peracetylated 2-acetamido-2-deoxy-alpha- and beta-d-glucose - Implications for the treatment of various amyloidoses, *Am J Pathol 164*, 2127-2137.
211. Maji, S. K., Perrin, M. H., Sawaya, M. R., Jessberger, S., Vadodaria, K., Rissman, R. A., Singru, P. S., Nilsson, K. P. R., Simon, R., Schubert, D., Eisenberg, D., Rivier, J., Sawchenko, P., Vale, W., and Riek, R. (2009) Functional amyloids as natural storage of peptide hormones in pituitary secretory granules, *Science 325*, 328-332.
212. Westerma.P, and Grimeliu.L. (1973) Pancreatic-islet cells in insular amyloidosis in human diabetic and non-diabetic adults., *Acta Pathol Microbiol Scand A 81*, 291-300.

213. Samsom, M., Szarka, L. A., Camilleri, M., Vella, A., Zinsmeister, A. R., and Rizza, R. A. (2000) Pramlintide, an amylin analog, selectively delays gastric emptying: potential role of vagal inhibition, *Am J Physiol Gastrointest Liver Physiol 278*, G946-951.
214. Mazor, Y., Gilead, S., Benhar, I., and Gazit, E. (2002) Identification and Characterization of a Novel Molecular-recognition and Self-assembly Domain within the Islet Amyloid Polypeptide, *J Mol Biol 322*, 1013-1024.
215. Dupuis, N. F., Wu, C., Shea, J.-E., and Bowers, M. T. (2011) The amyloid formation mechanism in human IAPP: Dimers have β-strand monomer−monomer interfaces, *J Am Chem Soc 133*, 7240-7243.
216. Buchanan, L. E., Dunkelberger, E. B., Tran, H. Q., Cheng, P. N., Chiu, C. C., Cao, P., Raleigh, D. P., de Pablo, J. J., Nowick, J. S., and Zanni, M. T. (2013) Mechanism of IAPP amyloid fibril formation involves an intermediate with a transient beta-sheet, *Proc Natl Acad Sci USA 110*, 19285-19290.
217. Nonoyama, A., Laurence, J. S., Garriques, L., Qi, H., Le, T., and Middaugh, C. R. (2008) A biophysical characterization of the peptide drug pramlintide (AC137) using empirical phase diagrams, *J Pharm Sci 97*, 2552-2567.
218. Green, J., Goldsbury, C., Mini, T., Sunderji, S., Frey, P., Kistler, J., Cooper, G., and Aebi, U. (2003) Full-length rat amylin forms fibrils following substitution of single residues from human amylin, *J Mol Biol 326*, 1147-1156.
219. Chen, M. S., Zhao, D. S., Yu, Y. P., Li, W. W., Chen, Y. X., Zhao, Y. F., and Li, Y. M. (2013) Characterizing the assembly behaviors of human amylin: a perspective derived from C-terminal variants, *Chem Commun 49*, 1799-1801.
220. Middleton, C. T., Marek, P., Cao, P., Chiu, C. C., Singh, S., Woys, A. M., de Pablo, J. J., Raleigh, D. P., and Zanni, M. T. (2012) Two-dimensional infrared spectroscopy reveals the complex behaviour of an amyloid fibril inhibitor, *Nat Chem 4*, 355-360.
221. Clark, A., Lewis, C. E., Willis, A. C., Cooper, G. J. S., Morris, J. F., Reid, K. B. M., and Turner, R. C. (1987) Islet amyloid formed from diabetes-associated peptide may be pathogenic in type-2 diabetes, *Lancet 2*, 231-234.
222. Koda, J. E., Fineman, M., Rink, T. J., Dailey, G. E., Muchmore, D. B., and Linarelli, L. G. (1992) Amylin concentrations and glucose control, *Lancet 339*, 1179-1180.
223. Fineman, M. S., Giotta, M. P., Thompson, R. G., Kolterman, O. K., and Koda, J. E. (1996) Amylin response following Sustacal(R) ingestion is diminished in type II diabetic patients treated with insulin, *Diabetologia 39*, 566-566.
224. Kruger, D. F., Gatcomb, P. M., and Owen, S. K. (1999) Clinical implications of amylin and amylin deficiency, *Diabetes Educ 25*, 389-397.
225. Seth, R., Terry, D. E., Parrish, B., Bhatt, R., and Overton, J. M. (2012) Amylin–leptin coadministration stimulates central histaminergic signaling in rats, *Brain Res 1442*, 15-24.
226. Trevaskis, J. L., Lei, C., Koda, J. E., Weyer, C., Parkes, D. G., and Roth, J. D. (2010) Interaction of leptin and amylin in the long-term maintenance of weight loss in diet-induced obese rats, *Obesity 18*, 21-26.
227. Roth, J. D., Roland, B. L., Cole, R. L., Trevaskis, J. L., Weyer, C., Koda, J. E., Anderson, C. M., Parkes, D. G., and Baron, A. D. (2008) Leptin responsiveness restored by amylin agonism in diet-induced obesity: Evidence from nonclinical and clinical studies, *Proc Natl Acad Sci 105*, 7257-7262.

228. Jha, S., Snell, J. M., Sheftic, S. R., Patil, S. M., Daniels, S. B., Kolling, F. W., and Alexandrescu, A. T. (2014) pH dependence of amylin fibrillization, *Biochemistry 53*, 300-310.
229. Charge, S. B. P., Dekoning, E. J. P., and Clark, A. (1995) Effect of pH and insulin on fibrillogenesis of islet amyloid polypeptide in-vitro, *Biochemistry 34*, 14588-14593.
230. Moriarty, D. F., and Raleigh, D. P. (1999) Effects of sequential proline substitutions on amyloid formation by human amylin20-29†, *Biochemistry 38*, 1811-1818.
231. Meng, F. L., Marek, P., Potter, K. J., Verchere, C. B., and Raleigh, D. P. (2008) Rifampicin does not prevent amyloid fibril formation by human islet amyloid polypeptide but does inhibit fibril thioflavin-T interactions: Implications for mechanistic studies beta-cell death, *Biochemistry 47*, 6016-6024.
232. Bucciantini, M., Giannoni, E., Chiti, F., Baroni, F., Formigli, L., Zurdo, J., Taddei, N., Ramponi, G., Dobson, C. M., and Stefani, M. (2002) Inherent toxicity of aggregates implies a common mechanism for protein misfolding diseases, *Nature 416*, 507-511.
233. Lambert, M. P., Barlow, A. K., Chromy, B. A., Edwards, C., Freed, R., Liosatos, M., Morgan, T. E., Rozovsky, I., Trommer, B., Viola, K. L., Wals, P., Zhang, C., Finch, C. E., Krafft, G. A., and Klein, W. L. (1998) Diffusible, nonfibrillar ligands derived from A beta(1-42) are potent central nervous system neurotoxins, *Proc Natl Acad Sci USA 95*, 6448-6453.
234. Bucciantini, M., Calloni, G., Chiti, F., Formigli, L., Nosi, D., Dobson, C. M., and Stefani, M. (2004) Prefibrillar amyloid protein aggregates share common features of cytotoxicity, *J Biol Chem 279*, 31374-31382.
235. Sciacca, Michele F. M., Kotler, Samuel A., Brender, Jeffrey R., Chen, J., Lee, D.-k., and Ramamoorthy, A. (2012) Two-step mechanism of membrane disruption by Aβ through membrane fragmentation and pore formation, *Biophys J 103*, 702-710.
236. Kayed, R., Head, E., Thompson, J. L., McIntire, T. M., Milton, S. C., Cotman, C. W., and Glabe, C. G. (2003) Common structure of soluble amyloid oligomers implies common mechanism of pathogenesis, *Science 300*, 486-489.
237. Porat, Y., Mazor, Y., Efrat, S., and Gazit, E. (2004) Inhibition of islet amyloid polypeptide fibril formation: A potential role for heteroaromatic interactions, *Biochemistry 43*, 14454-14462.
238. Mishra, R., Bulic, B., Sellin, D., Jha, S., Waldmann, H., and Winter, R. (2008) Small-molecule inhibitors of islet amyloid polypeptide fibril formation, *Angew Chem-Int Edit 47*, 4679-4682.
239. Meng, F., Abedini, A., Plesner, A., Verchere, C. B., and Raleigh, D. P. (2010) The flavanol (-)-epigallocatechin 3-gallate inhibits amyloid formation by islet amyloid polypeptide, disaggregates amyloid fibrils, and protects cultured cells against IAPP-induced toxicity, *Biochemistry 49*, 8127-8133.
240. Yan, L.-M., Velkova, A., Tatarek-Nossol, M., Rammes, G., Sibaev, A., Andreetto, E., Kracklauer, M., Bakou, M., Malideli, E., Göke, B., Schirra, J., Storr, M., and Kapurniotu, A. (2013) Selectively N-methylated soluble IAPP mimics as potent IAPP receptor agonists and nanomolar inhibitors of cytotoxic self-assembly of both IAPP and Aβ40, *Angew Chem Int Ed 52*, 10378-10383.
241. Fisher, S. K., Novak, J. E., and Agranoff, B. W. (2002) Inositol and higher inositol phosphates in neural tissues: homeostasis, metabolism and functional significance, *J Neurochem 82*, 736-754.

242. Michaelis, T., Helms, G., Merboldt, K. D., Hanicke, W., Bruhn, H., and Frahm, J. (1993) Identification of scyllo-inositol in proton NMR-spectra of human brain *in vivo*, *NMR Biomed 6*, 105-109.
243. McLaurin, J., Franklin, T., Chakrabartty, A., and Fraser, P. E. (1998) Phosphatidylinositol and inositol involvement in Alzheimer amyloid-beta fibril growth and arrest, *J Mol Biol 278*, 183-194.
244. McLaurin, J., Golomb, R., Jurewicz, A., Antel, J. P., and Fraser, P. E. (2000) Inositol stereoisomers stabilize an oligomeric aggregate of Alzheimer amyloid β peptide and inhibit Aβ-induced toxicity, *J Biol Chem 275*, 18495-18502.
245. Sinha, S., Du, Z., Maiti, P., Klärner, F.-G., Schrader, T., Wang, C., and Bitan, G. (2012) Comparison of three amyloid assembly inhibitors: the sugar scyllo-inositol, the polyphenol epigallocatechin gallate, and the molecular tweezer CLR01, *Acs Chem Neurosci 3*, 451-458.
246. Bleiholder, C., Do, T. D., Wu, C., Economou, N. J., Bernstein, S. S., Buratto, S. K., Shea, J. E., and Bowers, M. T. (2013) Ion mobility spectrometry reveals the mechanism of amyloid formation of A beta(25-35) and its modulation by inhibitors at the molecular level: epigallocatechin gallate and scyllo-inositol, *J Am Chem Soc 135*, 16926-16937.
247. McLaurin, J., Kierstead, M. E., Brown, M. E., Hawkes, C. A., Lambermon, M. H. L., Phinney, A. L., Darabie, A. A., Cousins, J. E., French, J. E., Lan, M. F., Chen, F. S., Wong, S. S. N., Mount, H. T. J., Fraser, P. E., Westaway, D., and St George-Hyslop, P. (2006) Cyclohexanehexol inhibitors of A beta aggregation prevent and reverse Alzheimer phenotype in a mouse model, *Nat Med 12*, 801-808.
248. Li, G., Rauscher, S., Baud, S., and Pomes, R. (2012) Binding of inositol stereoisomers to model amyloidogenic peptides, *J Phys Chem B 116*, 1111-1119.
249. Li, G., and Pomes, R. (2013) Binding mechanism of inositol stereoisomers to monomers and aggregates of A beta(16-22), *J Phys Chem B 117*, 6603-6613.